DYNAMIC RESPONSE OF TALL STRUCTURES TO WIND EXCITATION

A Thesis submitted for the Degree of

Doctor of Philosophy

UNIVERSITY OF EDINBURGH

DEPARTMENT

OF

CIVIL ENGINEERING BUILDING SCIENCE

by

Massoud Sohirad, Dip.Struct.Eng., M.Sc.(Dundee)

JUNE 1983

ABSTRACT

A system of measuring instantaneous localised wind characteristic profiles at three different heights above ground level was devised. The system made use of kites to support the wind mointoring instruments at the required levels and the transfer of data to ground by telemetery.

A 20 storey building was instrumented with displacement and acceleration transducers in order to determine its dynamic characteristics and to examine its dynamic response to wind excitation.

A reference on the local wind speed and direction profiles was established by means of a station at the top of the building.

Through the utilisation of an amplitude modulation/demodulation procedure extra recording channels were made available over and above those provided on the basic instrument taperecorder.

The dynamic characteristics of the building were established experimentally, and the results were compared with values computed by analytical methods.

The dynamic behaviour of the structure under wind excitation was studied and the measured response was compared with predictions based on two methods. The first method took into account the frequency dependence of a component of drag, and the second assumed the drag to be constant. The relationship of the magnitude of the response to human perception levels was considered.

An equivalent static drag coefficient was deduced for the dynamic response at the fundamental frequency in a particular wind

velocity. This value was hence was found to be in good agreement with values determined by wind tunnel studies, and was hence employed to predict the dynamic response of the structure to a 50 year return wind velocity.

ACKNOWLEDGEMENTS

The author wishes to thank a number of people and parties that have helped in various ways in the completion of this research.

Prof. A.W.Hendry, Head of the Department of Civil Engineering and Building Science for providing facilities, encouragement, and support through the technical staff of his department.

To Dr.R.Royles, a special word of thanks for his endless support and learned advice throughout.

The authour is indebted to the Housing Department of the City of Edinburgh District Council for the use of JRC building for the purpose of this project.

Special mentions are also given to Dr.J.H.Dripps, Electrical Engineering Department, and Mr.David C.Jeffrey, Department of Mechanical Engineering University of Edinburgh, for their technical advice and patience.

Strong appreciations of the financial support given by the Royal Society is truly expressed.

A word of gratitude to members of the BRE, Dynamic Loading Division for invaluable advice and kindness in making available soft ware and hard ware for calibration and analysis of data.

The authour wishes to thank all the post graduates, collegues, and Dr.John W. McCarter of Heriot Watt University for sacrificing their valuable time freely and voluntarily to help.

Blyth and Blyth Consulting Engineers, and City of Edinburgh District Council Housing Department are also thanked for providing technical drawings of the building.

Finally to my parents for their encouragement and financial support without which none of this would have been achieved.

CONTENTS

CHAPTER 3 JOHN RUSSEL COURT BUILDING

CHAPTER 4 INSTRUMENTATION

CHAPTER 5 SIGNAL CONDITIONING AND DATA ACQUISITION

CHAPTER 6 INTERPERTATION AND ANALYSIS OF RECORDED DATA

CHAPTER 7 GENERAL DISCUSSION AND CONCLUSIONS

NOTATION

A	Area
B	Bandwidth
C	Damping matrix
C_D	Damping drag coefficient
$C_D l$	An equivalent static drag coefficient
C_{qs}	Quasi static drag coefficient
D	Depth of building
F_r	Force causing the modal frequency response
H	Height of the building
K	Stiffness matix
K*	Von Karman's constant
L	Lift force
M	Mass matrix
M_r	Modal mass at the r^{th} term
T	Sampling time
U(t)	Instantaneous velocity or wind speed
U(z)	Hourly mean wind speed at the height z
U*	Friction velocity
Vn	Amplitude of response of damped system after n the cycle
$\ddot{X}_{max}$	Maximum acceleration
Z	Normalising factor
Z_G	Gradient height
Z_o	Roughness length
a	Amplitude
b	Bias error
d^o	Deflection of intial mode shape

f	Frequency
f_r	Modal frequency at the r^{th} mode
g	Gravity acceleration
h	Height
k	Stiffness
m	Mass
p	Peak factor
P_I	Intial load
q	Displacement
$\dot{q}$	Velocity
$\ddot{q}$	Acceleration
s	Variance error
t	Time
u_t	Fluctuating compoent of U(t)
v	Wind velocity
v	Relative deflection
w	Width of the building
x_r	Modal range at the r^{th} mode
z_r	Reference height (10 m)
α	Power law exponent of the mean wind speed profile
β	Diagonal matrix containing proportions of critical damping
γ	Average structural mass density
$\Delta(t)$	Longitudinal instantaneous displacement
$\bar{\Delta}(z)$	Mean displacement
$\delta(t)$	Fluctuating componet of Δ (t)
$\dot{\delta}(t)$	Longitudinal velocity of response
$\ddot{\delta}(t)$	Longitudinal acceleration of response
ζ	Structural damping ratio (fraction of critical)

$\mu_n(z)$	Modal shape of the n^{th} mode
ω	Natural circular frequency
ψ	Shape factor of initial mode shape
ρ	Air mass density
σ_u	R.M.S. value of u_T
σ_δ	R.M.S. value of $\delta(t)$
$\sigma_{\ddot{\delta}}$	R.M.s. value of $\ddot{\delta}(t)$
ε	Standard error

LIST OF FIGURES

LIST OF TABLES

LIST OF PLATES

CHAPTER 1

INTRODUCTION

1.1 INTRODUCTION

In recent years, arising from a desire to achieve material economies, structures have been constructed with decreased structural damping and increased slenderness. This, in turn, makes the structures more susceptible to dynamic loading. By definition, dynamic load may be described as a load in which the magnitude, direction or position varies with time. Such loads are derived from earthquakes, explosions, eccentrically mounted machinery, vehicular traffic, sea waves, and wind.

The perception of wind induced motion in some recently completed high-rise buildings has focused the attention of engineers on the serviceability requirement which must be considered in the design process. The static equivalent wind loading, as presented in building codes, are not adequate for a serviceability analysis because the basic problem requires an assessment of dynamic effects such as peak loads and their frequency of occurrence and the characteristics of a structure which influence its response to dynamic loadings.

In order to predict the response of a structure to wind, it is of utmost importance to understand the structure and dynamic characteristics of natural wind.

1.2 ORIGIN OF WIND

Atmospheric pressure differences, which arise from differences in

the amount of heat received from the sun, gives rise to wind. In addition to the forces produced by these pressure differences, Coriolis forces , which are due to the curvature and rotation of the earth, act on a given mass of air. At increasing heights above the earth's surface, where boundary layer effects can be ignored, quasi-static conditions exsist,(i.e. when the weather map is not changing rapidly). The resultant of these forces produces a steady motion which is parallel to the lines of equal barometric pressure on the weather map, (viz.,isobars). The motion is denoted by the gradient wind speed. In quasi-static conditions the gradient wind can be determined directly from the weather map if the latitude, radius of curvature of the isobars, and the pressure gradient or spacing of the isobars are known.

The lowest height at which the wind velocity is equal to the gradient velocity is known as the gradient height. This gradient height normally lies between 300 m and 3000 m above ground level, but depends on either the gradient wind speed or the roughness of the underlying terrain. Closer to the surface of the earth frictional effects predominate and cause fluctuations in the mean flow. This gives rise to a kinetic energy transfer from the mean wind speed into these fluctuations and results in gusting.

The turbulent fluctuations provide a vertical exchange of air mass and momentum. Application of the equations of fluid mechanics to the problem shows that this momentum exchange introduces a Reynolds stress. The result is that within the planetary boundary layer the mean wind direction is no longer parallel to the isobars, but changes systematically between the gradient height and the surface, an effect known for historical reasons, as the Ekmann

Spiral. Also, the mean wind speed decreases from the gradient speed at the gradient height to a value of zero at the earth's surface[1].

1.3 STRUCTURE OF WIND

Detailed studies of the wind or meteorological station records reveal two relevant facts,

(i) the variation in wind speeds which occur have a wide range of frequencies, Figure 1.1, and,

(ii) the variations are not regular like a sine wave signal, but are highly complex and irregular.

The most widely used wind structure description is that proposed by Davenport[2] and modified by Harris[3]. Their description of wind structure was a power law expression. However studies carried out by meteorologist show that a logarithmic expression can provide a better fit. Studies carried out by Harris and Deaves[1] represent a significant advance on previous formulations, where the wind structure is fully defined by a logarithmic expression using only two parameters, viz.,

(i) the representative upwind ground roughness length, and,

(ii) a reference wind speed.

1.3.1 Power law expression

Experiments which have been conducted to determine an hourly mean wind speed profile show that the theoretically derived logarithmic law is applicable for wind speed near ground level[4] i.e. only for the lower part of the boundary layer. The power law profile, however, can provide a better fit to measured data over a more

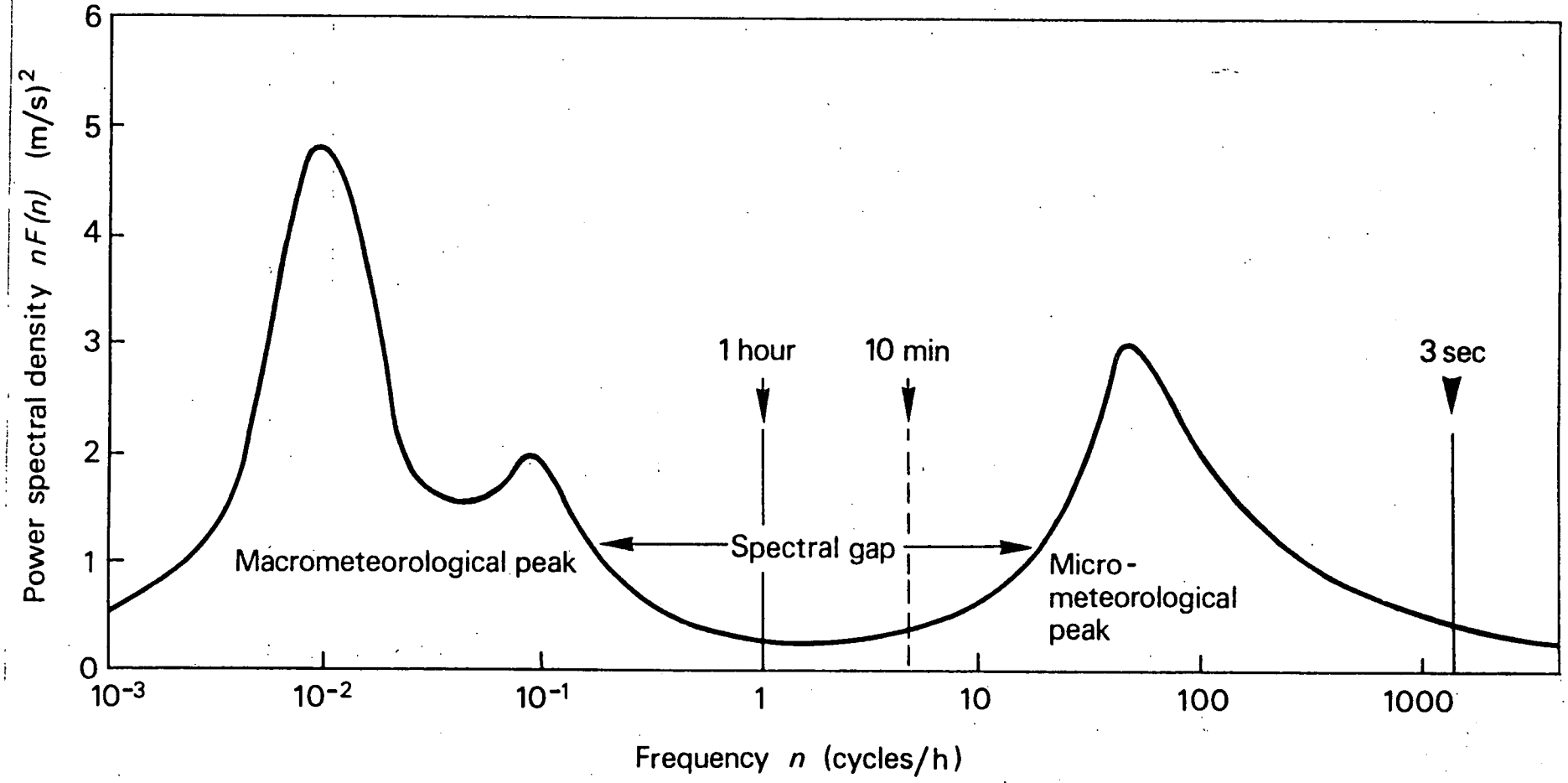

Figure 1.1 Spectrum of horizontal wind speed (after Van der Hoven)

extensive range of height. The power law expression is defined as

$$\bar{U}(Z) = \bar{U}(Z_r)\left(\frac{Z}{Z_r}\right)^{\alpha}$$

where,

$\bar{U}(Z)$ is the hourly mean wind speed at height Z

Z_r is the reference height and Z_r = 10 m is taken conventionally

α is the empirical power exponent.

1.3.2 Logarithmic expression

Most investigations of the profiles of mean wind speeds have been experimental, and measurements made in the lowest 50 m of the atmosphere. The flow in this lowest layer of the atmosphere is very similar to that adjacent to a rough wall in laboratory experiments, and on this basis, a logarithmic profile law is to expected. The modified logarithmic expression derived by Harris and Deaves[1] has shown that over level terrain of uniform roughness, in strong winds,(i.e. neutral stability), the results can be represented in the lowest 30 m or so, by the expression,

$$\bar{U}(Z) = \frac{U^*}{K^*} \ln\left(\frac{Z}{Z_o}\right)$$

where,

$\bar{U}(Z)$ is the mean wind speed at height Z

K^* is Von Karman's constant ($\simeq 0.4$)

U^* is the friction velocity (defined in terms of the surface frictional shear stress τ_o, by $U^* = \left[\tau_o/\rho\right]^{\frac{1}{2}}$)

Z_o is the roughness length or measure of the surface roughness,

constant for a surface of given roughness

1.4 WIND LOADING ON STRUCTURES

The natural wind is composed of a steady mean wind speed with a superimposed randomly fluctuating velocity component. Traditionally, the peak gust velocities resulting from this process have been applied in design as a quasi-static loading, with allowance for the size of the structure when assessing gust duration. The use of quasi-static gust loads is, however, unrepresentative of the true nature of turbulent wind loading[5]. On the one hand, there is no allowance for aerodynamic interaction between wind and structure, and on the other, there may be an inappropriate, conservative allowance for the lack of full correlation of gusts.

1.4.1 Codes of practice

The principal wind loading code in the U.K. is CP3 ChapterV:Part 2:1972[6], and considers wind loading by an equivalent static load on the structure. The code ignores the dynamic characteristics of wind. This code has proved inadequate in an increasing number of cases[7] and as a result, several supplementary codes[8,9,10,11,12] have been formulated to cover such special cases. Discrepancies have arisen between wind loading calculated by CP3 and the supplementary codes and, in some cases, has caused many problems for the designer to assertain the more correct loading. Therefore it is necessary to emphasise a need for a unification and modification of the current codes.

1.4.2 The effect of dynamic loading on structure

Bearman[13] has shown how the power spectrum of the total force on a structure can be evaluated by expressing the distribution between frequency components of the total variance of the force. The bulk of the variance is associated with frequencies lower than the lowest natural frequency of most structures. Since, however there is a spectrum of the frequencies in the wind load, it is certain that at least one of the natural frequencies of the structure would be contained within the spectrum[14].

It is therefore necessary to treat the problem by an appropriate dynamic analysis in terms of the natural modes of the structure. This is extremely well suited to the load formulation given by Bearman[13], as only minor modifications are necessary to the admittance (correlation) integral to give the spectra of the relevant modal generalised forces.

1.4.2.1 Dynamic along-wind response

The dynamic along-wind response of structures results from the action of wind turbulence superimposed on the mean wind drag force. The dynamic analysis procedures available are as follows.

(i) Full spectral analysis, in which allowance is made for the fluctuating wind loading. This obtained by applying an explicit wind regime to a stochastic dynamic analysis through the full range of gust frequencies, in combination with a steady mean loading. This method has been used widely for more than a decade and has become a highly developed analytical tool in design.

(ii) Part spectral/part correlation analysis (termed the component method) which is similar to (i), but with full dynamic analysis

only over frequencies close to the structure frequency (narrow band component), and a correlation analysis at lower gust frequencies (broad band component) again in combination with a steady mean loading.

Simplified gust response factor methods of analysis are presently available to the designer in a form suitable for design office use[15,16]. In these methods, the ratio of total response to mean response is usually obtained at the base of the structure. They are based on the full spectral method and formulations of the wind spectrum and profile description similar to those presented at the 1970 CIRIA Wind Conference[17]. These methods are relatively simple to apply and are to be found in several national wind codes,(e.g Australia[18], Canada[19], Czechoslovakia[20], Denmark[21], France[22], Netherlands[23], Sweden[24]). They are based on line like structures of uniform properties with a linear mode shape but are generally applicable to a wide range of practical structures. The structure input data required, in addition to that for a static analysis, are the natural frequency, and the structural and aerodynamic damping.

The component method of analysis provides the basis of a simple calculation procedure similar to that for existing gust factor methods[25]. The requisite design charts for evaluation of the base moment of constant exposed width structures are provided for the broad-band component. The narrow-band component and the influence of the gradient wind speed are determined by calculation[5].

The full spectral and component methods have their respective advantages and disadvantages. The full spectral method allows a consistent derivation of the peak response factor, while, in the component method, the peak response factor can similarly be

obtained for the narrow-band component, but there is not a similar analytical base for the broad-band component.

When applied in simple formulations the full spectral method may not allow for the correlation between modes in the broad-band zone, which the component method does take into account. This effect is not pronounced for structures of uniform exposed area and mass. There is a lower limit on the structure frequency that can be considered when applying the component method, depending on the structure height and mean wind speed. Wyatt[25] has indicated the limiting frequencies that can be considered for typical conditions. In situations of relatively high wind speed and low frequency the condition may not be satisfied in which case a full spectral analysis approach would be necessary.

1.4.2.2 Dynamic cross-wind response

Cross-wind response is particularly significant in lightweight structures of circular or prismatic cross section with low damping characteristics. It can become severe under certain critical conditions of low wind speed in laminar flow, resulting in a classical resonant vortex shedding type response.

Whereas the along-wind response of a structure has received much investigation , cross-wind response still requires further detailed studies because of the complexity of the fluctuation froces due to vortices. The forces due to vortices are affected by various factors, in particular, aspect ratio and wind profile.

Analytical approaches have been considered[26,27,28] but, it is evident that full scale studies are still required to verify or modify these theoretical predictions.

1.5 WIND TUNNEL STUDIES

The availability of statistical methods and computers has encouraged engineers to study non-steady wind loading on structures in wind tunnels. The aero-elastic models designed[29] to satisfy the scaling requirements for top deflections or base bending moments illustrated by Vickery and Davenport[30] and Kato, et al.[31], have their limitations. The results obtained are only applicable to that unique combination of shape, frequency and damping represented by the model.

However, a more general technique used by Ellis[32] was to obtain the wind load spectra and to compute the corresponding dynamic spectra for those combinations of model frequency and damping appropriate to a particular structure. In order to obtain the various modal force spectra, the response of an idealised areo-elastic model in a wind tunnel was found. These forces thus were used to predict the response for other prescribed combinations of frequency and damping.

Although wind tunnel techniques have undergone continuous development to provide more realistic estimates of wind loading required by modern analysis, there are still difficulties involved such as,

(i) simulation of the turbulent shear flow of the earth's boundary layer interacting with the flow generated by a building,

(ii) the achievement of a correct scaling factor value of aero-elastic model damping in relation to the actual structure, and,

(iii) the aero-elastic models are extremely prone to ground vibrations.

As an example experiment carried out by Dalgliesh et.al.[33] showed a good correlation between model and full-scale measurement of standard deviation of acceleration for most wind directions. However the scatter found in field data set practical limitations on the accuracy of their prediction.

Therefore, before the wind tunnel results can be reliably applied to structural design methods, there is a need for confirmation by tests on full scale structures.

1.6 FULL SCALE MEASUREMENTS

The dynamic parameters of mass and stiffness associated with a building can be estimated during the design, although doubt arises with the latter owing to the uncertainties surrounding soil-structure interaction at foundation level and the quality of member connections. An even more unpredictable parameter is that of damping inherent in the structure, and this characteristic can be established only after construction is completed.

In order to obtain the simultaneous structural response of a building at different floors to a wind of varying in direction and speed, sophisticated monitoring equipment must be employed. Consequently the length of the cables connecting the monitoring devices to the recorder becomes a problem. Furthermore as the instruments must be stable and maintenance free during long periods of mointoring , the cost of the experiment becomes expensive.

A long term approach to the design of tall buildings for dynamic loading is to establish a pool of information relating to the dynamic characteristics of existing structures of various types of construction, and in a wide range of materials and configurations,

so that a designer could refer to past experience for future guidance.

The present work has been undertaken as part of the long term approach and covers the procedure for obtaining localised wind data, the selection of a suitable structure, an assessment of its characteristics, the instrumentation of the structure, and analysis of the response of the structure to wind excitation.

CHAPTER 2

MEASUREMENT OF NATURAL WIND CHARACTERISTICS

2.1 INTRODUCTION

Currently in the U.K.structural design for wind loading purposes is carried out according to CP3 Chapter 5 Part 2: Sept.1972[6]. This document is based largely on data obtained from the Meteorological Office network of stations measuring mean wind speed and direction at a reference height of 10 m above ground level, and dynamic characteristics of the flow are not given.

Usually detailed information about the wind characteristics for a particular site are unavailable, and such a situation is not peculiar to the U.K. Consequently there is a need to establish a convenient means of measuring strong wind data within the earth's natural wind boundary layer both in open virgin locations and more congested urban sites.

The key to the problem lies mainly in the methods to be adopted for mounting instruments at different levels in good vertical alignment without the supporting structure unduly influencing the wind flow around the instruments.

Various approaches to the question of instantaneous measurement at different heights including the use of existing tall structures, portable mast, balloons, helicopters, and kites were considered. Detailed studies of these methods highlighted the advantages of the kite system over all the other systems.

This chapter outlines the kite based instrument lifting system approach to the problem. Choice of instruments, mountings,

transfer of data to the ground, recording and reduction of data are also discussed.

2.2 HISTORY AND DEVELOPMENT OF THE KITE

Even though its origin is obscure, it is generally accepted that the kite was first invented in China long before the beginning of written history. Many theories have been put forward as to the original inspiration of the kite, while all theories must remain speculative, as Chinese influence grew, kites along with many other cultural artefacts, were introduced into neighbouring countries.

From China,via Indo-China, the kite soon appeared throughout Japan, and subsequently spread to the Pacific. Appearing in various forms in Korea, Burma, through Indonesia, Melanesia and Polynesia, and New Zealand to the Easter Islands, acquiring even greater religious and ceremonial significance on the route. Carried by land, kites travelled across Southern Asia into Arabia possibly 1500 years ago[34]. The dispersionist view has it that it was then a short step to Europe.

The use of the kite as an adjunct to meteorological experiment was first extensively developed by the British meteorologist E.D.Archibald in 1833. He succeeded in lifting anemometers on kites, measuring wind speeds at various altitudes. However the first recorded scientific application of the kite was in a form of a meteorological experiment conducted by Alexander Wilson, at Camlachie, Scotland in 1749. Wilson measured the variation of temperature at different altitudes by raising thermometers on six kites flying in tandem to a height of 915 m. This experiment was the first of its kind to fly kites in tandem[35].

After the development of the Hargrave box kite, H.Wise succeeded in lifting himself in 1897. This was achieved by use of two separate trains of box kites. Each tandem consisted of a pilot box kite and a much larger lifter kite. The two flying trains were gathered at a point at which a pulley was attached. Through this pulley a line supporting a boatswain's chair was passed. On this apparatus Wise duly ascended to a height of 12 m.

Samuel Franklin Cody patented a winged variation of Hargrave's double cell box kite in 1901 which was a man lifter system. During 1907 he gave a demonstration of an instrument developed by the Meteorological Office, the meteorograph, capable of registering height, humidity, temperature and wind velocity. On one occasion he lifted the instrument to a height of 4268 m.

Considering the pace at which aviation technology accelerated into the second decade of the twentieth century, it seems hardly surprising that the kite was virtually forgotten for a period of thirty years or so. Apart from isolated military, meteorological and advertising applications during and between the two World Wars it was neglected by all except children. It was only in the mid fifties, through the work of Francis Rogallo of the National Aeronautical and Space Administration that the simple kite was once again reinstated as a potentially important tool of science. Rogallo worked towards the total elimination of rigid spars. Via a series of wings of cellular configuration using inflatable spars his experiments led to the invention of the limp wing, a totally unsupported sail area, capable of holding its shape solely by means of the distribution of the air load on the kite surface, counterbalanced by the tension of the shroud lines. In effect the

shroud lines form the central spine or keel of the kite, without recourse to rigid supports, the keel deflecting the wind into the supporting wing areas, giving the kite both form and lift with maximum economy.

William M.Allison patented the Allison or Scott sled in 1950. The concept of this kite was based on a semi-rigid canopy kite, supported only in its longitudinal plane, relying upon the wind to give lateral support to the structure by holding its canopy open.

The most recent innovation in the history of the kite is the parafoil, a totally original concept in kite design invented by D.C.Jalbert. His use of multi-cellular surfaces fitted with a double keel for increased manoeuvrability and stability reduced the spillage of air considerably and retained a greater volume of air than the conventional parachute.

The parafoil is the lightest, most efficient and economical non mechanised lifting surface yet devised, employing the principle known as ram-air inflation[35].

A further refinement of this basic idea was the inclusion of an automatic ventilator or flutter valve, sewn into the face of the centre cells. The use of this device, however, increased the drag coefficient of the parafoil. The valve ensures that the pressure within the cells is never great enough to distort their shape. The flutter valve principle was further extended in the parashed - a close relative of the parafoil - which also incorporates the valve into the leading edge intakes of the wing, ensuring that, in the event of a drop in wind velocity, the pressure within the cell is retained, thus preventing the kite from losing its essential form.

2.3 INSTRUMENTS AND INSTRUMENT STATION

2.3.1 Instruments

In order to produce a profile of natural wind speed with a certain degree of confidence, it was decided that three points at a staged height of 50 m below the bridle of the lifting kite would be sufficient. Hence the height above the ground level could be adjusted by raising or lowering the system, Figure 2.1.

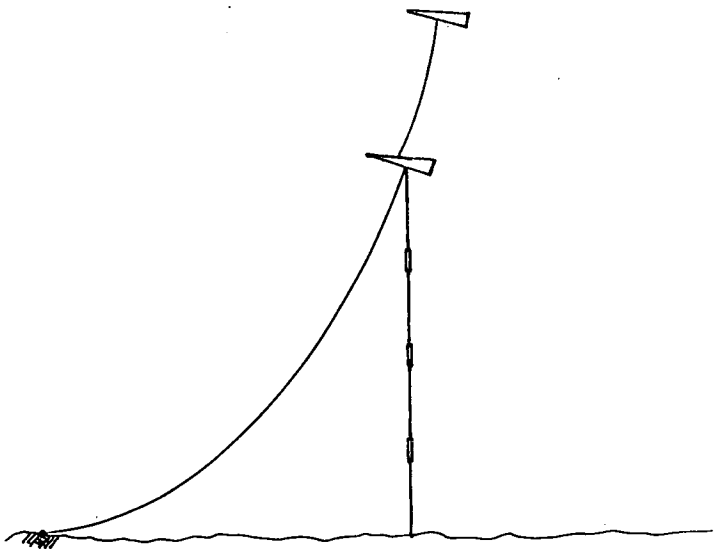

Figure 2.1 Configuration of anemometer stations in space

The instrument selected for the monitoring of wind speed was a VA-320 J-Tech wind speed and direction sensor. This device combined the technique of vortex counting for speed with several alternatives for direction measurement. Vortex speed sensing utilised the linear relationship between the frequency of vortex formation in the wake of a stationary rod and the speed of the air moving around it.

Ultrasonic transducers were used to sense the vortex formation and thus speed was sensed without the need for any moving parts.

The speed sensor was mounted high in the tail of a vane which in turn was free to rotate about a vertical axis.

Angular determination was achieved initially by a transducer which sensed the relative position of the vane with respect to the mounting.

The essential specifications of this device were

Speed range	1 to 60 m/s
Speed accuracy	+ 2%F.S. R.M.S.
Power	10 - 24 VDC at 30mA
Weight	3.5 kg
Operating Environment	Temp. $-30^{o}C$ to $70^{o}C$
	Rel.Humidity: 0-100%
	Vibration: MIL-STD-167 Type1
	Shock: 15 g at 0.011 s

In order to utilise the VA-320 anemometer in the kite line, modifications had to be made in the angular determination system, since the mounting was no more held in a fixed position.

The principle described below based on the magnetic compass is an outline of a solution to this problem.

2.3.2 Magnetic compass

The principles of the construction of this device was based upon the use of an encoded magnetic disc being sandwiched between a series of light emitters and detectors.

By arranging the light emitter/detectors on a radial arm attached to the shaft of the wind vane, the relative angle between the wind vane and magnetic north could be measured in the form of an analogue voltage signal. Hence wind direction could be established

to an accuracy dependent upon the code employed. For instance using a 2^8 bit encoder as illustrated in Figure 2.2, the angular measurement would have a resolution of 1.4 degrees of arc +50%.

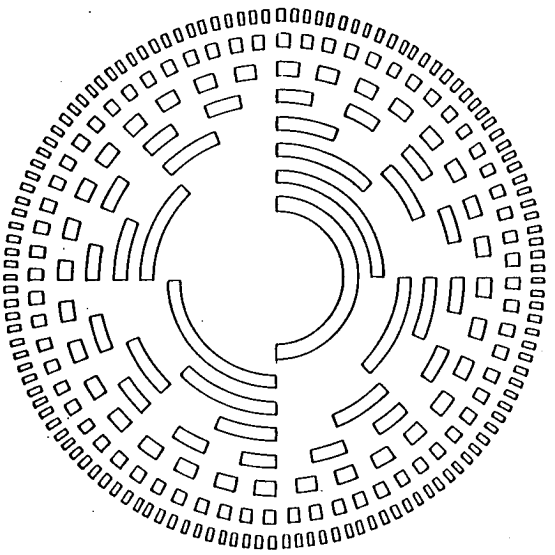

Figure 2.2 A 2^8 bit encoder

2.3.3 Instrument station (Figure 2.3)

Although the ruggedness and lightness of the frame was essential, due to the nature of the magnetic compass it was vital that no ferrous materials be used for the construction of the station. Therefore aluminium was the only suitable material for the construction of the frame.

Each rectangular station was designed for a tension force of 1225 N applied at the centre of each cross member,(i.e.the breaking strength of 2 mm dia. nylon braided line.)

The cross sectional area of this member was calculated to be 34x6 mm with a span of 660 mm.

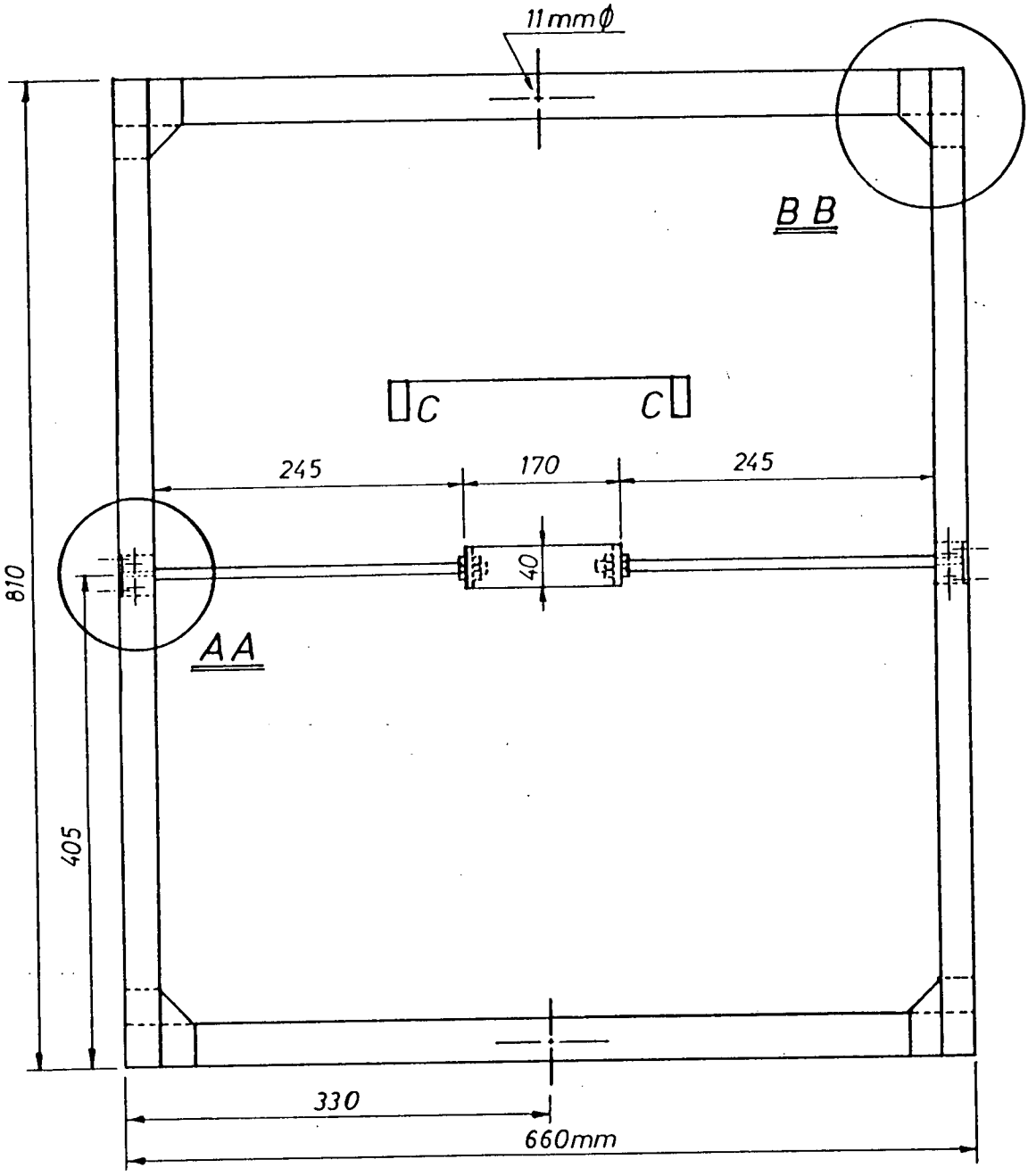

FIGURE 2.3
Aluminium frame for each instrument station

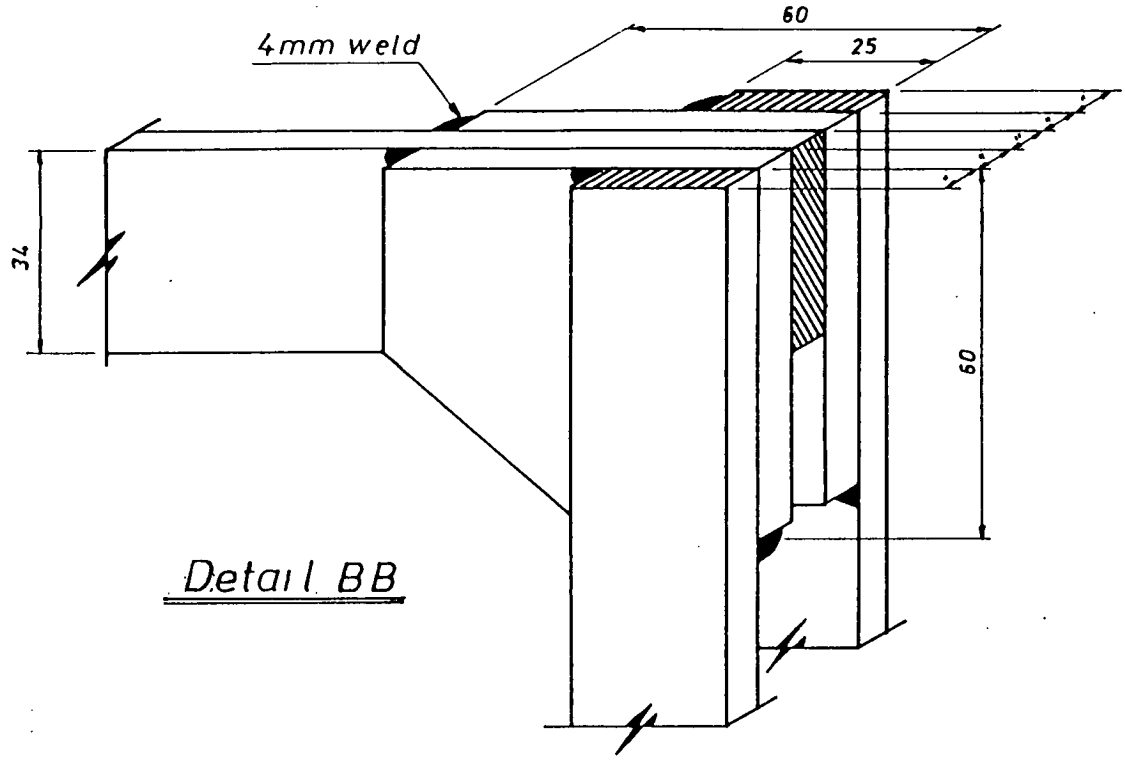

Detail BB

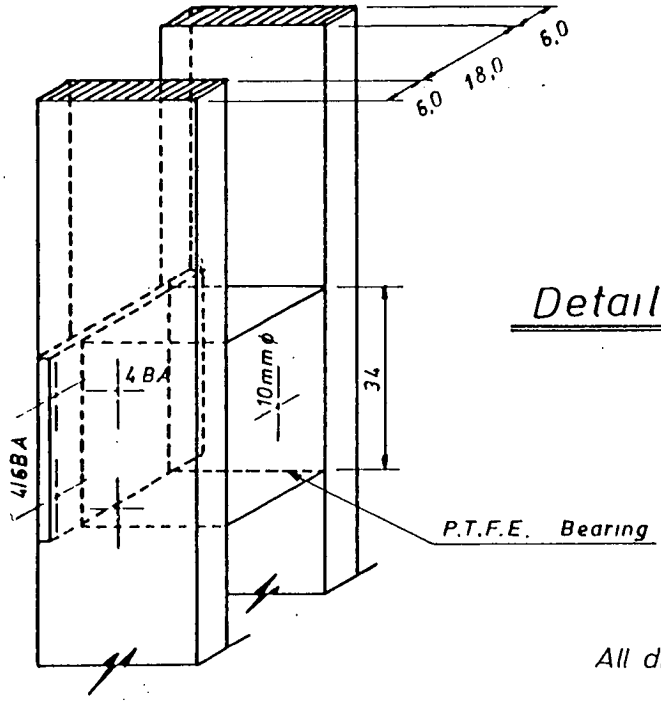

Detail AA

All dimensions in mm

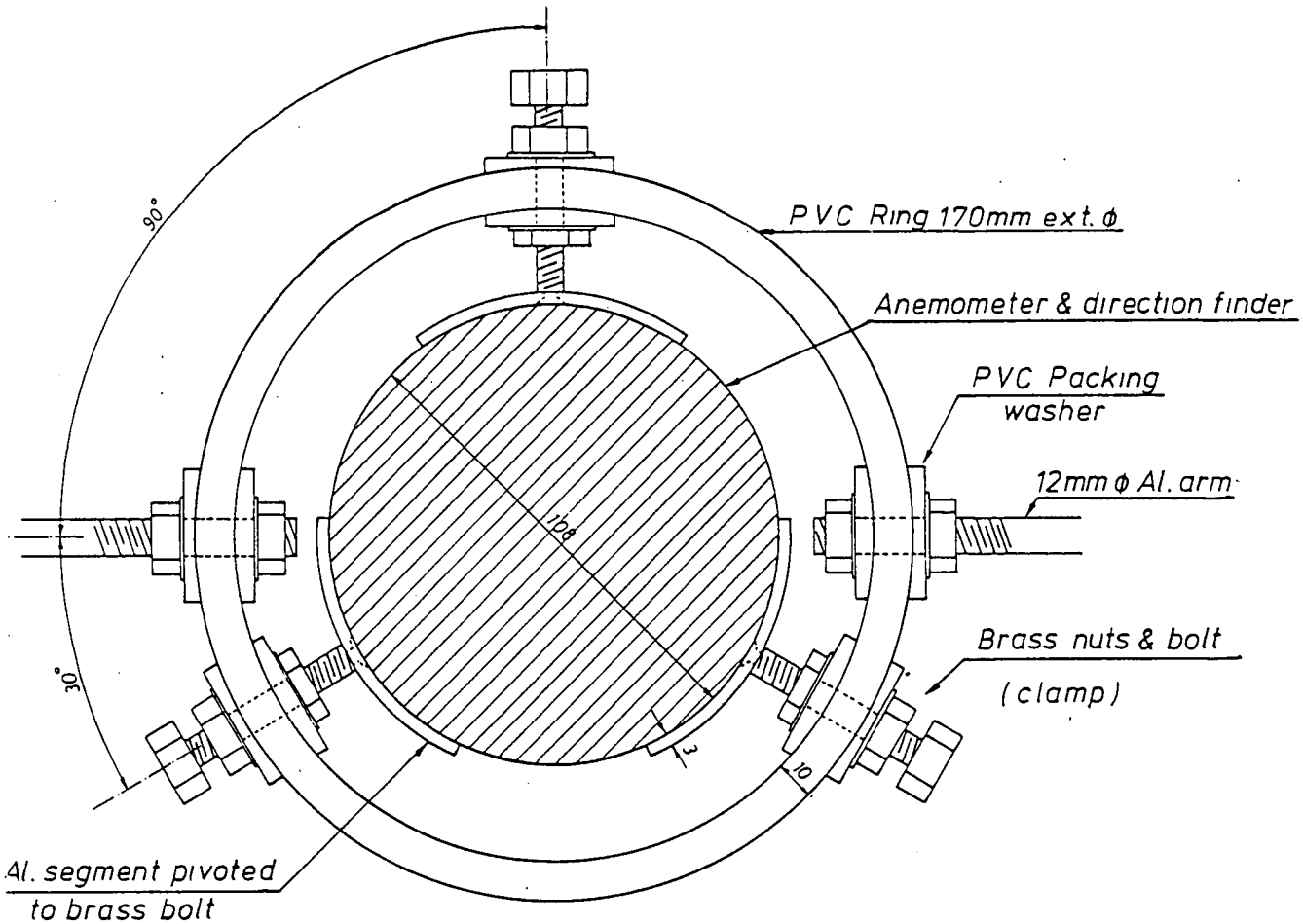
90°
30°
PVC Ring 170mm ext. ϕ
Anemometer & direction finder
PVC Packing
washer
12mm ϕ Al. arm
Brass nuts & bolt
(clamp)
Al. segment pivoted
to brass bolt
168
3
10

Detail CC

The upright of the frame was constructed of two 810 mm lengths of 25x6 mm sections.

The 660 mm wide and 810 mm long dimensions were dictated by the rotation arms of the modified VA-320 anemometer about the horizontal and vertical planes respectively.

To provide stiffness at the joints, two 6 mm thick gusset plates were welded to one side of each upright,(Detail BB). Thus the cross member was welded between the gusset plates. These plates ensured enough space between the two uprights to accommodate a bearing block for the suspension arm.

The bearing consisted of a block of 34x18x25 mm of P.T.F.E. which was secured at the mid height of the uprights by four screws. A 10 mm diameter hole was drilled through the block to receive the suspension arm,(Detail AA).

The magnetic compass and its circuitry was encased in an aluminium tube, 106 mm outside diameter (O.D.), a wall thickness of 1.5 mm and a length of 180 mm.

The compass housing and the anemometer were fixed together by means of a circular flange plate and four bolts.

The casing was held rigidly in a 170 mm O.D.,40 mm wide, and 10 mm thick P.V.C. ring by the means of three adjustable clamps set at 120^{o} on the perimeter of the ring,(Detail CC).

Each clamp consisted of a 3 mm thick aluminium circular segment, 65 mm long, pivoted centrally to a 12 mm brass bolt. The adjustment was provided by means of two brass locking nuts.

Each suspension arm was made up of 385 mm long, 12 mm diameter aluminium rods, threaded at one end and reduced to 10 mm at the other. These arms were fixed to the ring by means of two brass

locking nuts.

The reduction in the arm diameter was made so that the arm would not be able to travel through its P.T.F.E. bearing. To ensure this and to provide some lateral stiffness for the two uprights a 30x34x1.5 mm thick aluminium plate was fixed flush to the uprights.

An 11 mm diameter hole was drilled centrally in each cross member and a universal coupling connected the frame to the kite line. This joint ensured easy insertion of the station in the suspended line hanging from the bridle of the lifting kite, and also provided a pivot facility to eliminate twisting effect from the line.

The total weight of each station was 3.356 kg.

2.4 DESIGN OF THE KITE

2.4.1 Basic concepts of kite in flight

A kite is a tethered aircraft in a stalled state. As it is heavier than air, in order to stay aloft the weight of the kite must be counteracted by a upward supporting force. This is produced by positioning the kite surface - by means of the bridle - at a suitable angle to the wind, causing the wind to exert pressure upon it. This angle is known as the angle of attack α .The vertical component of the pressure force caused by flow of the wind over surface of the kite is the lift force.

This force is increased by a force created by the build-up of partial vacuum at the back of the kite in much the same way that an area of low pressure builds up on the top surface of a cambered areofoil in the wind flow. As the aerofoil is dependent upon forward momentum in order to maintain lift, so the kite in its captive state depends upon the resistance of the flying line, or

tether, to provide its momentum[35].

Three main forces are at work on a kite in flight; lift L, gravity G, and drag force C. For the sake of clarity each one of these forces is said to be concentrated upon a single point of balance upon the kite surface. The centre of lift is the point at which the air pressure against the entire surface is concentrated; the centre of gravity is the point where all weight forces of the kite are concentrated, and the centre of drag is the point where all resistant forces exerted by the air upon the kite are concentrated. All three forces are balanced at the centre of pressure, the point where all pressure forces P, may be said to act, Figure 2.4.

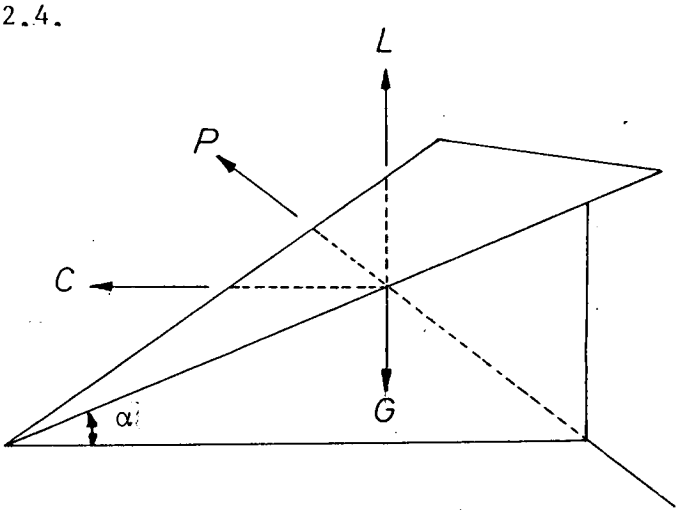

Figure 2.4 Forces acting on the kite

Consequently, if the kite is well balanced structurally, and the bridle is well set for the anticipated angle of attack that the kite is designed to adopt, then a good lift to drag ratio is achieved. A low lift to drag ratio on even the lightest kite will cause it to fly at a low angle to the horizon, whereas a more streamlined surface with a high lift to drag ratio will act through

the wind, climbing steadily along its arc, well up towards its zenith.

Another tool in the hands of the practised designer is the aspect ratio. This is the relationship of span to length of kite. A kite of high aspect ratio is capable of extremely buoyant flight, but it is difficult to stabilise. Conversely, a kite of low aspect ratio, though considerably more stable, has a high sink rate[35].

2.4.2 Choice of kite

After a great deal of deliberation, special attention was finally paid to the kites designed by Squadron leader D.Dunford. The flying machine and the twin keel delta 2500 kites were ultimately selected for trial flights. This selection was made entirely due to the need for a kite with a high lift to drag ratio.

However after several trial flights it was decided that the twin keel delta kite was the most appropriate design for the lifting system due to its higher lift to drag ratio and its low aspect ratio.

This kite consisted of Ripstop Nylon as the sail material and 12.5 mm diameter wooden spar as stiffners. A spine and cross bar opened up the sail and two other spars ensured the stiffness of the leading edges, Fig 2.5.

A twin keel with a 4mm diameter aluminium tube formed the bridle. A 500 mm long cord was suspended from the extremities of the tube to which the control line was attached.

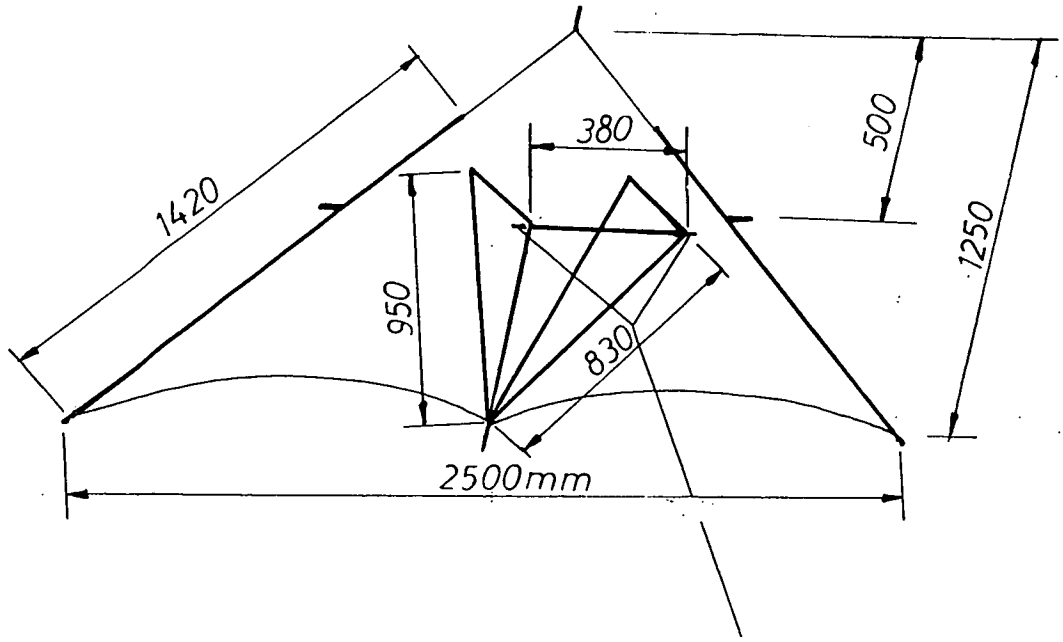

Figure 2.5 Dunford twin keel delta 2500 kite

2.4.3 Design procedure

In order to evaluate the required sail area to provide the necessary lift force (21 kg), the following expression was used

$$L = \tfrac{1}{2}\rho_{air} \cdot C_D \cdot v^2 \cdot A$$

where L is the lift force, ρ_{air} is the air density (1.226 kg/m^3 at 15^{o}C and 760 mm of Hg), C_D is the drag force coefficient, v is the wind velocity, and A is the sail area.

The value of C_D was found at the trial flights to be of the order of 0.02 for the twin keel delta. This value was calculated for the wind speed of 8 m/s at a reference height of 10 m above ground level. The estimated height of the kite was 200m above ground level. The wind velocity at 200 m above the ground level was converted to a wind velocity of 15 m/s at the kite height using the expression

$$\bar{U}(Z) = (\frac{2}{H})^{\alpha}\ \bar{U}(H)$$

where $\bar{U}(z)$ is the hourly mean wind velocity at the reference height

of z, $\overline{U}(H)$ is the mean wind velocity at the height H, and α is the power law exponent of the mean wind speed profile[6]. The value of α was chosen to be 0.22 for suburban terrains.

Assuming the value of C_d is constant for a fixed geometry, hence the sail area A = 21 x 2 / (1.226 x 15^2 x 0.02) = 7.613 m^2

Conclusively it was decided that a kite of 5 m span as the lifting kite and two 2.5 m span kites as pilot kites flown in tandem would provide the necessary lift with a safety factor of 1.23.

2.5 DESIGN OF WINCH (Fig.2.6)

In order to wind in the kite line after the completion of the operation the use of a powered winch was paramount. This equipment was designed for robustness and lightness.

Basically it consisted of a petrol driven motor with variable speed of 1200 to 3600 r.p.m. producing 5 Hp at 1200 r.p.m. The output shaft of the motor was coupled to a worm and wheel gear box with a 10:1 ratio by means of a spider flexible coupling. The output shaft of the gear box was connected to a 400 mm long 100 mm dia. drum by use of two pulleys with a ratio of 2:1 and a friction grip drive belt. (total reduction of the motor speed of 20:1)

A cranked lever attached to a tensioner pulley ensured the correct tension for the full drive and consequently acted as a clutch mechanisim for the engagement of the gear box to the drum.

The maximum capacity of the drum was designed for 2000 m of 2 mm diameter braided nylon line with a breaking strength of 1200 N.

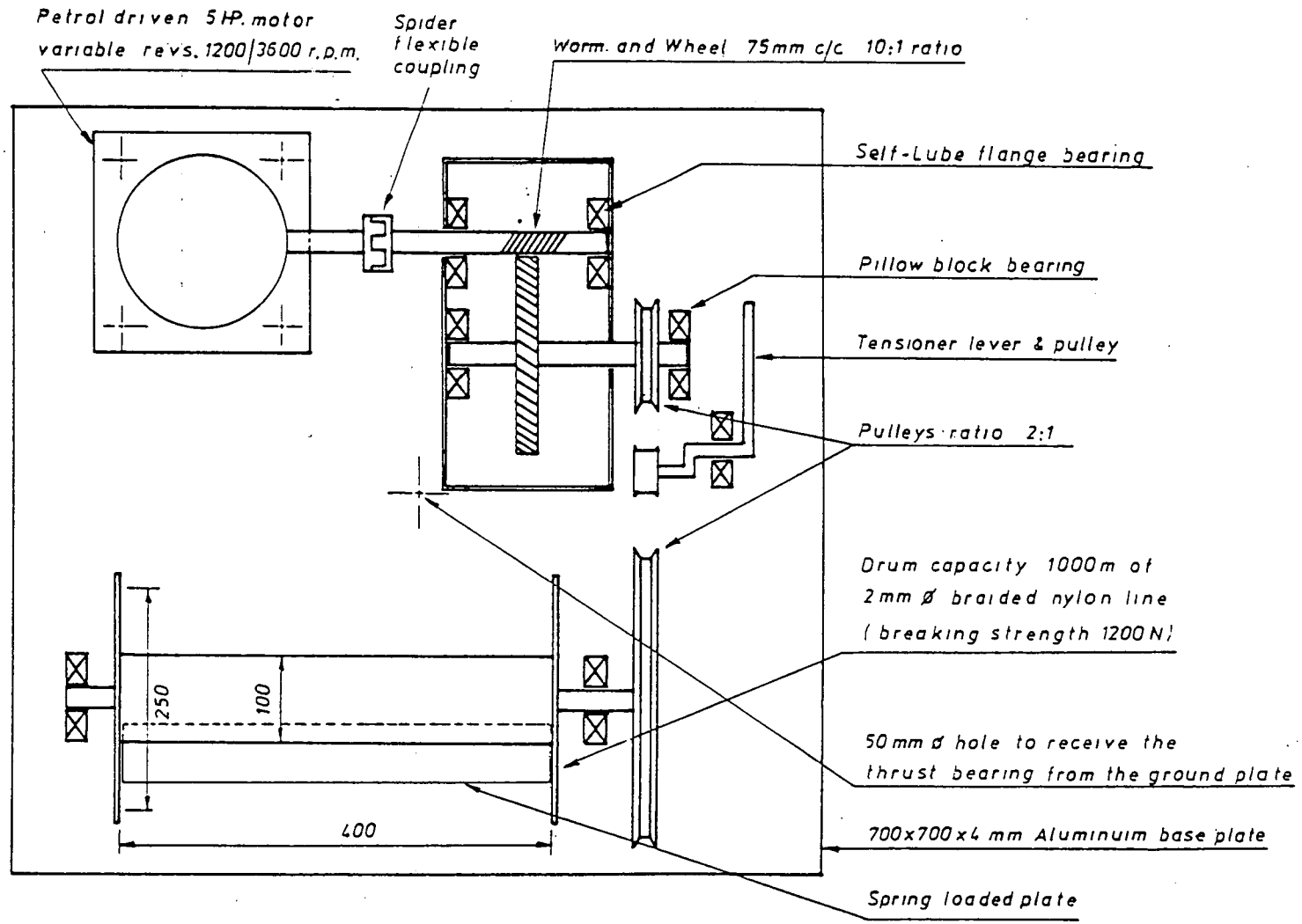

FIGURE 2.6 DESIGN OF A POWERED WINCH

In order to achieve a reasonable time for the a wind-in the required mean drum diameter was calculated to be 200 mm. This ensured a maximum full wind-in time of 27 min. at 2400 r.p.m.

A 400 mm long spring loaded plate was arranged to be in contact with the drum at all times, to prevent the over lapping of the line when wound on to the drum.

The winch was mounted upon a 700x700x4 mm aluminium base plate which in turn was pivoted on a ground plate by means of a trust bearing to allow rotation relative to the kites. The ground plate dimensions were 400x400x4 mm and was secured to ground by 4 steel pegs.

2.6 WIND DATA COLLECTION

there were two possible ways of transfering the voltage signals from an anemometer station suspended in space to a ground level recording station -(i) by means of a direct cable link, and (ii) by telemetry.

The first method was considered carefully but rejected because of the damage to the cable caused by the twisting of the kite line, the restraint that the cable would apply to the rotational freedom of an instrument station, and the additional pay load involved with any direct link.

The second method envisaged the use of telemetry with a two channel high frequency transmitter at each instrument station beaming the signals down to a ground level receiver from which the demodulated signals would be passed by direct lines to a multi-channel F.M. tape recorder. The distance over which the radio transmission was to take place was no more than two

kilometres and although some loss of quality in the signals might occur in comparison with those along a direct line it was felt that the data would be more than adequate for the analysis of spectral content, establishment of velocity and turbulence profiles and cross correlations between points in space regarding wind speed and direction.

CHAPTER 3

JOHN RUSSEL COURT BUILDING

3.1 INTRODUCTION

By courtesy of the City and Royal burgh of Edinburgh,the University of Edinburgh was granted permission to monitor the dynamic response of John Russel Court (JRC). This building is one of two 20 storey residential blocks in Couper Street,Leith , sited in the triangular area bounded by Commercial Street, Coburg Street and N.Junction Street, Figure 3.1.

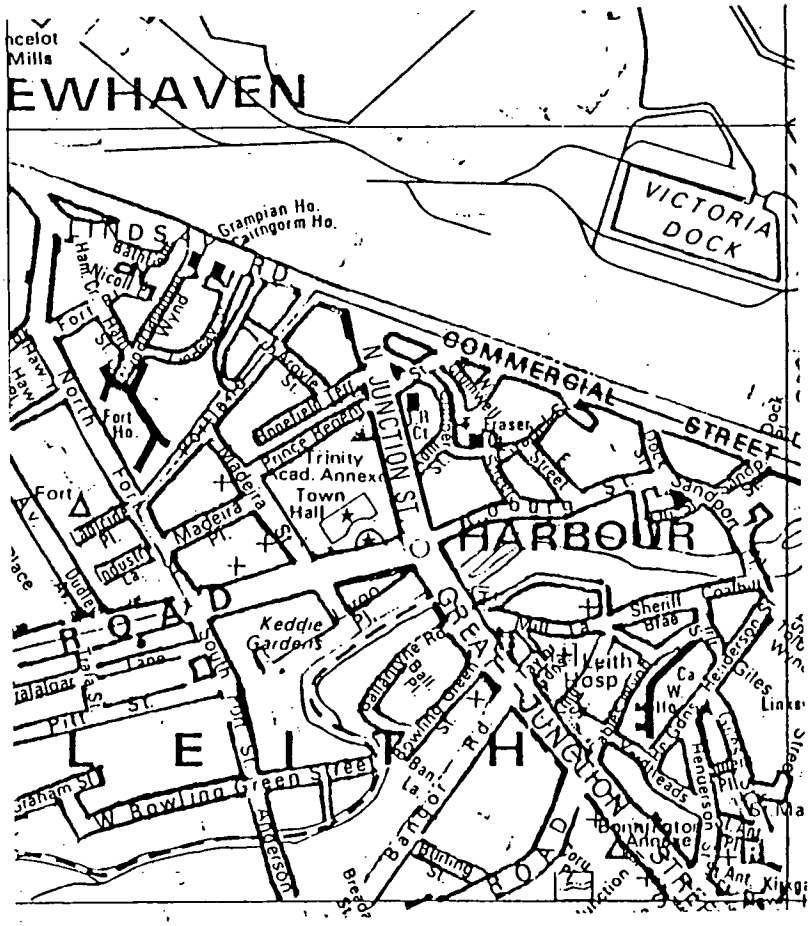

Figure 3.1 Location of John Russel Court

Plate 3.1 John Russel Court Building.

John Russel Court and Thomas Fraser Court were designed by Blyth and Blyth, consulting civil and structural engineers, Edinburgh, and built in 1961-62.

The building was designed as a reinforced concrete frame, with stair wells and lift shafts providing a central core also of reinforced concrete. Although the structural elements are beams, columns and floor slabs, the frames are infilled with a double leaf of 100mm lightweight concrete frames internally, and with precast concrete cladding panels externally.

The foundation of this building consists of 39 bored and reamed cast in-situ concrete piles of approximately 1.0 m diameter, designed to carry 350 tonnes, on which a raft system of large r.c.strip footings and inter connecting ground beams (main footing being 1.22 m thick) were constructed. The average depth of each pile being 7.8 m in a general substrata of a boulder clay[36]. It was assumed that any rotation of foundation under lateral loading of the superstructure would be negligible.

3.2.DETAILS AND DRAWINGS OF JRC BUILDING

Copies of drawing numbers
2513/60/2C dated Dec.1960,
2513/60/3C dated Jan.1961, and
2513/60/5C dated Dec.1960
are reproduced at the back of this thesis.

3.3 NATURAL CIRCULAR FREQUENCY

3.3.1 Choice of method

The essential physical properties of any linearly elastic

structure are its mass, stiffness, damping ratio, natural circular frequency and modal shape.

In order to predict the circular frequency of any structure using analytical or numerical methods it is quite straightforward although tedious, especially without the aid of a computer. The major problem is to employ the correct assumptions on which the theories are based. According to Jeary[37] there can be large discrepancies between predicted and actual natural circular frequency -as much as 100%. These variations are caused by movements in joints including foundations and cracks.

In the past this has been ascribed to a variable interaction with the ground. In recent years,however,it has been shown that different types of foundation exhibit remarkably similar dynamic characteristics[37].

However due to this large deficit between predictions and actual natural circular frequency of buildings, it is evident that, in some cases simple predictors are the most accurate.

Ellis[38] proposed a predictor $f = 46/H$, where f is the first mode natural frequency of free oscillations in Hz, and H is the height of the building in m, with a correlation coefficient of r=0.8828 for 163 rectangular plan buildings studied by BRE.

To examine Jeary and Ellis's conclusions three analytical approaches were applied:

1/ theoretical long hand method;

2/ computer simulation analysis; and

3/ experimental technique;

3.3.2 Theoretical long hand method

Improved Rayleigh method

This theory is based upon equating the potential energy from the work done in deflecting the structure by the inertia forces associated with the assumed deflected shape to the kinetic energy given by the original assumed shape. A better approximation can be obtained by computing the kinetic energy from the calculated shape.For a more detailed version of this theory,the reader is referred to Clough and Penzien[39].

3.3.2.1 Calculation of the mass of JRC

For conciseness of this section, a typical page of calculations for the mass of John Russel Court from appendix 3.1 is presented. Table 3.1 shows the integrated mass of John Russel Court building, which results from appendix 3.1.

TABLE 3.1 Integrated mass of JRC building

FLOOR LEVEL	MASS in kg
20	428E3
19	416E3
18	417E3
17	418E3
16	420E3
15	423E3
14	423E3
13	423E3
12	426E3
11	429E3
10	428E3
9	429E3
8	432E3
7	436E3
6	436E3
5	436E3
4	436E3
3	439E3
2	438E3
1	451E3
TOTAL	8584E3

Description		quantity	rate	mass in kg
floor area 1				
23.60x18.00	424.800			
area of cores cols				
	- 14.519			
area enclosed by cores				
3.72x2.36	- 8.779			
2.60x2.03	- 5.278			
2.03x2.03	- 4.121			
2.87x2.36	- 6.773			
	385.330	385.330 m^2	390.594 kg/m^2	
(210mm plank/pot floor)				
Total cross section area of conc. cores cols.= 17.109 at ht. of 4.763m		81.400 m^2	2400.000 kg/m^3	195576
1/2 of total cross section of conc.cores cols.above first floor = 7.216 at height of 2.591 m		18.80 m^2	2400.000 kg/m^3	45121
Floor finishing		385.330 m^2	195.297 kg/m^2	72254
Allowance for partitions		385.330 m^2	73.236 kg/m^2	28820
Partition walls claddings				
	12773 +			
	5613 +			
	10104 +			
	14840			
	43330			43330
Average beam (floor 9 taken as average)				05705
Superimposed load			195.297 kg/m^2	72205
Total dead load				450714
Total dead load + 1/2 super imp.				487000
Total dead load + super imp.				523000

3.3.2.2 Calculation of the stiffness for JRC

For ease of calculation, the stiffness of each storey is calculated in two parts - the stiffness of columns, and the stiffness of walls in both directions of motion. Let ky be the stiffness of columns about the Y axis (appropriate to motion normal to the Y axis), and kx be the stiffness, of columns about the X axis. Ixx and Iyy are second moments of area about the X and Y axes respectively.

A typical calculation of the stiffness for one storey is shown for illustration purposes, and a complete calculation is shown in appendix 3.2. The results of appendix 3.2 are summarised in Table 3.2a, and Table 3.2b.

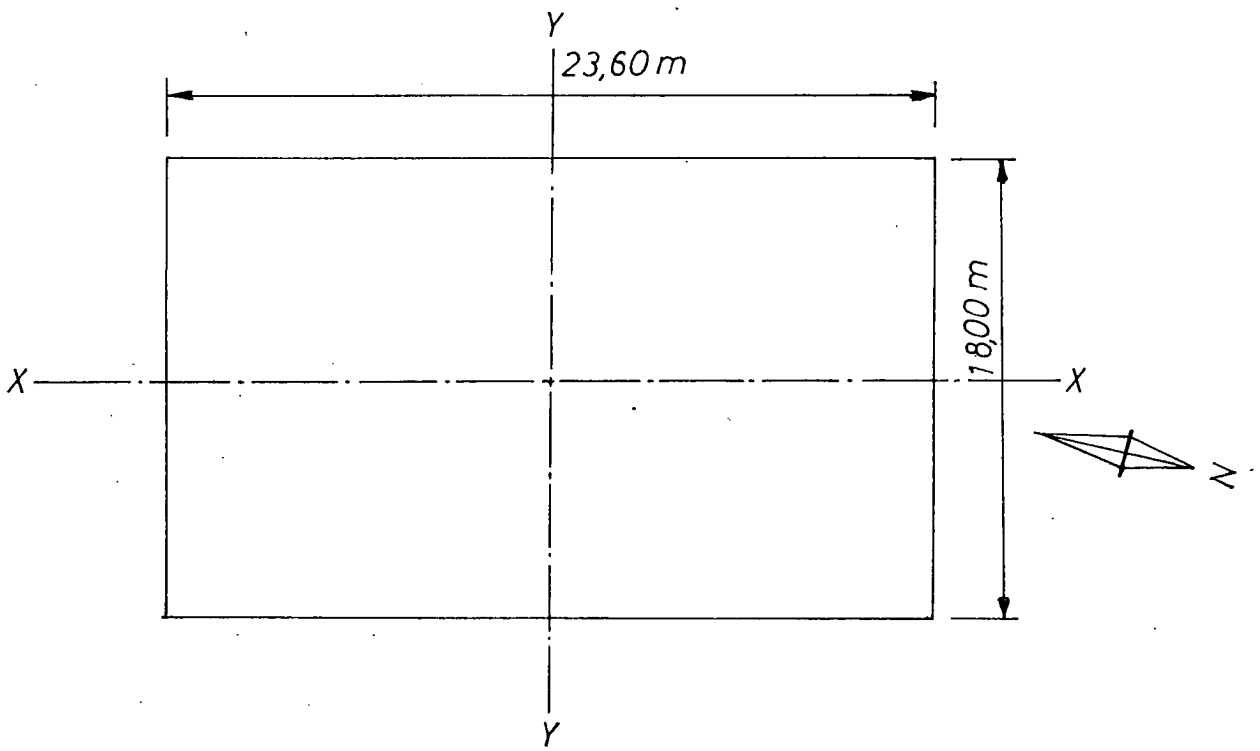

4-5 Level about XX axis			
Ixx gable cols.	$8x(25x99^3)/12$	= 0.162	m^4
Ixx int. cols.	$6x(38x107^3)/12$	= 0.233	m^4
Ixx ext. cols.	$6x(38x99^3)/12$	= 0.184	m^4
TOTAL Ixx cols.		0.579	m^4
Ixx walls	$= 15^3/12\ (478+290+234+478+281+290+234+62+62+478+478)+$	0.009	m^4
	$15/12\ (118^3+20^3+236^3+15^3+203^3 x4+236^3+178^3+15^3+5^3)$	0.838	m^4
TOTAL Ixx walls		0.847	m^4
E conc. walls		21.0E9	N/m^2
E conc. cols.		28.0E9	N/m^2
L cols.		2.591	m
k4 xx cols.	$= 12\ E\ I\ /\ L^3$	1.118E10	N/m
k4 xx walls	$= 12\ E\ I\ /\ L^3$	1.227E10	N/m
TOTAL k4x		2.345E10	N/m

4-5 Level about YY axis

Iyy gable cols.	$8x(99x25^3)/12$	=	0.001	m^4
Iyy int. cols.	$6x(99x38^3)/12$	=	0.003	m^4
Iyy ext. cols.	$6x(107x38^3)/12$	=	0.003	m^4
TOTAL Iyy cols.			0.007	m^4

$$I_{yy\ walls} = 15^3/12\ (236+118+20+15+203x3+236+178+15)+15/12\ (478^3+281^3+478^3+290^3\ x2+234^3\ x2+478^3\ x2+62^3+62^3)$$

TOTAL Iyy walls		6.678	m^4
k4 yy cols	$= 12\ E\ I\ /\ L^3$	0.128E10	N/m
k4 yy walls	$= 12\ E\ I\ /\ L^3$	9.771E10	N/m
TOTAL k4y		9.899E10	N/m

TABLE 3.2a Stiffness of JRC about XX axis

STOREY	kx cols. (N/m)	kx walls (N/m)	kx total (N/m)
G-1	0.312E10	0.357E10	0.669E10
1-2	1.373E10	1.045E10	2.418E10
2-3	1.335E10	1.227E10	2.562E10
3-4	1.118E10	1.184E10	2.519E10
4-5	1.118E10	1.227E10	2.345E10
5-6	1.118E10	1.045E10	2.163E10
6-7	1.118E10	1.227E10	2.345E10
7-8	0.578E10	1.184E10	2.302E10
8-9	0.578E10	1.227E10	1.805E10
9-10	0.578E10	1.045E10	1.623E10
10-11	0.578E10	1.227E10	1.805E10
11-12	0.317E10	1.184E10	1.762E10
12-13	0.317E10	1.227E10	1.544E10
13-14	0.317E10	1.045E10	1.362E10
14-15	0.317E10	1.227E10	1.544E10
15-16	0.151E10	1.184E10	1.501E10
16-17	0.151E10	1.227E10	1.378E10
17-18	0.151E10	1.045E10	1.196E10
18-19	0.151E10	1.227E10	1.378E10
19-20	0.085E10	1.181E10	1.266E10

TABLE 3.2b Stiffness of JRC about YY axis

STOREY	ky cols. (N/m)	ky walls (N/m)	ky total (N/m)
G-1	0.038E10	1.233E10	1.271E10
1-2	0.155E10	8.723E10	8.878E10
2-3	0.135E10	9.776E10	9.911E10
3-4	0.135E10	8.519E10	8.654E10
4-5	0.135E10	9.771E10	9.899E10
5-6	0.128E10	8.723E10	8.851E10
6-7	0.128E10	9.675E10	9.803E10
7-8	0.128E10	8.519E10	8.648E10
8-9	0.104E10	9.675E10	9.779E10
9-10	0.104E10	8.723E10	8 827E10
10-11	0.104E10	9.675E10	9.779E10
11-12	0.104E10	8.517E10	8.621E10
12-13	0.085E10	9.675E10	9.760E10
13-14	0.085E10	8.723E10	8.808E10
14-15	0.085E10	9.675E10	9.760E10
15-16	0.085E10	8.519E10	8.604E10
16-17	0.068E10	9.675E10	9.743E10
17-18	0.068E10	8.723E10	8.791E10
18-19	0.068E10	9.675E10	9.743E10
19-20	0.052E10	8.099E10	8.151E10

3.3.2.3 Calculation of natural circular frequency

This is achieved using the improved Rayleigh method as outlined by Clough and Penzien[39].

about XX axis

The mass of JRC frame was assumed as lumped in the floors, with values as shown in Table 3.1. Also, the floors were assumed to be rigid, so that the columns in each storey act as simple lateral springs with stiffness coefficients about the XX direction as indicated in Table 3.2a.

For an initial deflected shape of $v_i^{\circ} = d^{\circ}\psi_i^{\circ} \sin \omega t$ the initial loads are $m_i \ddot{v}_i^{\circ}$, and the maximum values of which are,

$$p_i^{\circ} = m_i \omega^2 d^{\circ} \psi_i^{\circ}$$

where m_i is the mass of each storey, ω is the natural circular frequency of the structure and d°, ψ° are deflections amplitude and shape factor of the initial mode shape.

The relative deflections $v_i^1 - v_{i-1}^{\circ}$ resulting from p_i° for this structure are shown in the Table 3.3. These deflections can be calculated since the deformation in each storey is given by the storey shear, p_i°, divided by the stiffness Ki. The actual maximum deflection at a floor level relative to ground is $v_i^1 = \Sigma_{i=1}^{i} v_i^1 - v_{i-1}^1$

The maximum potential energy for this shape is therefore,

$$P.E^1.\ max = \tfrac{1}{2} \Sigma p_i^{\circ} v_i^{\circ}$$

where $v_i^1 = d^1 \psi_i^1$, and $d^1 \psi^1$ are the amplitude and shape factor for the mode shape due to p_i°

Consequently

$$P.E^1\ max = \tfrac{1}{2} \omega^4 d^{\circ} \frac{d^1}{\omega^2} \Sigma m_i \psi_i^{\circ} \psi_i^1$$

For $v_i^o=1$ it can be assumed that $d^o = \psi_i^o=1$, and by letting $Z = d^1/\omega^2$ then,

$$P.E^1_{max} = \tfrac{1}{2}\,\omega^4 Z\,\Sigma\, m_i\psi_i^1$$

The maximum P.E. was calculated in a tabular way and is illustrated in Table 3.4 yielding,

$$P.E^1max = 5943052\ \omega^4 Z/2$$

The maximum K.E. of the system can be represented initially as,

$$K.E^omax = \tfrac{1}{2}\,\Sigma\, m_i\,(v_i^o)^2 = \tfrac{1}{2}\,\Sigma\, m_i\,(\omega d^o\psi_i^o)^2$$

which becomes,

$$K.E^omax = \tfrac{1}{2}\,\omega^2\,\Sigma\, m_i$$

when $v_i^o=1$ and the assumption $d^o=\psi_i^1 = 1$ is made.

Thus from Table 3.3

$$K.E^omax = \tfrac{1}{2}\omega^2\Sigma m_i = \tfrac{1}{2}8584000$$

Equating kinetic energy, K.E., to potential energy,

$$\omega^2 = \frac{1}{Z}\ \ (\ 8584000/5934052\ )\ \text{where } Z = 536.410E\text{-}6$$

Hence,

$$\omega = 16.41\ \text{rads/s}$$

In order to improve the accuracy of this value, K.E.max. was recalculated using the improved shape factor ψ_1^1 as follows,

$$K.E.^{1}_{max} = \tfrac{1}{2}\,\omega^{2}\,(d^{1})^{2}\,\Sigma\, m_i(\psi_i^{1})^{2}$$

$$= \tfrac{1}{2}\,\omega^{6}\,z^{2}\,\Sigma\, m_i(\psi_i^{1})^{2}$$

For convenience, results are shown in Table 3.5 from which

$$K.E.^{1}_{max} = \tfrac{1}{2}\,\omega^{6}\,z^{2}\,4629758$$

and equating K.E.max to P.E.max, yields,

$$\omega^{2} = 1/z\ (5943052/4629758)$$

$$= 15.47 \text{ rads/s}$$

$$\omega = 2.46 \text{ Hz}$$

Similarly it was found that about the YY axis, the natural circular frequency of JRC was 27.73 rads/s , or 4.41 Hz.

LEVEL i	MASS m_i (kg)	STIFFNESS K_i (N/m)	EQUIVALENT SHEAR ABOVE A LEVEL (N)	REL. DEFLECTIONS $v_i - v_{i-1}$ (m)
20	428E3		$428E3\omega^2$	$3.381E-5\omega^2$
		1.266E10		
19	416E3		$844E3\omega^2$	$6.125E-5\omega^2$
		1.378E10		
18	417E3		$1261E3\omega^2$	$10.544E-5\omega^2$
		1.196E10		
17	418E3		$1679E3\omega^2$	$12.184E-5\omega^2$
		1.378E10		
16	420E3		$2099E3\omega^2$	$13.984E-5\omega^2$
		1.501E10		
15	423E3		$2522E3\omega^2$	$16.334E-5\omega^2$
		1.544E10		
14	423E3		$2945E3\omega^2$	$21.623E-5\omega^2$
		1.362E10		
13	423E3		$3368E3\omega^2$	$21.813E-5\omega^2$
		1.544E10		
12	426E3		$3794E3\omega^2$	$21.532E-5\omega^2$
		1.762E10		
11	429E3		$4223E3\omega^2$	$23.396E-5\omega^2$
		1.805E10		
10	428E3		$4651E3\omega^2$	$28.657E-5\omega^2$
		1.623E10		
9	429E3		$5080E3\omega^2$	$28.144E-5\omega^2$
		1.805E10		
8	432E3		$5512E3\omega^2$	$23.944E-5\omega^2$
		2.302E10		
7	436E3		$5948E3\omega^2$	$23.365E-5\omega^2$
		2.345E10		
6	436E3		$6384E3\omega^2$	$29.515E-5\omega^2$
		2.163E10		
5	436E3		$6820E3\omega^2$	$29.083E-5\omega^2$
		2.345E10		
4	436E3		$7256E3\omega^2$	$28.805E-5\omega^2$
		2.519E10		
3	439E3		$7695E3\omega^2$	$30.035E-5\omega^2$
		2.562E10		
2	438E3		$8133E3\omega^2$	$33.635E-5\omega^2$
		2.418E10		
1	451E3		$8584E3\omega^2$	$128.311E-5\omega^2$
		0.669E10		
$\sum_{i}$	m_i =8584E3			

Table 3.3 Mass and stiffness per storey, horizontal shear above a floor level, and resulting relative deflections.

Table 3.4 Calculation of maximum potential energy of improved shape .

Let Z = 536.410E-5

Level i	Displacement relative to ground $v_i - v_o$	Normalised Displacement	$P.E._{max_i}$
20	$536.410E-5w^2$	$Z(1.000)w^2$	$428000w^4 Z^4/2$
19	$533.029E-5w^2$	$Z(0.994)w^2$	$413504w^4 Z^4/2$
18	$526.904E-5w^2$	$Z(0.982)w^2$	$409494w^4 Z^4/2$
17	$516.360E-5w^2$	$Z(0.963)w^2$	$394800w^4 Z^4/2$
16	$504.176E-5w^2$	$Z(0.940)w^2$	$386622w^4 Z^4/2$
15	$490.192E-5w^2$	$Z(0.914)w^2$	$373550w^4 Z^4/2$
14	$473.858E-5w^2$	$Z(0.883)w^2$	$356589w^4 Z^4/2$
13	$452.235E-5w^2$	$Z(0.843)w^2$	$341652w^4 Z^4/2$
12	$430.422E-5w^2$	$Z(0.802)w^2$	$341652w^4 Z^4/2$
11	$408.890E-5w^2$	$Z(0.762)w^2$	$326898w^4 Z^4/2$
10	$385.494E-5w^2$	$Z(0.719)w^2$	$307732w^4 Z^4/2$
9	$356.837E-5w^2$	$Z(0.665)w^2$	$285285w^4 Z^4/2$
8	$328.693E-5w^2$	$Z(0.613)w^2$	$264816w^4 Z^4/2$
7	$304.749E-5w^2$	$Z(0.568)w^2$	$247648w^4 Z^4/2$
6	$279.384E-5w^2$	$Z(0.521)w^2$	$227156w^4 Z^4/2$
5	$249.869E-5w^2$	$Z(0.466)w^2$	$203176w^4 Z^4/2$
4	$220.786E-5w^2$	$Z(0.412)w^2$	$179632w^4 Z^4/2$
3	$191.981E-5w^2$	$Z(0.358)w^2$	$153940w^4 Z^4/2$
2	$161.946E-5w^2$	$Z(0.302)w^2$	$132276w^4 Z^4/2$
1	$128.311E-5w^2$	$Z(0.239)w^2$	$107789w^4 Z^4/2$

$$P.E._{max} = \sum_i P.E._{max_i} = 5943052w^4 Z^4/2$$

Table 3.5 Calculations of the K.E.max using the new shape factor

LEVEL i	New shape factor (ψ_i^1)	$(\psi_i^1)^2$	$m\ (\psi_i^1)^2$
20	1.000	1.000	428000
19	0.994	0.988	411008
18	0.982	0.964	401988
17	0.963	0.927	387486
16	0.940	0.884	371280
15	0.914	0.835	353205
14	0.883	0.780	329940
13	0.843	0.711	300753
12	0.802	0.643	273918
11	0.762	0.581	249249
10	0.719	0.520	222560
9	0.665	0.442	189618
8	0.613	0.376	162432
7	0.568	0.323	140828
6	0.521	0.271	118156
5	0.466	0.217	94612
4	0.412	0.170	74120
3	0.358	0.128	55040
2	0.302	0.091	39858
1	0.239	0.057	25707
		$\Sigma\ m_i (\psi_i^1)^2 =$	4629758

3.3.3 Computer simulation analysis

3.3.3.1 ICES Strudl computer package analysis

Strudl-II provides a broad and integrated set of dynamic analysis capabilities for linear elastic structures undergoing small displacement response.

Virtually any structure that can be analysed statically in Strudl can also be analysed dynamically.

The equations of dynamic equilibrium may be written in matrix form as

$$M\ddot{X} + C\dot{X} + KX = F(t)$$

where M, C and K are the mass, damping and stiffness matrices, respectively and X, $\dot{X}$, and $\ddot{X}$ are the time dependent displacement, velocity, and acceleration vectors respectively. The vector F(t) is the forcing function. It should be noted that the above equation implies viscous damping, (damping proportional to velocity).

There are two ways in which the equations of motion, either generated by Strudl from the structural data, or input directly in matrix form, can be solved. The equation can be directly integrated to obtain the response. This is called a physical analysis. Alternatively, the equations can be transformed to a new coordinate system to yield uncoupled linear equations. This coordinate system is called normal mode analysis. The advantage of this method is that the frequencies and mode shapes of the structure can be obtained. The equation of motion after

transformation to normal coordinates become

$$\ddot{q} + 2 \beta \omega \dot{q} + \omega^2 q = \phi' F (t)$$

where q, $\dot{q}$, and $\ddot{q}$ are the displacements, velocities, and accelerations respectively in normal coordinates, ω is a diagonal matrix containing the modal frequencies of vibration, β is a diagonal matrix containing the proportions of critical damping in each mode, and ϕ is a square matrix which gives the transformation between physical and normal coordinates. The contents of ϕ are the eigenvectors or mode shapes of a structure. The frequencies and mode shapes are for an undamped structure since

1/ the normal mode technique will not work for an arbitrary damping matrix C, and

2/ the uncertainty as to the content of C is very high. Thus to perform a normal mode analysis, the diagonal matrix β from the equation of motion after transformation is input directly since this is known with more certainty from experimental evidence.

3.3.3.2 Results

For an explanation of the format,the reader is referred to ICES Strudl users manual[40].

ICES Strudl analysis of the natural circular frequencies of the JRC building was indentical to the analysis preformed by the PAFEC computer package. To avoid duplication, the reader is referred to the results of the PAFEC analysis which is presented in the appendix 3.3.

From appendix 3.3 the first natural circular frequency of JRC in the XX and YY axes with 1.00% damping ratio,is 2.45 and 4.40 Hz respectively.

3.3.3.3 PAFEC Computer package analysis

Dynamic analysis by the Pafec computer package[41] is based upon the development of the stiffness matrices for one of the most simple kinds of finite elements- that of a beam subjected to flexure.

The finite element method is associated with the strain energy stored in the beam element. The principles involved are explained concisely in appendix 3.3 where a summary of the results of a dynamic analysis of the JRC building are given.

3.3.4 Experimental technique

A forced vibration technique was employed using contra-rotating masses.

The principle of the vibrator was based upon two contra-rotating masses of 5 kg fixed on the perimeter of each of two wheels of diameter 700 mm, powered by an electric motor. Each wheel experiencing a centrifugal force of

$\frac{1}{2} m . a . \omega^2$ Where 2a is the amplitude (diameter of the wheel), ω is the frequency of vibration and m is the eccentric mass. The rotating force of $\frac{1}{2} . m . a . \omega^2$ is resolved into vertical and horizontal components of $\frac{1}{2} m.a.\omega^2 . \cos \omega t$ and $\frac{1}{2} m.a.\omega^2 . \sin \omega t$ respectively. The result of motion is that vertical forces cancel each other and net result of vibrating force of $m.a.\omega^2 . \sin \omega t$ is achieved in the horizontal direction, Figure 3.2.

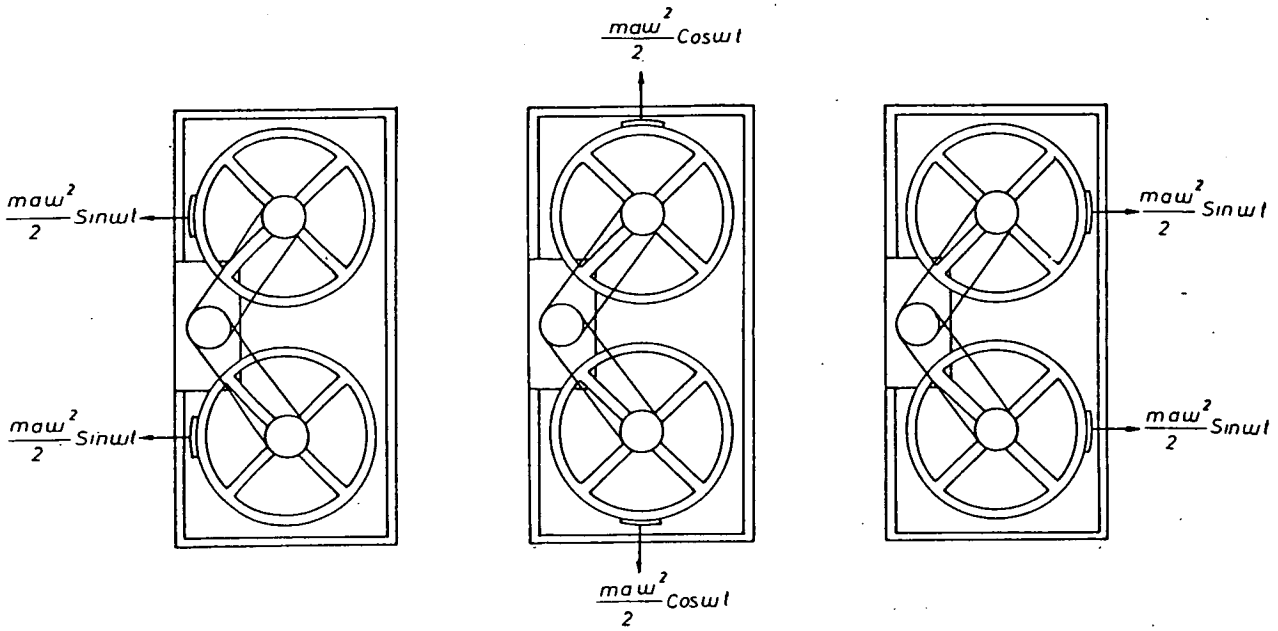

Figure 3.2 Vibrating forces induced by the vibrator

The vibrator was placed at the 19th floor and secured by means of four scaffolding jacks between the larger liftshaft and corridor wall which was supported by the 8th and 9th column. In this case the response of JRC parallel to the X X axis was of interest (Plate 3.2).

The vibrator was then transported to the 17th floor level where it was secured between the two liftshafts by means of 4 scaffolding jacks. Hence the JRC building was excited and responded to forced vibration parallel to the Y axis.

The reason that the vibrator was transported to the 17th floor was due to the unsuitability of the spacing of the structural walls for securing the vibrator for operation about both the XX and YY axes of the building.

The vibrator was driven by a 1.5 h.p. 1500 r.p.m. AC motor and the frequency of vibration was mointored by a frequency counter.

Two Sensonics ANS/1H accelerometers (section 4.5.1) were secured orthogonally and horizontally on a main structural column (Figure 4.3, column 8) as near as possible to the geometric centre in plan and parallel to the axes of the building at the 20th floor level, to monitor the response.

The signals from the accelerometers were fed through a differential stage, low pass filter and amplifier, high pass filter and finally to an F.M. taperecorder (section 5.3) and a Bell and Howell Tungsten Halogen recorder.

Plate 3.2 Position of the vibrator at the 19th floor level

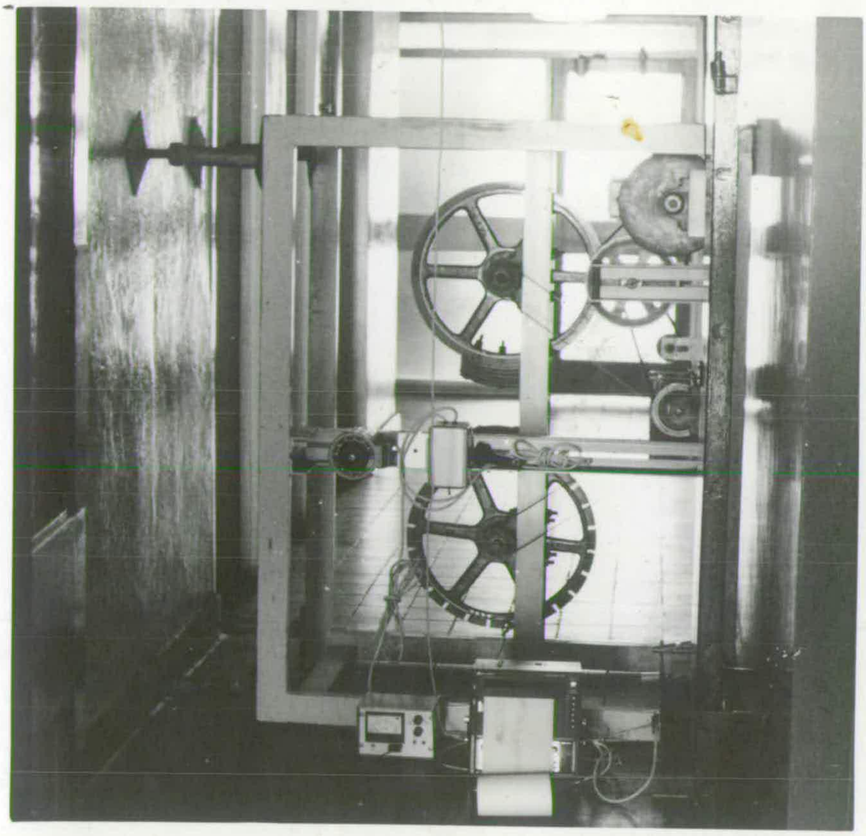

By increasing the frequency of the vibrator gradually, the first natural circular frequency was reached.This was indicated by a resonant response of the two recorders. At this stage the excitation was stopped so that the free oscillation decay curve could be mointored.

3.3.4.1 Results

From the hard copies of the recorder the first natural circular frequency of JRC about XX and YY axis was found to be 1.00 Hz and 1.18 Hz respectively. The corresponding average damping ratio were 1.07% and 0.64%. Typical response characteristic about XX and YY axes are presented in Plate 3.3.

These results were obtained by considering 6 traces about XX axis and 1 trace about YY axis. Table 3.6 and 3.7 illustrates in details the method used to achieve the obtained results and the reduction used. It was based on the following expression,

$$\zeta = \frac{V_n - V_{n+m}}{2\ m\ \pi\ V_{n+m}}$$

where ζ is the damping ratio in per-cents, Vn is the amplitude of response of damped system after n cycles , and Vn+m is the amplitude of response of damped system after n+m cycles.

Table 3.6 Natural Circular Frequency of JRC about XX axis

Trace number	Vn mm	Vm mm	m-n	Damping ratio%	Mean damping ratio %	Frequency Hz
1	56	21	50	0.53	0.65	0.99
	56	31	25	0.51		
	47	23	25	0.66		
	45	19	25	0.90		
2	50	21	25	0.88	0.73	1.03
	50	30	20	0.53		
	47	21	20	0.99		
	48	29	20	0.52		
3	36	12	20	1.59	1.31	1.00
	36	20	10	1.27		
	30	12	15	1.59		
	36	15	15	0.78		
4	50	14	25	1.64	1.48	0.98
	50	20	20	1.19		
	40	14	20	1.48		
	45	15	20	1.59		
5	46	15	25	1.32	1.18	0.99
	46	19	20	1.13		
	38	15	20	1.22		
	38	19	15	1.06		
6	43	15	25	1.19	1.08	1.00
	43	22	20	0.83		
	41	15	20	1.38		
	41	22	15	0.98		
Average					1.07%	1.00Hz

Plate 3.3 Typical response characteristics of JRC

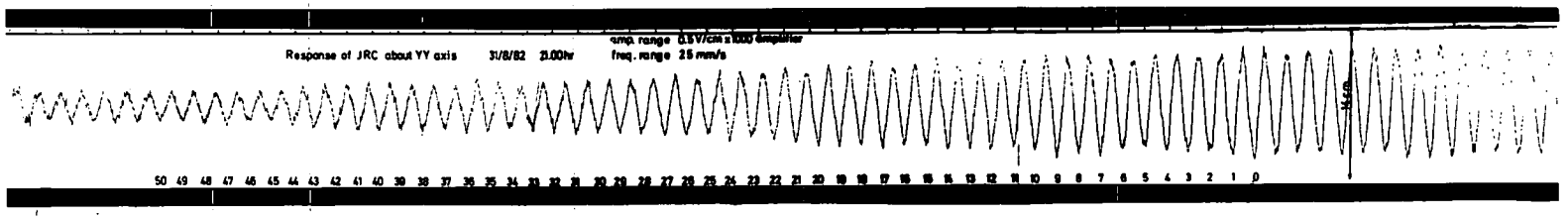
Response of JRC about YY axis 31/8/82 21.00hr
amp. range 0.5 V/cm x 1000 amplifier
freq. range 25 mm/s
50 49 48 47 46 45 44 43 42 41 40 39 38 37 36 35 34 33 32 31 30 29 28 27 26 25 24 23 22 21 20 19 18 17 16 15 14 13 12 11 10 9 8 7 6 5 4 3 2 1 0

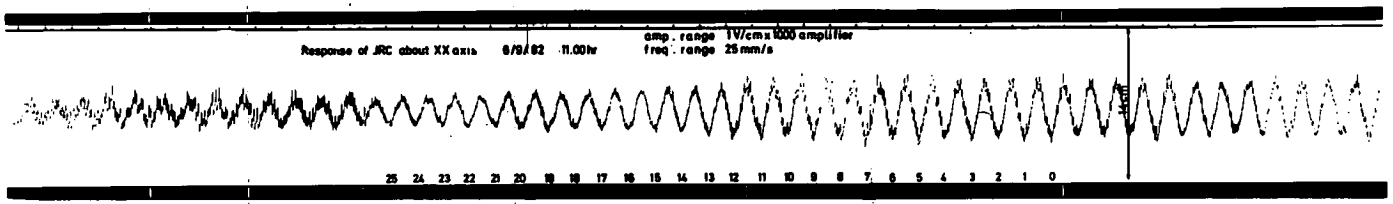
Response of JRC about XX axis 6/9/82 11.00hr
amp. range 1V/cm x 1000 amplifier
freq. range 25 mm/s
25 24 23 22 21 20 19 18 17 16 15 14 13 12 11 10 9 8 7 6 5 4 3 2 1 0

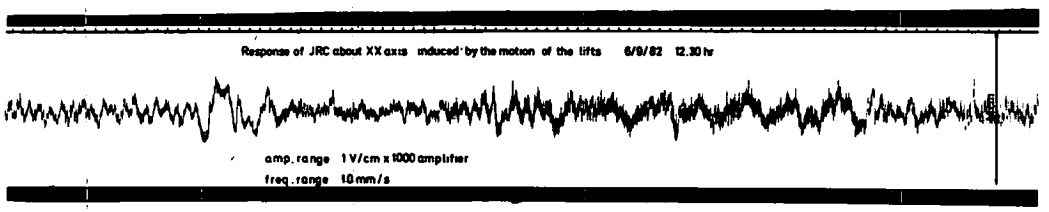
Response of JRC about XX axis induced by the motion of the lifts 6/9/82 12.30 hr
amp. range 1 V/cm x 1000 amplifier
freq. range 10 mm/s

Table 3.7 Natural Circular Frequency of JRC about YY axis

Trace number	Vn mm	Vm mm	m-n	Damping ratio%	Mean damping ratio %	Frequency Hz
1	106	27	50	0.93	0.64	1.18
	106	48	25	0.77		
	89	47	25	0.57		
	75	44	25	0.45		
	48	27	25	0.50		

Table 3.8 Comparison of obtained results of natural circular frequency (Hz)

Method	about XX	about YY
Improved Rayleigh method	2.46	4.41
Strudl	2.45	4.40
Pafec	2.45	4.40
Forced vibration	1.00	1.18
Predictor 46/H	0.85	0.85

3.4 DISCUSSION OF RESULTS

Table 3.8 shows the results for the of natural circular frequency of the JRC building using the improved Rayleigh method, computer package analysis (Strudl and Pafec), and forced vibration technique.

The obtained results show that the computer simulations and the long hand techniques agree closely. They took a similar length of time and effort to obtain.

However the predictor suggested by Ellis[38] ($f = 46/H$) and the forced vibration technique results showed that the discrepancies between these results were of the order of 150% to 370% greater than the measured frequencies depending on the direction of the motion.

A explanation for these large differences could be attributed to the following factors.

1/ Overestimation of the stiffness of the building.

2/ Underestimation of the mass of the building.

3/ Rotation of the building at the foundation level.

4/ Dynamic soil/foundation interaction.

In the cases 3 and 4, Ellis[38] believe that one reasonably can ignore the dynamic soil-structure interaction.

This conclusion was based upon the fact that most tall buildings so far tested show no indication of significant movement at ground level and the large uncertainties in predicting natural frequencies of a rigid based structure are likely to overshadow the effect of soil-structure interaction.

In the first case, the values calculated for the stiffness of each storey height was based on the assumptions that,

1/ The materials were homogeneous.

2/ The central core of the building, shear walls, columns,and floor slabs were interconnected and the overall stiffness of each storey was the accumulation of the stiffnesses of all columns and walls.

3/ Floor slabs do not contribute towards the overall stiffness of each storey.

4/ The deformation of each storey was of the double curvature type, and the stiffness was calculated on the basis of

$$K = 12 E I / L^3$$

Studies carried out on the behaviour of the Sheraton Universal Hotel during the San Fernando earthquake in 1971 by U.S. Department of Commerce[42] throws some light on this subject.

Basically the fundamental frequency changed from a pre-earthquake value of 0.79Hz to 0.45 Hz during the earthquake, and the damping ratio during the earthquake appeared to be about 10% critical, whereas most buildings have a damping ratio between 0.5% and 2.5% for low amplitude motions. Hence it was concluded that these results indicate a loss of stiffness in the structure and can be attributed to damage (or plastic deformation) caused by the earthquake.

Although it is acceptable to believe that some overestimation of the stiffness in the theoretical analysis could occur, but to over estimate the stiffness of the building to the extent that it caused an error of the order of 190% in the calculation of the natural circular frequencies is also unrealistic.

Considering the second case,i.e. under estimation of the mass of the building.

This value was calculated on an accurate quantity survey of the whole of the building, and it is an accumulative figure of the mass of materials used. If the discrepancey between the measured and predicted frequencies were to be attributed entirely to underestimate of the mass, this quantity would have to be increased by a factor of approximately 14. Such a large error seemed unlikely in this case.

Understandably to quantify the error in each case and hence to minimise it, is an enormous time consuming task.

Therefore it can only be concluded that this large and alarming difference between the actual and the theoretical values of natural circular frequency of the building, is due to an accumulation of errors arising from a combination of the factors mentioned earlier.

CHAPTER 4

INSTRUMENTATION

4.1 INTRODUCTION

Measurement of the alongwind dynamic response of the JRC, was made using an instrumentation system which consisted of 7 accelerometers, 7 translational displacement transducers, a cup anemometer, a wind direction finder, a 14 F.M. channel taperecorder, and a modulation/ demodulation system to provide four extra recording channels.

Sangamo N8RT/1.5mm displacement transducers were used to measure the relative displacement of two floors at various levels. Plate 4.1

Sensonic ANS/1H accelerometers were utilised to monitor the dynamic response of the building in the X and Y directions at the same levels. Plate 4.2

Munro mark II cup anemometer and a wind direction finder were used to give a datum point on the wind velocity / height profile.

An EMI SE Labs 3000 tape recorder was employed to record the signals from all the instruments simultaneously during the period of a storm.

Plate 4.1 Sangamo N8RT/1.5 mm displacement transducer

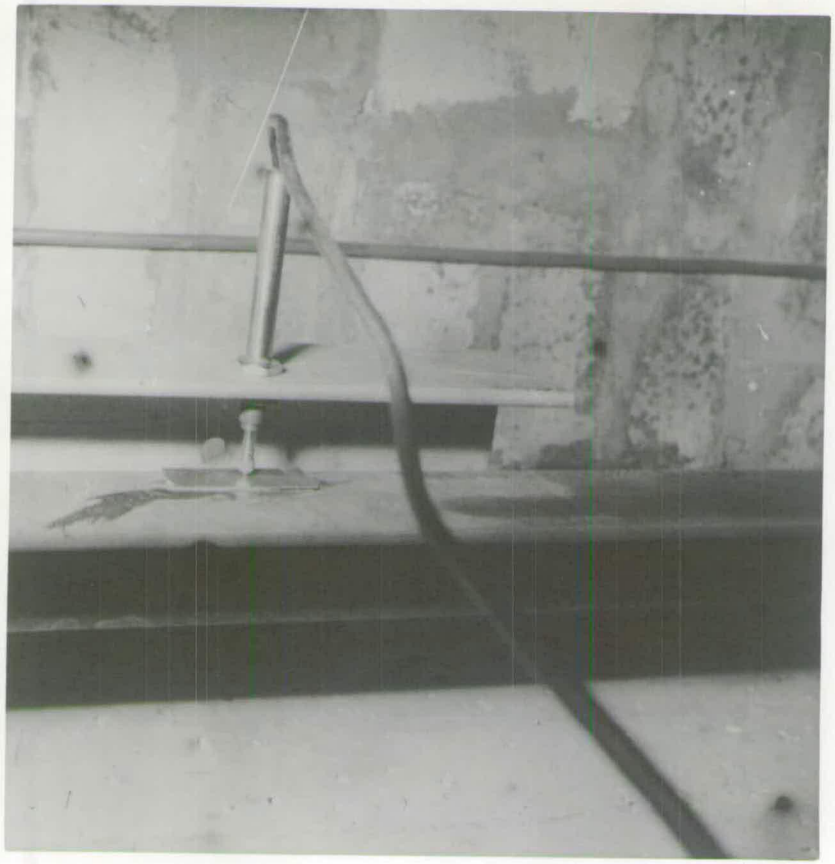

Plate 4.2 Sensonic ANS/1H horizontal accelerometer

4.2 LOCATION OF INSTRUMENTS

It was decided that up to the fourth flexural mode response characteristics of JRC to a horizontal wind force was of a great interest. Therefore the fourth mode of vibrations of a cantilever was considered, and the points of contraflexure were estimated. The points of contraflexure were related to storey heights of JRC and the corresponding levels were calculated to be at ground to 1 , 6 to 7 , 12 to 13 and at the top storey, Figure 4.1.

Three accelerometers were fixed to top floor, one of which was placed at the corner of the building to measure torsional effects, in order that it could be taken into consideration at that level. The other two were fixed as near as possible to the geometrical centre of the plan form to measure the acceleration of the building in the X and Y directions.These accelerometers were placed orthogonally, Figure 4.2.

The remaining 4 accelerometers were fixed at the 13th and 7th floor to measure the response of the building in the X and Y directions at these levels.

Three displacement transducers were fixed between ground and first floor to measure displacments in the X and Y directions,and torsional movements. Dynamic torsion at this level is of the first mode (linear mode shape assumed) , and was measured by one displacement transducer. This transducer was fixed at the most accessible extreme point at this level. The other two orthogonal displacement transducers were fixed as near as possible to the geometrical centre of the plan form.

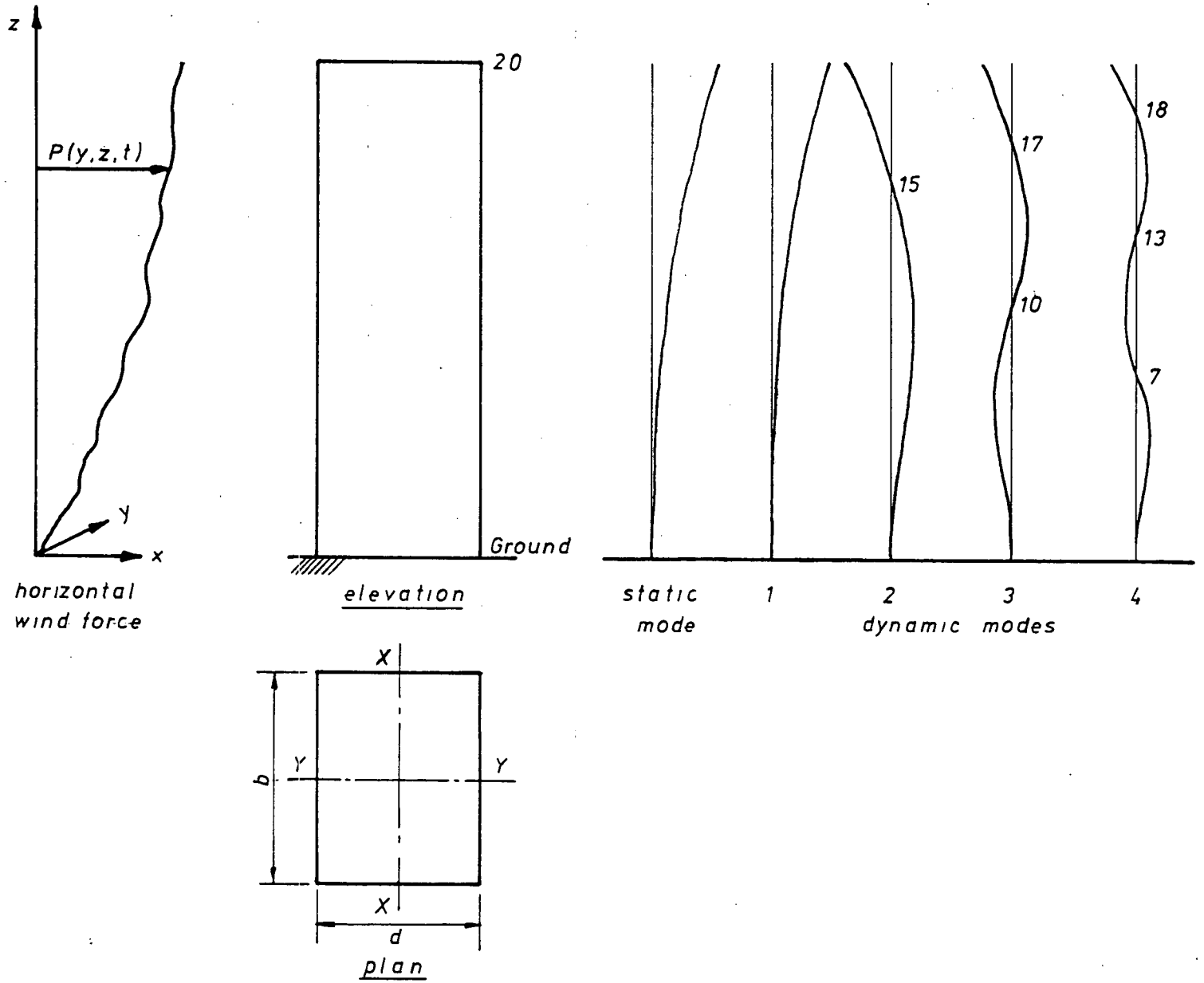

Fig.4.1 Typical flexural response to horizontal wind force

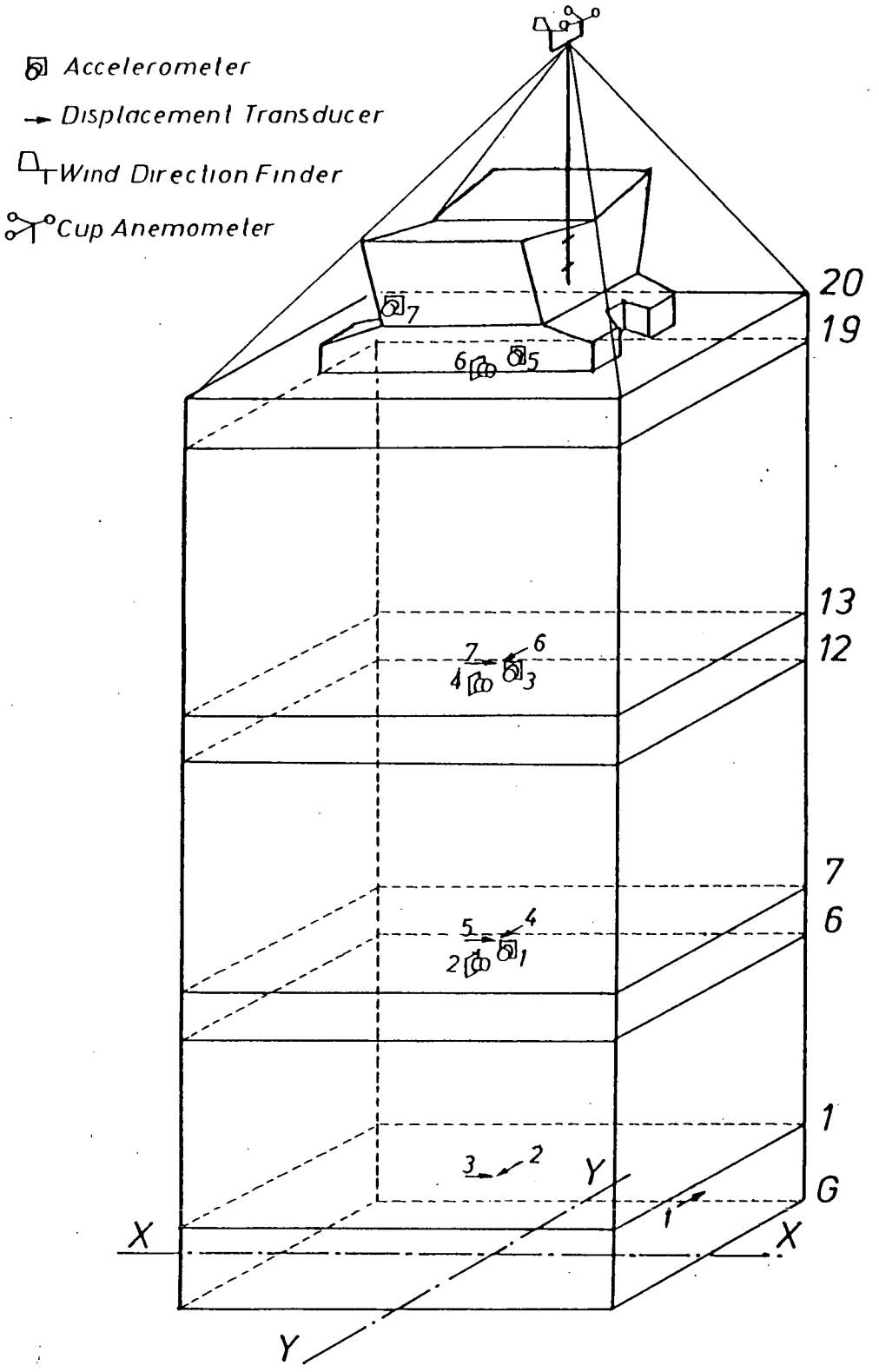

Figure 4.2 Schematic position of transducers

These transducers measured the X and Y movements of first floor relative to the ground floor. The other 4 sets were used at the 6-7th and 12-13th floor to measure the relative movements at these floors in the X and Y directions only.

4.3 CALCULATION OF GEOMETRICAL CENTRE COORDINATES

The position of the geometrical centre was obtained by assuming the first floor level plan as a typical floor plan, see Fig 4.3. The position of geometrical centre of this floor level was assumed not to differ by more than a few millimetres with the other floor levels.

Although the exact position of the geometrical centre of each floor was essential for use in the calculations, this assumption was justified since the availability of space and accessibility to this point was the governing factor.

By considering each wall (staircase and lift shafts) also as columns, taking moments of area about the X and Y axes, the coordinates of the geometrical centre of the first floor level were found to be 11.62m and 9.20m respectively.

For details of this calculation, the reader is referred to appendix 4.1.

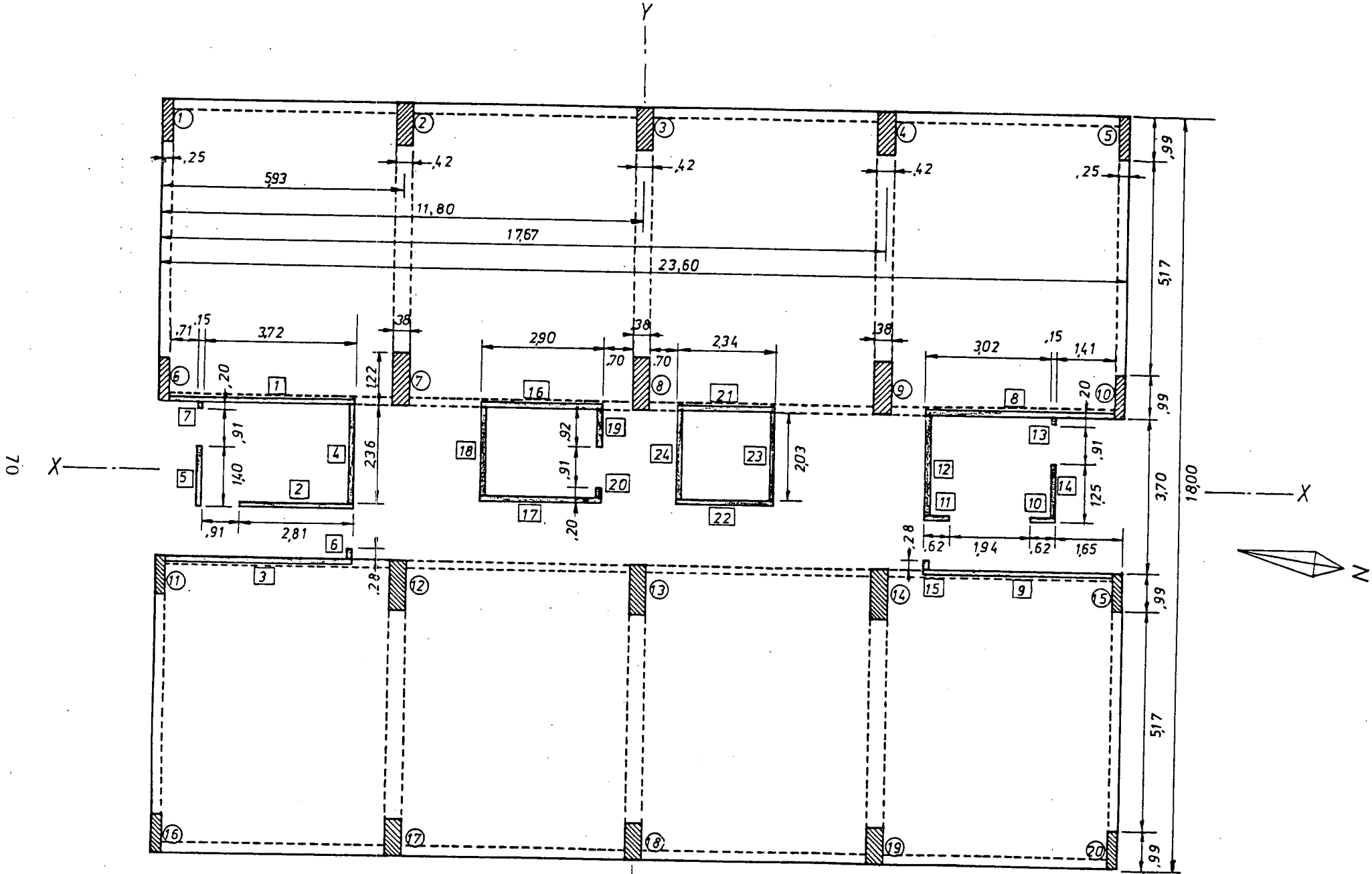

Figure 4.3 Typical floor plan of JRC Building

4.4 DISPLACEMENT TRANSDUCERS AND TRANSDUCER AMPLIFIER

4.4.1 Description

The Sangamo NT9 transducer amplifier is a general purpose analogue signal conditioning unit which was employed for amplifying and detecting the outputs of seven Sangamo linear displacement transducers type N8RT/1.5mm. These gauging transducers had a non-rotating (2^{o} maximum) spring return actuator running in a precision linear ball bearing. This arrangement provided a repeatability of measurement of better than 0.1 micron.

A flexible nitrite rubber gaiter protects the bearing , permitting operation in slurries, cutting oils and most degreasing agents.

Each N8RT was fitted with a 3 mm dia. Tungsten Carbide ball end which was mounted at the end of the actuator.

The total stroke was 3.0 mm with a nominal maximum permitted error of 0.3 per cent of total stroke. Sensitivity was 80.32 mV/V/mm with a load impedance of 1K ohms.

The NT9 transducer amplifier converted the modulated AC transducer signal by means of a synchronous detector and amplifier to give a voltage and current output. The conversion from input to output was linear and in most cases the linearity of the measuring system was determined by the transducer itself. The transducer output could be offset to zero at any point within its internal switch setting. A range control provided 400 to 1 range expansion; full scale output could be obtained from 100 per cent and in six steps down to 0.25 per cent of transducer stroke.The gauge factor control , in conjunction with an internal switch, adjusted the amplifier gain to suit the transducer sensitivity gauge factor

directly. It was calibrated to read in terms of transducer gauge factor directly, and so measurements could be made without external calibration. An internal calibration facility enabled fine gain adjustment to be made to check and compensate for small variations in oscillator voltage and amplifier gain.

4.4.2 Calibration of displacement transducers

Each N8RT transducer was mounted vertically on a stand on a flat table in the laboratory.Each transducer was in turn connected to the amplifier and energised.

By raising the actuator of the N8RT transducer with a slip gauge of known thickness, voltages produced by the transducer were recorded against the slip gauge size. This procedure was carried out over the actuator's full stroke range.

Each N8RT translational transducer was calibrated by the same method under constant laboratory conditions.

The results obtained were tabulated and reduced to a graphical format for each transducer. Hence the sensitivity and linearity of each transducer was determined. Good agreement with the manufacturer's specification was obtained in each case, the linearity being typically 0.1% over the displacement range.

4.4.3 Design of supporting columns.

The inaccessibility of the geometrical centre of each floor imposed practical restrictions with regard to the positioning of the displacement transducers. Due to these restrictions, the design of supports for transducers had to be more carefully considered.

The supports for transducers consisted of two over lapping columns, one was held rigidly to the suffit of the first floor level and suspended towards the ground, and the other column was fixed to the floor level.

The translational transducers were mounted orthogonally on one column through 6 mm diameter holes so that their actuators were touching the other column, Figure 4.4.

This design had to be modified for the 6th and 12th floor levels to incorporate brackets for the accelerometers. In this case the upper column was replaced by a 200 mm length of 203x76x23.6 kg/m channel section. The channel was fixed to the beam joining columns 7, 8, and 9 at ceiling level by one of its flanges, Figure 4.5, and Plate 4.3.

For security reasons at the 6th and 12th floor level the instruments were encased with a Dexion frame work which was held rigidly to the ceiling and smaller lift shaft wall. The side panellings of the enclosure were constructed from 5.0 mm thick chipboard panels.

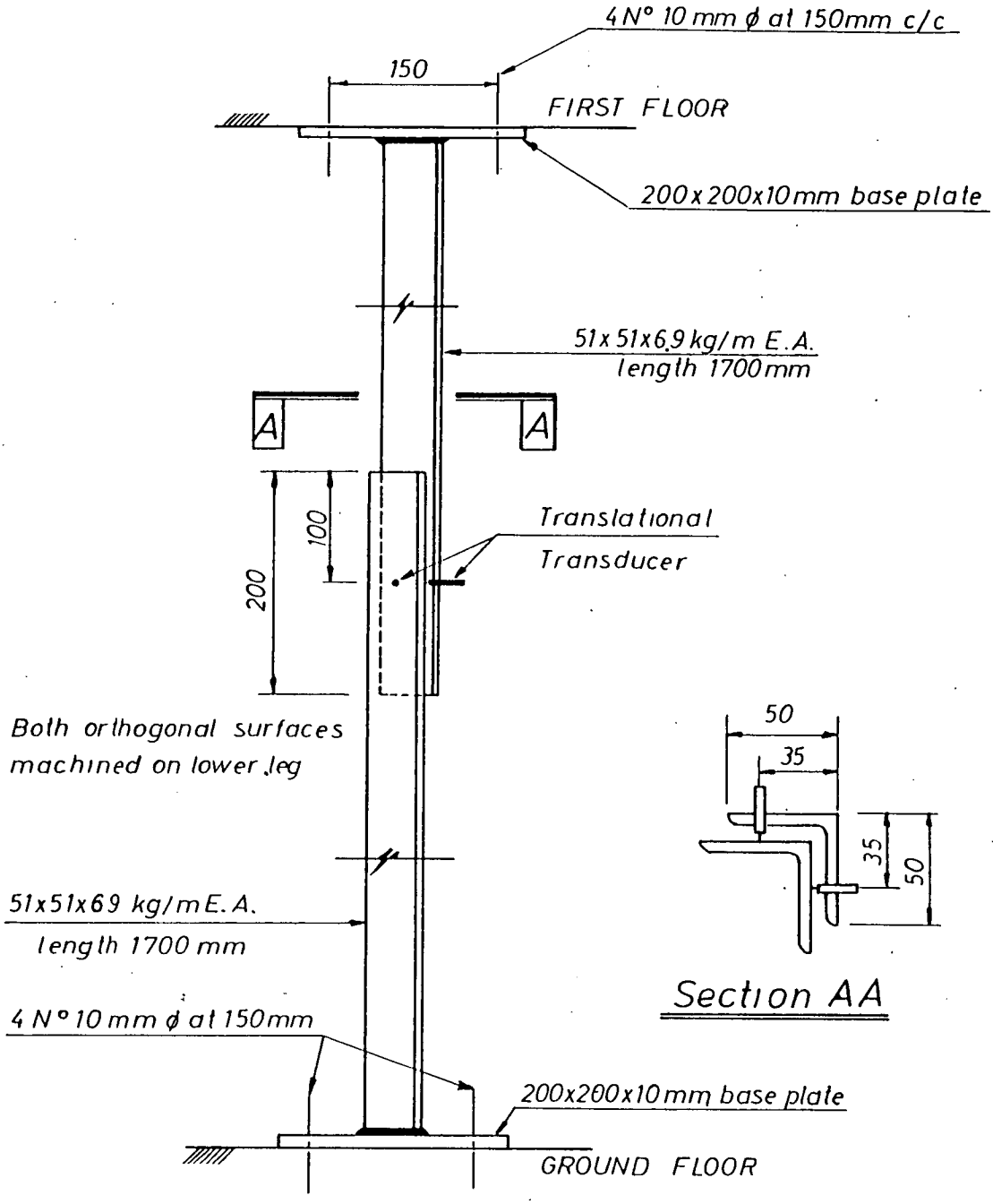

Note

All dimensions in mm

Figure 4.4 Supporting columns for dispt. transducers at ground level

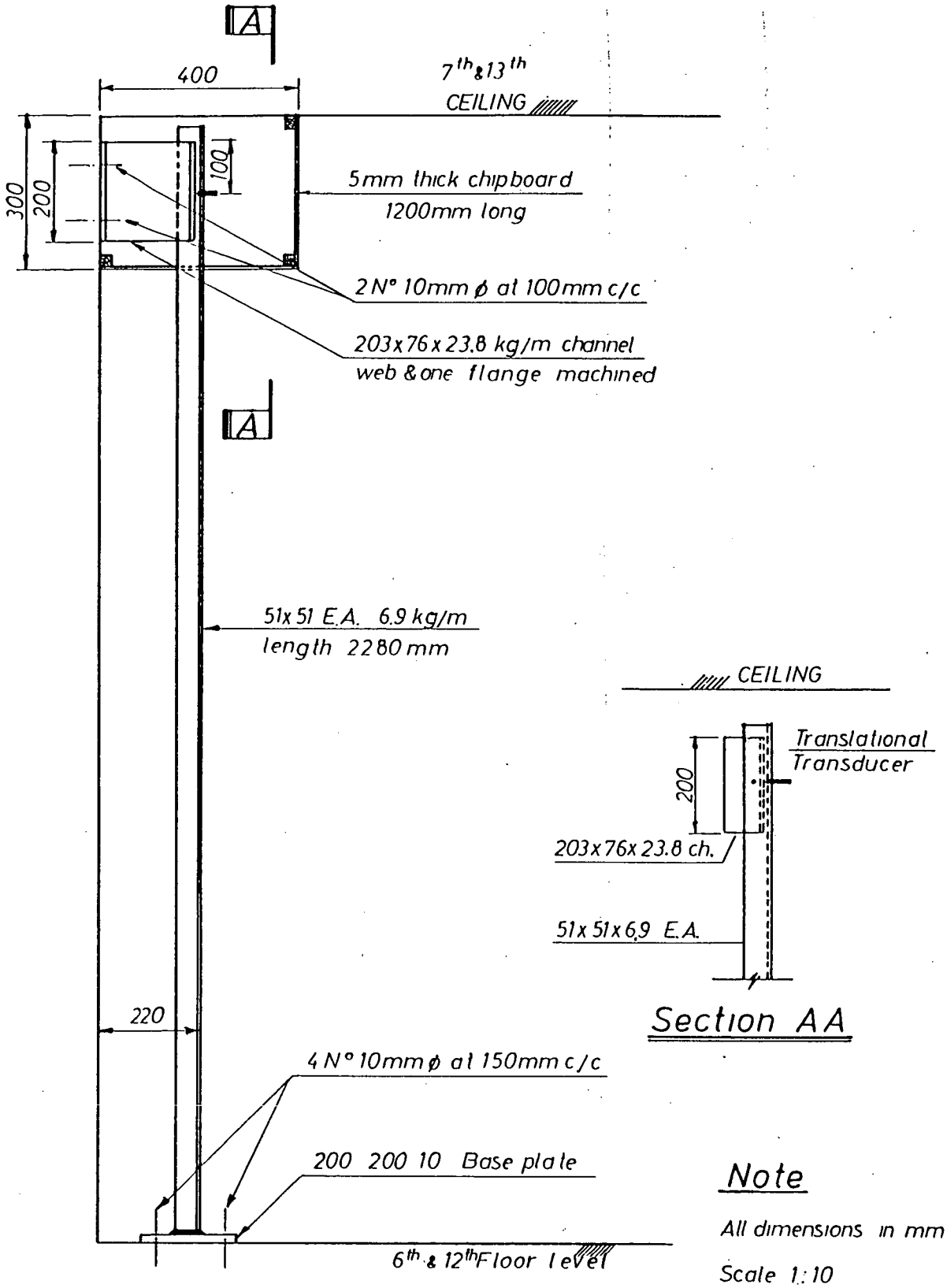

Figure 4.5 Supporting column and channel for displacement transducers at the 6th and 12th floor level

Plate 4.3 Accelerometers and displacement transducers at the 6^{th} floor level

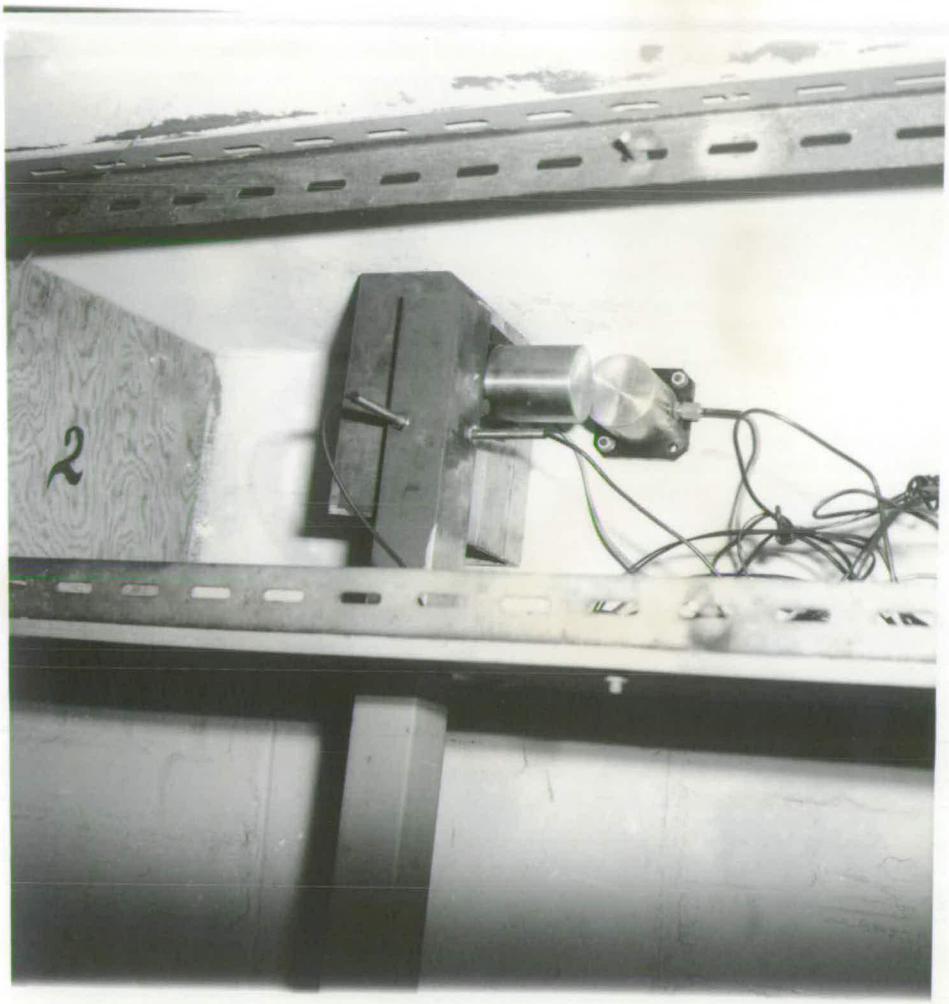
2

4.5 ACCELEROMETERS

4.5.1 Description

The Sensonic ANS/1H accelerometer is a low frequency, low level acceleration sensing device. The acceleration sensing element is an inductive device excited by alternating current (AC) from an integral solid state oscillator. The resulting AC output signal is amplified and demodulated by an electronic unit contained within the transducer body. The filtered DC output signal is directly proportional to the applied acceleration.

The sensitivity of an ANS/1H is of the order of + 10V/g with a resolution of 0.0001g. Frequency ranges between 0 and 40 Hz with frequency response of + 1 db over 0 to 25 Hz. The input supply and current are + 15 VDC (stablised) and + 25 mA maximum respectively.

The physical dimensions of the device are

1/ height of cylinderical body	70.0 mm
2/ diameter of cylinderical body	63.5 mm
3/ base plate dimensions	83x83x9.25 mm
4/ weight	1.05 kg

4.5.2 Calibration of accelerometers

Calibration of each individual accelerometer was carried out before its installation in the JRC building. The procedure consisted of mounting a Bruel and Kjear 4366 standard accelerometer and a Sensonic ANS/1H accelerometer back to back on the probe of an electro-mechanical vibrator.

The Bruel and Kjear 4366 accelerometer was energised through a charge amplifier which was set at 46.2 pc/g to produce 1 volt/g. The output signal was then fed to a Levell AC micro-voltmeter.

The Sensonic accelerometer was energised by a +15 volts DC power supply and the output signal was fed to a Levell transistor AC micrometer.

The vibrator was energised by a Linstead function Generator, G250, and the frequency of vibration was controlled by use of a frequency counter.

4.5.3 Experimental results

The response of the ANS/1H accelerometer was monitored over a range of frequencies between 10 Hz and 50 Hz while the response of the Bruel and Kjear standard accelerometer was kept constant by varying the amplitude of the vibrations at all frequencies.

The test procedure was repeated for each ANS/1H accelerometer. A typical response curve is shown in Fig.4.6 where the response as a proportion of that of the standard accelerometer is presented.

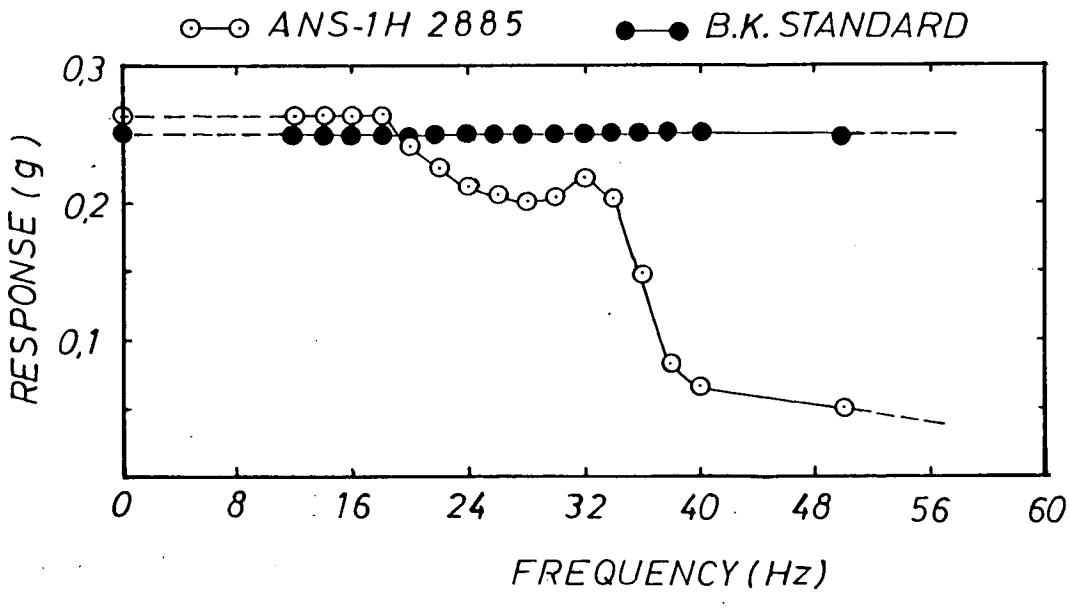

Figure 4.6 Frequency response of an ANS/1H accelerometer

The discontinuity in a response curve was attributable to resonance phenomena. An examination of all seven response curves revealed a peak at approximately 30 Hz. This was consistant with a resonance in the dual accelerometer and mounting bracket system at this frequency. Some slight variation occurred in the shape of the curves at their peaks and these could be explained by the fact that it was difficult to establish exactly the same mounting position on the vibrator for each system.

4.5.4 Design of fixing brackets

Each ANS/1H accelerometer was mounted on a base plate which had 4 fixing holes of 8 mm diameter at 60 mm centre to centre.

At level 20 within the Penthouse, column 8 and the beam running between columns 7, 8,and 9 were exposed. Hence 2 ANS/1H accelerometers were fixed orthogonally to two adjacent faces of column 8.

The method of attachment was by the use of two 6 mm diameter rawlbolts anchored diagonally at a distance of 85 mm centre to centre. By shimming one corner of the base plate of the accelerometer , it was possible to ensure that an accelerometer was horizontal.

At level 7 and 13 the web of the existing 200 mm long channel was utilised for connecting one accelerometer and the other accelerometer was mounted to the beam column connection.

4.6 MUNRO MARK II CUP ANEMOMETER MET.REF.992

4.6.1 Description

The spindle of the cup anemometer carries a 12 pole permanent

magnet rotor whose motion within a wound stator induces an alternating voltage,(approximately proportional to wind speed),in the stator windings. This voltage is sufficient to operate up to six indicators and one recorder, connected in parallel, at distance up to several hundred meters from the head.

No external source of electricity is required. The indicator essentially consists of a metal rectifier, a temperature correcting element, and a moving coil DC voltmeter calibrated directly in wind speed.

The specification of this instrument is summarised below and for more detailed version, the reader is referred to Munro Mark II cup anemometer specification hand book.

Effective velocity range	5-90 knot	(9-160 km/h)
Accuracy from	1/2 knot at 5 knots to 2 knots at 90 knots	
Generator output	approximately 30V per 1000 r.p.m.	
	3 volts per 10 kt.	
Dimensions		
Anemometer height	265 mm	
Anemometer radius	228 mm	
Indicator radius	111 mm	
Anemometer weight	4.5 kg	
Indicator weight	1.4 kg	

4.6.2 Calibration of cup anemometer

The anemometer was mounted on a base board flush with the floor of the test section of a Keith Blackman Tornado wind tunnel of 50 m/s nominal maximum speed, Plate 4.4.

Plate 4.4 Calibration of Munro cup anemometer in the wind tunnel

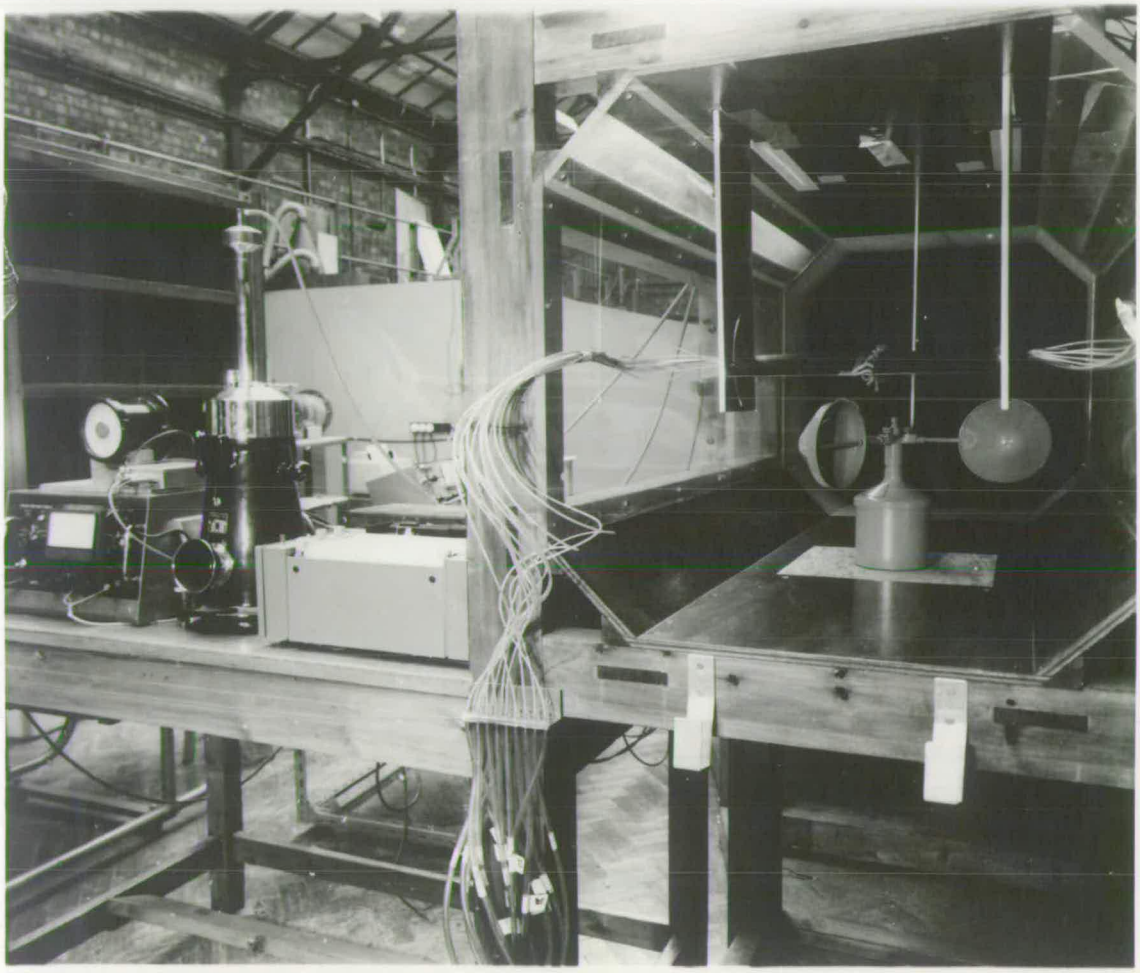

11 A pitot tube was fixed to the test section so that the orifice was 400 mm upstream of the cup anemometer and at the same height of the centre line of the cups, and in line with the longitudinal axis of test section.

The pitot tube was connected to a Schiltknecht water manometer which read directly to 0.1 mm of water.

Since the output signal of the anemometer was specified to be 30 V AC at 100 knots it was necessary to rectify and attenuate the output signal to 1.0V DC to match the input requirement of the taperecorder.

A rectifier, filter, and buffer circuit was designed and built for this purpose. The circuit diagram of this device is shown in Figure 4.7.

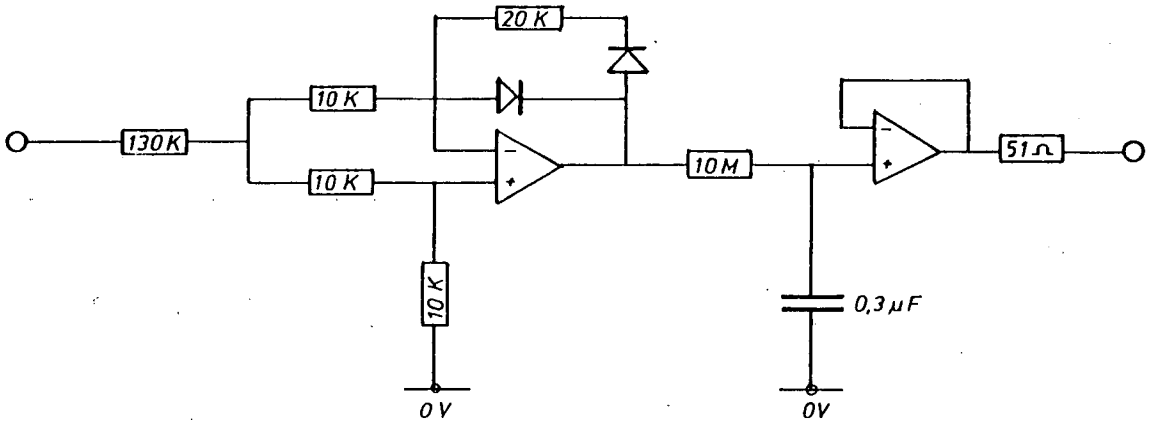

Figure 4.7 Rectifier, Filter, & Buffer circuit for the Munro Cup Anemometer

The conditioned signal from the anemometer was passed to a penchart recorder.

The Schiltknecht water manometer readings were converted to mean wind tunnel velocities using the expression,

$$V = \sqrt{\frac{2 \times 1000 \times 9.81 \times h \times 10^{-3}}{\rho_{air}}}$$

where

h is in mm of water

ρ air is in kg/m^3 and

ρ water is 1000 kg/m^3

Assuming ρ air at 15 degrees C at 760 mm Hg is 1.226 kg/m^3 the ambient room characteristics were measured to be

Ambient air temperature	=	23.0 degrees C
Ambient room pressure	=	747.7 mm Hg
Relative humidity	=	60 %

From this informations and use of conversion and correction charts, ρ air was calculated to be 1.178 kg/m^3. Figure 4.8 is the calibration chart of the Munro Mark II cup anemometer where the output signal is plotted against corresponding wind speed.

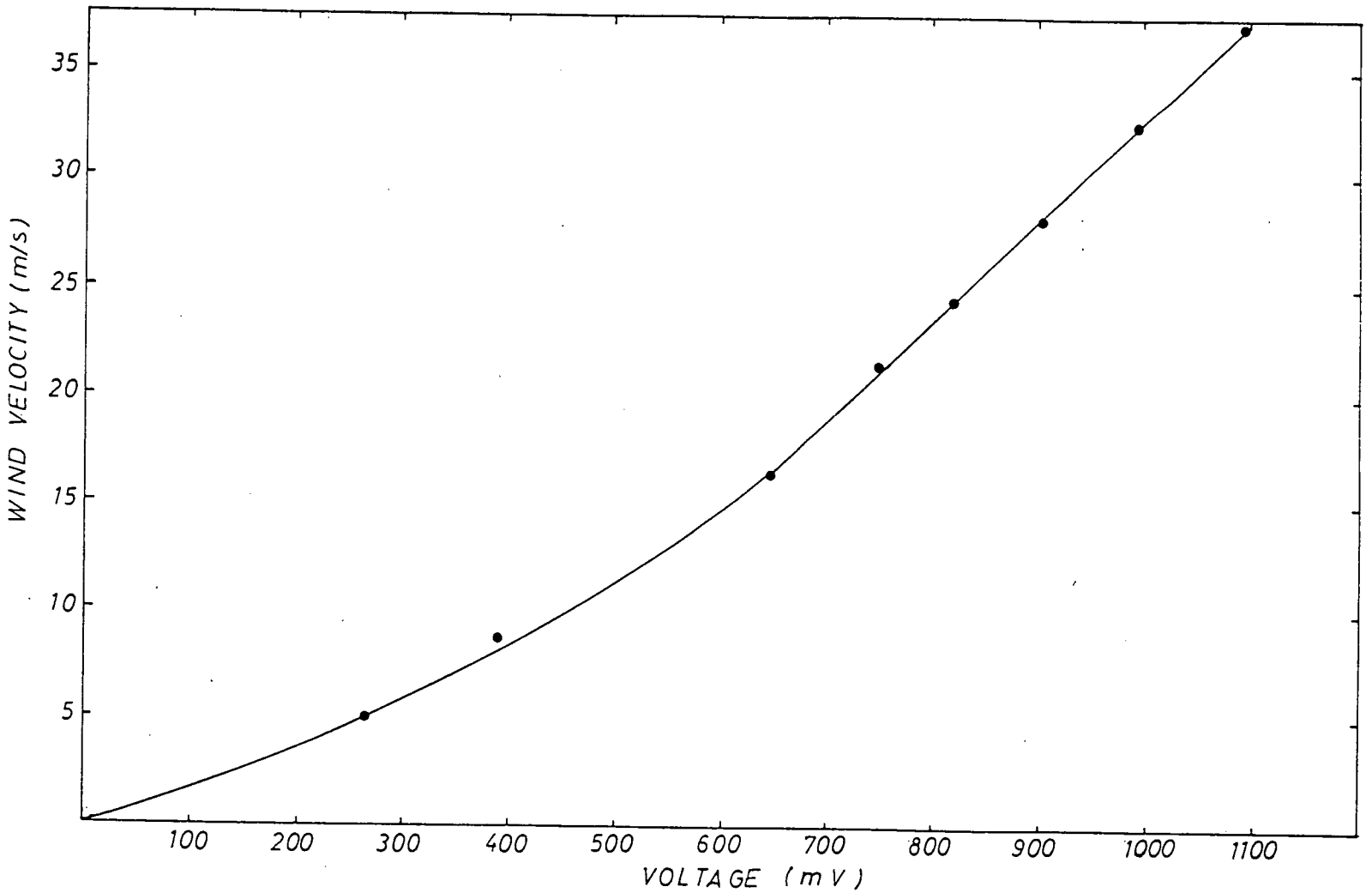
WIND VELOCITY (m/s)
35
30
25
20
15
10
5
100
200
300
400
500
600
700
800
900
1000
1100
VOLTAGE (mV)

4.7 WIND DIRECTION FINDER

4.7.1 Description

The wind direction indicator consisted of a 10 mm diameter shaft mounted vertically in two single row radial ball bearings. The upper part of the shaft was connected to the rotating arm, 700 mm long carrying a wind vane at one extremity. The lower part of the shaft was connected to a Penny and Giles Sine/Cosine potentiometer type RCP 20/18/SC ref.D20616.

The potentiometer was mounted on a circular base plate and the assembly aligned with and connected to the main shaft by means of a coupling. The base plate was fixed to the casing of the direction finder.

The potentiometer was energised by $\pm$ 10.000 V DC. This was achieved by use of a +10.000 voltage reference semi-conductor and inverted by use of a 741 operational amplifier to supply -10.000 V DC.

The circuit was energised by a 15 volt DC power supply and the output signal of the potentiometer was passed through a buffer circuit. This circuit prevents excessive loading of the potentiometer by any external circuitry. This circuit was housed within the casing of the direction finder on the same circuit board as the voltage reference and inverter.

Figure 4.9 illustrates in detail the design of the wind direction finder. Figure 4.10 shows the circuit diagram for the voltage reference and the buffer.

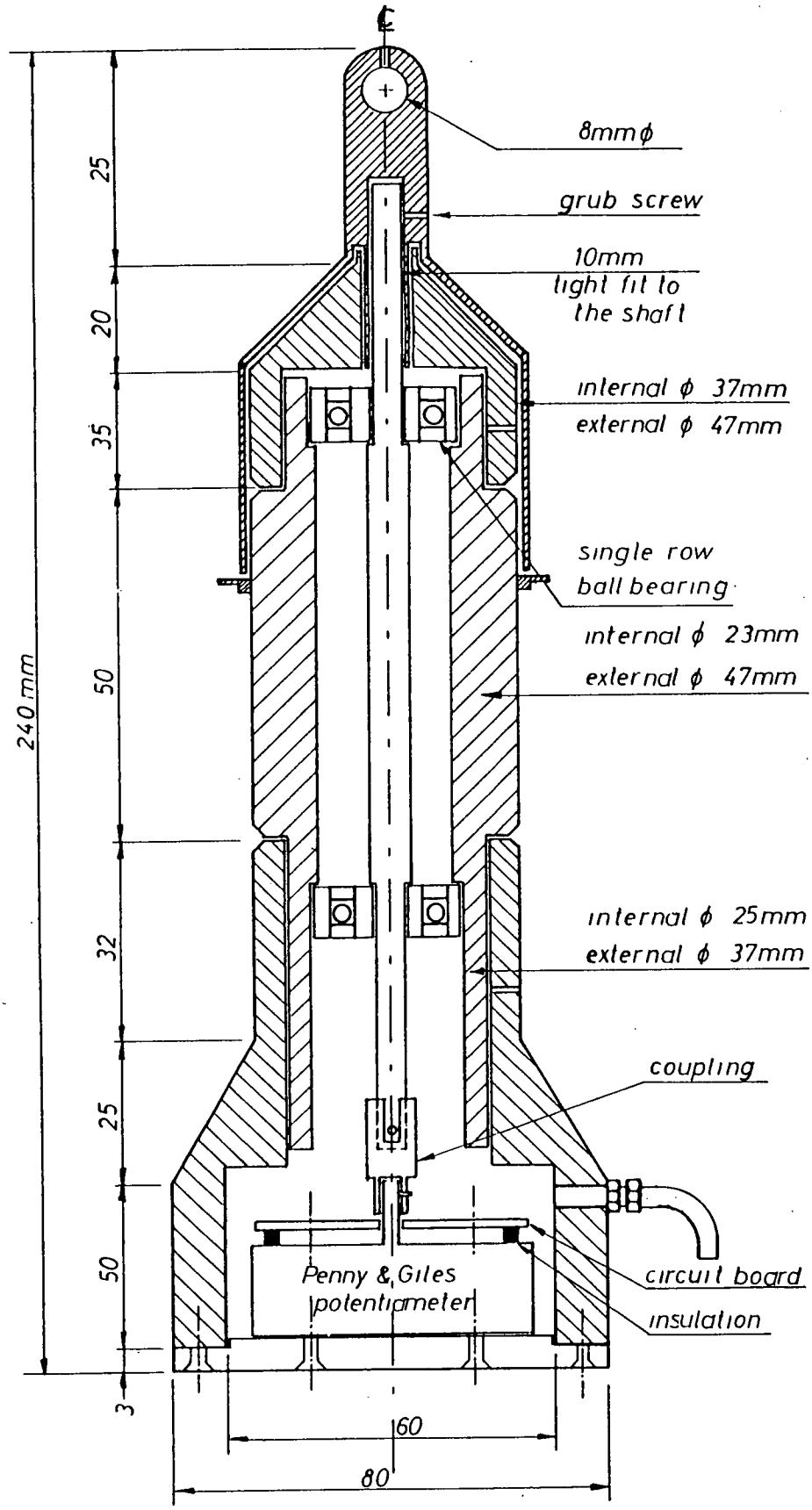

Figure 4.9 Design of a wind direction finder

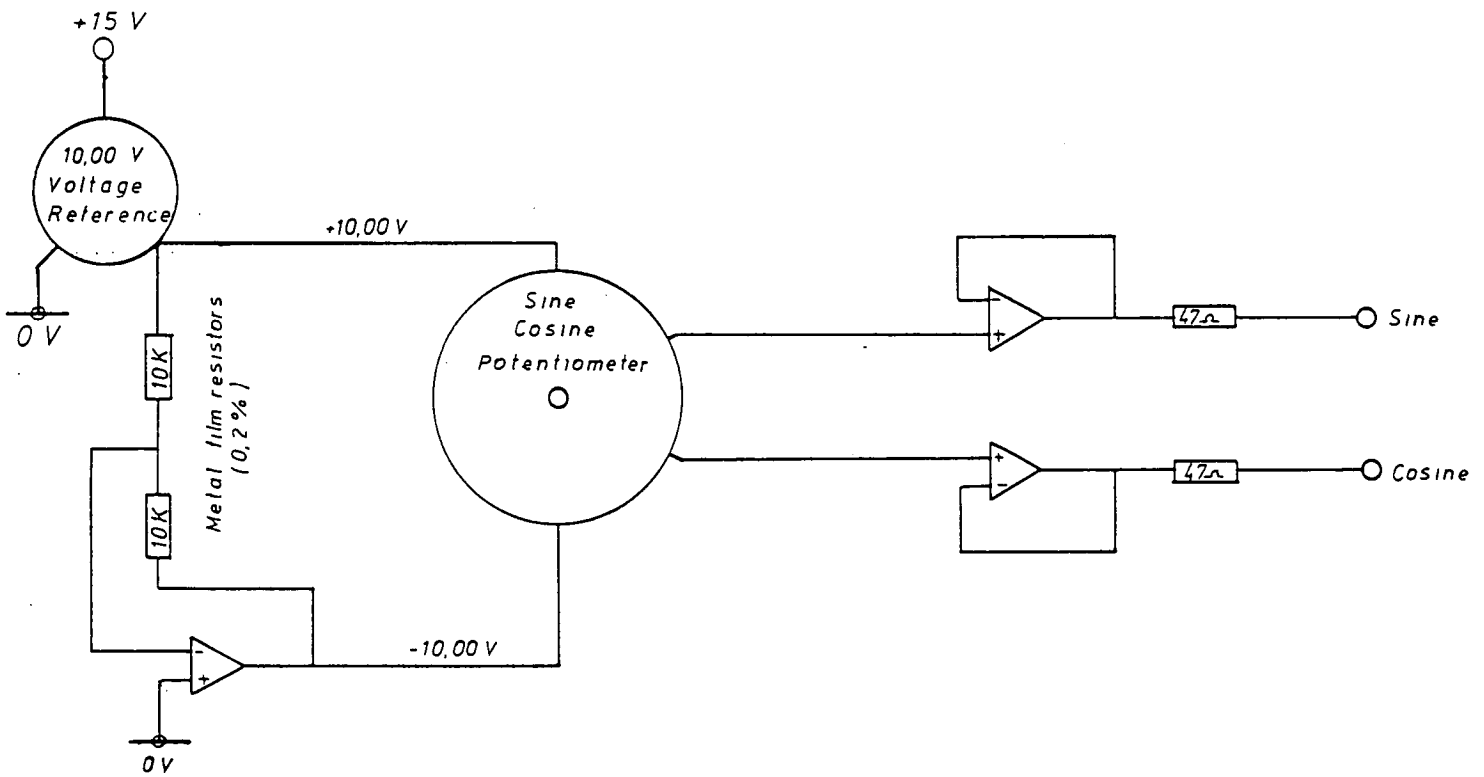

Figure 4.10 Voltage reference & buffer circuit for the direction finder

4.7.2 Calibration of direction finder

Using a prismatic compass, the assumed north direction was established. This was an assumed position since true north could not be established in the laboratory.

An arrow marking north was painted on the body of the direction finder as a reference point, and the direction finder was energised by a 15 V DC power supply.

By pointing the arrow and the wind vane to north a set of sine and cosine signals from the potentiometer were recorded via the buffer and a digital voltmeter.

The body of the direction finder was fixed and the wind vane was rotated through 360 degrees in 30 degrees increments.

Sine and cosine signals were recorded as the wind vane was rotated through one full turn. The results given in Fig 4.9 are the mean of four such rotations.

In order to obtain angular position from these values, the following steps were taken.

Step 1/ If sine and cosine are positive,find arcsine.

Step 2/ If sine is positive and cosine is negative, find arcsine and subtract from 180 degrees.

Step 3/ If sine is negative and cosine is negative, find arcsine and add 180 degrees.

Step 4/ If sine is negative and cosine is positive, fine arcsine and subtract from 360 degrees.

N.B. All values of sine and cosine were divided by 10, since the potentiometer was energised by $\pm$10V.

These angles were related to true north by pointing the direction

finder to magnetic north and applying the appropriate correction angle. The corresponding voltage readings were subtracted algebraically from those for the other positions.

4.8 CABLE STAYED MAST

This consist of four 50 mm dia. aluminium lengths of scaffolding tube joined together,(total 11.5m). A cross bar (50 mm dia ,700 mm long) was formed at the top, so that the cup anemometer and the wind direction finder could be attached to the mast.

The cup anemometer was fixed to a circular base plate, which was welded to a 50 mm dia ,300 mm long tube. This assembly was connected to the cross bar by a scaffolding clamp.

The wind direction finder was connected to the opposite end of the cross bar by means of another 50 mm dia ,300 mm long tube and two clamps.

The mast was fixed rigidly to the side of the concrete wall of the penthouse by two brackets at 1.5 m apart. Each bracket was fixed to the wall by four 10 mm dia ,75 mm long rawlbolts.

To increase rigidity and minimise deflection, the mast was stayed at three points with four 3 mm dia steel cables. Each cable was anchored to the roof with 10 mm dia ,75 mm long rawlbolts.

In order to rise above most of the wind flow turbulence caused by the edges of the building, the centre line height of the instruments was adjusted to 10.0 m above the penthouse roof level.

CHAPTER 5

SIGNAL CONDITIONING AND DATA ACQUISITION

5.1 INTRODUCTION

In any full scale field measurement of the dynamic response characteristics of a bluff structure, sophisticated electronic measuring techniques are required to separate the response from extraneous noise.

Preliminary testing highlighted the main problem area to be one concerning the length of the conducting cables between the transducers and instrumentation control room, Plate 5.1. As the length of these cables increased, the signal to noise ratio decreased. The instrumentation room was located on the 20th floor, within the penthouse external walls and the smaller lift shaft.

This chapter describes the problem of signal conditioning and the necessary hardware required to deal with the noise problem.

5.2 SIGNAL CONDITIONING

The Sensonic ANS-111 accelerometer produced nominally 10V for 1g, with a resolution of 0.0001g. In voltage terms this resolution was equivalent to 1 mV.

A Sangamo N8RT displacement transducer and the transducer meter C56 were capable of measurements better than 0.1 microns, which in turn produced 5 mV.

Initially the cables used were two plain copper stranded 7/0.25 mm conductors insulated by a flat figure 8, P.V.C. sheath. The reasons for choosing this cable were economy and availability.

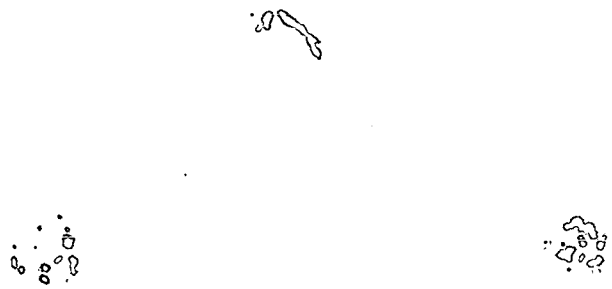

Plate 5.1 Instrumentation room

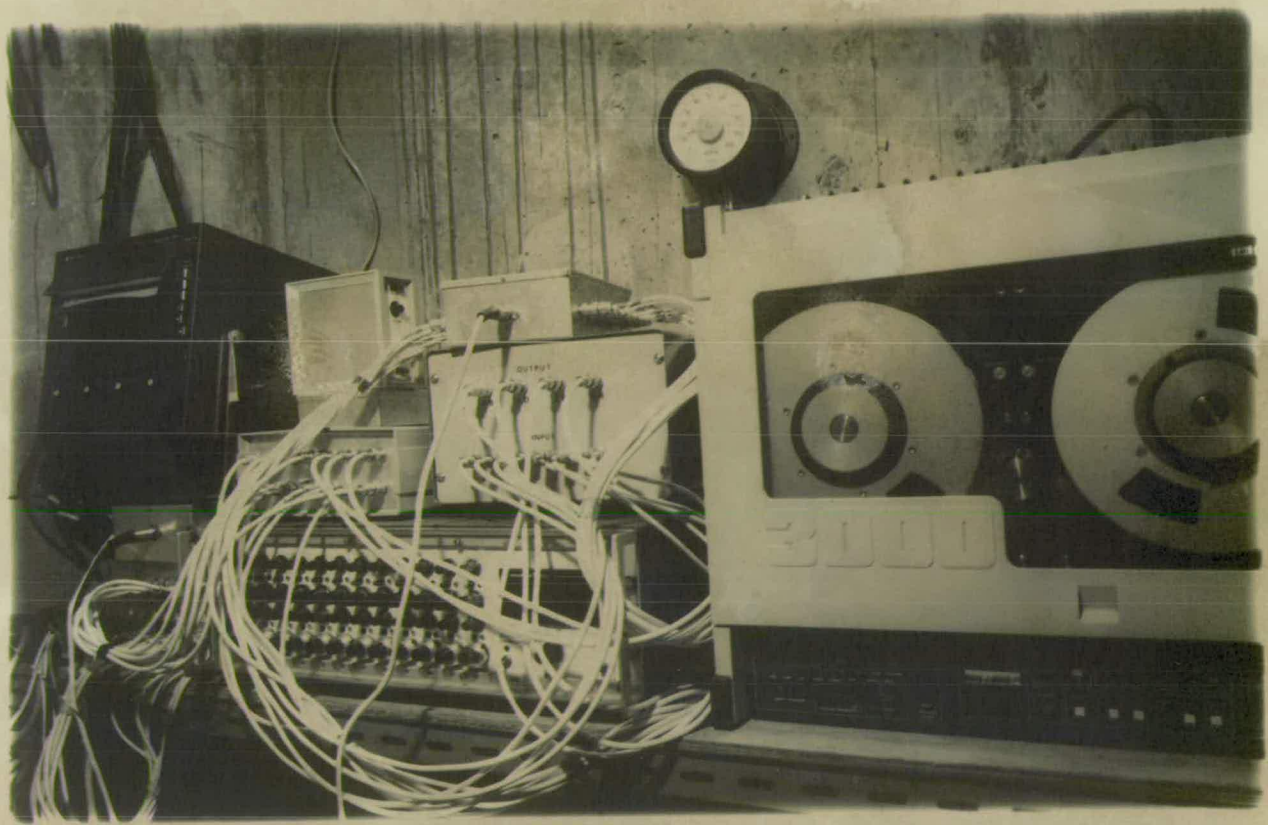

In order to meet safety standards and regulations, the cables were cut to length for each transducer and passed through the smaller lift shaft. These cables were gathered and fastened at 2m intervals to the lift shaft wall.

The length of the cables varied between 5m and 70m depending on the position of the transducers from the instrumentation room.

Energisation and the first trial run proved that, for the length and the type of the cable used, data acquisition was impossible due to excessively low signal to noise ratio. In order to increase this ratio to a reasonable level, it was concluded that an elaborate system of differential amplifiers and filters was essential. At the same time it was found futile to build a sophisticated monitoring system with poor conducting cables. Unscreened cable has a tendency to act as an antenna for electro-magnetic interference (E.M.I.).

Therefore multicore 7/0.1 mm tinned copper stranded conductors covered by 0.2 mm P.V.C. with overall tinned copper braided screened cable was substituted to connect the transducers to their associated energisers through the lift shaft.

However the unscreened cables were utilised for two-way communication with an 'inter-com' between the instrumentation room and various levels. This was necessary for the set zero positions of the transducers.

It was evident that in order to monitor the dynamic response characteristics of the building additional circuitry would be required. This was designed and built by the author and is described in the following sections.

5.2.1 Differential Amplifier

The term instrumentation amplifier is used to denote a high gain DC coupled differential amplifier with single ended output, high input impedance, and high common mode rejection ratio (CMRR). They are used to amplify small differential signals coming from transducers in which there may be a large common mode signal.

The circuit chosen is shown in Fig.5.1 which is one of the simplest forms of differential amplifier.

The Sensonics ANS-III accelerometer transducer has an output impedance of 75 ohms, and with the large input impedance of the circuit there was no longer any problem with the source impedance, at least at DC level. At frequencies of approximately 60 Hz it became important to have matched source impedances relative to the common mode signal, since common mode AC power-line pickup is frequently a problem. In consequence, a 75 ohm resistor was inserted very close to the transducer in the reference line[43].

5.2.2 Active filter

There are several commonly used and readily available active filters, each of which can be used to generate response functions such as the Butterworth, Chebyshev,and Bessel[43]. The reason why such variety is required is that the various filter realisations excel in one or another desirable property, so there is no all round best circuit.

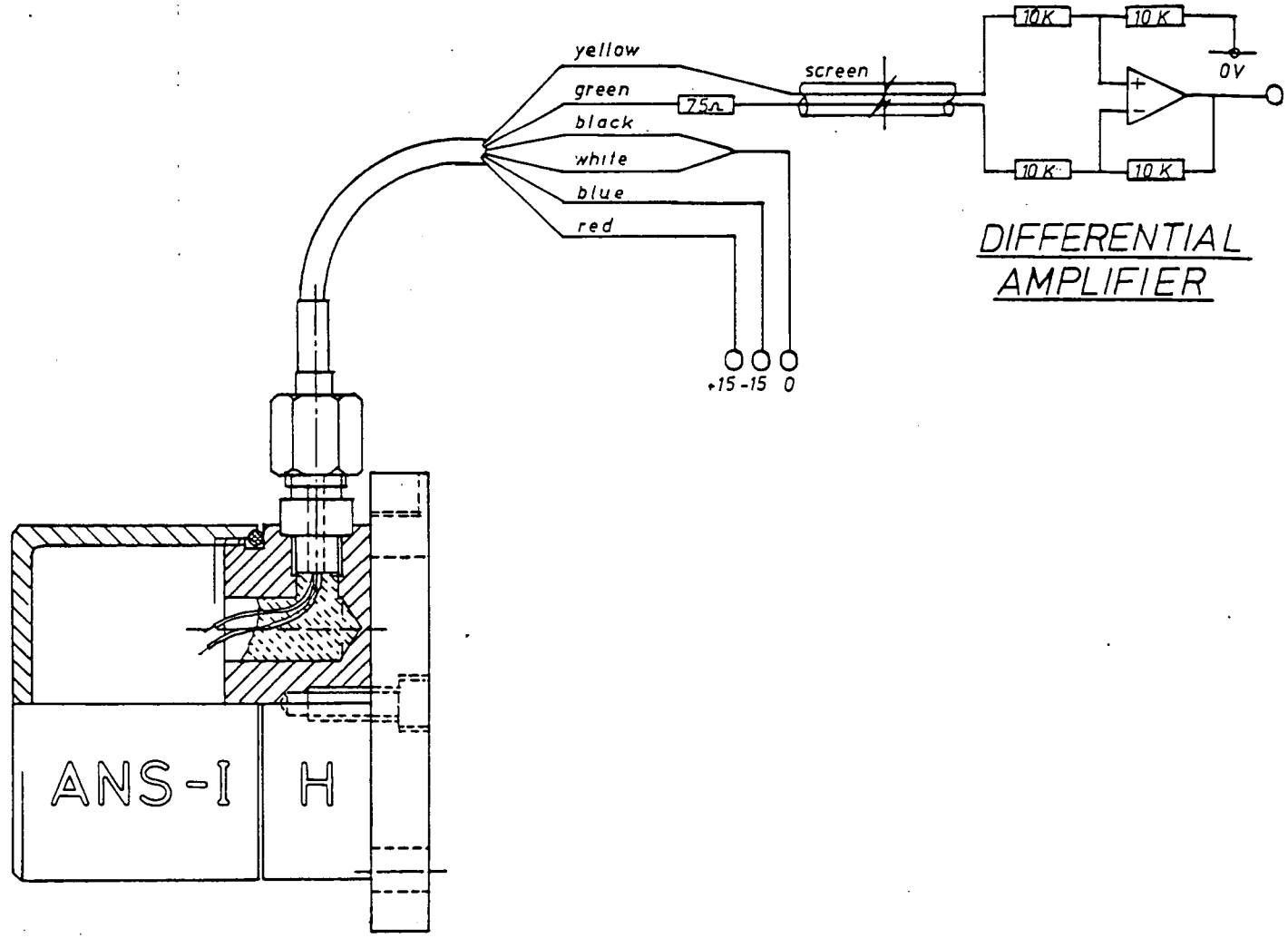

FIGURE 5.1 ACCELERATION TRANSDUCER & DIFFERENTIAL AMPILIFER

The Butterworth filter produces the flattest pass band response, at the expense of steepness in the transition region from pass band to stop band when compared with Chebyshev. Chebyshev like the Butterworth has phase characteristics that are less linear than Bessel types.

5.2.2.1 Low pass active filter

After consideration of several designs, circuit diagrams shown in Figs.5.2, 5.3, 5.4, and 5.5 were built for their response curve analysis. Hence it was deduced that eight cascaded Sallen Key filters (96 dB/octave) were the most appropriate filter for conditioning an accelerometer transducer output signal. A modified form of the Butterworth type filter was employed for conditioning the signals from the displacement transducers after the Sangamo transducer meter. Fig. 5.6 illustrates the response characteristics of the filters tested by a frequency response analyser.

In order to overcome the mains noise, these filters were designed for a cut off frequency of 50 Hz. The transition from pass band to stop band is 12 dB/octave.

Low pass filter

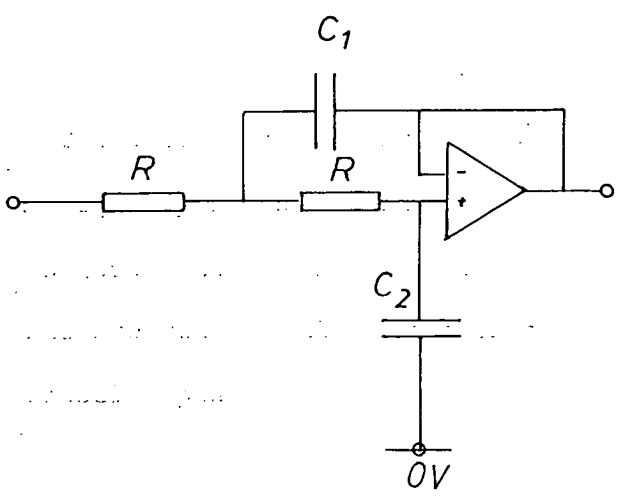

High pass filter

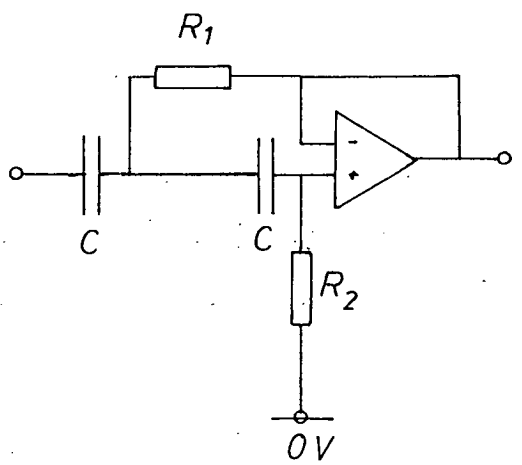

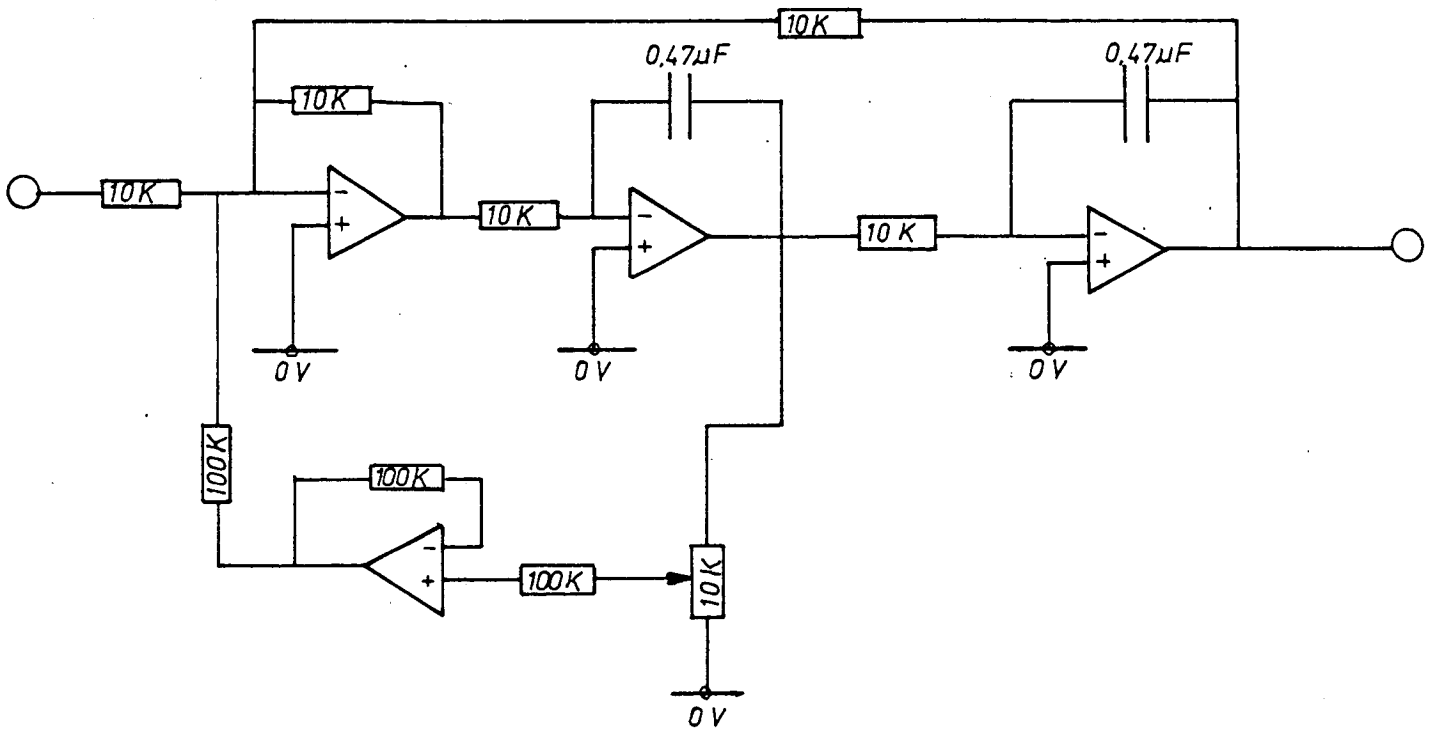

FIGURE 5.2 2nd ORDER LOWPASS FILTER

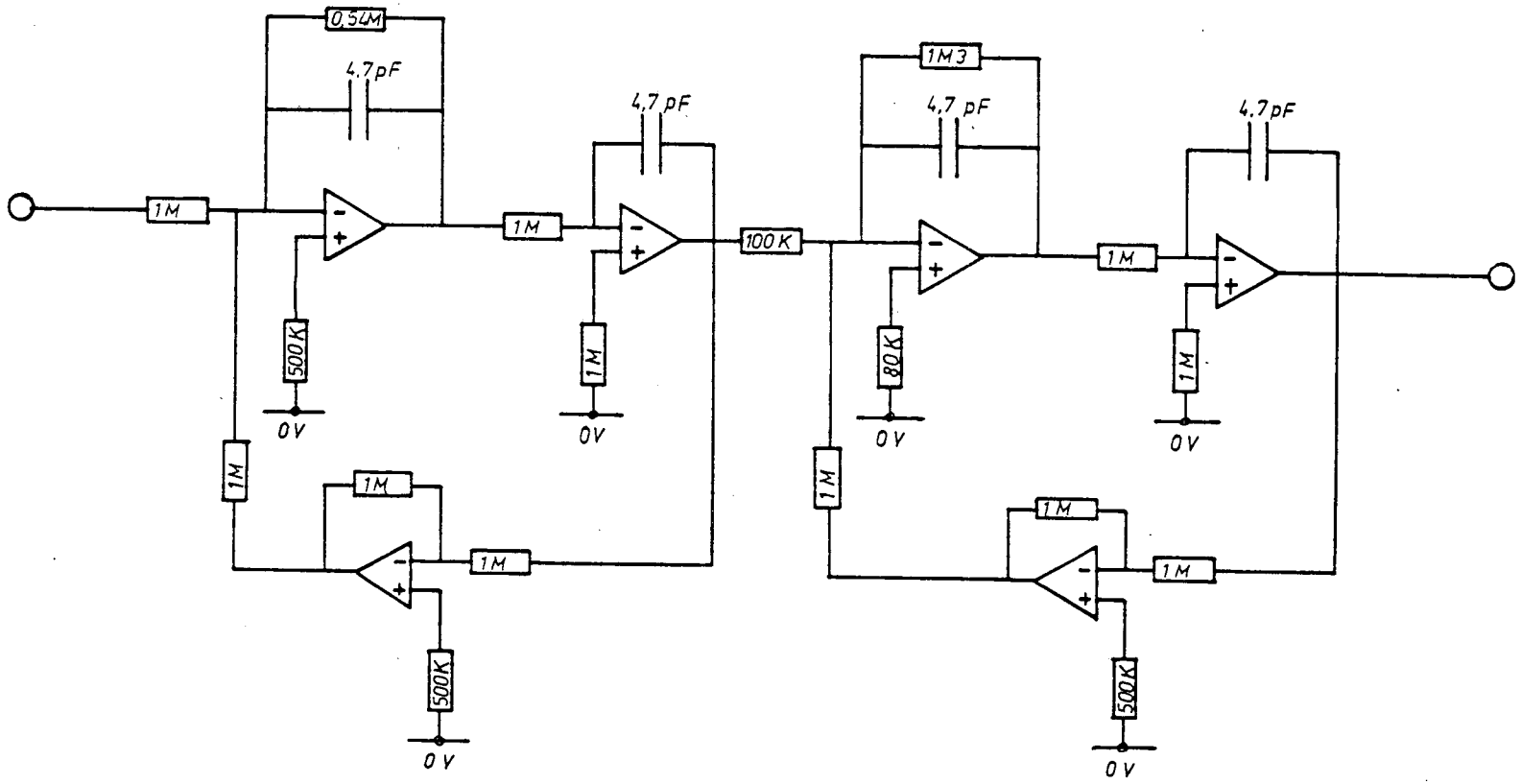

FIGURE 5.3 4th ORDER LOWPASS FILTER WITH GAIN=10

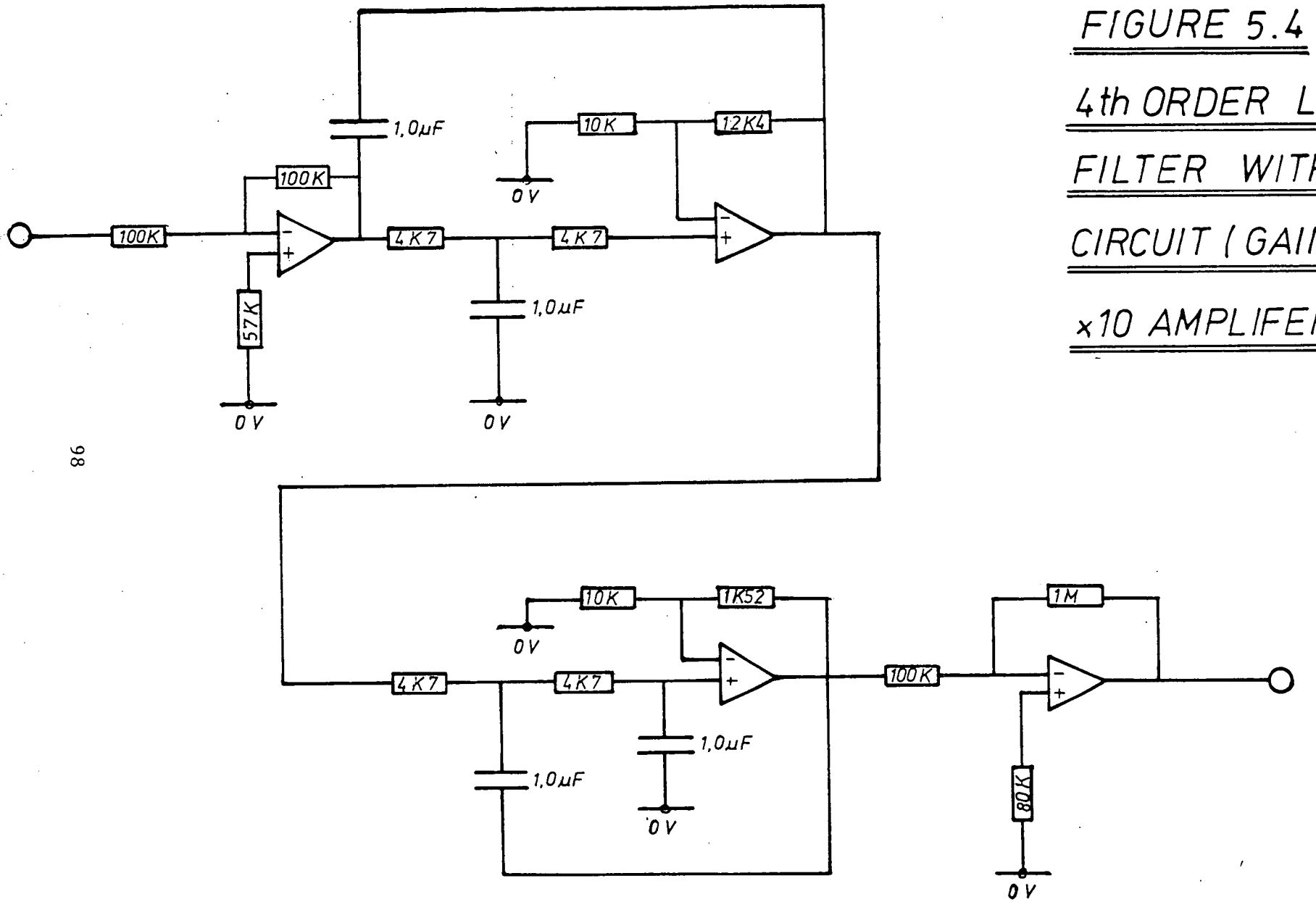

FIGURE 5.4

4th ORDER LOWPASS FILTER WITH BUFFER CIRCUIT (GAIN=1) & x10 AMPLIFER

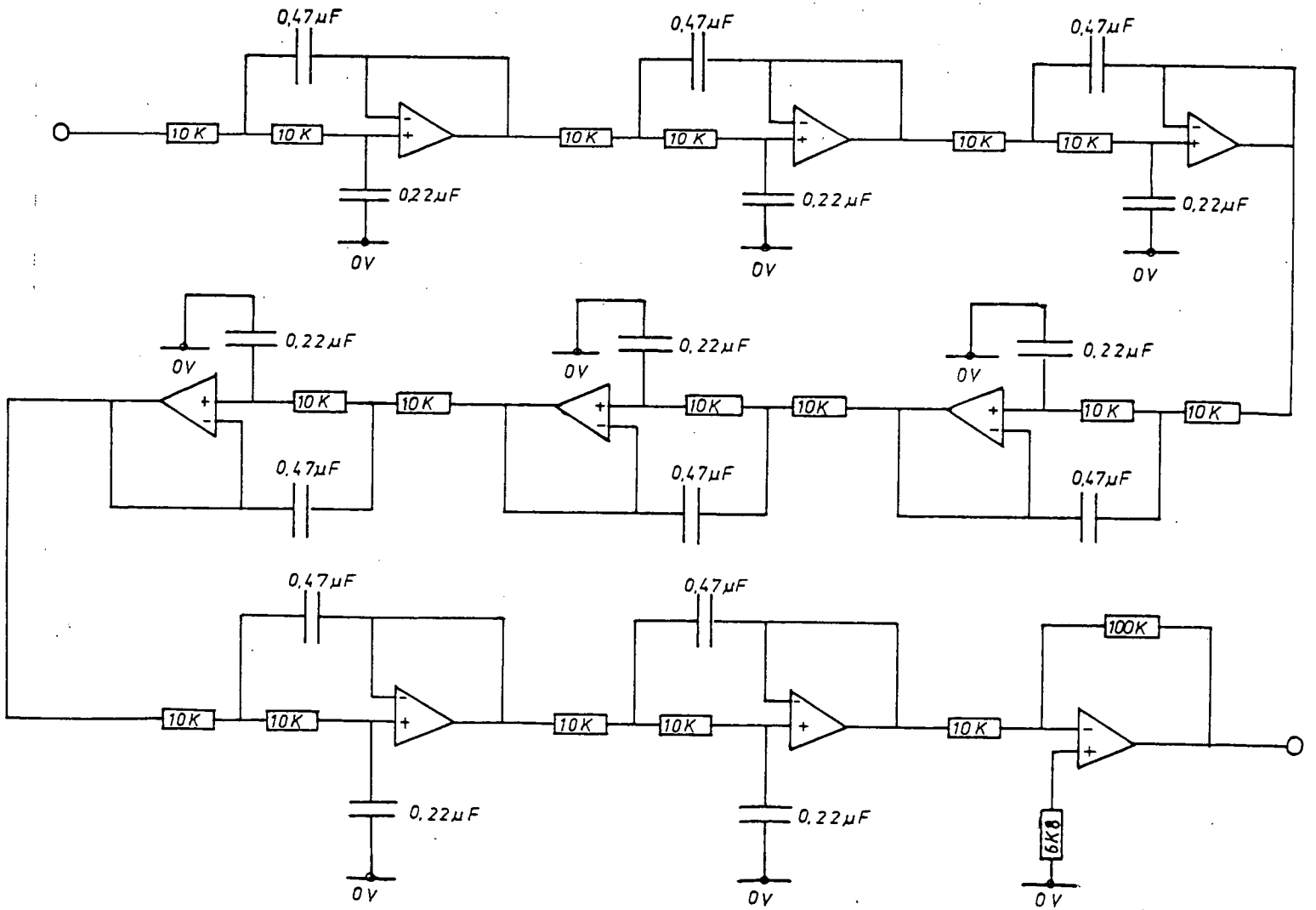

FIG.5.5 8 SALLEN & KEY 2nd ORDER LOWPASS FILTERS + ×10 AMPLIER

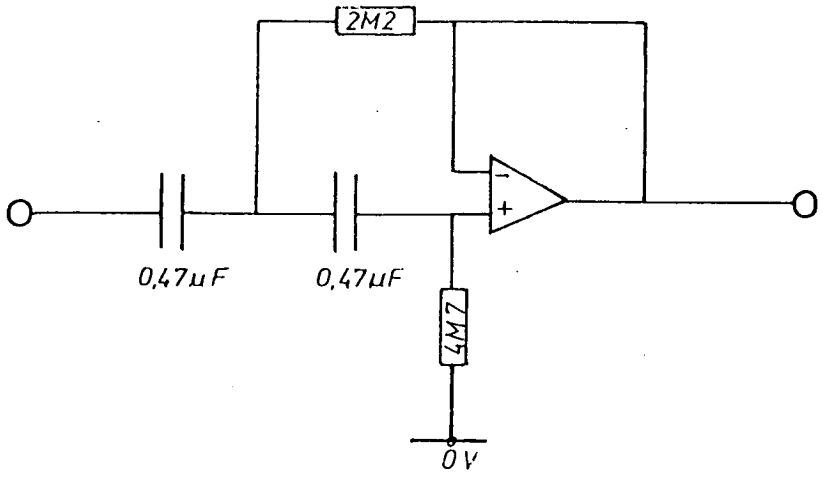

FIGURE 5.7 2nd ORDER HIGHPASS FILTER

cut off freq. = 0,1 Hz

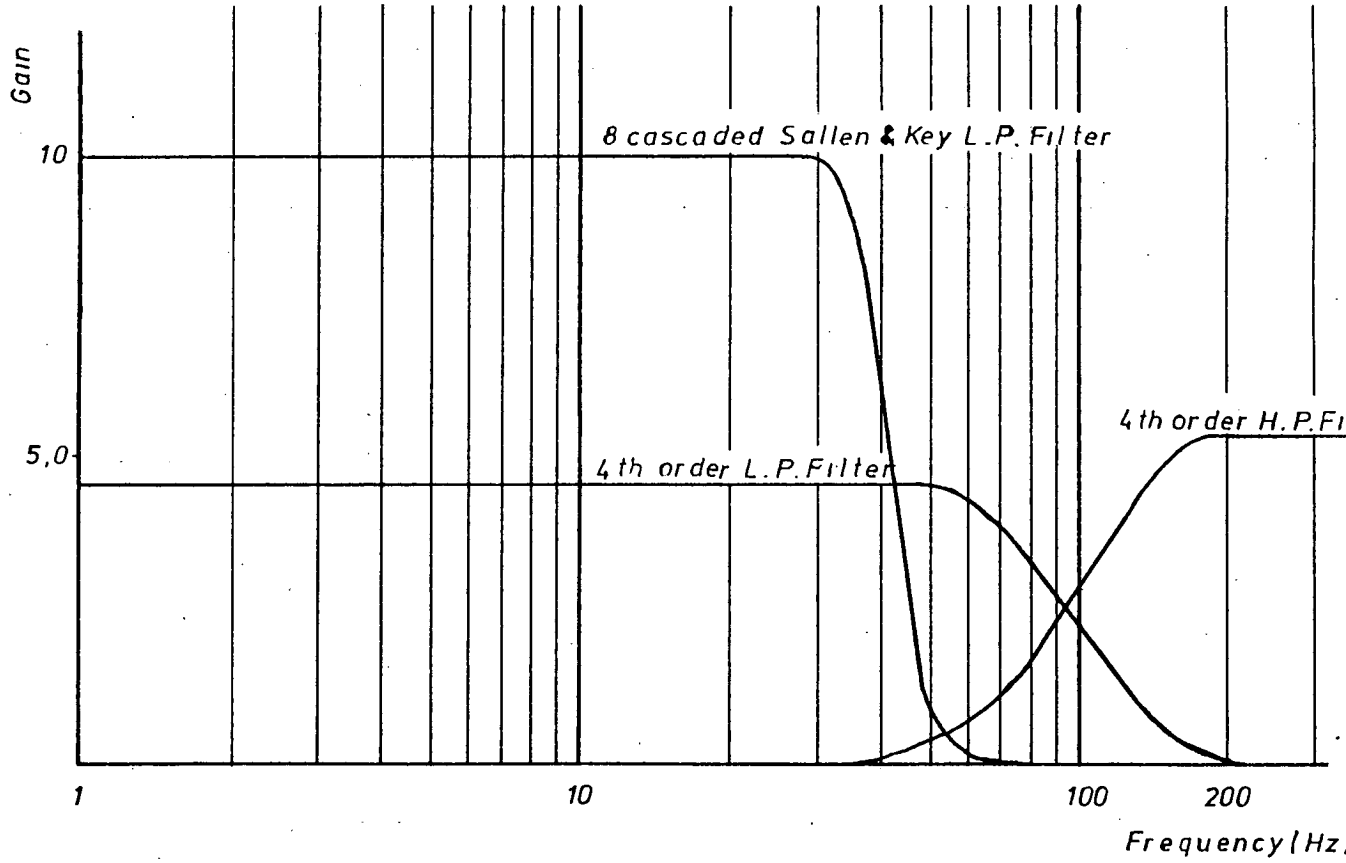

FIGURE 5.6 Response characteristics of filters

The expression for calculating the values of the capacitors and the resistors is given by[44]

$$f = \frac{1}{2 \pi R \sqrt{C_1 C_2}}$$

where f is the cut off frequency in Hz, R is value of resistors in ohms, and C1 , C2 are the values of the capacitors in farads.

5.2.2.2 High pass active filter

These filters were used for two purposes, to eliminate any DC offset after signal conditioning and in an amplitude demodulation system explained in section 5.3.2.

In order to eliminate any DC offset, the design used was of the second order Sallen Key type. Fig.5.7. The expression used for calculating the values of the capacitors and the resistors was given by[44]

$$f = \frac{1}{2 \pi C \sqrt{R_1 R_2}}$$

The value of the cut-off frequency was chosen to be 0.1 Hz. The operational amplifier used in this circuit was of the type LF351 which has a very low bias current.

It was assumed that most large civil engineering structures have a first mode natural frequency in the range of 0.5 to 5 Hz. Consequently frequency components in the natural wind outside the band of 0.1 to 10 Hz have little effect on the dynamic response of such structures[45].

The results obtained by Davenport[45] suggest that the largest response generally occur in the lowest mode or modes of vibration of the structure with higher frequencies relatively quiescent.

Principally the reason being that the greatest energy in the wind almost invariably exist at the lower frequencies. However Lam and Lam[46] have reported that there could be some significant effects on structures from very low frequency components.

5.3 DATA ACQUISITION

The general concept of this research was based upon monitoring the 14 channels of data (7 accelerations and 7 displacements) on an EMI SE Labs 3000 FM taperecorder, plus an extra 3 channels of natural wind data (two for the direction and one for speed) from the weather station at roof level , on a Racal Store 4D taperecorder. By recording one signal on both taperecorders, it was assumed that both tapes could be synchronised for digitisation. This assumption was proved not to be valid when studied at greater length.

The hardware described below, Fig.5.8, was constructed to solve the problem of recording 17 channels of data on a 14 channel taperecorder.

The taperecorder channels were capable to accept a signal of 0 to 313 Hz at a recording speed of 11.9 mm/s (15/32 in/s) on the wide band range. This frequency increased as the recording speed increased, (maximum 40 kHz at the recording speed of 1520 mm/s) . The record attenuator facility offered a range between 0.3 to 30 V peak to peak in order to select the level of input signal which is to produce a + 40% carrier deviation.

In order to record a reasonable length of data it was decided to use a recording speed of 23.8 mm/s on the intermediate band mode which offered a 313 Hz bandwidth.

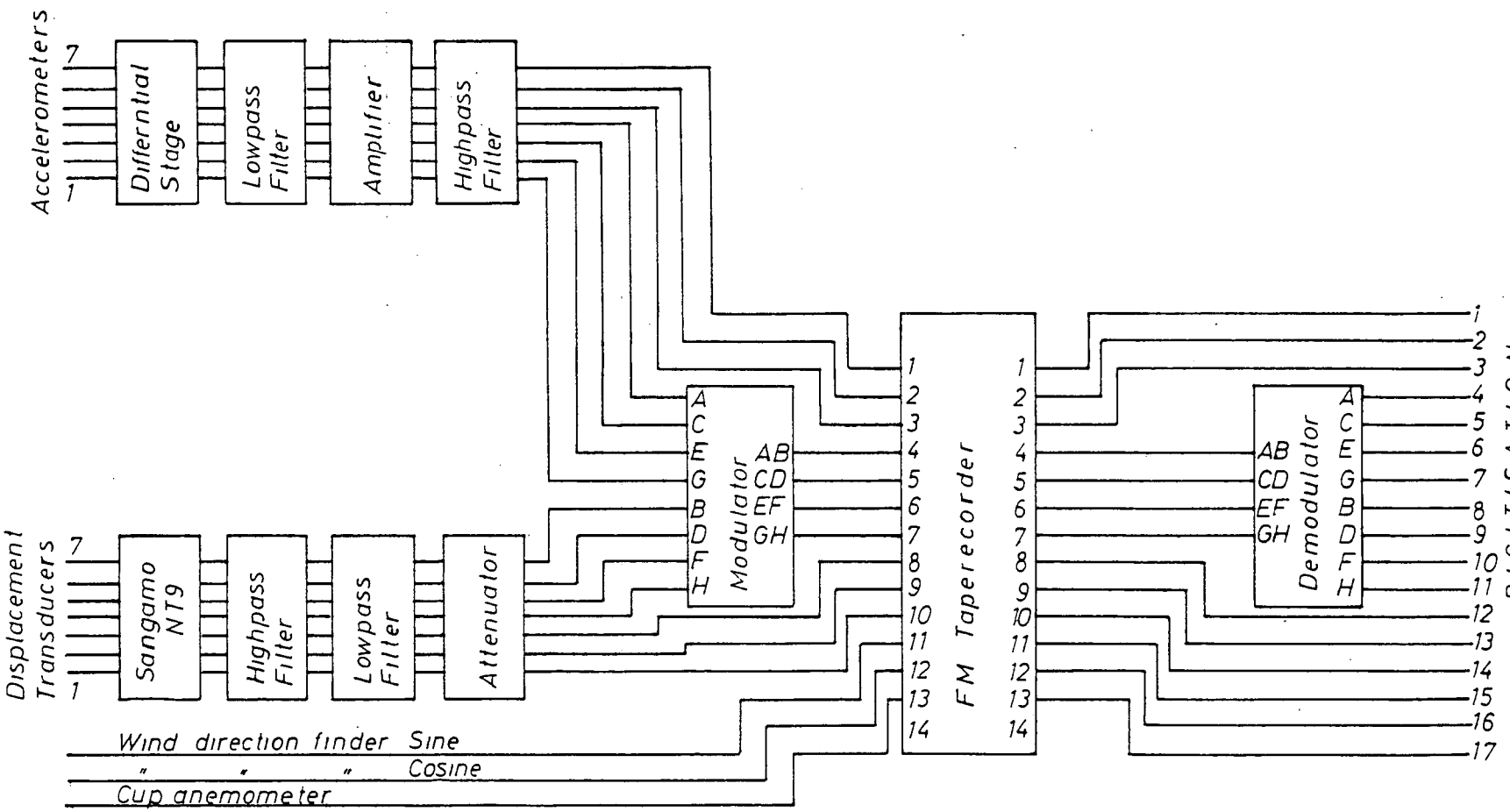

FIGURE 5.8

Signal conditioning and data aquisition

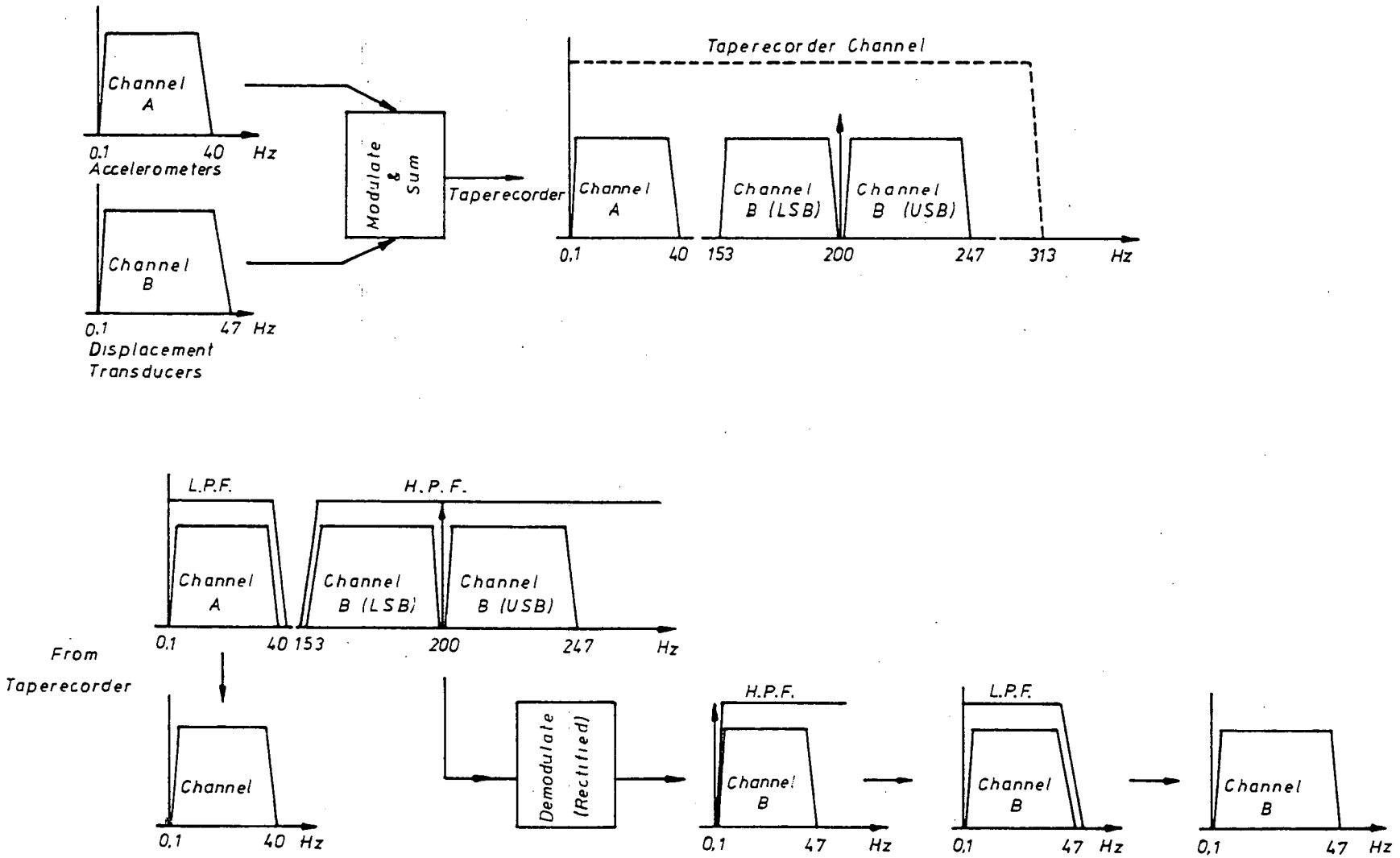

FIGURE 5.9 AMPLITUDE MODULATION/DEMODULATION

The data of interest were in the 0.1 to 10 Hz band and thus any given taperecorder channel had excess capacity which could be utilised to carry one or more extra 10 Hz bandwidth channels. This was achieved by suitable translation of the base band channel spectrum to band pass before addition to the existing base band signal on the given taperecorder channel,Fig.5.9.

5.3.1 Signal Modulation

Possible modulation schemes were amplitude modulation (AM), or frequency modulation (FM). The former was chosen for reasons of hardware utility and ease of implementation taking into consideration the need to produce 4 sets of hardware for the four channels 4,5,6,and 7 (Fig.5.10). A single carrier frequency was generated at 200 Hz by clocking a 2716 (2Kx8bit) EPROM at 51.2 kHz. This clock frequency was set and trimmed by a voltage regulator (VR1).

The prom was coded with a sinewave sampled at 256 points and stored in addresses 00 to FF (Hex). The 8 bit digital output from the prom was latched to suppress glitches due to setting time and presented to the digital inputs of a multiplying digital to analogue convertor (MDAC). This 8 bit binary number selected a fraction of the analogue (or reference) input current (I ref.) to the MDAC. This fraction (M/256) of I ref. was presented at the current sinking output of the MDAC as Io while (1-M/256)Iref. was presented at the complementary current sinking output $\overline{Io}$. When these currents were summed in a current summing amplifier (Fig.5.10), the output was an AM signal. A second voltage regulator,VR2, adjusted the depth of modulation.

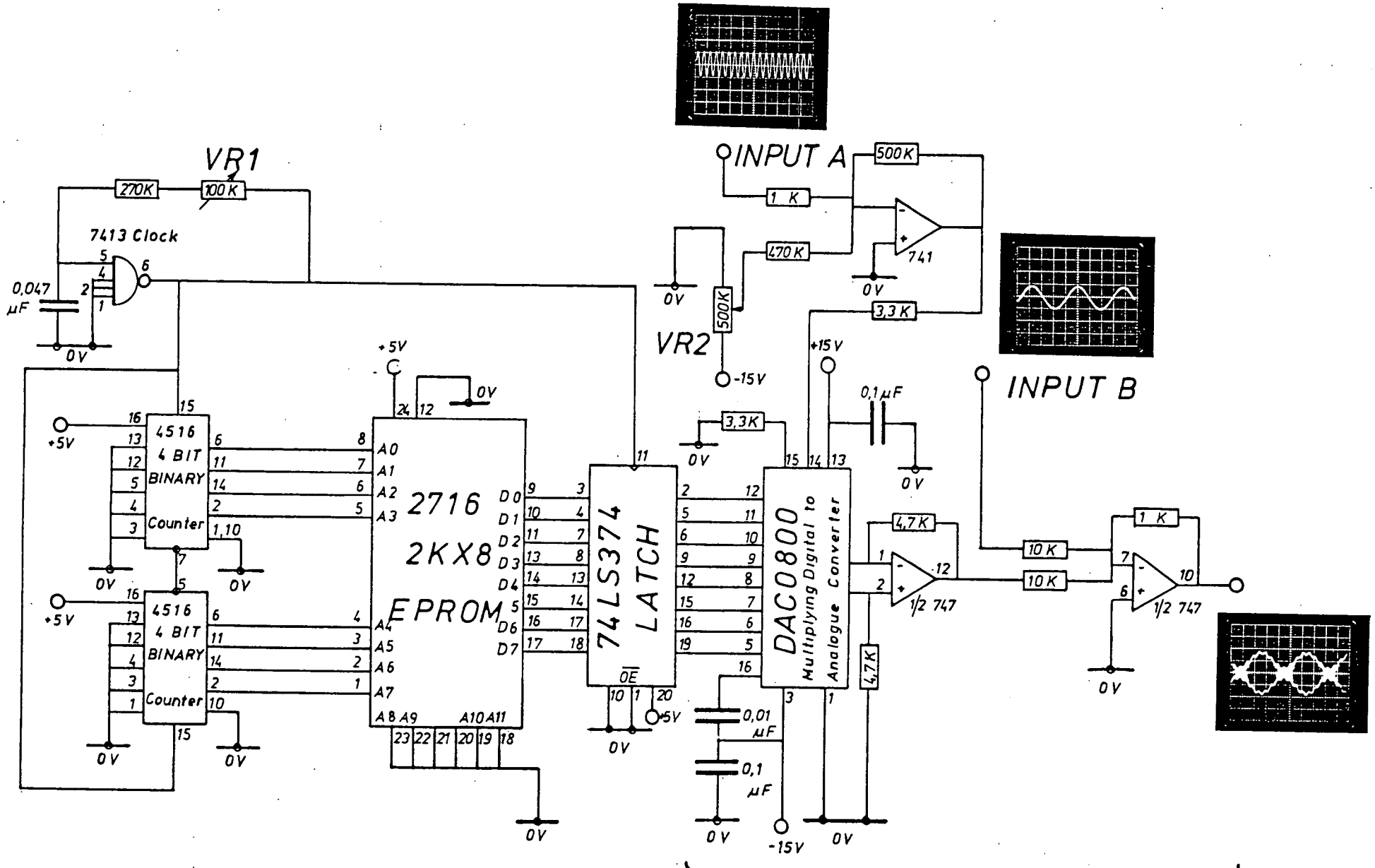

FIGURE 5.10 Modulation Stage

Four duplicate circuits for 8 signals

This AM output had a band pass spectrum consisting of upper and lower side bands disposed about the 200 Hz carrier frequency and occupying the spectral region 160 Hz to 240 Hz (Fig.5.9). This band pass signal was orthogonal to the base band signals. The composite signal lies in the range zero Hz to 240 Hz, and may be regarded as a single base band signal and recorded on any of the 14 recorder channels in the usual manner.

5.3.2 Signal demodulation (Fig.5.11)

Demodulation of the composite playback signal began by separating the two component signals using low pass (Fig.5.12) and high pass filters (Fig.5.13) to accept the base band and band pass signals respectively.

The order of these filters was chosen to make the cross-talk between the two channels negligible. The base band channel merely required low pass filtering (Fig.5.12). The band pass channels had to be rectified (Fig.5.14) to bring them back down to base band. Following rectification it was high pass filtered (Fig.5.15) to remove the unwanted DC term and attenuated to prevent overload of the succeeding low pass filter stage. Finally the signal was low pass filtered to remove all trace of the carrier ripple.

Attenuators (Fig.5.16) were used on all channels to prevent overload and to permit the overall gain from modulator input to demodulator output to be adjusted to unity. Modulation/demodulation was thus made totally transparent to the user.

The system was setup and adjusted in the laboratory with the modulator and demodulator "back to back". Two sinewaves with

different frequencies and an amplitude of 1 Volt were generated as test signals. These generated signals were each split into two parts, one of which were fed directly to the Bell and Howell minirecorder and the others were fed to the channel A and channel B of the system.

As it is evident from Plate 5.2 there is a delay of 0.01 s between the generated test signal and the signal which is subjected to the modulation / demodulation operation (channel B). The signal which was fed through the channel A was delayed with a insignificant time increment.

Cross-talk from the band pass to the base band channel was measured to be of the order of ± 1% of full scale, while cross-talk from the base band to the band pass channels was too small to be measured.

To sychronise all the signals to the cup anemometer signal, the channels which were passed through the modulation-demodulation system were digitised at an advance time of 0.01s.

5.4 SYSTEM CALIBRATION

Due to the effects of mis-match of imput impedance of the signal conditioning circuitery, it was necessary to obtain a calibration factor for each transducer as a whole system.

The actuator of the each displacement transducers was displaced several times by an 0.1 mm slip gauge and an average calibration factor was obtained, Table 5.1.

Each acceleration transducer was rotated through 5^{o} in increments of 30 minutes by use of a inclinometer and the results are presented in Table 5.2.

TABLE 5.2 CALIBRATION OF ACCELERATION TRANSDUCERS

Number	Serial Number ANS-1H	Calibration factor (V/g)
1	1991	110.58
2	2883	108.75
3	2882	110.30
4	2884	110.23
5	2885	108.24
6	2900	118.69
7	2886	124.20

TABLE 5.1 CALIBRATION OF DISPLACEMENT TRANSDUCERS

Number	Serial Number Sangamo	Calibration factor (V/mm)
1	32551	43.20
2	32549	10.20
3	32552	40.58
4	32550	48.90
5	32543	45.60
6	32544	64.20
7	32546	45.50

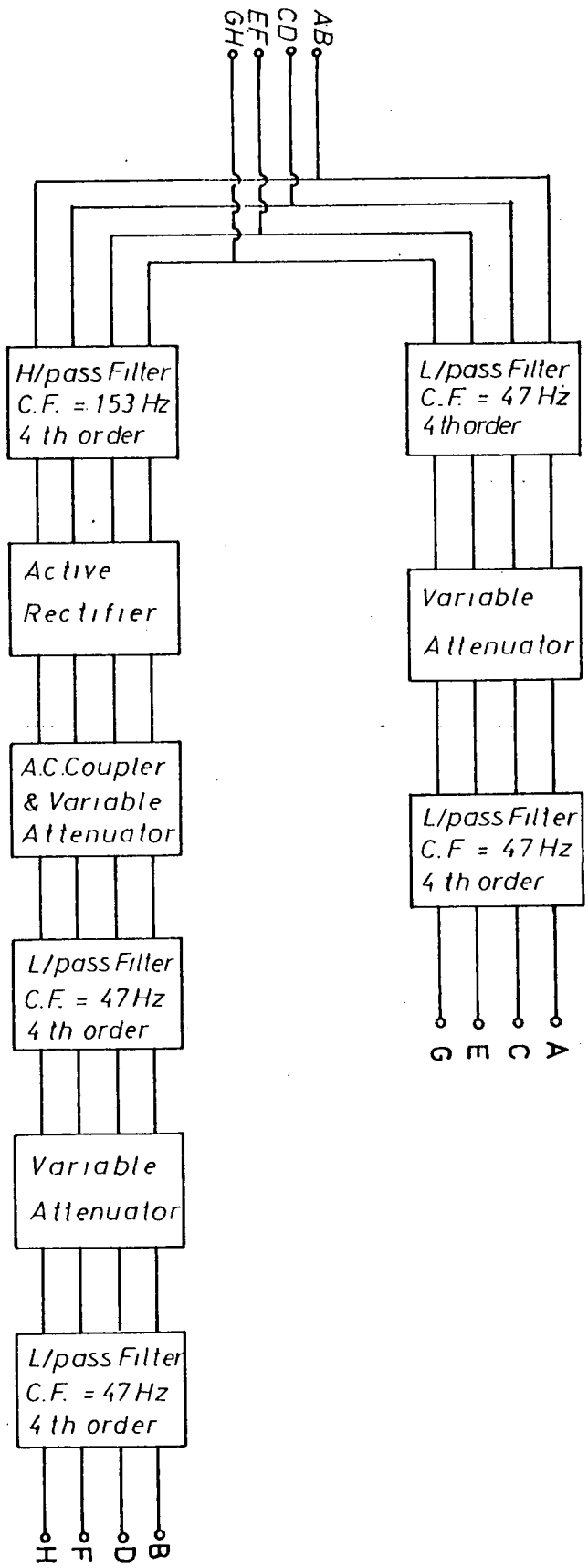

FIGURE 5.11 Demodulation Stage

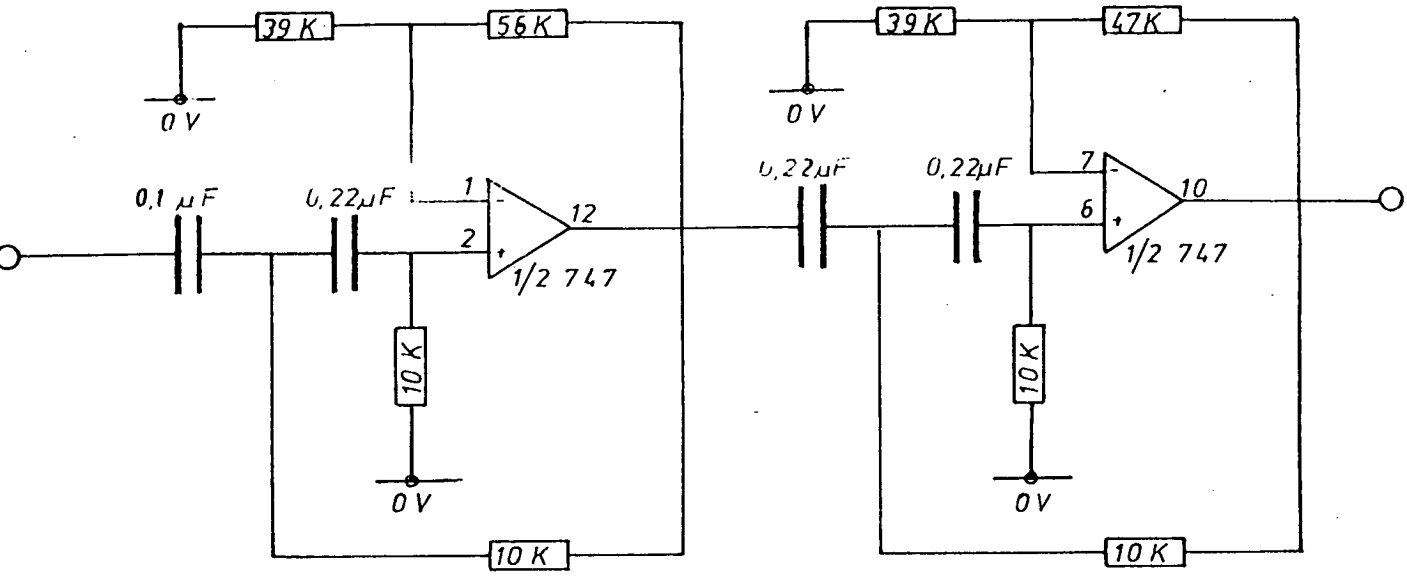

FIGURE5.13 Active 4th order Highpass Filter

cutoff freq. = 153 Hz

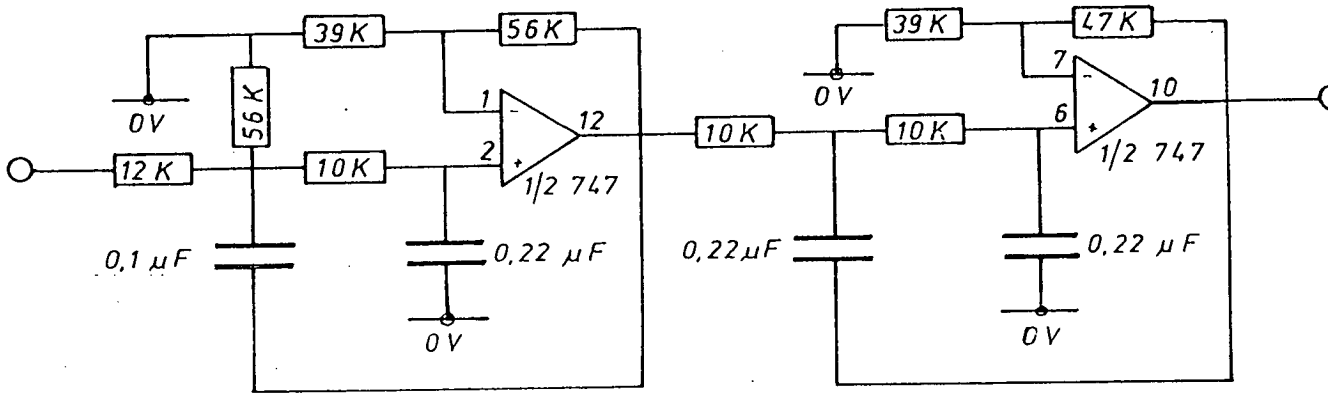

FIGURE 5.12 Active 4th order Lowpass Filter

cut off freq. = 47 Hz

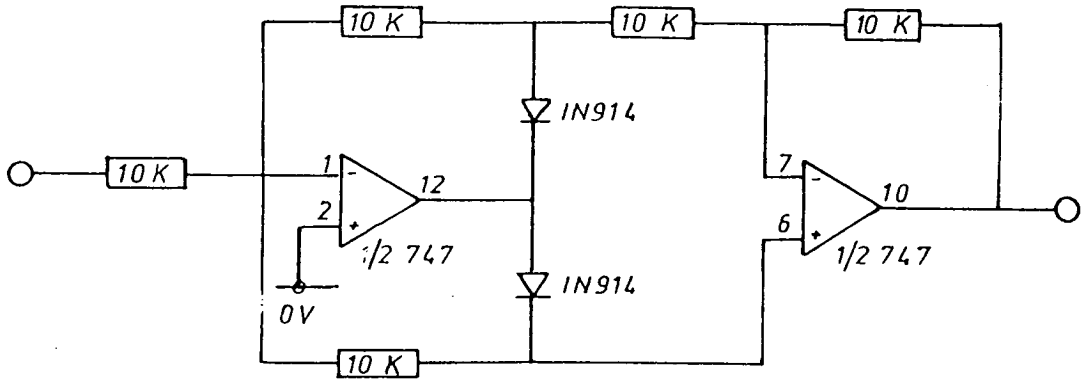

FIGURE 5.14 Active Fullwave Rectifier

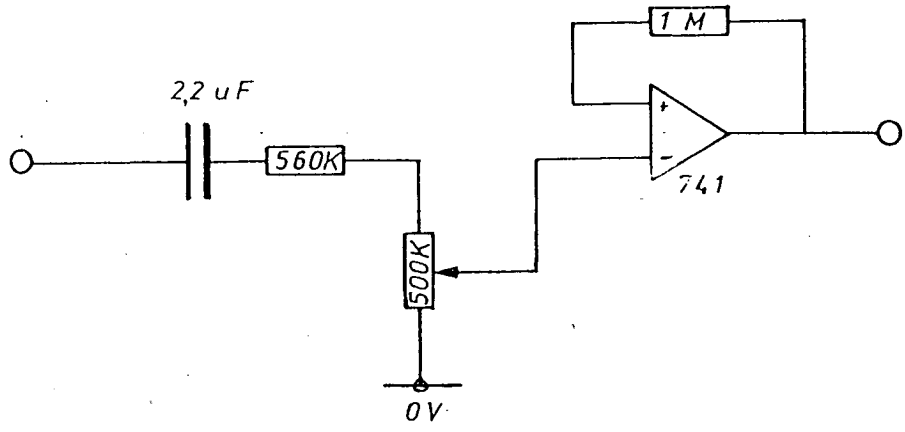

FIGURE 5.15 A.C. Coupler & Variable Attenuator

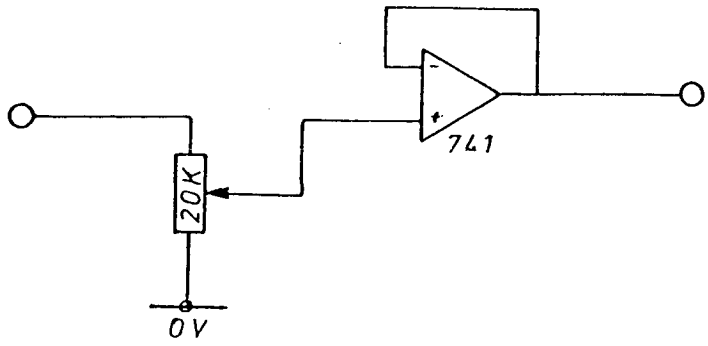

FIGURE 5.16 Variable Attenuator

Plate 5.2 Phase difference of generator signal with mod / demodulated signal

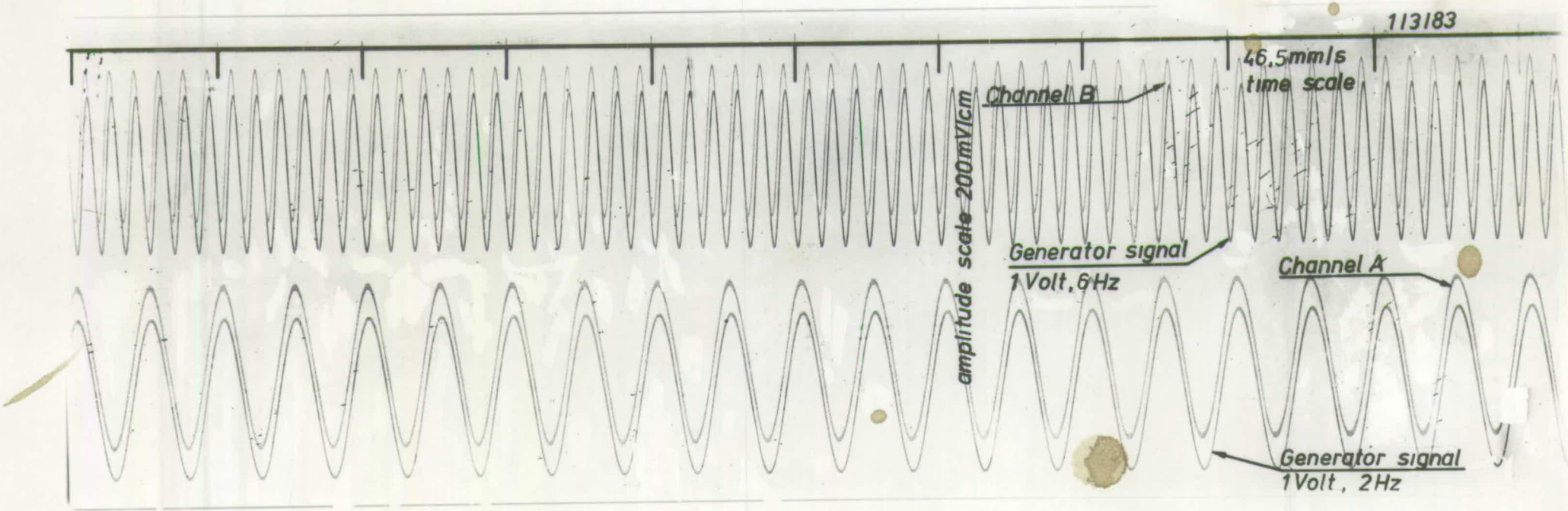
113183
46.5mm/s
time scale
Channel B
amplitude scale 200mV/cm
Generator signal
1Volt, 6Hz
Channel A
Generator signal
1Volt, 2Hz

CHAPTER 6

INTERPRETATION AND ANALYSIS OF RECORDED DATA

6.1 INTRODUCTION

In order to carry out a suitable analysis on the wind excitation response of JRC building, its dynamic characteristics had to be fully established. As it was concluded in chapter 3, the theoretical (long hand and computer package analysis) evaluation of these characteristics were prone to large errors. Hence it was decided that a forced vibration technique would be a more appropriate method to determine the required characteristics.

The vibrator used to excite the building at the first fundamental translational frequencies proved to have limited capability in range of frequency and induced force. It was therefore clear that a joint venture between the University of Edinburgh and the Building Research Establishment (BRE) could be beneficial to both parties.

The cooperation was based on the following circumstances.

1/ The BRE has been conducting full-scale vibration test on tall buildings during the last eight years and their interest in a long term approach analysis of any tall building to wind excitation was expressed.

2/ The BRE possessed an elaborate system of forced vibration testing equipment (Plate 6.1) and a computer package for analysis of the recorded data.

3/ The JRC building was fully instrumented already by the University of Edinburgh.

4/ The results obtained could be jointly used.

Consequentely an invitation was sent to the BRE with the proposal. The agreement with the BRE for the calibration of JRC was endorsed by the Edinburgh City Council Housing Department, the owners of the building. Accordingly a mutually convenient date was set for the calibration and to eliminate any cause for concern, the JRC building tenants were notified of the nature of the experiment.

6.2 CALIBRATION OF JRC

The vibration system used by the BRE[47] consisted of four purpose built eccentric mass exciters. Each exciter consisted essentially of two motor driven sets of contra-rotating masses. By addition of extra weights to the exsisting sets, the induced force could be varied. The force produced in this fashion was calibrated using a load cell and was well within the $\pm$ 3% accuracy of the specification. A maximum force of approximately one tonne peak to peak (p-p) could be produced by the system at one Hertz.

Each exciter had its own 'slave' control unit driven by a master unit which controlled the whole system. The required frequency was clocked from a crystal oscillator and it was claimed to be accurate to one part in 10^6. The use of a servo control technique allowed the frequency to be controlled to 0.001Hz accuracy. Each unit could be set to run either at 0^o or at 180^o out of phase and was and could be adjusted to an accuracy of 0.6^o relative phase difference. The exciters were mounted on steel rings designed so

Plate 6.1 Vibration system used by the BRE

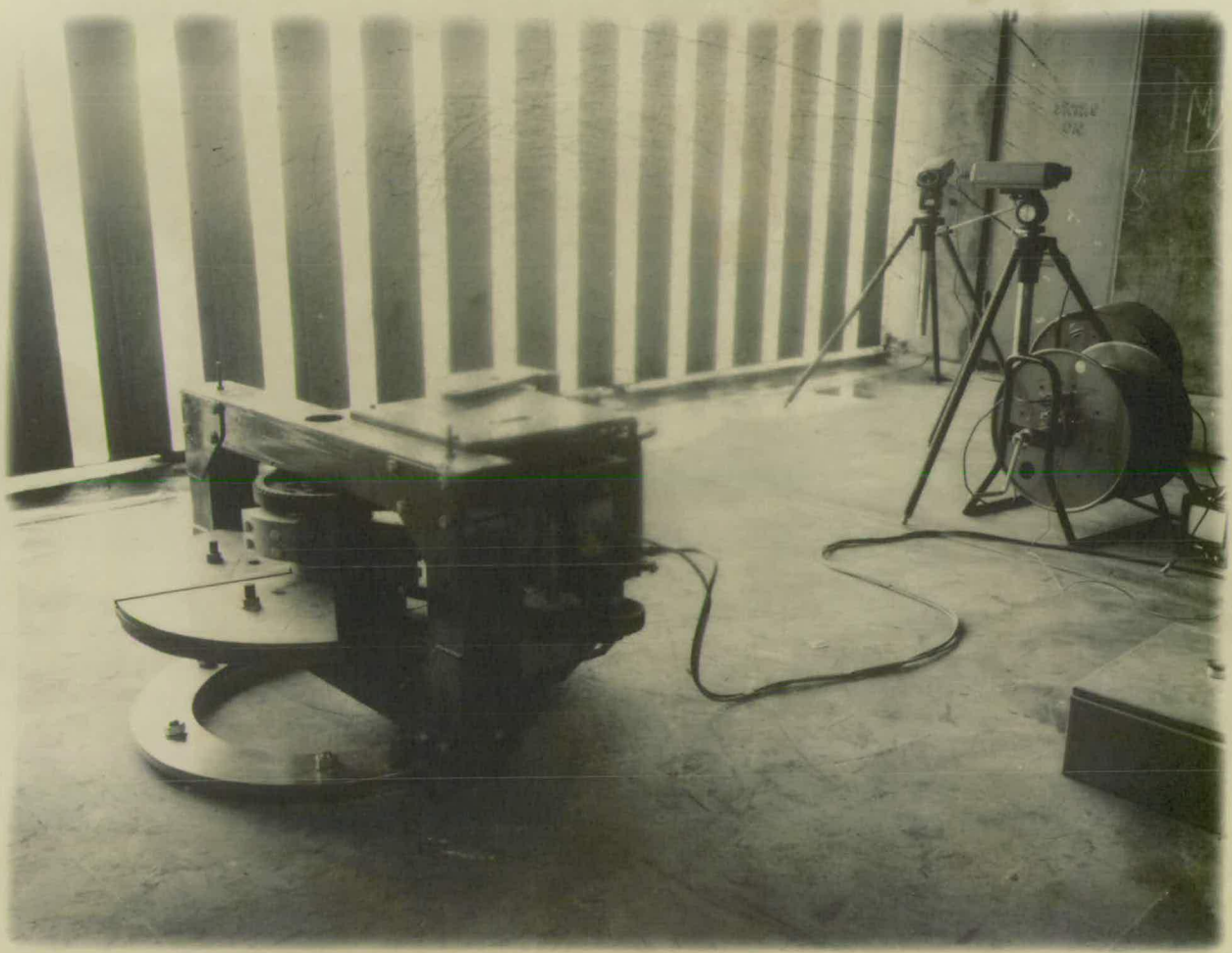

that each unit was capable of rotation in any desired orientation in the horizontal plane.

In case of the JRC building, the excitation was generated by only two exciters. Each exciter was positioned at the 19th floor level close to the extreme corner of the building in two diagonally opposite drying rooms.

After establishment of the natural circular frequencies by trial excitations, the JRC building was set in a steady state mode of vibration at a particular natural frequency with a known excitation force. By using two accelerometers (one as reference and the other as the roving measuring device) the modal shape of that frequency was plotted. Figures 6.1, 6.2, and 6.3 shows the modal shapes for the first three natural frequencies, (2 translational modes and one torsional).

In translational modes the exciters were set in-phase and in torsional modes the exciters were set in anti-phase with respect to each other.

In order to obtain the damping ratio as a percentage of critical damping, a trace of the decay curve was obtained at the 19th floor level when the excitation ceased, (c.f. Chapter 3).

The modal mass calculation was based on the expression

$$M_r = \frac{F_r}{8 \zeta \pi^2 f_r^2 x_r}$$

where

F_r is the applied force in N causing the modal frequency response.

ζ is the fraction of critical damping %

f_r is the modal frequency in Hz

x_r is the range of vibration in the r th mode in m (p-p)

also assuming the power law exponent of first modal shape α =1

then, for r = 1

$$M_1 = \int_o^H m(z)\,\Phi^2(z)\,dz$$

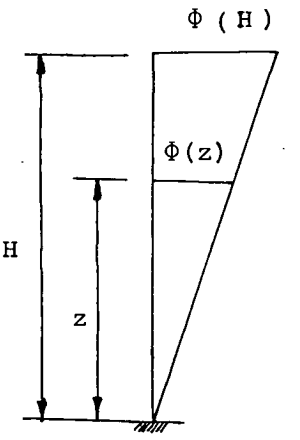

for $\Phi = z/H$

$$M_1 = \int_o^H m(z)(z/H)^2\,dz$$

$$= [z^3/3H^2 \,.\, m(z)]_o^H$$

$$= H^3/3H^2 \,.\, m(z)$$

assuming $m(z).H = M_T$ (total mass)

therefore

$$M_1 = M_T/3$$

The modal inertia calculation was also based on the above expression, but instead of amplitude of vibration and applied force, angular displacement and applied torque were used respectively.

By varying the magnitude of the applied force at each natural circular frequency range of angular displacement, amplitude, damping ratio, modal mass, and modal inertia were established and the results are tabulated in the Table 6.1.

The torsional centre was found by applying a torsional force only to the structure in the first torsional resonant mode and measuring two orthogonal components of acceleration at each of several different points (x_i, y_i) at the 19th floor level.

Since

$$\ddot{X}_i = l_{yi}\,\ddot{\theta}$$

$$\ddot{Y}_i = l_{xi} \ddot{\theta}$$

where l_{xi} and l_{yi} are the normal distances between the lines of measured accelerations X_i and Y_i and corresponding lines through the torsional centre. Thus for each point (x_i, y_i) the radial distance $\sqrt{(l_{yi}+l_{xi})}$ from the torsional centre was computed. Then the torsional centre was determined from the intersection of the arcs, using these radii from the measured points. The coordinates of this point were found to be 11.8 m and 9.85 m from a datum at South East corner.(see Figure 4.3)

6.3 RECORDED DATA

On Monday 9th May 1983, between 17:00 and 18:30 hours, the system was activated and the response of JRC building due to wind excitation was recorded. The wind speed and direction were measured and later confirmed by the Turnhouse Meterological Office, Edinburgh as 11 knots at 250° in azimuth from true north.

The longitudinal axis of JRC building (XX) was oriented at an angle of 350 degrees of azimuth. Hence the wind direction was almost normal to this axis.

6.4 ANALYSIS OF DATA

The BRE computer package analysis was performed on the recorded data for the Power Spectral Density (PSD) analysis for the estimation of frequency response functions of JRC building.

The concept of the analysis is briefly described and for more comprehensive description reader is referred to the BRE Note N70/76[48].

TABLE 6.1 RESULT OF CALIBRATION OF JOHN RUSSEL COURT BUILDING

MODE	TORQUE (Nm p-p)	FORCE (N p-p)	FREQ. (Hz)	ANG.DISP. xE-6 (rads p-p)	AMPL. (mm p-p)	DAMPING %	MODAL MASS (kg)	MODAL INERTIA kgm/rad
YY 1	-	405.4	0.990	-	0.230	0.71	3.27E6	-
	-	804.2	0.986	-	0.433	0.84	2.94E6	-
	-	1608.4	0.986	-	0.560	0.91	4.19E6	-
	-	2383.3	0.980	-	0.840	0.99	3.85E6	-
	-	3158.3	0.977	-	1.470	1.00	2.91E6	-
	-	3907.6	0.972	-	1.810	1.15	2.57E6	-
XX 1	-	577.8	1.182	-	0.176	1.08	2.80E6	-
	-	1142.1	1.175	-	0.292	1.12	3.27E6	-
	-	2260.8	1.169	-	0.577	1.27	2.92E6	-
	-	3373.9	1.166	-	0.870	1.24	2.97E6	-
	-	4490.8	1.165	-	1.162	1.21	3.04E6	-
	-	5555.8	1.159	-	1.402	1.44	2.64E6	-
θ 1	14240	-	1.142	19.85	-	-	-	-
	28182	-	1.136	40.08	-	-	-	-
	55179	-	1.124	63.60	-	1.15	-	7.56E8
	81888	-	1.118	91.42	-	-	-	-
	108015	-	1.112	128.44	-	2.34	-	3.68E8
	134049	-	1.108	141.79	-	-	-	-
YY 2	-	9717.2	3.445	-	0.111	2.46	-	-
XX 2	-	6044.9	3.823	-	0.055	1.60	-	-
θ2	259175	-	3.445	23.49	-	2.26	-	-
YY 3	-	10278.5	7.050	-	0.009	-	-	-
XX 3	-	10720.5	7.200	-	-	-	-	-
θ3	223621	-	6.400	2.60	-	-	-	-

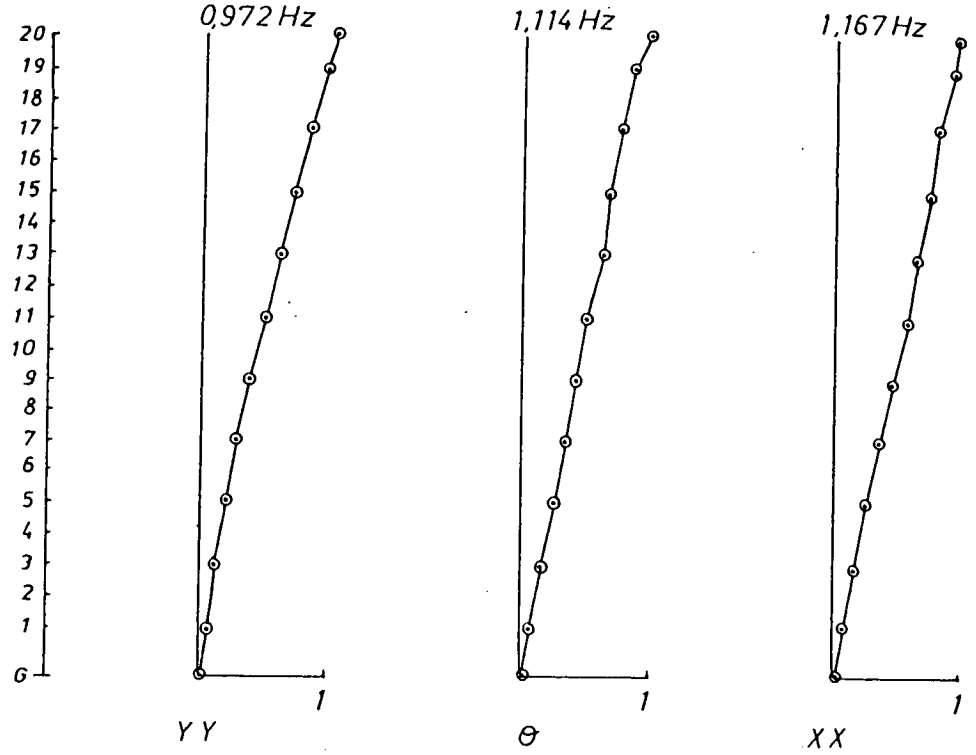

Figure 6.1 First mode shapes

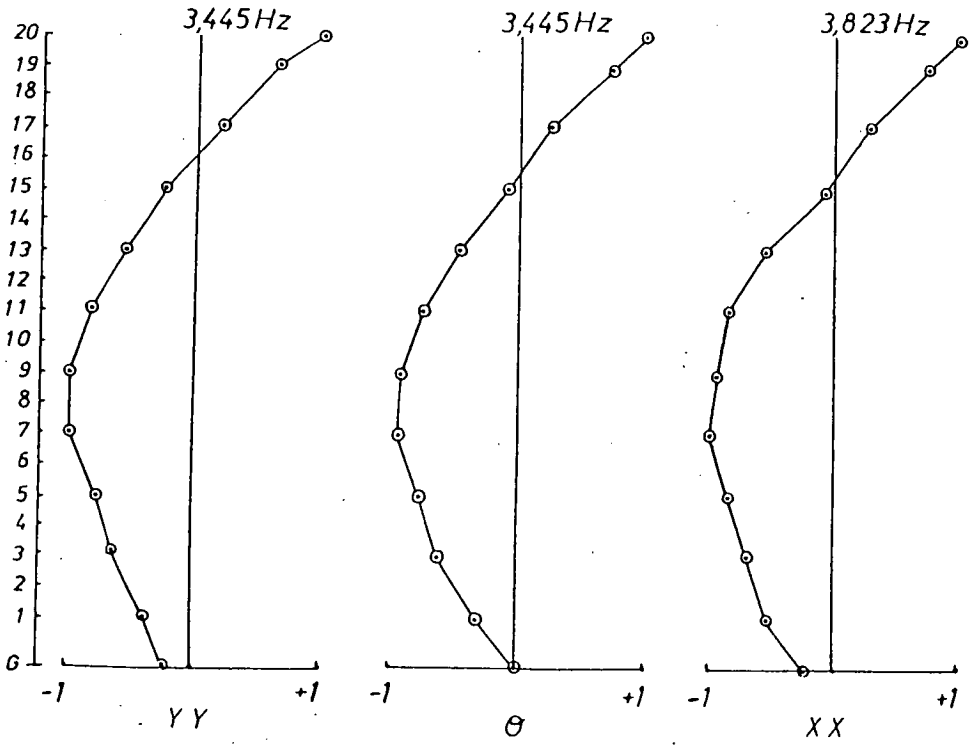

Figure 6.2 Second mode shapes

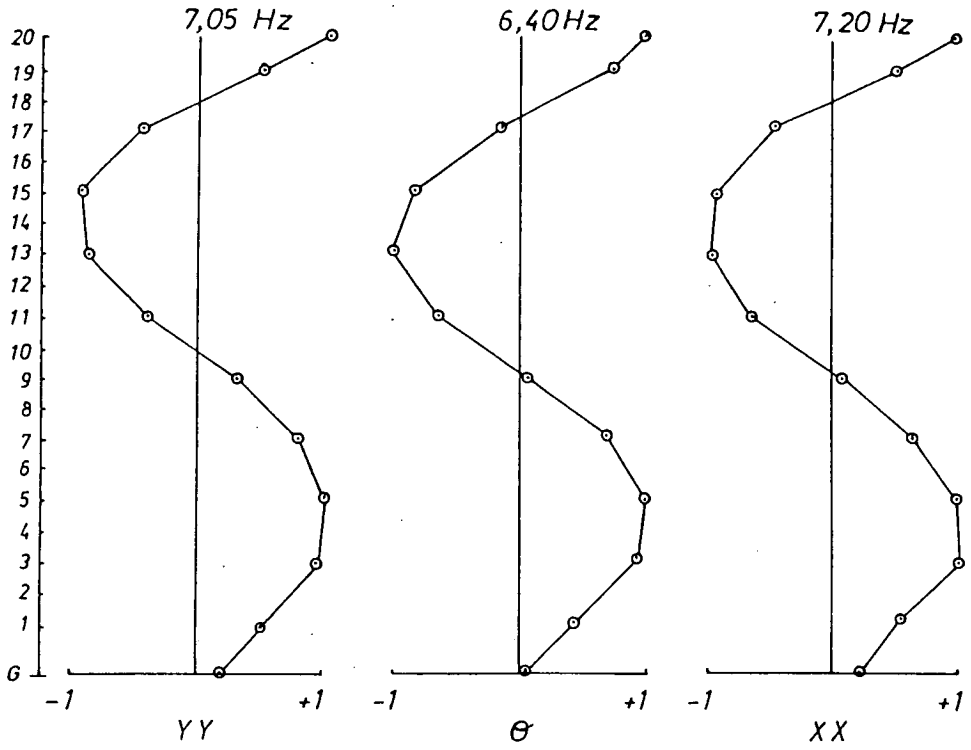

Figure 6.3 Third mode shapes

6.4.1 Concept of analysis

Prior to the actual analysis, a 'quick look' analysis was perfomed. This involved using an analysis parameter (such as sampling frequency and number of data) which were known to give large errors in the estimated function, but it also indicated the nature of the parameter to be used and the most beneficial type of analysis.

The available analysis was categorised into three functions; (i) time, (ii) amplitude, and (iii) frequency domain functions.

The quick look analysis indicated that the frequency domain function was the more appropriate type of analysis to use.

The useful quantity for this analysis of time varying data was considered to be the PSD.

It is defined as in the limit $T \rightarrow \infty$ and $B \rightarrow 0$

$$G_y(f) = \frac{1}{BT} \int_0^T y_B^2 \ (f,t)$$

where B is a bandwidth in which $y_B(f,t)$ is observed and T is the time for which it is observed, (sampling time).

Since it is not possible to observe an infinitely long data, therefore the function is estimated as,

$$\hat{G}_y(f) = \frac{1}{BT} \int_0^T y_B^2 \ (f,t)$$

The function $G_y(f)$ is the single sided PSD and is no longer computed digitally by this means.

In practice the PSD is found by taking the Fourier Transform of time history. This procedure produced a function $S_y(f)$ which is

two sided PSD. $G_y(f)$ could be obtained from $S_y(f)$ from the relationship,

$$S_y(f) = 1/2 \quad G_y(f) \qquad f \geqslant 0$$

also $S_y(f)$ is an even function.

As a taperecorder was used for recording the data, it was possible to speed up the analysis by playing the tape faster,(x32). In this case, the analysis output needed to be multiplied by the speed up factor. This was because the speed up process had itself reduced the density of the data before the normalising process.

6.4.2 Error

The errors which occur due to estimation of the real values in the analysis of functions are characterised as bias and variance errors.

If a quantity Φ is estimated by $E[\overline{\Phi}]$, then the normalised standard error is defined as,

$$\varepsilon \left[\overline{\Phi} \right] = \frac{\sqrt{E \left[(\Phi - \overline{\Phi})^2 \right]}}{\Phi}$$

This is a dimensionless quantity which is equal to the square root of the mean square error, divided by the true value. In practice the standard error should be as small as possible and is used to estimate the confidence limits that can be placed on a measurement.

The standard error (ε) is equal to the sum of the bias (b) and the variance (s) errors.

The bias error in a PSD measurement can be avoided by choosing B

such that there are many estimates of the mean square value when $G_y(f)$ is changing rapidly. In practice this occurs when a resonent response occurs. If four estimates are chosen throughout the bandwidth of the response then the bias error is 5% and if 10 are used the bias error is 1%.

For the PSD when the bias error is negligible the standard error $\varepsilon \simeq 1/\sqrt{BT}$ [48]

The aim is normally to use a product of BT at least 100 (giving ε =0.1 or more).

In the analysis of JRC building data, due to the short length of recording time a BT of 50 was used, giving $\varepsilon = 1/\sqrt{50} = 14\%$

6.4.3 Results

The PSD for each transducer was obtained and presented in Figures 6.4 to 6.14. The reduction of the PSD plots produced the range (p-p) of vibration. The results for the accelerometers are tabulated in the Table 6.2. For illustration purposes the procedure of reduction for acceleration transducer 5 is shown below, (i.e. acceleration in the YY direction measured close to torsional centre at 20th floor level).

From Figure 6.6 peak response of - 5.5 db occurred at 0.99 Hz (1st YY)

peak response of -22.5 db occurred at 3.45 Hz (2nd YY)

1st YY

To convert the db to ratio use $10^{0.1 \times db}$ (e.g. $-3db = 10^{-0.3}$)

i.e. $10^{-.55} = 2.818E\text{-}1$

which when multiplied by the scaling factor of 0.00001 gives

$$S_y(f) = 2.818E\text{-}6 \ V^2/Hz$$

and so

$$G_y(f) = 5.637E\text{-}6\ V^2/Hz$$

To obtain V r.m.s.value, take square root, hence

$$\sqrt{G_y(f)} = 2.374E\text{-}3\ V\ r.m.s.$$

Due to the speed up process, multiply by 32

$$= 7.597E\text{-}2\ V\ r.m.s.$$

Calibration factor of accelerometer 6 is 118.69V/g (Table 5.2)

Therefore the resonant accelerations at the top of JRC building was

$$\ddot{X} = 7.019E\text{-}4\ g\ r.m.s.$$

which is equivalent to

$$\ddot{X}_{max} = 7.019E\text{-}4\ \sqrt{2}$$

$$= 9.9\ \ E\text{-}4\ g$$

To convert maximum acceleration to range of displacement at the top of the building in mm assuming harmonic motion, multiply by

$$2\ g\ 10^3/(2\omega)^2 f^2$$

$$= 5.03E\text{-}1\ \ mm\ p\text{-}p$$

For the reduction of PSD to mm p-p for the displacement transducers, the only step to be omitted from the above reduction process is the conversion of g r.m.s. to mm r.m.s. Table 6.3 illustrates the reduced results for the displacement transducers.(For calibration factors of displacement transducers see Table 5.1)

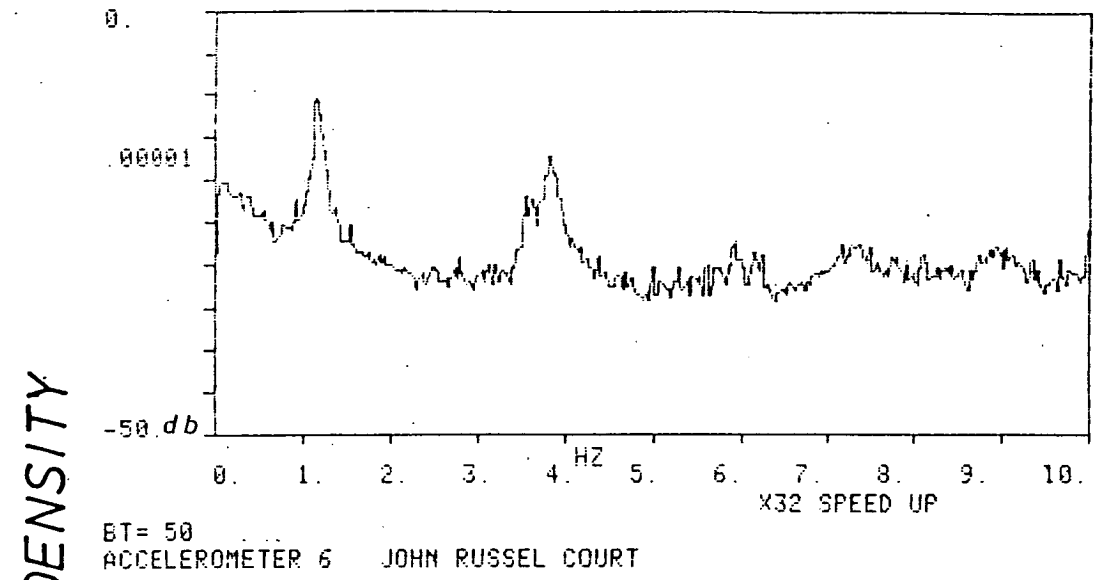

Figure 6.5

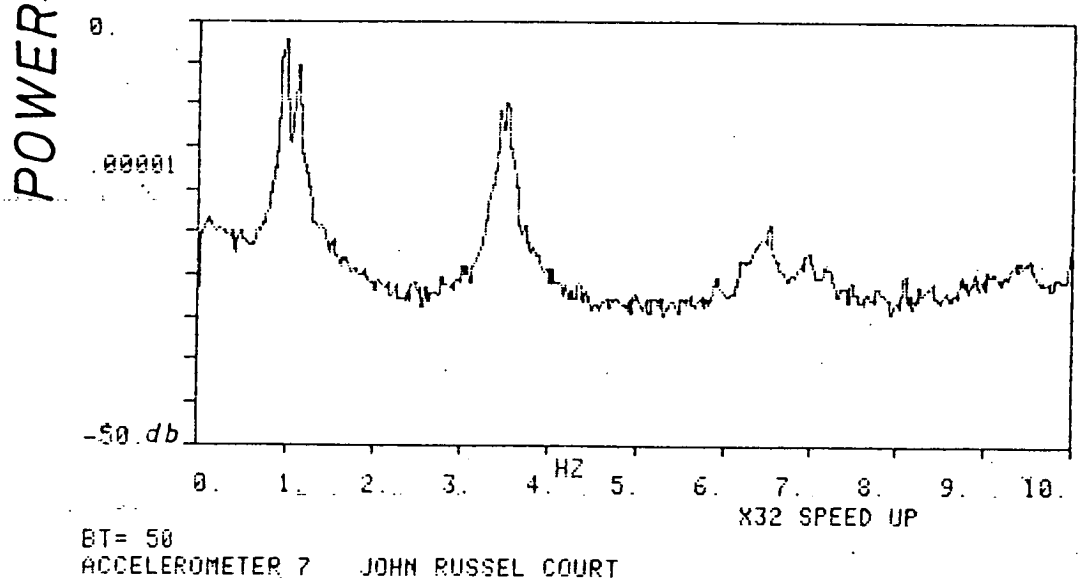

Figure 6.4

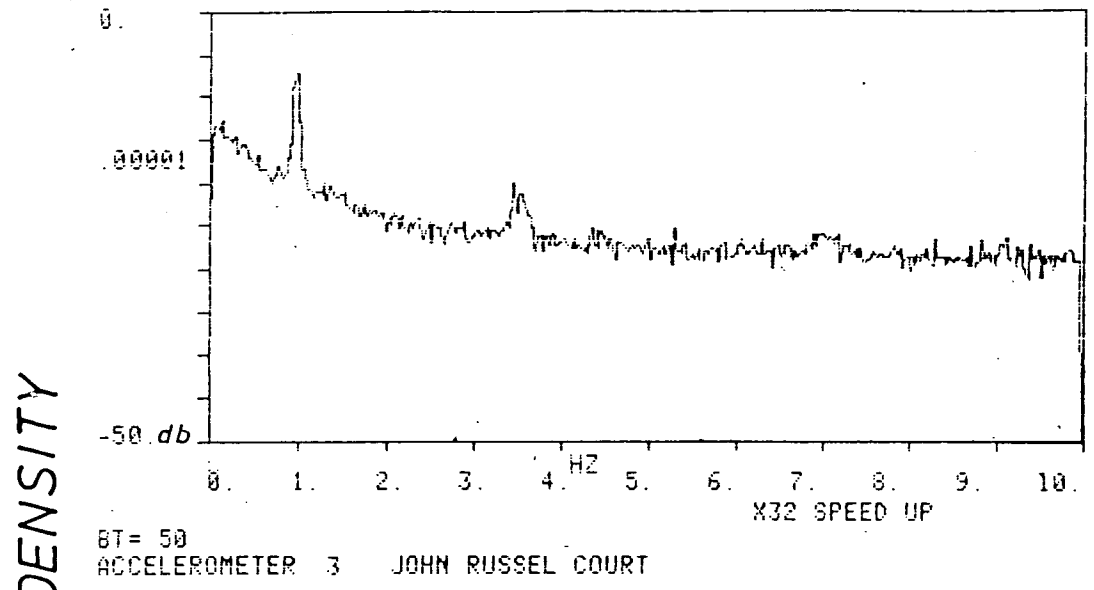

POWER SPECTRAL DENSITY

Figure 6.7

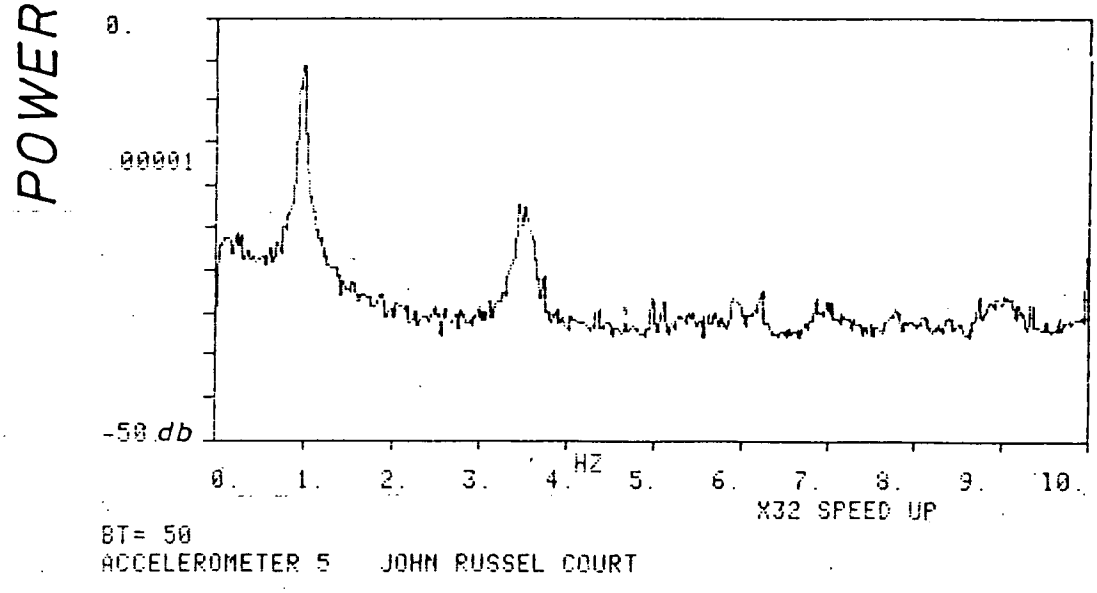

Figure 6.6

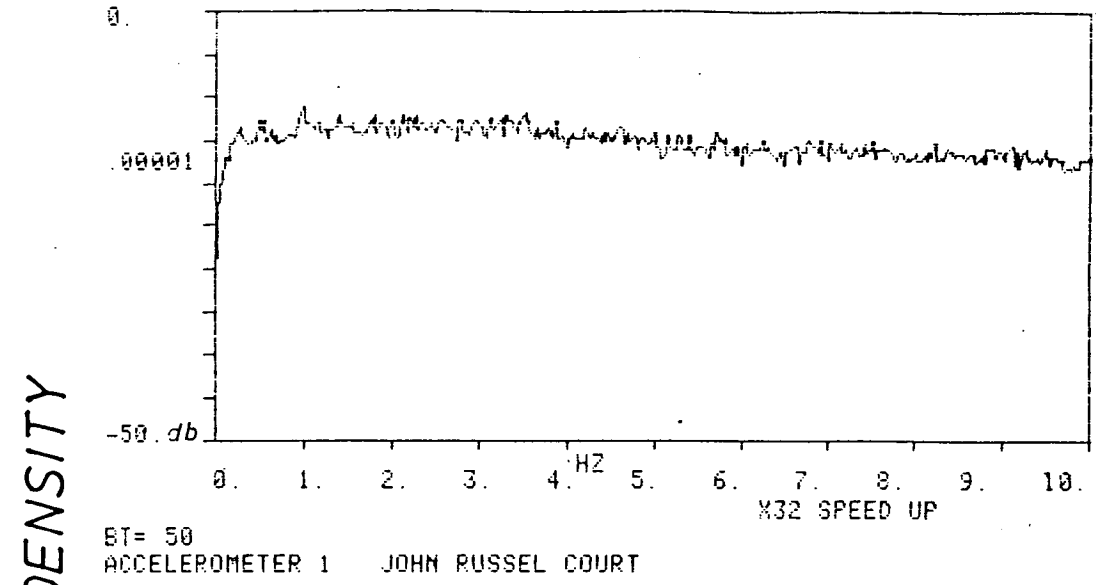

Figure 6.9

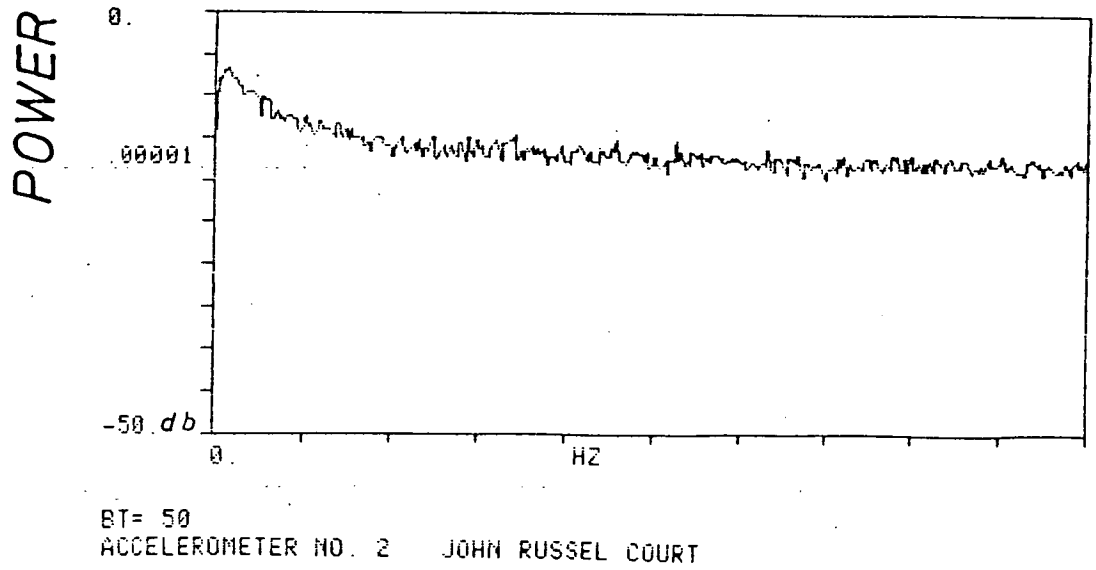

Figure 6.8

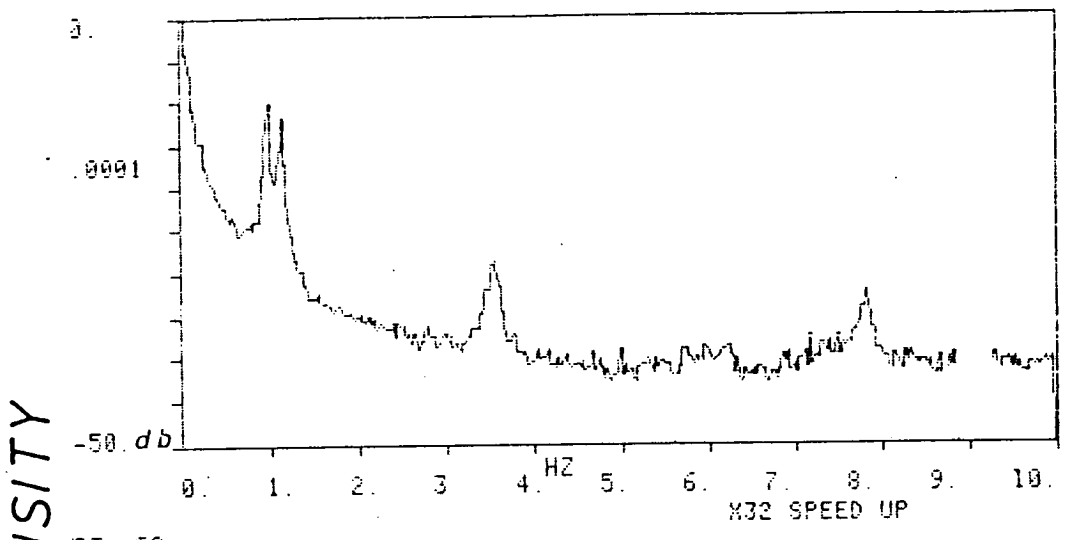

Figure 6.10 a

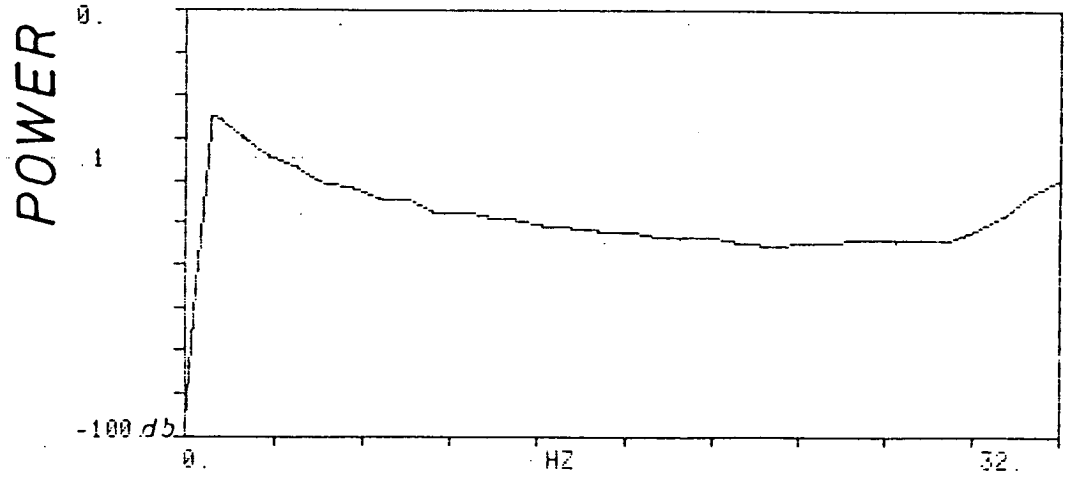

Figure 6.10 b

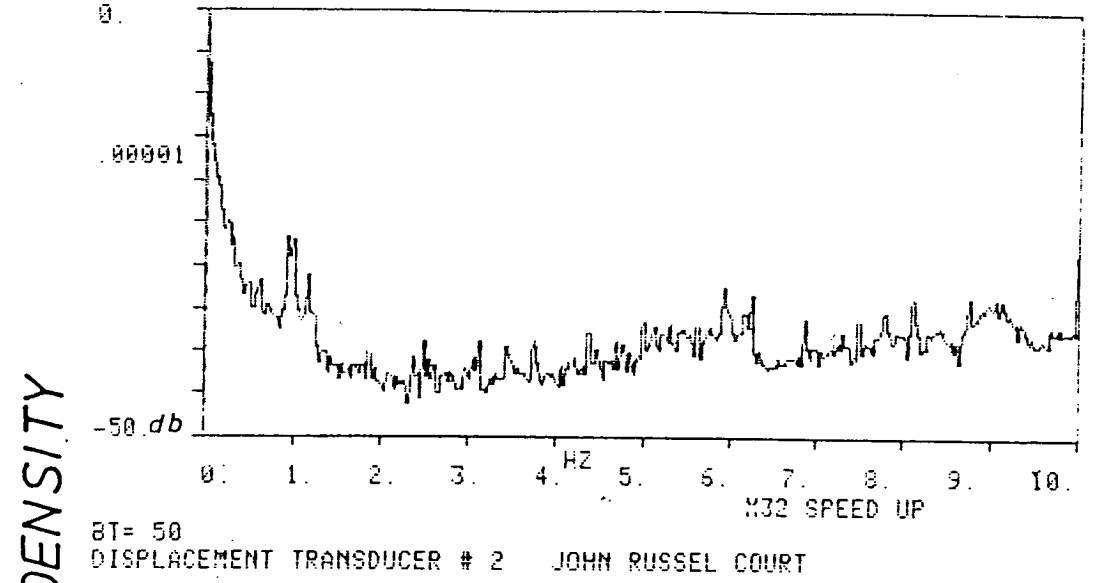

Figure 6.11

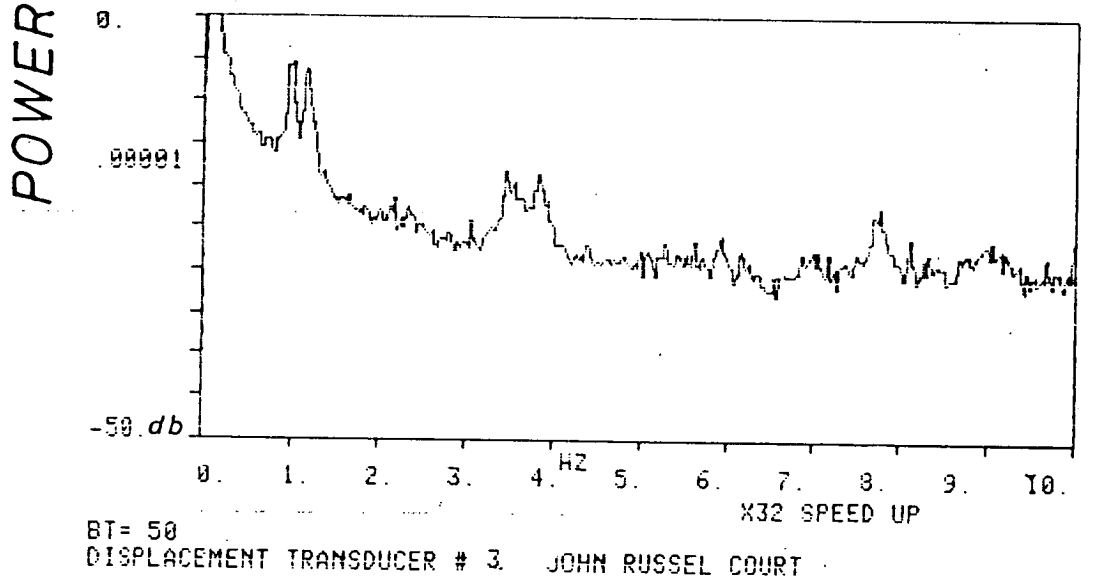

Figure 6.12

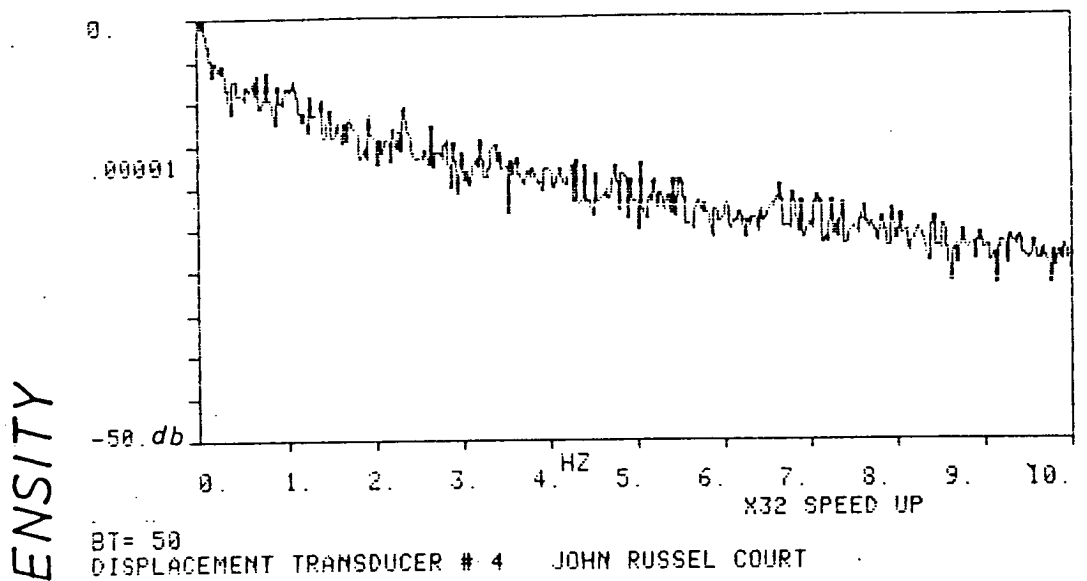

Figure 6.13

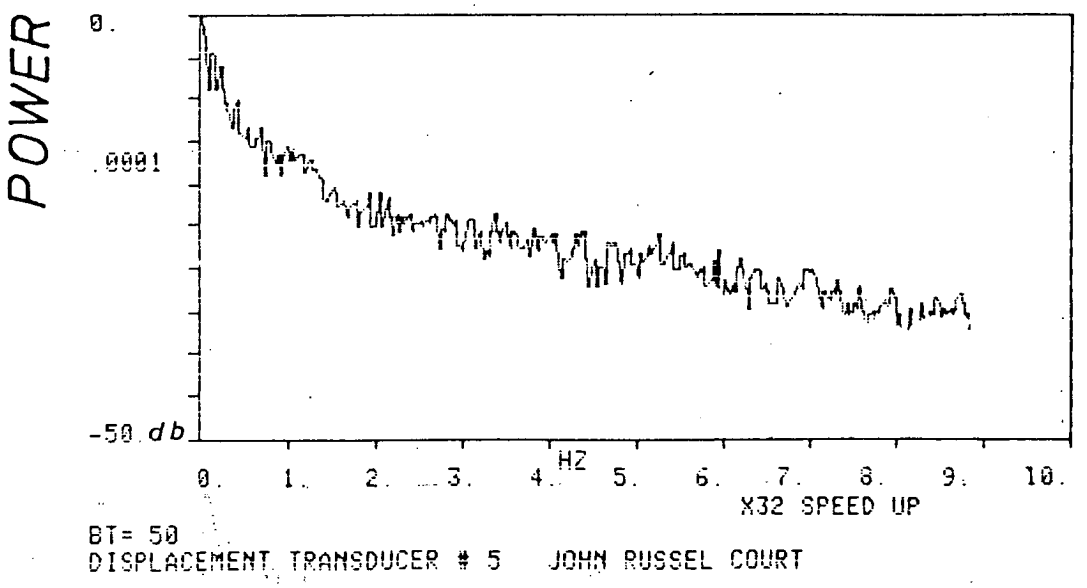

Figure 6.14

TABLE 6.2 ACCELERATION RESPONSE OF JRC DUE TO WIND EXCITATION*

ACCELERATION TRANSDUCER	PEAK RESPONSE (dB)	FREQUENCY (Hz)	DIRECTION	MODE	RANGE (mm p-p)
7	- 2.5	0.990	YY	1	6.13E-1
7	-10.0	3.445	YY	2	2.13E-2
7	-23.0	6.400	YY	3	1.39E-3
7	- 6.0	1.180	θ	1	2.89E-1
7	-10.0	3.450	θ	2	2.13E-2
7	-23.0	6.400	θ	3	1.39E-3
6	-11.0	1.180	XX	1	1.69E-1
6	-17.0	3.82	XX	2	8.12E-3
5	- 5.5	0.990	YY	1	5.03E-1
5	-22.5	3.450	YY	2	5.80E-3
4	-	-	XX	1	-
4	-	-	XX	2	-
3	- 7.0	0.990	YY	1	4.11E-1
3	-20.0	3.445	YY	2	7.61E-3
2	-	-	XX	1	-
2	-	-	XX	2	-
1	-	-	YY	2	-
1	-	-	YY	2	-

* Mean hourly wind speed = 6.05 m/s at 10 m reference height
wind direction 250° in azimuth

TABLE 6.3 DISPLACEMENT RESPONSE OF JRC DUE TO WIND EXCITATION*

DISPLACEMENT TRANSDUCER	PEAK RESPONSE (dB)	FREQUENCY (Hz)	DIRECTION	MODE	RANGE (mm p-p)
1	-10.0	0.990	YY	1	9.28E-3
1	-28.0	3.450	YY	2	1.17E-3
1	-12.0	1.180	θ	1	7.37E-3
1	-32.0	7.800			7.37E-4
2	-27.0	0.990	YY	1	1.76E-3
3	- 6.0	0.990	YY	1	4.95E-3
3	-18.0	3.450	XX, θ	2	1.24E-3
3	- 7.0	1.180	XX	1	4.41E-3
3	-18.0	3.450	XX, θ	2	1.24E-3
3	-18.0	3.90			1.24E-3
3	-24.0	7.80			6.23E-4
4	-	-	-	-	-
5	-	-	-	-	-
6	-	-	-	-	-
7	-	-	-	-	-

* Mean hourly wind speed = 6.05 m/s at 10 m reference height
wind direction 250^{0} in azimuth

6.5 RESPONSE PREDICTION

The response prediction of JRC building was calculated using two different methods.(i) Computer analysis method (RESPONSE), and (ii) the method described in ESDU 76001[49].

6.5.1 Computer program (RESPONSE)

The computer program (RESPONSE) was a slightly modified version of WREANO1[4] which was derived on the approach described by Etkin[50] dealing with the along-wind response of a vertical 'line like' structure. The theory from which WREANO1 was derived is concisely described in appendix 6.1. The preparation of data for the use of RESPONSE is presented below.

H=54.0 m B=23.6 m D=18.0 m f=0.99 Hz γ =374 kg/m^3 α =1.0 zeta=0.71%

$U(z_r)$ =6.1 m/s

α =0.3 from Table 1 ESDU 76001

α_T=0.08 ESDU 75001[51]

$Z_G = 900 Z_o^{0.18}$

$Z_o = 150 \exp(-1.39/0.3)$

Assume Z_o = 1.0 for consistencecy with ESDU 76001

therefore Z_G =900 m

$\bar{U}(Z_r) = (Z_r/H)^{\alpha} \bar{U}(H)$

Therefore

$\bar{U}(H)$ = 10.12 m/s

$2\sigma_u(H)/\bar{U}(H)$ = 0.47 Kanda[4] (Fig.B, see appendix 6.2)

$\sigma_u(H)$ = 2.378

$\sigma_u(Z_r) = (Z_r/H)^{\alpha_T} \sigma_u(H)$

= 2.721

Therefore $\sigma_u(Z_r)/U(Z_r)$ = 2.721/6.1 =0.446

$L(Z_G) = 3.3Z_G + 1500$

$=4470$ m

$L(Z_r) = 4470(10/900)^{0.5}$

$=471$

$\alpha_L = 0.5 - \alpha_\mu$

$=0.2$

$k_y(Z_r) = 7.0(10/900)^{-0.19}$

$=16.46$

$k_z(Z_r) = 6.0(10/900)^{-0.19}$

$=14.11$

$= 2.0$ Harris[52] and ESDU74031[53]

$C_{D_o} = 1.4$ NAKAGUCHI[54] and BEARMAN[55]

$\tilde{C}_{D_{qs}}/C_{D_o} = 0.8$

$\tilde{C}_{D_1}/C_{D_o} = 1.1$ Kanda[4] (Figure 4.14,see appendix 6.2)

The results obtained by the use of the RESPONSE program are presented in appendix 6.3.

6.5.2 ESDU 76001 method

The prediction method described by the ESDU 76001 document[49] was based on the assumptions that the total response or load effect could be considered in three parts. (i)mean value, (ii) a non-resonant fluctuating component, and (iii) a dynamic or resonant fluctuating component for which there may be significant contributions from more than one mode of vibration.

The main advantage of the component method was in its relative simplicity. Additionally any cross coupling effects between various modes due to the incident gusts were automatically

included. However according to Jeary and Ellis[56] the predictions made by the Canadian code[19] lay much closer to actual measurements than the predictions made by the ESDU 76001 document. Their views were based on the analysis of some good quality data for which, overall, the correlation between measurement and prediction was poor.

The procedure outlined by the use of this method is presented in Appendix 6.4.

6.6 DISCUSSION OF RESULTS

Considering the dynamic calibration tests on the JRC building, the results illustrated the fact that the damping ratio of the building was a function of the modal force for each fundamental frequency, Figure 6.15.

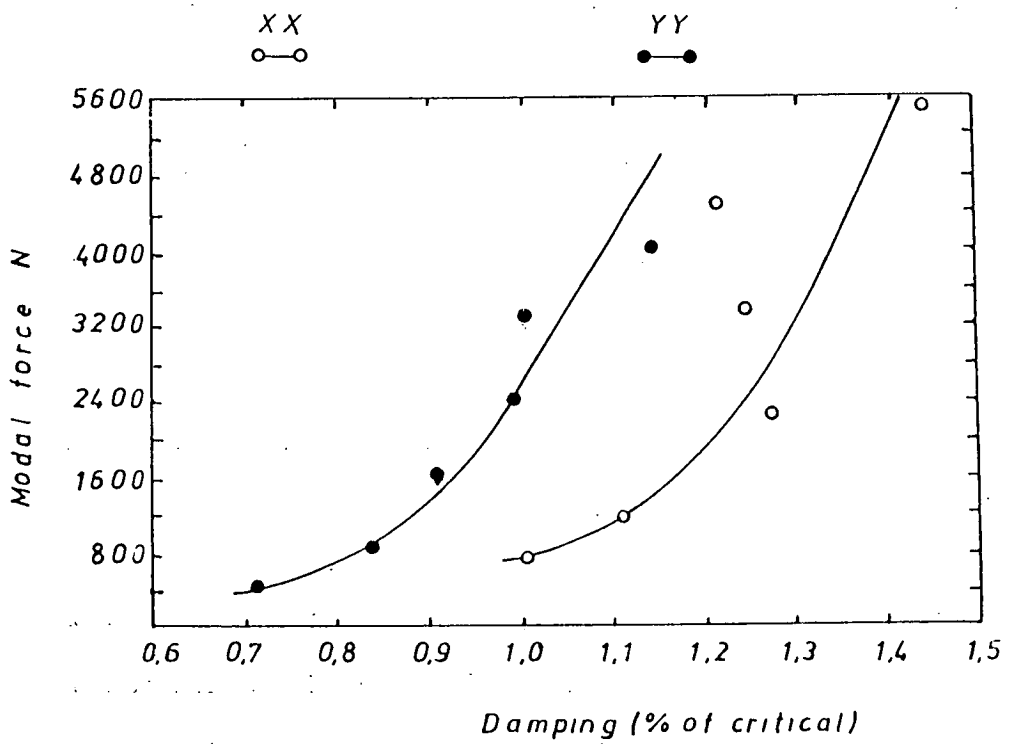

Figure 6.15 Relationship between the modal force and the damping ratio at the translational fundamental frequencies

These results support the view that a structure could be considered as a system made of several elements with different degrees of fixity relative to each other, and that its damping capacity depended primarily on the friction forces set up during motion. When such a system was resonated with a modal force, a certain amount of relative movement between elements would be set up depending on the amount of static friction to be overcome.

By increasing the displacement of the system due to an increase of modal force it could be expected that more sliding friction would be brought into play with a consequent increase in damping capacity.

It was clear also from the forced excitation work that the mode shape, whether it was in translation or torsion, was not dependent on the magnitude of the modal force, see Figures 6.1, 6.2, and 6.3. However at the higher modes some movement was evident at the base (see Figure 6.2 and 6.3) which had not occurred at the fundamental frequency, see Figure 6.1. The movement suggested some degree of partial fixity at the base and although it was not detectable at the fundamental frequencies this could be attributed to the level of the modal force being insufficient.

The experimental mode shapes for the first three modes conform very closely with those predicted for a cantilever type structure as can be seen by comparing Figures 6.1, 6.2, and 6.3 with the theoretical ones for the corresponding modes given in Figure 4.1

In a mean hourly speed of 6.05 m/s (measured at the reference height of 10 m above ground level at Turnhouse airport 10 km South West of the building) acting almost parallel to the YY axis of the structure a significant response occurred. The loading was

sufficient to cause a measurable response in the form of horizontal accelerations at the 12th and 19th floor levels, and relative horizontal shear displacement between ground and first floor level, as can be seen from Table 6.2 and 6.3 respectively.

Since the wind excitation causing these responses was approximately parallel to the YY axis of the building it could be expected that the responses in this direction would be greater. Using the peak to peak range of translational response in the YY direction from transducer 3, Table 6.3, the r.m.s. translational response, δ 01 can be obtained in that direction. Using the corresponding stiffness computed for the structural elements in that floor level, see section 3.3.2.2, an equivalent static drag coefficient, C_D1, associated with the first mode frequency can be deduced as follows.

Table 6.3 gives δ 01 = 1.76E-3/2$\sqrt{2}$ = 0.62E-3 mm

Using the relationship, δ 01 x k 1 = F

where

k01 is the stiffness of the building between the first floor and ground (Table 3.2 a), and

F is the force above the level 0-1 which induce the displacement δ01, and also

$$F = 1/2 \quad air.C_{D1}[\bar{U}(h/2)]^2.b.H$$

where

$\bar{U}(h/2)$ is the mean hourly wind speed at h/2 = $6.1(25.8/10)^{0.3}$ m/s,

b is the width of the structure, and

h is the height of the structure (H) minus half of first storey height

i.e. h = H - (h0-1)/2

= 51.6 m

Therefore

$$C_D1 = 2x1.75E-6x0.699E10x9.81/\ 1.23x(8.1)^2x23.6x51.6$$

$$C_D1 = 2.44$$

This value of C_D1 is comparable with the static drag coefficient, $C_D = 2.4$[54,55] and indicates that the method of determination of the stiffness of a storey height was not unreasonable.

In the above deductions of a value for C_D the response component in the YY direction from displacement transducer number 3 was utilised. This transducer was orientated along the XX axis and located very near to the torsional centre. Consequently any response in the YY direction could be considered due to translation only. It would have been better to have utilised transducer number 2 located in the same position and orientated along the YY axis but some doubt had arisen over its calibration, see Table 5.1. The fact that XX and YY response components were obtained from transducer number 3 indicated translation in both those directions was taking place in addition to the torsion represented by the difference between the YY component from transducer numbers 1 and 2.

The two methods of forced excitation testing of the structure revealed very good agreement for the dynamic characteristics of the structure in the YY directions, see Tables 3.6,3.7, and 6.1. The extended forced vibration testing yielded also dynamic characteristics in translation and torsion for modal frequencies up to approximately 7 Hz. Above this level frequencies would be excited only by low energy components in the wind and would have an insignificant effect on the response. Consequently modes higher than the third were not sought.

The modal mass determinations in the extended forced vibration tests provided a means of checking the estimated total mass of the structure. It was shown in section6.2 that the modal mass is one third of the total mass assuming a linear first mode shape, and consequently estimates of the total mass were made and compared in Table 6.4 with a direct estimate of mass from the original design drawings,(Table 3.1).

TABLE 6.4 Estimates of mass of JRC building

Mass deduced from design calculations and drawings kg x E-6	Estimates of mass from modal force		
	Direction of force	Mean total mass kg x E-6	Overall mean total mass kg x E-6
8.584	XX	8.82	
	YY	9.86	9.34

The agreement between the two approaches for estimating the mass is quite good considering the nature of the drawing from which a typical floor level was used to compute the mass of the beams in the structure. and the assumption of a linear first mode shape. Also there were a maximum deviations from the experimental means of the mass deduced from excitation about the two orthogonal axes of the order of 27%.

The response of the building in a 6.05 m/s (10 m reference height) mean hourly wind speed is summarised in Table 6.5 in terms of the peak acceleration response at the fundamental frequency in the YY direction.

Table 6.5 Peak accelerations at 20th floor level in YY direction	
Source	Maximum accelerations xE-4 g
Transducer No.5 YY direction	9.9
Prediction using RESPONSE program	5.6 (see appendix 6.3)
Prediction using ESDU procedure	19.6 (see appendix 6.4)

These accelerations are small. The predicted acceleration by the RESPONSE program method being lower but of the same order as the experimentally measured value and the ESDU method of prediction giving a value almost twice that measured.

CHAPTER 7

GENERAL DISCUSSION AND CONCLUSIONS

7.1 GENERAL DISCUSSION

The difference between the measured and predicted frequencies has been highlighted by the results obtained in both chapters 3 and 6 from which it could be seen that the predictions were of the order of 150% greater for the YY direction and 370% for the XX direction.

The extended forced vibration tests reported in chapter 6 indicated that the direct estimate of the total mass of the structure and that obtained via the modal mass approach differed by less than 9%.

Some confidence in the approach to the stiffness estimation of the building structure was derived in chapter 6 from the deductions relating to the equivalent static drag coefficient at the fundamental frequency in the YY direction.

Thus it would appear unlikely that errors in mass and superstructure stiffness estimates could account for the large discrepancy between measured and predicted fundamental frequencies.

In chapter 6 the extended forced vibration tests revealed that there was movement at the base, see Figures 6.2 and 6.3. Consequently the assumption of a rigid base in the methods of prediction is called into question. It is indicative that some interaction between soil and structure was occurring.

By contrast Ellis[38] from an examination of structures of a similar construction had found no base movement and felt that

soil-structure interaction had little influence on the dynamic characteristics of those structures.

The foundation of this structure comprised a series of bearing piles on stiff boulder clay supporting a base slab through three heavy strip pile caps. There was no evidence of any differential settlement in the structure.

The measurement of actual response to wind excitation were confined to one fairly light wind of mean hourly speed of 6.05 m/s. The predictive methods of response were at variance with one another as can be seen in Table 6.5. The RESPONSE program approach was closer to the measured value, but below it whereas the ESDU[49] approach was much greater than the measured value. However the measured value itself was based on only one hour of the one and half hours of measurement. More measurements would be required to increase the reliability of the results obtained.

It should be noted that the fundamental frequencies of the building were very close to each other - 0.99 Hz, 1.14 Hz, and 1.18 Hz in translation parallel to YY, translation parallel to XX and torsion respectively (see Table 6.1) - and hence coupling of modal displacements could be expected. The measured modal value of acceleration in a particular direction would be augmented by such effects. In the second mode Table 6.1 shows that coupling between torsion and translation parallel to the YY axis would be more marked since those modal frequencies were equal. However the degree of separation between first and second mode frequencies would ensure no coupling between them.

In the ESDU approach only one drag coefficient, a static one, equal to 1.0 was employed. By comparison a static drag coefficient

= 2.4 was adopted in the RESPONSE program method with a quasi static drag coefficient = 2.0 and a dynamic drag coefficient of 2.4, (based on these experimental findings).

It is interesting to extend the methods of prediction to estimate response in a strong wind, say 32.5 m/s mean hourly wind speed at the 10 m reference height. This is the 50 year return wind speed for the Edinburgh area[6].

The results of such an exercise are presented in the Appendices 6.3 and 6.4 and are summarised in Table 7.1 in terms of the maximum accelerations, and the associated r.m.s.amplitude of displacement.

Table 7.1 Predicted translational response at top of structure in a 32.5 m/s mean hourly wind speed (10 m reference height)

Source	Maximum acceleration x g	R.M.S amplitude of displacement mm
RESPONSE program	0.126* 0.053**	8.3* 4.5**
ESDU method	0.037	6.6

* corresponds to the use of $\widetilde{C}_D$ = 5.76

** corresponds to the use of $\widetilde{C}_D$ = 2.40

At this higher wind speed the RESPONSE program method gives a much higher prediction of the response. In this case the RESPONSE program approach uses C_{D_o}= 2.4, C_{Dqs}= 2.0, and $\widetilde{C}_D$= 5.76, the latter value being obtained from Figure B in Appendix 6.2. By comparison, at the lower mean hourly wind speed of 6.05 m/s a value of $\widetilde{C}_D$= 2.4 was used based on the deductions from the measured data. No such full scale experimental information was available for the higher wind speed. It is worth mentioning that if the value used for $\widetilde{C}_D$

at 6.05 m/s i.e. $\widetilde{C}_D = 2.4$, were employed at the 32.5 m/s wind speed the RESPONSE program prediction for the maximum acceleration and r.m.s. displacement at the top of the structure would be of the order of that from the ESDU procedure but still above it.

The static drag coefficient used in the ESDU computations and the drag ratios taken from Kanda's proposals (see Figure B in appendix 6.2) were based on two dimensional wind tunnel tests. The real building is a three dimensional body and drag both of a static and dynamic nature could be dependent on spatial distribution effects. Also Figure B in appendix 6.2 shows the ratio of dynamic to static drag increasing towards infinity as the reduced velocity approaches zero. This is not physically feasible since at very low reduced velocity the turbulence component in the wind will reduce in magnitude and have little energy to excite much dynamic behaviour. Consequently the ratio $\widetilde{C}_D/C_{D_o}$ must drop to zero at zero reduced velocity and the family of curves shown in the Figure B must turn over at a peak value and reduce to zero. Therefore the value of $\widetilde{C}_D = 5.76$ at the higher mean hourly wind speed could be an overestimate.

Further experimental information is required to clarify these points.

It is quite apparent that the magnitude of the predicted responses is well above threshold limits of human preception[57] and is consistent with a private survey[58] of the building in which it was found that all tenants in the building living between levels 12 and 19 at the time of the Edinburgh hurricane in Jan. 1968 (3 second gust speeds $\simeq$ 45 m/s at 10 m reference height) were aware of building motion. This awareness seemed to increase with height as might be expected.

Both methods of prediction make use of power law expressions for the variation with height of various wind characteristics. These expressions are based on limited amounts of available data from a few sites in various parts of the world. Discrepancies between the predictions of both methods with actual measurements could be explained more thoroughly if localised wind data could be obtained. The system outlined in chapter 2 for wind data collection could be very helpful in this respect. More measurements of the structure's dynamic behaviour at different mean hourly wind speeds are required in order to have a better chance of understanding the behaviour and verifying or improving the capabilities of the prediction method.

An area of great interest in this work was centred on drag coefficients in an endeavour to determine whether there was any dependence of drag on height of a structure and on modal frequency. The system devised for measuring horizontal relative wind shear displacements was sensitive enough to detect a dynamic response in the first floor level at the fundamental frequencies in translation. However at higher modes the exciting force was not large enough to cause a measurable dynamic response. Similarly at the intermediate storeys (7th and 13th) which were instrumented in the same way the power spectra showed no discernible dynamic peaks. However the wind speed involved was quite low and the overall indications are that at higher velocities such responses might be detected premitting the derivation of drag coefficients for the parts of the structure above the level of measurement. Hence it should be possible to investigate whether there is any frequency and/or height dependence of drag in a tall bluff structure.

7.2 CONCLUSIONS

1/ The fundamental translational frequencies of JRC building were 1.18 Hz, and 0.99 Hz in the directions parallel to the XX and YY axes respectively. The fundamental torsional frequency was 1.14 Hz.

2/ The second mode translational frequencies of JRC building were 3.82 Hz, and 3.45 Hz in the directions parallel to the XX and YY axes respectively. The second mode torsional frequency was 3.45 Hz.

3/ The third mode translational frequencies of JRC building were 7.20 Hz, and 7.05 Hz in the directions parallel to the XX and YY axes respectively. The third mode torsional frequency was 6.40 Hz.

4/ The method used for the estimation of the mass of JRC building compared well with the experimentally found value.

5/ The damping ratio of JRC building was found to be a function of the modal force.

6/ An equivalent static drag force coefficient, C_D associated with the first mode frequency was experimentally found to be equal to 2.44.

7/ The normalised mode shape was found to be constant irrespective of the magnitude of the force causing the

displacements.

8/ The amplitude modulation/demodulation system to increase the number of record channels on the taperecorder proved very successful. The cross-talk from band pass to the base band channels was measured to be of the order of 1% of full scale deflection, while cross-talk from the base band to the band pass channels was too small to be measured.

9/ The maximum acceleration of JRC building at the 20th floor level in YY direction due to a wind speed of 6.05 m/s mean hourly at a reference height of 10 m was 9.9E-4 g.

10/ The structure moves dynamically at its base level.

11/ A sufficiently sensitive system has been devised for measuring relative horizontal wind shear displacement.

12/ The prediction methods used (RESPONSE program and the method outlined by ESDU 76001) confirmed that, the structural excitation caused by a wind speed of 32.5 m/s at 10 m reference height (50 year return wind speed of 50 m/s, 3 second gust at a reference height of 10 m) would be well above the human preception level.

REFERENCES

1 HARRIS,R.I. and DEAVES,D.M.

'The structure of strong wind'

CIRIA Wind Egineering in the Eighties Nov. 1980

2 DAVENPORT,A.G.

'The application of statistical concepts to the wind loading of structure'

Proceding of Institute of Civil Engineers Aug.61,Vol.19

3 HARRIS,R.I.

'The nature of wind'

Proc.of a Seminar on the modern design of wind sensitive structures, June 1970

4 KANDA,J.

'Dynamic along-wind response of tall bluff structures in strong wind'

Ph.D. Thesis, University of Edinburgh, 1979

5 BELL,M.H. and SHEARS,M.

'The assessment of wind effects in design practice'

Wind engineering in the eighties CRIA, Nov. 1980

6 BRISTISH STANDARD INSTITUTE

'CP3 Chapter5: Part2: 1972'

7 MAYNE,J.R.

'Unification of codes of practice'

Wind engineering in the eighties. CIRIA, Nov.1980

8 BRITISH STANDARD INSTITUTE

'Steel, concrete and composite bridges, Part 2 Specification for loads'

B.S.5400, 1978

9 DRAFT CODE OF PRACTICE

'Lattice towers and masts (loading)'

B.S.I.Document 78/13085

10 BRITISH STANDARD INSTITUTE

'Design of buildings and structures for agriculture Section Section 1.2

Design, construction and loading'

B.S.5502, 1978

11 BRITISH STANDARD INSTITUTE

'Slating and tiling'

B.S.5534, 1978

12 BRITISH STANDARD INSTITUTE

'Specification for steel chimneys'

B.S.4076, 1978

13 BEARMAN,P.W.

'Areodynamic loads on buildings and structures'

Wind engineering in the eighties.

CIRIA Nov.1980

14 WYATT,T.A.

'The dynamic behaviour of structures subject to gust loading'

Wind engineering in the eighties. CIRIA Nov.1980

CIRIA Nov.1980

15 VICKERY,B.J.

'Notes on wind forces on tall buildings'

Australian standard 1170, Part 2, 1973

16 NATIONAL BUILDING CODE OF CANADA, 1970

'NRC Number 11246 and NRC Number 11530'

17 THE PROCEDINGS OF A SEMINAR ON THE MODERN DESIGN OF WIND SENSITIVE STRUCTURES

CIRIA 1970

18 AUSTRALIAN STANDARD

'Rules for minimum design loads on structures known as the SAA loading code Part 2 Wind forces'

AS 1170, Part 2, 1975

19 NATIONAL BUILDING CODE OF CANADA 1970 PART 4

'Design section 4.1 Structural loads and procedures'

20 CZESKOSLOVENSKA ATATNF NORMA

'Loading of building structures'

CSN 730035z 30.3.1967, Ueinnost od 1.2.1978

21 DANSK INGENIORFORENING'S CODE OF PRACTICE

'For loads for the design of building structures'

Dansk Standard DS 410.2 Oct.1977

22 DOCUMENT TECHNIQUE UNIFIE

'Regles definissant les effects de la neige et du vent sur sis constructions et annexes'

Regles, N.V.65 Revisees 1967 et Annexes Jan.1968

23 NETHERLANDS NORMALISATIVE INSTITUUT

'Regulations for the calculations of building structures'

'General considerations and loading'

NEN 3850 1e druk, Dec.1972

24 SVENSK BYGGNORM 67 SUPPLEMENT SBN-S 21:64

'Vindlastens dynamiska inveskan

25 WYATT,T.A

'Evaluation of gust response in practice'

Wind engineering in the eighties. CIRIA Nov.1980

26 BEARMAN,P.W.

'Wind induced oscillations of class E buildings and structures'

Wind engineering in the eighties. CIRIA Nov.1980

27 MELBOURNE,W.H.

'Cross-wind response of structures to wind action'

Proc.of 4th Conf. on wind effects on buildings and

structures. Heathrow, England 1975

28 BEARMAN,P.W.

'Dynamic loads on buildings and structures'

Wind engineering in the eighties. CIRIA Nov.1980

29 WHITBREAD,R.E.

'Model simulation of wind effects on structures'

Proc. Symp. on wind effects on structures. H.M.S.O.

London 1963

30 VICKERY,B.J. and DANENPORT, A.G.

'An investigation of the behaviour of the proposed Centre

Point Tower in Sydney, Australia.

University of Western Ontario, Faculty of Engineering.

Eng.Sci.Res.Rep.BLWT-1-70, 1970

31 KATO,B.A. , AKIYABN,H., KAWABATA,S. AND KANDA,J.

'Wind tunnel test for dynamic response of tall buildings'

Proc. 3rd Inter. Conf. on wind effects on buildings and structures. Tokyo 1971

32 ELLIS,N.

'A technique for evaluating the fluctuating aerodynamic forces on a flexible building'

Proc. Inter. Symp. on vibration problems in industry

UKAEA Windscale, 1973

33 DALGLIESH,W.A., COOPER,K.A. and TEMPLIN,J.T.

'Comperison of model and full-scale accelerations of a high-rise building'

Sixth Inter.Conference on Wind Engineering,

Australia March 1983, New Zealand April 1983

34 LLOYD,A. and THOMAS

'Kites and kite flying'

Hamlyn London 1978

35 PELHAM,D.

'Kites'

Penguin books limited, 1979

36 BLYTH and BLYTH CONSULTING ENGINEERS

'Private communication'

Edinburgh 1976

37 JEARY,A.P.

'Vibration theory gets a shake up'

NCE 3 Sept. 1981

38 ELLIS,B.R.

'An assessment of the accuracy of predicting the fundamental natural frequencies of buildings and the implications concerning the dynamic analysis of structures'

Proc. Instn. Civil Engrs. Part 2 Vol. 2 Sept.1980

39 CLOUGH,R.W. and PENZIEN,J.

'Dynamics of structures'

McGraw-Hill 1975

40 OHTMER,O.

'ICES-STRUDL Application Manual Vol.1 and 2'

EUROCOPI 1976

41 PAFEC 75

'PAFEC Theory handbook'

Pafec limited

Nottingham 1978

42 EARTHQUAKE OF FEB.1971,

'U.S.Government Printing Office, Washington 1973'

43 HOROWITZ and HILL

'The art of electronics'

Cambridge University Press 1980

44 HAMILTON,T.D.S.

'Handbook of linear integrated electronics for research'

McGraw-Hill 1977

45 DAVENPORT,A.G.

'Gust loading factors'

Journal of the structural division

Proc. of the American Soc. of Civil Engrs. June 1967 St.3

46 LAM,L.C.H. and LAM,R.P.

'Observation on some salient features of fullscale dynamic wind forces on a multistorey building'

Proc.I.C.E. Part 2 Dec.1982

47 JEARY,A.P.

'Induced vibration testing'

Inernational Association for Bridge and Structural Engineering'

Colloquim on Instrumentation of Structures.

Cambridge, 11-14 July 1983.

48 JEARY,A.P.

'Acquisition and analysis of time varying data'

Building Research Establishment Note N70/76 A 30.4.

May 1976

49 ESDU

'The response of flexible structures to atmospheric turbulence'
Data Item Number 76001
ESDU London, 1976

50 ETKIN, B.
'Theory of the response of a slender vertical structure to a turbulent wind with shear'
Compliation of papers persented at the meeting on Ground Wind Load Problems in relation to Launch Vehicles, NASA Langley Research Centre, Paper 21, June 1966

51 ESDU
'Characteristics of atmospheric turbulence near the ground- Part III: Variation in space and time for strong winds'
Data Item Number 75001
ESDU London, 1975

52 HARRIS, R.I.
'The nature of the wind'
Proc.Seminar on the modern design of wind-sensitive structures, London, 1970
CIRIA 1971

53 ESDU
'Characteristics of atmospheric turbulence near the ground_ Part II Single point data'
Data Item Number 74031
ESDU London, 1974

54 NAKAGUCHI,I.,HASHIMOTO,K. and MUTO,S.
'An experimental study on aerodynamic drag of rectangular cylinders'
J.Japan Society of Aero and Space Sciences, Vol.16,No 168, Japan 1968

55 BEARMAN,P.W. and TUREMAN,D.M.
'An investigation of the flow around rectangular cylinders'
Aero.Quart.Vol.23
1972

56 JEARY,A.P. and ELLIS,B.R.
'On predicting the response of tall buildings to wind excitation'
Sixth International Conference on Wind Engineering
Australia, March 1983, New Zealand, April 1983

57 CHANG,F.K.
'Human response to motions in tall buildings'
Proc.ASCE, 99(St6)
1973

58 MASTERTON,G.A. and ROYLES,R.
'Private communication based on a private survey of preception levels of JRC tenants at the time of the Edinburgh hurricane in Jan.1968.'

APPENDIX 3.1

CALCULATION OF THE MASS OF JRC BUILDING

Description		quantity	rate	mass in kg
floor area 1				
23.60x18.00	424.800			
area of cores cols				
	- 14.519			
area enclosed by cores				
3.72x2.36	- 8.779			
2.60x2.03	- 5.278			
2.03x2.03	- 4.121			
2.87x2.36	- 6.773			
	385.330	385.330 m^2		
(210mm plank/pot floor)			390.594 kg/m^2	150508
Total cross section area of conc. cores cols.= 17.109 at ht. of 4.763m		81.400 m^2	2400.000 kg/m^3	195576
1/2 of total cross section of conc.cores cols.above first floor =	7.216			
at height of 2.591 m		18.80 m^2	2400.000 kg/m^3	45121
Floor finishing		385.330 m^2	195.297 kg/m^2	72254
Allowance for partitions		385.330 m^2	73.236 kg/m^2	28820
Partition walls claddings				
	12773 +			
	5613 +			
	10104 +			
	14840			
	43330			43330
Average beam (floor 9 taken as average				50705
Superimposed load			195.297 kg/m^2	72205
Total dead load				451000
Total dead load + 1/2 super imp.				487000
Total dead load + super imp.				523000

Description		quantity	rate	mass in kg
floor area 2				
23.60x18.00	424.800			
area of cores cols				
	- 14.519			
area enclosed by cores				
3.62x2.36	- 8.543			
2.60x2.03	- 5.278			
2.03x2.03	- 4.121			
2.88x2.36	- 6.797			
	384.840	384.840 m^2		
(210mm plank/pot floor)			390.594 kg/m^2	150316
Total cross section area of conc. cores columns= 1/2 (14.512+14.519) at height of 2.591 m		37.610 m^3	2400.000 kg/m^3	90263
Floor finishing		385.840 m^2	195.297 kg/m^2	75158
Allowance for partitions		385.840 m^2	73.236 kg/m^2	28184
Partition walls claddings				
	12773 +			
	5613 +			
	10104 +			
	14840			
	43330			43330
Average beam (floor 9 taken as average)				50705
Superimposed load			195.297 kg/m^2	72254
Total dead load				438000
Total dead load + 1/2 super imp.				474000
Total dead load + super imp.				510000

Description		quantity	rate	mass in kg
floor area 3				
23.60x18.00	424.800			
area of cores cols				
	- 14.274			
area enclosed by cores				
3.72x2.36	- 8.779			
2.60x2.03	- 5.278			
2.03x2.03	- 4.121			
2.87x2.36	- 6.797			
	385.575	385.575 m^2		
(210mm plank/pot floor)			390.594 kg/m^2	150603
Total cross section area of conc. cores columns 1/2 (14.519+14.274) at height of 2.591 m		37.287 m^3	2400.000 kg/m^3	89489
Floor finishing		385.575 m^2	195.297 kg/m^2	75302
Allowance for partitions		385.575 m^2	73.236 kg/m^2	28238
Partition walls claddings	12773 +			
	5613 +			
	10104 +			
	14840			
	43330			43330
Average beam (floor 9 taken as average)				50705
Superimposed load			195.297 kg/m^2	72254
Total dead load				439000
Total dead load + 1/2 super imp.				475000
Total dead load + super imp.				511000

Description		quantity	rate	mass in kg
floor area 4				
23.60x18.00	424.800			
area of cores cols				
	- 14.519			
area enclosed by cores				
3.62x2.36	- 8.543			
2.60x2.03	- 5.278			
2.03x2.03	- 4.121			
2.88x2.36	- 6.797			
	384.840	384.840 m^2	390.594 kg/m^2	150316
(210mm plank/pot floor)				
Total cross section area of conc. cores columns 1/2 (14.274+14.177) at height of 2.591 m		36.858 m^3	2400.000 kg/m^3	88460
Floor finishing		384.840 m^2	195.297 kg/m^2	75158
Allowance for partitions		384.840 m^2	73.236 kg/m^2	28184
Partition walls claddings				
	12773 +			
	5613 +			
	10104 +			
	14840			
	43330			43330
Average beam (floor 9 taken as average)				50705
Superimposed load			195.297 kg/m^2	72254
Total dead load				436000
Total dead load + 1/2 super imp.				472000
Total dead load + super imp.				508000

Description		quantity	rate	mass in kg
floor area 5				
23.60x18.00	424.800			
area of cores cols				
	- 13.933			
area enclosed by cores				
3.72x2.36	- 8.779			
2.60x2.03	- 5.278			
2.03x2.03	- 4.121			
2.88x2.36	- 6.773			
	385.916	385.916 m^2	390.594 kg/m^2	150737
(210mm plank/pot floor)				
Total cross section area of conc. cores columns 1/2 (14.177+13.933) at height of 2.591 m		36.417 m^3	2400.000 kg/m^3	87400
Floor finishing		385.916 m^2	195.297 kg/m^2	75367
Allowance for partitions		385.916 m^2	73.236 kg/m^2	28263
Partition walls claddings	12773 +			
	5613 +			
	10104 +			
	14840			
	43330			43330
Average beam (floor 9 taken as average)				50705
Superimposed load			195.297 kg/m^2	72254
Total dead load				436000
Total dead load + 1/2 super imp.				472000
Total dead load + super imp.				508000

Description		quantity	rate	mass in kg
floor area 6				
23.60x18.00	424.800			
area of cores cols				
	- 14.177			
area enclosed by cores				
3.62x2.36	- 8.543			
2.60x2.03	- 5.278			
2.03x2.03	- 4.121			
2.88x2.36	- 6.797			
	385.182	385.182 m^2	390.594 kg/m^2	150450
(210mm plank/pot floor)				
Total cross section area of conc. cores columns 1/2 (13.932+14.177) at height of 2.591 m		36.415 m^3	2400.000 kg/m^3	87397
Floor finishing		385.182 m^2	195.297 kg/m^2	75225
Allowance for partitions		385.182 m^2	73.236 kg/m^2	28209
Partition walls claddings	12773 +			
	5613 +			
	10104 +			
	14840			
	43330			43330
Average beam (floor 9 taken as average)				50705
Superimposed load			195.297 kg/m^2	72254
Total dead load				436000
Total dead load + 1/2 super imp.				472000
Total dead load + super imp.				508000

Description		quantity	rate	mass in kg
floor area 7				
23.60x18.00	424.800			
area of cores cols				
	- 13.932			
area enclosed by cores				
3.72x2.36	- 8.779			
2.60x2.03	- 5.278			
2.03x2.03	- 4.121			
2.87x2.36	- 6.773			
	385.917	385.917 m^2	390.594 kg/m^2	150737
(210mm plank/pot floor)				
Total cross section area of conc. cores columns 1/2 (14.177+13.931) at height of 2.591 m		36.414 m^3	2400.000 kg/m^3	87393
Floor finishing		385.917 m^2	195.297 kg/m^2	75369
Allowance for partitions		385.917 m^2	73.236 kg/m^2	28263
Partition walls claddings				
	12773 +			
	5613 +			
	10104 +			
	14840			
	43330			43330
Average beam (floor 9 taken as average)				50705
Superimposed load			195.297 kg/m^2	72254
Total dead load				436000
Total dead load + 1/2 super imp.				472000
Total dead load + super imp.				508000

Description		quantity	rate	mass in kg
floor area 8				
23.60x18.00	424.800			
area of cores cols				
	- 12.828			
area enclosed by cores				
3.62x2.36	- 8.543			
2.60x2.03	- 5.278			
2.03x2.03	- 4.121			
2.88x2.36	- 6.797			
	386.531	386.531 m^2		
(210mm plank/pot floor)			390.594 kg/m^2	150977
Total cross section area of conc. cores columns 1/2 (13.931+12.828) at height of 2.591 m		34.666 m^3	2400.000 kg/m^3	83199
Floor finishing		386.531 m^2	195.297 kg/m^2	75488
Allowance for partitions		386.531 m^2	73.236 kg/m^2	28820
Partition walls claddings				
	12773 +			
	5613 +			
	10104 +			
	14840			
	43330			43330
Average beam (floor 9 taken as average)				50705
Superimposed load			195.297 kg/m^2	72254
Total dead load				432000
Total dead load + 1/2 super imp.				468000
Total dead load + super imp.				505000

Description		quantity	rate	mass in kg
floor area 9				
23.60x18.00	424.800			
area of cores cols				
	- 12.583			
area enclosed by cores				
3.72x2.36	- 8.779			
2.60x2.03	- 5.278			
2.03x2.03	- 4.121			
2.87x2.36	- 6.773			
	387.266	387.266 m^2		
(210mm plank/pot floor)			390.594 kg/m^2	151264
Total cross section area of conc. cores columns 1/2 (12.828+12.583) at height of 2.591 m		32.920 m^3	2400.000 kg/m^3	79008
Floor finishing		387.266 m^2	195.297 kg/m^2	75632
Allowance for partitions		387.266 m^2	73.236 kg/m^2	28362
Partition walls claddings				
	12773 +			
	5613 +			
	10104 +			
	14840			
	43330			43330
Average beam (floor 9 taken as average)				50705
Superimposed load			195.297 kg/m^2	72254
Total dead load				429000
Total dead load + 1/2 super imp.				465000
Total dead load + super imp.				501000

Description		quantity	rate	mass in kg
floor area 10				
23.60x18.00	424.800			
area of cores cols				
	- 12.828			
area enclosed by cores				
3.62x2.36	- 8.543			
2.60x2.03	- 5.278			
2.03x2.03	- 4.121			
2.88x2.36	- 6.797			
	386.531	386.531 m^2		
(210mm plank/pot floor)			390.594 kg/m^2	150977
Total cross section area of conc. cores columns 1/2 (12.583+12.828) at height of 2.591 m		32.920 m^3	2400.000 kg/m^3	79008
Floor finishing		386.531 m^2	195.297 kg/m^2	75488
Allowance for partitions		386.531 m^2	73.236 kg/m^2	28308
Partition walls claddings	12773 +			
	5613 +			
	10104 +			
	14840			
	43330			43330
Average beam (floor 9 taken as average)				50705
Superimposed load			195.297 kg/m^2	72254
Total dead load				428000
Total dead load + 1/2 super imp.				464000
Total dead load + super imp.				500000

Description	quantity	rate	mass in kg
floor area 11			
23.60x18.00 424.800			
area of cores cols			
- 12.582			
area enclosed by cores			
3.72x2.36 - 8.779			
2.60x2.03 - 5.278			
2.03x2.03 - 4.121			
2.87x2.36 - 6.773			
387.267	387.267 m^2		
(210mm plank/pot floor)		390.594 kg/m^2	151264
Total cross section area of conc. cores columns 1/2 (12.828+12.582) at height of 2.591 m	32.919 m^3	2400.000 kg/m^3	79005
Floor finishing	387.267 m^2	195.297 kg/m^2	75632
Allowance for partitions	387.267 m^2	73.236 kg/m^2	28362
Partition walls claddings			
12773 +			
5613 +			
10104 +			
14840			
43330			43330
Average beam (floor 9 taken as average)			50705
Superimposed load		195.297 kg/m^2	72254
Total dead load			429000
Total dead load + 1/2 super imp.			465000
Total dead load + super imp.			501000

Description		quantity	rate	mass in kg
floor area 12				
23.60x18.00	424.800			
area of cores cols				
	- 11.844			
area enclosed by cores				
3.62x2.36	- 8.543			
2.60x2.03	- 5.278			
2.03x2.03	- 4.121			
2.88x2.36	- 6.797			
	387.515	387.515 m^2		
(210mm plank/pot floor)			390.594 kg/m^2	151361
Total cross section area of conc. cores columns 1/2 (12.582+11.844)				
at height of 2.591 m		31.644 m^3	2400.000 kg/m^3	75945
Floor finishing		387.515 m^2	195.297 kg/m^2	75680
Allowance for partitions		387.515 m^2	73.236 kg/m^2	28380
Partition walls claddings				
	12773 +			
	5613 +			
	10104 +			
	14840			
	43330			43330
Average beam (floor 9 taken as average)				50705
Superimposed load			195.297 kg/m^2	72254
Total dead load				426000
Total dead load + 1/2 super imp.				462000
Total dead load + super imp.				498000

Description		quantity	rate	mass in kg
floor area 13				
23.60x18.00	424.800			
area of cores cols				
	- 11.599			
area enclosed by cores				
3.72x2.36	- 8.779			
2.60x2.03	- 5.278			
2.03x2.03	- 4.121			
2.87x2.36	- 6.773			
	388.250	388.250 m^2		
(210mm plank/pot floor)			390.594 kg/m^2	151648
Total cross section area of conc. cores columns 1/2 (11.844+11.599) at height of 2.591 m		30.370 m^3	2400.000 kg/m^3	72889
Floor finishing		388.250 m^2	195.297 kg/m^2	75824
Allowance for partitions		388.250 m^2	73.236 kg/m^2	28434
Partition walls claddings	12773 +			
	5613 +			
	10104 +			
	14840			
	43330			43330
Average beam (floor 9 taken as average)				50705
Superimposed load			195.297 kg/m^2	72254
Total dead load				423000
Total dead load + 1/2 super imp.				459000
Total dead load + super imp.				495000

Description		quantity	rate	mass in kg
floor area 14				
23.60x18.00	424.800			
area of cores cols				
	- 11.848			
area enclosed by cores				
3.62x2.36	- 8.543			
2.60x2.03	- 5.278			
2.03x2.03	- 4.121			
2.88x2.36	- 6.797			
	387.515	387.515 m^2		
(210mm plank/pot floor)			390.594 kg/m^2	151361
Total cross section area of conc. cores columns 1/2 (11.599+11.844) at height of 2.591 m		30.370 m^3	2400.000 kg/m^3	72889
Floor finishing		387.515 m^2	195.297 kg/m^2	75680
Allowance for partitions		387.515 m^2	73.236 kg/m^2	28380
Partition walls claddings				
	12773 +			
	5613 +			
	10104 +			
	14840			
	43330			43330
Average beam (floor 9 taken as average)				50705
Superimposed load			195.297 kg/m^2	72254
Total dead load				423000
Total dead load + 1/2 super imp.				459000
Total dead load + super imp.				495000

Description		quantity	rate	mass in kg
floor area 15				
23.60x18.00	424.800			
area of cores cols				
	- 11.598			
area enclosed by cores				
3.72x2.36	- 8.779			
2.60x2.03	- 5.278			
2.03x2.03	- 4.121			
2.87x2.36	- 6.773			
	388.251	388.251 m^2		
(210mm plank/pot floor)			390.594 kg/m^2	151649
Total cross section area of conc. cores columns 1/2 (11.844+11.598) at height of 2.591 m		30.369 m^3	2400.000 kg/m^3	72886
Floor finishing		388.251 m^2	195.297 kg/m^2	75824
Allowance for partitions		388.251 m^2	73.236 kg/m^2	28434
Partition walls claddings				
	12773 +			
	5613 +			
	10104 +			
	14840			
	43330			43330
Average beam (floor 9 taken as average)				50705
Superimposed load			195.297 kg/m^2	72254
Total dead load				423000
Total dead load + 1/2 super imp.				459000
Total dead load + super imp.				495000

Description		quantity	rate	mass in kg
floor area 16				
23.60x18.00	424.800			
area of cores cols				
	- 10.857			
area enclosed by cores				
3.62x2.36	- 8.543			
2.60x2.03	- 5.278			
2.03x2.03	- 4.121			
2.88x2.36	- 6.797			
	388.502	388.502 m^2		
(210mm plank/pot floor)			390.594 kg/m^2	151747
Total cross section area of conc. cores columns 1/2 (11.598+10.857) at height of 2.591 m		29.090 m^3	2400.000 kg/m^3	69817
Floor finishing		388.502 m^2	195.297 kg/m^2	75873
Allowance for partitions		388.502 m^2	73.236 kg/m^2	28452
Partition walls claddings				
	12773 +			
	5613 +			
	10104 +			
	14840			
	43330			43330
Average beam (floor 9 taken as average)				50705
Superimposed load			195.297 kg/m^2	72254
Total dead load				420000
Total dead load + 1/2 super imp.				456000
Total dead load + super imp.				493000

Description		quantity	rate	mass in kg
floor area 17				
23.60x18.00	424.800			
area of cores cols	- 10.606			
area enclosed by cores				
3.72x2.36	- 8.779			
2.60x2.03	- 5.278			
2.03x2.03	- 4.121			
2.87x2.36	- 6.773			
	389.243	389.243 m^2	390.594 kg/m^2	152036
(210mm plank/pot floor)				
Total cross section area of conc. cores columns 1/2 (10.857+10.606) at height of 2.591 m		27.805 m^3	2400.000 kg/m^3	66733
Floor finishing		389.243 m^2	195.297 kg/m^2	76018
Allowance for partitions		389.243 m^2	73.236 kg/m^2	28507
Partition walls claddings	12773 +			
	5613 +			
	10104 +			
	14840			
	43330			43330
Average beam (floor 9 taken as average)				50705
Superimposed load			195.297 kg/m^2	72254
Total dead load				418000
Total dead load + 1/2 super imp.				454000
Total dead load + super imp.				490000

Description		quantity	rate	mass in kg
floor area 18				
23.60x18.00	424.800			
area of cores cols				
	- 10.857			
area enclosed by cores				
3.62x2.36	- 8.543			
2.60x2.03	- 5.278			
2.03x2.03	- 4.121			
2.88x2.36	- 6.797			
	388.502	388.502 m^2		
(210mm plank/pot floor)			390.594 kg/m^2	151747
Total cross section area of conc. cores columns 1/2 (10.606+10.857) at height of 2.591 m		27.805 m^3	2400.000 kg/m^3	66733
Floor finishing		388.502 m^2	195.297 kg/m^2	75873
Allowance for partitions		388.502 m^2	73.236 kg/m^2	28452
Partition walls claddings	12773 +			
	5613 +			
	10104 +			
	14840			
	43330			43330
Average beam (floor 9 taken as average)				50705
Superimposed load			195.297 kg/m^2	72254
Total dead load				417000
Total dead load + 1/2 super imp.				453000
Total dead load + super imp.				489000

Description		quantity	rate	mass in kg
floor area 19				
23.60x18.00	424.800			
area of cores cols				
	- 9.818			
area enclosed by cores				
3.72x2.36	- 8.779			
2.60x2.03	- 5.278			
2.03x2.03	- 4.121			
2.87x2.36	- 6.773			
	390.031	390.031 m^2		
(210mm plank/pot floor)			390.594 kg/m^2	152344
Total cross section area of conc. cores columns 1/2 (10.857+9.818) at height of 2.591 m		26.784 m^3	2400.000 kg/m^3	64283
Floor finishing		390.031 m^2	195.297 kg/m^2	76172
Allowance for partitions		390.031 m^2	73.236 kg/m^2	28564
Partition walls claddings	12773 +			
	5613 +			
	10104 +			
	14840			
	43330			43330
Average beam (floor 9 taken as average)				50705
Superimposed load			195.297 kg/m^2	72254
Total dead load				416000
Total dead load + 1/2 super imp.				452000
Total dead load + super imp.				488000

Description		quantity	rate	mass in kg
floor area roof				
23.60x18.00	424.800			
area enclosed by cores				
3.62x2.36	- 8.543			
2.60x2.03	- 5.278			
2.03x2.03	- 4.121			
2.88x2.36	- 6.797			
	399.359	399.359 m^2	390.594 kg/m^2	155987
(210mm plank/pot floor)				
Total cross section area of conc. cores columns				
1/2(9.818)x2.591+	12.719			
0.15x1.75x5.486x4+	+ 5.760			
0.15x1.75x3.700x2+	+ 1.943			
1.75x0.38x0.40	+ 0.266	20.688 m^3	2400.000 kg/m^3	49651
Approximate vol. of Penthouse		20.688 m^3	2400.000 kg/m^3	49651
Waterproofing roofing		399.359 m^2	195.297 kg/m^2	77994
Partition walls claddings				
	12773 +			
	5613 +			
	10104 +			
	14840			
	43330			43330
Average beam (floor 9 taken as average)				50705
Superimposed load			195.297 kg/m^2	72254
Total dead load				428000
Total dead load + 1/2 super imp.				464000
Total dead load + super imp.				500000

APPENDIX 3.2

CALCULATIONS OF THE STIFFNESS OF JRC BUILDING

Ground-1 about XX axis

Ixx corner cols.	$4x(40x107^3)/12$	=	0.163	m^4
Ixx int. cols.	$6x(42x107^3)/12$	=	0.257	m^4
Ixx gable cols.	$4x(38x99^3)/12$	=	0.242	m^4
Ixx int. cols.	$6x(38x122^3)/12$	=	0.345	m^4
TOTAL Ixx cols.			1.007	m^4
Ixx walls =	$15^3/12(540+372+236+128+43+290+234+30+112+408+408)+$		0.009	m^4
	$15/12(145^3+15^3+130^3+248^3+278^3+99^3+142^3+36^3+36^3+370^3+203^3+91^3+20^3+203^3+203^3)$		1.530	m^4
TOTAL Ixx walls			2.546	m^4
E conc. walls			21.0E9	N/m^4
E conc. cols.			28.0E9	N/m^4
L cols.			4.763	m
kl xx cols. =	$12 E I / L^3$		0.312E10	N/m
kl xx walls =	$12 E I / L^3$		0.357E10	N/m
TOTAL klx			0.669E10	N/m

Ground - 1 about YY axis

Iyy corner cols.	$4x(107x40^3)/12$	=	0.023	m^4
Iyy int.cols.	$6x(107x42^3)/12$	=	0.040	m^4
Iyy gable cols.	$4x(122x40^3)/12$	=	0.026	m^4
Iyy int. cols.	$6x(122x38^3)/12$	=	0.033	m^4
TOTAL Iyy cols.			0.122	m^4

$$I_{yy\ walls} = 15^3/12(145+130+99+15+248+278+142+370+203+36+36+91+20+203+203)$$ 0.006 m^4

$$+15/12(540^3+372^3+236^3+128^3+290^3+290^3+234^3+112^3+408^3+408^3+30^3+43^3)$$ 5.289 m^4

TOTAL Iyy walls	5.417	m^4
kl yy cols. = $12 E I / L^3$	0.038E10	N/m
kl yy walls = $12 E I / L^3$	1.233E10	N/m
TOTAL kly	1.271E10	N/m

1-2 Level about XX axis

Ixx gable cols.	$8x(25x99^3)/12$	=	0.162	m^4
Ixx ext. cols.	$6x(42x99^3)/12$	=	0.204	m^4
Ixx int. cols.	$6x(38x122^3)/12$	=	0.345	m^4
TOTAL Ixx cols.			0.711	m^4
Ixx walls =	$15^3/12(458+281+458+290+290+234+$			
	$234+458+458+62+62)+$		0.009	m^4
	$15/12(236^3+20^3+140^3+28^3+203^3 x3+$			
	$236^3+125^3+92^3+20^3+20^3+28^3)$		0.712	m^4
TOTAL Ixx walls			0.721	m^4
E conc. walls			21.0E9	N/m^4
E conc. cols.			28.0E9	N/m^4
L cols.			2.591	m
k2 xx cols. =	$12 E I / L^3$		1.373E10	N/m
k2 xx walls =	$12 E I / L^3$		1.045E10	N/m
TOTAL k2x			2.418E10	N/m

1-2 Level about YY axis

Iyy gable cols.	$8x(99x25^3)/12$	=	0.010 m^4
Iyy ext. cols.	$6x(99x42^3)/12$	=	0.037 m^4
Iyy int. cols.	$6x(107x38^3)/12$	=	0.033 m^4
TOTAL Iyy cols.			0.080 m^4

$$Iyy\ walls = 15^3/12(236+140+20+28+203x3+92+20+20+236+125+28)+$$

$$15/12(458^3+281^3+458^3+290^3+290^3+234^3+234^3+458^3+458^3+62^3+62^3)$$

		0.004 m^4
		6.017 m^4
TOTAL Iyy walls		6.021 m^4
k2 yy cols. =	$12 E I / L^3$	0.155E10 N/m
k2 yy walls =	$12 E I / L^3$	8.723E10 N/m
TOTAL k2y		8.878E10 N/m

2-3 Level about XX axis

Ixx gable cols.	$8x(25x99^3)/12$	= 0.162	m^4
Ixx int. cols.	$6x(38x122^3)/12$	= 0.345	m^4
Ixx ext. cols.	$6x(38x99^3)/12$	= 0.184	m^4
TOTAL Ixx cols.		0.691	m^4
Ixx walls =	$15^3/12(478+281+478+290+290+234+234+478+478+62+62)+$	0.009	m^4
	$15/12(118^3+20^3+236^3+15^3+203^3+203^3x3+236^3+178^3+15^3+5^3)$	0.838	m^4
TOTAL Ixx walls		0.844	m^4
E conc. walls		21.0E9	N/m^4
E conc. cols.		28.0E9	N/m^4
L cols.		2.591	m
k3 xx cols. =	$12 E I / L^3$	1.335E10	N/m
k3 xx walls =	$12 E I / L^3$	1.227E10	N/m
TOTAL k3x		2.562E10	N/m

2-3 Level about YY axis

Iyy gable cols.	$8x(99x25^3)/12$	=	0.010	m^4
Iyy int. cols.	$6x(99x38^3)/12$	=	0.027	m^4
Iyy ext. cols.	$6x(122x38^3)/12$	=	0.033	m^4
TOTAL Iyy cols.			0.070	m^4

$$I_{yy\ walls} = 15^3/12(236+118+20+15+203+203+203+236+178+15+5) + 0.004\ m^4$$

$$+15/12(478^3+281^3+478^3+290^3+290^3+234^3+234^3+478^3+478^3+62^3+62^3) \quad 6.674\ m^4$$

TOTAL Iyy walls	6.748	m^4
k3 yy cols. = $12\ E\ I\ /\ L^3$	0.135E10	N/m
k3 yy walls = $12\ E\ I\ /\ L^3$	9.776E10	N/m
TOTAL k3y	9.911E10	N/m

3-4 Level about XX axis

Ixx gable cols.	$8x(25x99^3)/12$	=	0.162	m^4
Ixx int. cols.	$6x(38x122^3)/12$	=	0.345	m^4
Ixx ext. cols.	$6x(38x99^3)/12$	=	0.184	m^4
TOTAL Ixx cols.			0.691	m^4
Ixx walls =	$15^3/12(458+458+281+290+290+234+30+112+458+458+62+62)+$		0.009	m^4
	$15/12(237^3+20^3+140^3+28^3+203^3+203^3 x3+125^3+236^3+20^3+28^3)$		0.808	m^4
TOTAL Ixx walls			0.817	m^4
E conc. walls			21.0E9	N/m^4
E conc. cols.			28.0E9	N/m^4
L cols.			2.591	m
k4 xx cols. =	$12 E I / L^3$		1.335E10	N/m
k4 xx walls =	$12 E I / L^3$		1.184E10	N/m
TOTAL k4x			2.519E10	N/m

3-4 Level about YY axis

Iyy gable cols.	$8x(99x25^3)/12$	=	0.010	m^4
Iyy int.cols.	$6x(99x38^3)/12$	=	0.027	m^4
Iyy ext. cols.	$6x(122x38^3)/12$	=	0.033	m^4
TOTAL Iyy cols.			0.070	m^4

$$Iyy\ walls = 15^3/12(237+140+20+28+203x4+236+20+125+28)+$$
$$15/12(458^3+281^3+458^3+290^3+290^3+234^3+458^3+458^3+112^3+30^3+62^3+62^3)$$

	5.875	m^4
TOTAL Iyy walls	5.880	m^4
k4 yy cols. = $12\ E\ I\ /\ L^3$	0.135E10	N/m
k4 yy walls = $12\ E\ I\ /\ L^3$	8.519E10	N/m
TOTAL k4y	8.654E10	N/m

4-5 Level about XX axis

Ixx gable cols.	$8x(25x99^3)/12$	=	0.162	m^4
Ixx int. cols.	$6x(38x107^3)/12$	=	0.233	m^4
Ixx ext. cols.	$6x(38x99^3)/12$	=	0.184	m^4
TOTAL Ixx cols.			0.579	m^4
Ixx walls =	same as floor 2		0.009	m^4
			0.838	m^4
TOTAL Ixx walls			0.847	m^4
E conc. walls			21.0E9	N/m^4
E conc. cols.			28.0E9	N/m^4
L cols.			2.591	m
k5 xx cols. =	$12 E I / L^3$		1.118E10	N/m
k5 xx walls =	$12 E I / L^3$		1.227E10	N/m
TOTAL k5x			2.345E10	N/m

4-5 Level about YY axis

Iyy gable cols.	$8x(99x25^3)/12$	=	0.010 m^4
Iyy int. cols.	$6x(99x38^3)/12$	=	0.027 m^4
Iyy ext. cols.	$6x(107x38^3)/12$	=	0.029 m^4
TOTAL Iyy cols.			0.066 m^4
Iyy walls =	same as floor 2		0.004 m^4
			6.674 m^4
TOTAL Iyy walls			6.744 m^4
k5 yy cols. =	$12 E I / L^3$		0.128E10 N/m
k5 yy walls =	$12 E I / L^3$		9.771E10 N/m
TOTAL k5y			9.899E10 N/m

5-6 Level about XX axis

Ixx gable cols.	$8x(25x99^3)/12$	=	0.162	m^4
Ixx int. cols.	$6x(38x107^3)/12$	=	0.233	m^4
Ixx ext. cols.	$6x(38x99^3)/12$	=	0.184	m^4
TOTAL Ixx cols.			0.579	m^4
Ixx walls =	same as floor 1		0.009	m^4
			0.712	m^4
TOTAL Ixx walls			0.721	m^4
E conc. walls			21.0E9	N/m^4
E conc. cols.			28.0E9	N/m^4
L cols.			2.591	m
k6 xx cols. =	$12 E I / L^3$		1.118E10	N/m
k6 xx walls =	$12 E I / L^3$		1.045E10	N/m
TOTAL k6x			2.163E10	N/m

5-6 Level about YY axis

Iyy gable cols.	$8x(99x25^3)/12$	=	0.010	m^4
Iyy int. cols.	$6x(99x38^3)/12$	=	0.027	m^4
Iyy ext. cols.	$6x(107x38^3)/12$	=	0.029	m^4
TOTAL Iyy cols.			0.066	m^4
Iyy walls =	same as floor 1		0.004	m^4
			6.017	m^4
TOTAL Iyy walls			6.021	m^4
k6 yy cols. =	$12 E I / L^3$		0.128E10	N/m
k6 yy walls =	$12 E I / L^3$		8.723E10	N/m
TOTAL k6y			8.851E10	N/m

6-7 Level about XX axis

Ixx gable cols.	$8x(25x99^3)/12$	=	0.162	m^4
Ixx int. cols.	$6x(38x107^3)/12$	=	0.233	m^4
Ixx ext. cols.	$6x(38x99^3)/12$	=	0.184	m^4
TOTAL Ixx cols.			0.579	m^4
Ixx walls =	same as floor 2		0.009	m^4
			0.838	m^4
TOTAL Ixx walls			0.847	m^4
E conc. walls			21.0E9	N/m^4
E conc. cols.			28.0E9	N/m^4
L cols.			2.591	m
k7 xx cols. =	$12 E I / L^3$		1.118E10	N/m
k7 xx walls =	$12 E I / L^3$		1.227E10	N/m
TOTAL k7x			2.345E10	N/m

6-7 Level about YY axis

Iyy gable cols.	$8x(99x25^3)/12$	=	0.010 m^4
Iyy int.cols.	$6x(99x38^3)/12$	=	0.027 m^4
Iyy ext. cols.	$6x(107x38^3)/12$	=	0.028 m^4
TOTAL Iyy cols.			0.066 m^4
Iyy walls =	same as floor 2		0.004 m^4
			6.674 m^4
TOTAL Iyy walls			6.678 m^4
k7 yy cols. =	$12 E I / L^3$		0.128E10 N/m
k7 yy walls =	$12 E I / L^3$		9.675E10 N/m
TOTAL k7y			9.803E10 N/m

7-8 Level about XX axis

Ixx gable cols.	$8x(25x99^3)/12$	=	0.162	m^4
Ixx int. cols.	$6x(38x107^3)/12$	=	0.233	m^4
Ixx ext. cols.	$6x(38x99^3)/12$	=	0.184	m^4
TOTAL Ixx cols.			0.579	m^4
Ixx walls =	same as floor 3		0.009	m^4
			0.808	m^4
TOTAL Ixx walls			0.817	m^4
E conc. walls			21.0E9	N/m^4
E conc. cols.			28.0E9	N/m^4
L cols.			2.591	
k8 xx cols. =	$12 E I / L^3$		1.118E10	N/m
k8 xx walls =	$12 E I / L^3$		1.184E10	N/m
TOTAL k8x			2.302E10	N/m

7-8 Level about YY axis

Iyy gable cols.	$8x(99x25^3)/12$	=	0.010 m^4
Iyy int. cols.	$6x(99x38^3)/12$	=	0.027 m^4
Iyy ext. cols.	$6x(107x38^3)/12$	=	0.029 m^4
TOTAL Iyy cols.			0.066 m^4
Iyy walls =	same as floor 3		0.005 m^4
			5.875 m^4
TOTAL Iyy walls			5.880 m^4
k8 yy cols. =	$12 E I / L^3$		0.128E10 N/m
k8 yy walls =	$12 E I / L^3$		8.519E10 N/m
TOTAL k8y			8.647E10 N/m

8-9 Level about XX axis

Ixx gable cols.	$8x(25x76^3)/12$	=	0.073	m^4
Ixx int. cols.	$6x(38x76^3)/12$	=	0.083	m^4
Ixx ext. cols.	$6x(38x91^3)/12$	=	0.143	m^4
TOTAL Ixx cols.			0.299	m^4
Ixx walls =	same as floor 2		0.009	m^4
			0.838	m^4
TOTAL Ixx walls			0.847	m^4
E conc. walls			21.0E9	N/m^4
E conc. cols.			28.0E9	N/m^4
L cols.			2.591	m
k9 xx cols. =	$12 E I / L^3$		0.578E10	N/m
k9 xx walls =	$12 E I / L^3$		1.227E10	N/m
TOTAL k9x			1.805E10	N/m

8-9 Level about YY axis

Iyy gable cols.	$8x(76x25^3)/12$	=	0.008	m^4
Iyy int.cols.	$6x(76x38^3)/12$	=	0.021	m^4
Iyy ext. cols.	$6x(91x38^3)/12$	=	0.025	m^4
TOTAL Iyy cols.			0.054	m^4
Iyy walls =	same as floor 2		0.004	m^4
			6.674	m^4
TOTAL Iyy walls			6.678	m^4
k9 yy cols. =	$12 E I / L^3$		0.104E10	N/m
k9 yy walls =	$12 E I / L^3$		9.675E10	N/m
TOTAL k9y			9.779E10	N/m

9-10 Level about XX axis

Ixx gable cols.	$8x(25x76^3)/12$	=	0.073	m^4
Ixx int. cols.	$6x(38x76^3)/12$	=	0.083	m^4
Ixx ext. cols.	$6x(38x91^3)/12$	=	0.143	m^4
TOTAL Ixx cols.			0.299	m^4
Ixx walls =	same as floor 1		0.009	m^4
TOTAL Ixx walls			0.721	m^4
E conc. walls			21.0E9	N/m^4
E conc. cols.			28.0E9	N/m^4
L cols.			2.591	m
k10xx cols. =	$12 E I / L^3$		0.578E10	N/m
k10xx walls =	$12 E I / L^3$		1.045E10	N/m
TOTAL k10x			1.623E10	N/m

9-10 Level about YY axis

Iyy gable cols.	$8x(76x25^3)/12$	=	0.008	m^4
Iyy int. cols.	$6x(76x38^3)/12$	=	0.021	m^4
Iyy ext. cols.	$6x(91X38^3)/12$	=	0.025	m^4
TOTAL Iyy cols.			0.054	m^4
Iyy walls =	same as floor 1		0.004	m^4
			6.017	m^4
TOTAL Iyy walls			6.021	m^4
k10yy cols. =	$12 E I / L^3$		0.104E10	N/m
k10yy walls =	$12 E I / L^3$		8.723E10	N/m
TOTAL k10y			8.827E10	N/m

10-11 Level about XX axis

Ixx gable cols.	$8x(25x76^3)/12$	=	0.073	m^4
Ixx int. cols.	$6x(38x76^3)/12$	=	0.083	m^4
Ixx ext. cols.	$6x(38x91^3)/12$	=	0.143	m^4
TOTAL Ixx cols.			0.299	m^4
Ixx walls =	same as floor 2		0.009	m^4
			0.838	m^4
TOTAL Ixx walls			0.847	m^4
E conc. walls			21.0E9	N/m^4
E conc. cols.			28.0E9	N/m^4
L cols.			2.591	m
k11xx cols. =	$12 E I / L^3$		0.578E10	N/m
k11xx walls =	$12 E I / L^3$		1.227E10	N/m
TOTAL k11x			1.805E10	N/m

10-11 Level about YY axis

Iyy gable cols.	$8x(76x25^3)/12$	=	0.008	m^4
Iyy int. cols.	$6x(76x38^3)/12$	=	0.021	m^4
Iyy ext. cols.	$6x(91x38^3)/12$	=	0.025	m^4
TOTAL Iyy cols.			0.054	m^4
Iyy walls =	same as floor 2		0.008	m^4
			6.674	m^4
TOTAL Iyy walls			$6.678X10^8$	m^4
klyy cols. =	$12 E I / L^3$		0.104E10	N/m
klyy walls =	$12 E I / L^3$		9.675E10	N/m
TOTAL kly			9.779E10	N/m

11-12 Level about XX axis

Ixx gable cols.	$8x(25x76^3)/12$	=	0.073	m^4
Ixx int. cols.	$6x(38x76^3 9/12$	=	0.083	m^4
Ixx ext. cols.	$6x(38x91^3)/12$	=	0.143	m^4
TOTAL Ixx cols.			0.299	m^4
Ixx walls =	same as floor 3		0.009	m^4
			0.808	m^4
TOTAL Ixx walls			0.817	m^4
E conc. walls			21.0E9	N/m^4
E conc. cols.			28.0E9	N/m^4
L cols.			2.591	m
k12xx cols. =	$12 E I / L^3$		0.578E10	N/m
k12xx walls =	$12 E I / L^3$		1.184E10	N/m
TOTAL k12x			1.762E10	N/m

11-12 Level about YY axis

Iyy gable cols.	$8x769x25^3)/12$	=	0.008 m^4
Iyy int. cols.	$6x(76x38^3)/12$	=	0.021 m^4
Iyy ext. cols.	$6x(91x38^3)/12$	=	0.025 m^4
TOTAL Iyy cols.			0.054 m^4
Iyy walls =	same as floor 3		0.004 m^4
			5.875 m^4
TOTAL Iyy walls			5.879 m^4
k12yy cols. =	$12 E I / L^3$		0.104E10 N/m
k12yy walls =	$12 E I / L^3$		8.517E10 N/m
TOTAL k12y			8.621E10 N/m

12-13 Level about XX axis

Ixx gable cols.	$8x(25x61^3)/12$	=	0.038	m^4
Ixx int. cols.	$6x(38x61^3)/12$	=	0.043	m^4
Ixx ext. cols.	$6x(38x76^3)/12$	=	0.083	m^4
TOTAL Ixx cols.			0.164	m^4
Ixx walls =	same as floor 2		0.009	m^4
			0.838	m^4
TOTAL Ixx walls			0.847	m^4
E conc. walls			21.0E9	N/m^4
E conc. cols.			28.0E9	N/m^4
L cols.			2.591	m
k13xx cols. =	$12 E I / L^3$		0.317E10	N/m
k13xx walls =	$12 E I / L^3$		1.227E10	N/m
TOTAL k13x			1.544E10	N/m

12-13 Level about YY axis

Iyy gable cols.	$8x(61x25^3)/12$	=	0.006	m^4
Iyy int. cols.	$6x(61x38^3)/12$	=	0.017	m^4
Iyy ext. cols.	$6x(76x38^3)/12$	=	0.021	m^4
TOTAL Iyy cols.			0.044	m^4
Iyy walls =	same as floor 2		0.004	m^4
			6.674	m^4
TOTAL Iyy walls			6.678	m^4
k13yy cols.	$= 12 E I / L^3$		0.085E10	N/m
k13yy walls	$= 12 E I / L^3$		9.675E10	N/m
TOTAL k13y			9.760E10	N/m

13-14 Level about XX axis

Ixx gable cols.	$8x(25x61^3)/12$	=	0.038	m^4
Ixx int. cols.	$6x(38x61^3)/12$	=	0.043	m^4
Ixx ext. cols.	$6x(38x76^3)/12$	=	0.083	m^4
TOTAL Ixx cols.			0.164	m^4
Ixx walls =	same as floor 1		0.009	m^4
			0.712	m^4
TOTAL Ixx walls			0.721	m^4
E conc. walls			21.0E9	N/m^4
E conc. cols.			28.0E9	N/m^4
L cols.			2.591	m
k14xx cols. =	$12 E I / L^3$		0.317E10	N/m
k14xx walls =	$12 E I / L^3$		1.045E10	N/m
TOTAL k14x			1.362E10	N/m

13-14 Level about YY axis

Iyy gable cols.	$8x(61x25^3)/12$	=	0.006	m^4
Iyy int. cols.	$6x(61x38^3)/12$	=	0.017	m^4
Iyy ext. cols.	$6x(76x38^3)/12$	=	0.021	m^4
TOTAL Iyy cols.			0.164	m^4
Iyy walls =	same as floor 1		0.004	m^4
			6.017	m^4
TOTAL Iyy walls			6.021	m^4
k14yy cols. =	$12 E I / L^3$		0.085E10	N/m
k14yy walls =	$12 E I / L^3$		8.723E10	N/m
TOTAL k14y			8.808E10	N/m

14-15 Level about XX axis

Ixx gable cols.	$8x(25x61^3)/12$	=	0.038	m^4
Ixx int. cols.	$6x(38x61^3)/12$	=	0.043	m^4
Ixx ext. cols.	$6x(38x76^3)/12$	=	0.083	m^4
TOTAL Ixx cols.			0.164	m^4
Ixx walls =	same as floor 2		0.009	m^4
			0.838	m^4
TOTAL Ixx walls			0.847	m^4
E conc. walls			21.0E9	N/m^4
E conc. cols.			28.0E9	N/m^4
L cols.			2.591	m
k15xx cols. =	$12 E I / L^3$		0.317E10	N/m
k15xx walls =	$12 E I / L^3$		1.227E10	N/m
TOTAL k15x			1.544E10	N/m

14-15 Level about YY axis

Iyy gable cols.	$8x(61x25^3)/12$	=	0.006	m^4
Iyy int. cols.	$6x(61x38^3)/12$	=	0.017	m^4
Iyy ext. cols.	$6x(76x38^3)/12$	=	0.021	m^4
TOTAL Iyy cols.			0.044	m^4
Iyy walls =	same as floor 2		0.004	m^4
			6.674	m^4
TOTAL Iyy walls			6.678	m^4
k15yy cols. =	$12 E I / L^3$		0.085E10	N/m
k15yy walls =	$12 E I / L^3$		9.675E10	N/m
TOTAL k15y			9.760E10	N/m

15-16 Level about XX axis

Ixx gable cols.	$8x(25x61^3)/12$	=	0.038	m^4
Ixx int. cols.	$6x(38x61^3)/12$	=	0.043	m^4
Ixx ext. cols.	$6x(38x76^3)/12$	=	0.083	m^4
TOTAL Ixx cols.			0.164	m^4
Ixx walls =	same as floor 3		0.009	m^4
			0.808	m^4
TOTAL Ixx walls			0.817	m^4
E conc. walls			21.0E9	N/m^4
E conc. cols.			28.0E9	N/m^4
L cols.			2.591	m
k16xx cols. =	$12 E I / L^3$		0.317E10	N/m
k16xx walls =	$12 E I / L^3$		1.184E10	N/m
TOTAL k16x			1.501E10	N/m

15-16 Level about YY axis

Iyy gable cols.	$8x(61x25^3)/12$	=	0.006	m^4
Iyy int. cols.	$6x(99x38^3)/12$	=	0.017	m^4
Iyy ext. cols.	$6x(76x38^3)/12$	=	0.021	m^4
TOTAL Iyy cols.			0.044	m^4
Iyy walls =	same as floor 3		0.005	m^4
			5.875	m^4
TOTAL Iyy walls			5.880	m^4
k16yy cols. =	$12 E I / L^3$		0.085E10	N/m
k16yy walls =	$12 E I / L^3$		8.519E10	N/m
TOTAL k16y			8.604E10	N/m

16-17 Level about XX axis

Ixx gable cols.	$8x(25x46^3)/12$	=	0.016	m^4
Ixx int. cols.	$6x(38x46^3)/12$	=	0.019	m^4
Ixx ext. cols.	$6x(38x61^3)/12$	=	0.043	m^4
TOTAL Ixx cols.			0.078	m^4
Ixx walls =	same as floor 2		0.009	m^4
			0.838	m^4
TOTAL Ixx walls			0.847	m^4
E conc. walls			21.0E9	N/m^4
E conc. cols.			28.0E9	N/m^4
L cols.			2.591	m
k17xx cols. =	$12 E I / L^3$		0.151E10	N/m
k17xx walls =	$12 E I / L^3$		1.227E10	N/m
TOTAL k17x			1.378E10	N/m

16-17 Level about YY axis

Iyy gable cols.	$8x(46x25^3)/12$	=	0.005	m^4
Iyy int. cols.	$6x(46x38^3)/12$	=	0.013	m^4
Iyy ext. cols.	$6x(61x38^3)/12$	=	0.017	m^4
TOTAL Iyy cols.			0.035	m^4
Iyy walls =	same as floor 2		0.004	m^4
			6.674	m^4
TOTAL Iyy walls			6.678	m^4
k17yy cols. =	$12 E I / L^3$		0.068E10	N/m
k17yy walls =	$12 E I / L^3$		9.675E10	N/m
TOTAL k17y			9.743E10	N/m

17-18 Level about XX axis

Ixx gable cols.	$8x(25x46^3)/12$	=	0.016	m^4
Ixx int. cols.	$6x(38x46^3)/12$	=	0.019	m^4
Ixx ext. cols.	$6x(38x61^3)/12$	=	0.943	m^4
TOTAL Ixx cols.			0.078	m^4
Ixx walls =	same as floor 1		0.009	m^4
			0.712	m^4
TOTAL Ixx walls			0.721	m^4
E conc. walls			21.0E9	N/m^4
E conc. cols.			28.0E9	N/m^4
L cols.			2.591	m
k18xx cols. =	$12 E I / L^3$		0.151E10	N/m
k18xx walls =	$12 E I / L^3$		1.045E10	N/m
TOTAL k18x			1.196E10	N/m

17-18 Level about YY axis

Iyy gable cols.	$8x(46x25^3)/12$	=	0.005 m^4
Iyy int. cols.	$6x(46x38^3)/12$	=	0.013 m^4
Iyy ext. cols.	$6x(61x38^3)/12$	=	0.017 m^4
TOTAL Iyy cols.			0.035 m^4
Iyy walls =	same as floor 1		0.004 m^4
			6.017 m^4
TOTAL Iyy walls			6.021 m^4
k18yy cols. =	$12 E I / L^3$		0.068E10 N/m
k18yy walls =	$12 E I / L^3$		8.723E10 N/m
TOTAL k18y			8.791E10 N/m

18-19 Level about XX axis

Ixx gable cols.	$8x(25x99^3)/12$	=	0.016	m^4
Ixx int. cols.	$6x(38x46^3)/12$	=	0.019	m^4
Ixx ext. cols.	$6x(38x61^3)/12$	=	0.043	m^4
TOTAL Ixx cols.			0.847	m^4
Ixx walls =	same as floor 2		0.009	m^4
			0.838	m^4
TOTAL Ixx walls			0.847	m^4
E conc. walls			21.0E9	N/m^4
E conc. cols.			28.0E9	N/m^4
L cols.			2.591	m
k19xx cols. =	$12 E I / L^3$		0.151E10	N/m
k19xx walls =	$12 E I / L^3$		1.227E10	N/m
TOTAL k19x			1.378E10	N/m

18-19 Level about YY axis

Iyy gable cols.	$8x(46x25^3)/12$	=	0.005 m^4
Iyy int. cols.	$6x(46x38^3)/12$	=	0.013 m^4
Iyy ext. cols.	$6x(61x38^3)/12$	=	0.017 m^4
TOTAL Iyy cols.			0.035 m^4
Iyy walls =	same as floor 2		0.004 m^4
			6.674 m^4
TOTAL Iyy walls			6.678 m^4
k19yy cols. =	$12 E I / L^3$		0.068E10 N/m
k19yy walls =	$12 E I / L^3$		9.675E10 N/m
TOTAL k19y			9.743E10 N/m

19-20 Level about XX axis

Ixx gable cols.	$8x(25x46^3)/12$	=	0.016	m^4
Ixx ext. cols.	$6x(38x46^3)/12$	=	0.019	m^4
Ixx int. cols.	$4x(38x27^3)/12$	=	0.003	m^4
Ixx int. cols.	$2x(38x46^3)/12$	=	0.006	m^4
TOTAL Ixx cols.			0.044	m^4
Ixx walls =	$15^3/12(458+281+458+234+234+234+112+30+458+62+62+458)$		0.009	m^4
	$15/12(236^3+20^3+140^3+28^3+203^3 x4+236^3+20^3+125^3+28^3)$		0.806	m^4
TOTAL Ixx walls			0.815	m^4
E conc. walls			21.0E9	N/m^4
E conc. cols.			28.0E9	N/m^4
L cols.			2.591	m
k20xx cols. =	$12 E I / L^3$		0.085E10	N/m
k20xx walls =	$12 E I / L^3$		1.181E10	N/m
TOTAL k20x			1.266E10	N/m

19-20 Level about YY axis

Iyy gable cols.	$8x(46x25^3)/12$	=	0.005	m^4
Iyy ext. cols.	$6x(46x38^3)/12$	=	0.013	m^4
Iyy int. cols.	$4x(27x38^3)/12$	=	0.005	m^4
Iyy int. cols.	$2x(46x38^3)/12$	=	0.004	m^4
TOTAL Iyy cols.			0.027	m^4

$$Iyy\ walls = 15^3/12(236+20+140+28+203x4+$$

$$236+20+125+28)+$$

$$15/12(458^3+281^3+458^3+234^3\ x3+$$

$$+112^3+30^3+458^3+62^3+62^3+458^3)$$

	0.005	m^4
	5.585	m^4
TOTAL Iyy walls	5.590	m^4
k20yy cols. = $12\ E\ I\ /\ L^3$	0.052E10	N/m
k20yy walls = $12\ E\ I\ /\ L^3$	8.099E10	N/m
TOTAL k20y	8.151E10	N/m

APPENDIX 3.3

THEORY OF DYNAMIC ANALYSIS BY PAFEC

The finite element method is associated with the strain enery stored in the beam element. This theory is based on the assumptions that,

1/ The beam is to lies with its neutral axis along the X coordinate axis;

2/ The cross section of the beam is uniform and is to be arranged so that the Y and Z directions are principal bending directions.

3/ The bending of the beam in the Y direction is not coupled with torsion.

4/ The cross sectional dimensions of the beam are to be small in relation to the length so that there is no warping and all the deformation is due to bending and none is due to shear.

5/ The first four assumptions relate to the original undeflected element. One further assumptions is needed in order to describe the manner in which deflection varies along the length of the beam. It is concerned with the displacement u in the Y direction and it is assumed that, it varies along the length of the beam according to

$$u_y = \alpha_1 + \alpha_2 x + \alpha_3^2 x + \alpha_4 x^3 \qquad (3.1)$$

where the α's are arbitrary constant.

This equation can also be written in matrix form as

$$u_y = [P] \{\alpha\} \qquad (3.2)$$

where α is a list of constants, and

$[P]$ is the polynominal matrix $[P] = [1 \quad x \quad x^2 \quad x^3]$

Hence an expression for strain energy in terms of the displacments is developed. By use of a Castigliano second theorem which states that the first derivative of strain energy with respect to displacement gives the force in the direction of that displacement, the derived expression is differentiated to give the forces at the nodes in terms of the displacements. This leads to the equilibrium conditions between elements in terms of forces and then in terms of displacements.

A set of system equations for the displacements is solved and by knowing the nodal displacements on each element the bending moments or stresses can be found.

In the dynamic analysis it is assumed that all displacements in a structure vary sinusoidally in time at frequency ω.

The kinetic energy of a single simple beam element is considered as

$$\text{K.E.} = \int_0^l \tfrac{1}{2} \rho A u_y^2 \omega^2 \, dx \qquad (3.3)$$

omitting the factor $\sin \omega t$ or $\exp(i \omega t)$.

The fact that equation (3.3) may be rewritten in terms of the nodal values $\{u_e\}$ is used to express the kinetic energy as

$$K.E. = \tfrac{1}{2} \omega^2 \{u_e\}^T [M_e] \{u_e\} \tag{3.4}$$

$[M_e]$ is known as the element mass matrix and is given by

$$[M_e] = \rho A [A]^T \int_0^1 [P]^T [P] \, dx \, [A]^{-1} \tag{3.5}$$

Differentiating the kinetic energy with respect to $\{u_e\}$ yields the forces required to produce the accelerations. Since the acceleration is in the opposite direction to the displacement the forces required to overcome the inertia are

$$\{F_e\}_{\text{inertia}} = -\omega^2 [M_e] \{u_e\} \tag{3.6}$$

The total force acting on an element in order to overcome both stiffness and inertia is

$$\{F_e\} = [S_e] \{u_e\} - \omega^2 [M_e] \{u_e\} \tag{3.7}$$

where $[Se]$ is the stiffness matrix for element.

Thus forces may be merged in exactly the same way as the

stiffness forces were merged in the static analysis. The process yields a system set of equations as

$$[S_s]\{u_s\} - \omega^2 [M_s]\{u_s\} = ([S_s] - \omega^2 [M_s])(u_s) = \{F_s\} \quad (3.8)$$

where $[Ms]$ is the system mass matrix and $\{Fs\}$ is a vector of the harmonically varying forces which are applied to the system.

To calculate natural frequency at which the structure will vibrate naturally without external loads the equations 3.8 is considered with $\{F\}=\{0\}$

$$([S_s] - \omega^2 [M_s])\{u_s\} = \{0\} \quad (3.9)$$

These equations are transformed to obtain,

$$[M_s] = [L][L^T] \quad (3.10)$$

where $[L]$ is a lower triangular matrix and $[L^T]$ is its upper triangular transpose.

The degrees of freedom $\{u\}_s$ are then transformed using

$$\{u'\} = [L]^T \{u_s\} \quad (3.11)$$

Equation 3.11 is substituted into equation 3.9 and $\{u\}_s$ is eliminated.

On premultiplying by $[L]^{-1}$

$$([S'] - \omega^2[I])\{u'\} = \{0\} \tag{3.14}$$

where $[S']$ is the symmetric matrix $[S'] = [L]^{-1}[S_s][L]^{-T}$ and $[I]$ is a unit matrix.

Equation 3.12 will be recongised by numerical analysts as a symmetric real eigenvalue problem. This equation is solved to determine the eigenvalues ω and the corresponding vectors $\{u'\}$. From a $\{u'\}$ vector the corresponding $\{u_s\}$ is calculated using equation 3.11

For a full description of this theory and the format used to process the structural data, the reader is referred to the Pafec 75 Theory results handbook[41].

PAFEC ANALYSIS OF JRC ABOUT XX AXIS

NATURAL FREQUENCY NUMBER 1 FREQUENCY= 2.444484 HZ

EIGENVECTORS

-0.197774 -0.251622 -0.301430 -0.350848 -0.402394

-0.456364 -0.504144 -0.550564 -0.606657 -0.665257

-0.714227 -0.760290 -0.807908 -0.855970 -0.892834

-0.924819 -0.953010 -0.977633 -0.992025 -1.000000

NATURAL FREQUENCY NUMBER 2 FREQUENCY= 6.694538 HZ

EIGENVECTORS

0.495257 0.615939 0.711206 0.786171 0.840835

0.870112 0.868493 0.837740 0.763045 0.644288

0.510476 0.351408 0.152726 -0.080897 -0.283060

-0.476901 -0.662327 -0.835013 -0.940185 -1.000000

NATURAL FREQUENCY NUMBER 3 FREQUENCY= 11.29682 HZ

EIGENVECTORS

0.649263 0.767887 0.813702 0.788855 0.688269

0.509322 0.296554 0.051513 -0.267210 -0.586090

-0.802800 -0.926322 -0.938519 -0.805495 -0.576971

-0.259981 0.125226 0.547001 0.829673 1.000000

NATURAL FREQUENCY NUMBER 4 FREQUENCY= 15.95567 HZ

EIGENVECTORS

-0.774015 -0.843069 -0.763381 -0.548622 -0.215409

0.189482 0.527541 0.771492 0.897037 0.798351

0.519355 0.106462 -0.394250 -0.838809 -1.000000

-0.882573 -0.484305 0.144688 0.646600 0.979373

NATURAL FREQUENCY NUMBER 5 FREQUENCY= 20.43636 HZ

EIGENVECTORS

-0.873597 -0.846643 -0.582553 -0.146562 0.366710

0.801293 0.956506 0.815918 0.314646 -0.379965

-0.855987 -1.000000 -0.709433 -0.016758 0.601837

0.958509 0.865333 0.259329 -0.396028 -0.894801

NATURAL FREQUENCY NUMBER 6 FREQUENCY= 25.55480 HZ

EIGENVECTORS

-0.692227 -0.550880 -0.174673 0.286438 0.644460

0.697695 0.412362 -0.079657 -0.658001 -0.852794

-0.506613 0.166020 0.815530 0.898839 0.337466

-0.485175 -1.000000 -0.692116 0.115075 0.896190

NATURAL FREQUENCY NUMBER 7 FREQUENCY= 29.74460 HZ

EIGENVECTORS

-0.950976 -0.594552 0.096865 0.741122 0.951890

0.510211 -0.228526 -0.829882 -0.903076 -0.150721

0.650602 0.918204 0.338723 -0.685631 -0.933154

-0.269247 0.740553 1.000000 0.168209 -0.930225

NATURAL FREQUENCY NUMBER 8 FREQUENCY= 33.82008 HZ

EIGENVECTORS

-0.794528 -0.345181 0.345382 0.775935 0.586991

-0.152133 -0.706168 -0.666605 0.104268 0.837134

0.599769 -0.302782 -0.955540 -0.355474 0.613613

0.829620 -0.076887 -1.000000 -0.434736 0.825587

NATURAL FREQUENCY NUMBER 9 FREQUENCY= 37.81161 HZ

EIGENVECTORS

-0.735962 -0.164791 0.533292 0.718712 0.163652

-0.624304 -0.695942 -0.024933 0.864517 0.563908

-0.461109 -0.877468 0.013868 1.000000 0.323558

-0.886924 -0.679657 0.899892 0.733774 -0.807958

NATURAL FREQUENCY NUMBER10 FREQUENCY= 41.64748 HZ

EIGENVECTORS

0.751360	-0.000391	-0.709432	-0.583964	0.294290
0.840240	0.274063	-0.658132	-0.768412	0.499759
0.828604	-0.215978	-1.000000	0.237883	0.883584
-0.157298	-0.962796	0.413311	0.751220	-0.571278

NATURAL FREQUENCY NUMBER11 FREQUENCY= 45.58994 HZ

EIGENVECTORS

0.711019	-0.180436	-0.768672	-0.267753	0.678819
0.582291	-0.395090	-0.776718	0.261917	0.848955
-0.274967	-0.876992	0.421417	0.819405	-0.671519
-0.652354	1.000000	0.036038	-0.890092	0.501741

NATURAL FREQUENCY NUMBER12 FREQUENCY= 48.69165 HZ

EIGENVECTORS

-0.672034	0.315253	0.742592	-0.034084	-0.809075
-0.122809	0.723914	0.303128	-0.912568	-0.006855
0.822749	-0.202341	-0.849630	0.886386	0.144846
-1.000000	0.605748	0.474295	-0.983193	0.454276

NATURAL FREQUENCY NUMBER13 FREQUENCY= 51.81670 HZ

EIGENVECTORS

-0.459584 0.321885 0.476127 -0.246544 -0.536948

0.295471 0.480969 -0.295669 -0.536065 0.698531

0.052937 -0.745031 0.523227 0.238484 -0.705246

0.430672 0.276601 -0.925619 1.000000 -0.387069

NATURAL FREQUENCY NUMBER14 FREQUENCY= 53.69574 HZ

EIGENVECTORS

-0.352603 0.298434 0.332138 -0.292444 -0.344463

0.389477 0.242193 -0.429977 -0.115865 0.582073

-0.361388 -0.326342 0.738536 -0.665094 0.170762

0.482804 -0.852283 1.000000 -0.836858 0.293827

NATURAL FREQUENCY NUMBER15 FREQUENCY= 56.54392 HZ

EIGENVECTORS

0.638697 -0.688241 -0.455458 0.783180 0.275762

-0.975962 0.159846 0.934738 -0.900767 0.063164

0.740855 -0.841670 0.283499 0.447681 -0.955571

1.000000 -0.716959 0.467601 -0.290341 0.088866

NATURAL FREQUENCY NUMBER16 FREQUENCY= 58.06448 HZ

EIGENVECTORS

-0.278305 0.335606 0.151342 -0.387124 -0.007525

0.424203 -0.227357 -0.317936 0.579351 -0.461011

0.058513 0.401095 -0.680912 0.907214 -1.000000

0.789092 -0.463290 0.248905 -0.135502 0.038717

NATURAL FREQUENCY NUMBER17 FREQUENCY= 61.55550 HZ

EIGENVECTORS

0.268850 -0.406874 -0.004103 0.416240 -0.289887

-0.181347 0.423137 -0.159912 -0.330993 0.787475

-1.000000 0.810945 -0.469353 0.259769 -0.161624

0.086243 -0.036969 0.014344 -0.006050 0.001491

NATURAL FREQUENCY NUMBER18 FREQUENCY= 63.95702 HZ

EIGENVECTORS

0.556565 -0.965828 0.263781 0.772017 -1.000000

0.333995 0.561643 -0.924277 0.752937 -0.595678

0.472631 -0.291265 0.134719 -0.058035 0.028687

-0.012658 0.004608 -0.001506 0.000548 -0.000123

NATURAL FREQUENCY NUMBER19 FREQUENCY= 69.42547 HZ

EIGENVECTORS

-0.261746 0.594797 -0.531715 0.085788 0.445604

-0.873439 1.000000 -0.695514 0.309570 -0.129661

0.060418 -0.024774 0.008068 -0.002380 0.000812

-0.000257 0.000070 -0.000017 0.000005 -0.000001

NATURAL FREQUENCY NUMBER20 FREQUECNY= 73.36635 HZ

EIGENVECTORS

-0.278214 0.747500 -1.000000 0.925978 -0.663592

0.455484 -0.311870 0.161630 -0.056512 0.018304

-0.006652 0.002198 -0.000590 0.000142 -0.000812

0.000010 -0.000002 0.000000 -0.000000 0.000000

ANALYSIS OF JRC ABOUT YY AXIS

NATURAL FREQUENCY NUMBER 1 FREQUENCY= 4.403820 HZ

EIGENVECTORS

-0.402663 -0.458744 -0.507427 -0.561210 -0.606337

-0.654520 -0.695795 -0.739901 -0.776400 -0.813946

-0.845109 -0.877239 -0.902687 -0.927567 -0.946942

-0.965356 -0.978431 -0.989361 -0.995980 -1.000000

NATURAL FREQUENCY NUMBER 2 FREQUENCY= 13.96330 HZ

EIGENVECTORS

0.836041 0.923040 0.969573 0.985006 0.965104

0.906251 0.822090 0.694770 0.558564 0.386773

0.218676 0.019623 -0.156859 -0.346618 -0.506304

-0.668285 -0.789156 -0.894233 -0.959583 -1.000000

NATURAL FREQUENCY NUMBER 3 FREQUENCY= 24.54265 HZ

EIGENVECTORS

0.960749 0.982235 0.898259 0.693730 0.442265

0.109220 -0.203033 -0.532687 -0.768222 -0.940377

-0.997901 -0.945068 -0.800311 -0.548512 -0.264744

0.088100 0.390665 0.681823 0.875138 1.000000

NATURAL FREQUENCY NUMBER 4 FREQUENCY= 35.41715 HZ

EIGENVECTORS

0.989190 0.881961 0.592892 0.112896 -0.331355

-0.747377 -0.958388 -0.958306 -0.748590 -0.336089

0.109098 0.587199 0.882585 1.000000 0.891339

0.551073 0.132946 -0.361764 -0.731461 -0.988493

NATURAL FREQUENCY NUMBER 5 FREQUENCY= 46.25438 HZ

EIGENVECTORS

-1.000000 -0.714094 -0.191438 0.489158 0.902181

0.988744 0.695470 0.066802 -0.514017 -0.946476

-0.986950 -0.618040 -0.064336 0.575311 0.941966

0.966736 0.636620 0.015083 -0.551176 -0.990431

NATURAL FREQUENCY NUMBER 6 FREQUENCY= 56.92428 HZ

EIGENVECTORS

-0.967578 -0.477314 0.231697 0.893335 0.968416

0.442132 -0.284598 -0.924911 -0.968413 -0.414519

0.317539 0.945789 0.972631 0.404835 -0.332029

-0.959076 -0.983930 -0.412985 0.328289 1.000000

NATURAL FREQUENCY NUMBER 7 FREQUENCY= 67.24819 HZ

EIGENVECTORS

-0.946218 -0.223511 0.600221 1.000000 0.563148

-0.420694 -0.974940 -0.725635 0.067117 0.887131

0.934116 0.157520 -0.651195 -0.988984 -0.528579

0.457634 0.976349 0.722410 -0.058728 -0.938910

NATURAL FREQUENCY NUMBER 8 FREQUENCY= 77.19874 HZ

EIGENVECTORS

-0.914931 0.047613 0.860326 0.764275 -0.111695

-0.961933 -0.723012 0.405572 0.981974 0.497685

-0.451946 -1.000000 -0.457168 0.660894 0.995987

0.224046 -0.684886 -0.926059 -0.211138 0.896933

NATURAL FREQUENCY NUMBER 9 FREQUENCY= 86.63617 HZ

EIGENVECTORS

-0.897546 0.325024 0.994541 0.266349 -0.717878

-0.770782 0.197272 1.000000 0.400781 -0.840242

-0.870737 0.378612 0.992481 0.260346 -0.734725

-0.793146 0.168399 0.996806 0.480079 -0.863584

NATURAL FREQUENCY NUMBER10 FREQUENCY= 95.34606 HZ

EIGENVECTORS

0.903855 -0.614626 -1.000000 0.379243 0.985534

-0.078720 -0.913966 -0.206948 0.746334 0.500633

-0.507532 -0.744699 0.212368 0.906848 0.123032

-0.983176 -0.438980 0.913263 0.730548 -0.825958

NATURAL FREQUENCY NUMBER11 FREQUENCY= 101.4190 HZ

EIGENVECTORS

0.930645 -0.855868 -0.920281 0.901636 0.881817

-0.904237 -0.883759 0.948934 0.867226 -0.934786

-0.900024 0.958070 0.901254 -0.919257 -0.944390

0.912441 0.954998 -0.841742 -1.000000 0.883244

NATURAL FREQUENCY NUMBER12 FREQUENCY= 112.8582 HZ

EIGENVECTORS

-0.520171 0.734080 0.226331 -0.932491 0.119651

1.000000 -0.441566 -0.956303 0.712822 0.819951

-0.887876 -0.603440 0.972205 0.370427 -0.979924

-0.089231 0.890755 -0.152854 -0.765529 0.466699

NATURAL FREQUENCY NUMBER13 FREQUENCY= 119.8111 HZ

EIGENVECTORS

-0.518928 0.900685 -0.083377 -0.970686 0.676460

0.630251 -1.000000 0.009231 0.878526 -0.578076

-0.459076 0.970517 -0.167309 -0.972774 0.689550

0.654074 -0.975110 -0.153204 0.959986 -0.485909

NATURAL FREQUENCY NUMBER14 FREQUENCY= 126.2069 HZ

EIGENVECTORS

0.479242 -0.983032 0.438911 0.667322 -0.981226

0.214438 0.694258 -0.963018 0.246708 0.832936

-0.930287 -0.019350 0.838388 -0.742994 -0.145236

0.981827 -0.684313 -0.484823 1.000000 -0.434439

NATURAL FREQUENCY NUMBER15 FREQUENCY= 131.8567 HZ

EIGENVECTORS

-0.426689 1.000000 -0.755349 -0.135641 0.816189

-0.878899 0.273690 0.633161 -0.968831 0.488290

0.336689 -0.985262 0.798784 0.142622 -0.873806

0.921825 -0.219990 -0.767487 0.993160 -0.381389

NATURAL FREQUENCY NUMBER16 FREQUENCY= 136.5176 HZ

EIGENVECTORS

-0.381413	0.989569	-1.000000	0.453813	0.254131
-0.890256	0.989752	-0.550751	-0.122811	0.790438
-0.930607	0.524413	0.125522	-0.760010	0.864354
-0.419612	-0.222589	0.774486	-0.764763	0.267086

NATURAL FREQUENCY NUMBER17 FREQUENCY= 140.8366 HZ

EIGENVECTORS

0.267206	-0.757456	0.945909	-0.860714	0.528436
0.043724	-0.546194	0.941570	-1.000000	0.654734
-0.095531	-0.574324	0.965701	-0.959411	0.559267
0.128958	-0.686354	0.965548	-0.779956	0.250655

NATURAL FREQUENCY NUMBER18 FREQUENCY= 143.9276 HZ

EIGENVECTORS

-0.195207	0.587818	-0.835224	1.000000	-0.997588
0.787073	-0.464377	0.031741	0.355758	-0.699270
0.851304	-0.854278	0.688531	-0.306082	-0.118813
0.571313	-0.833329	0.850346	-0.606864	0.184226

NATURAL FREQUENCY NUMBER19 FREQUENCY= 146.0786 HZ

EIGENVECTORS

0.108532 -0.340396 0.524750 -0.726944 0.876086

-0.966659 0.991427 -1.000000 0.960633 -0.800374

0.561096 -0.246733 -0.053053 0.376198 -0.609956

0.797615 -0.855928 0.739993 -0.488137 0.142587

NATURAL FREQUENCY NUMBER20 FREQUENCY= 147.8633 HZ

EIGENVECTORS

0.018431 -0.059746 0.098126 -0.150718 0.204717

-0.268182 0.334371 -0.437746 0.548653 -0.660125

0.742540 -0.855719 0.956365 -1.000000 0.975317

-0.922693 0.834344 -0.642580 0.398646 -0.112861

APPENDIX 4.1

CALCULATION OF GEOMETRICAL CENTRE OF THE JRC

Considering the first floor level as a typical floor level, Fig 4.3, and adpating a numbering system as shown in the Fig 4.3, i.e. numbers in the circles repersent the column numbers and the numbers in the squares repersent the reinforced concrete walls.

The coordinates of the geometrical centre was found to be at 11.60 m and 9.17 m from the dutum at South East corner. These calculations are represented in a tabular format in the following two tables.

TABLE 1 TAKING FIRST MOMENT OF AREA ABOUT THE EXTREME EDGE

PARALLEL TO XX AXIS

column number		first moment of area
○		cm^3
1,5	25x99x2x1750.5	8.665E6
2,3,4	42x99x3x1750.5	21.836E6
6,10	25x99x2x1134.5	5.616E6
7,8,9	38x122x3x1146.0	15.939E6
11,15	25x99x2x665.5	3.294E6
12,13,14	38x122x3x654.0	9.906E6
16,20	25x99x2x49.5	0.245E6
17,18,19	42x99x3x49.5	0.618E6
□		
1	6870x(1085+7.5)	7.505E6
2	4215x(1085-236-7.5)	3.547E6
3	6870x(715-7.5)	4.860E6
4	3540x(1085-118)	3.423E6
5	2100x(1085-236-15+70)	1.898E6
6	420x(715+14)	0.316E6
7	300x(1085-10)	0.323E6
8	6870x(1085+7.5)	7.506E6
9	6870x(715-7.5)	4.861E6
10	930x(1085-236-7.5)	0.783E6
11	930x(1085-236-7.5)	0.783E6
12	3540x(1085-118)	3.423E6
13	300x(1085-10)	0.323E6
14	1875x(1085-236+62.5)	1.709E6
15	420x(715+14)	0.306E6
16	4350x(1085+7.5)	4.752E6
17	4350x(1085-203-7.5)	3.804E6
18	3045x(1085-101.5)	2.995E6
19	1380x(1085-46)	1.434E6
20	300x(1085-203+10)	0.268E6
21	3510x(1085+7.5)	3.835E6
22	3510x(1085-203-7.5)	3.070E6
23	3045x(1085-101.5)	2.995E6
24	3045x(1085-101.5)	2.995E6
	145119Y	133.013E6

$\bar{Y} = 917$ cm

TABLE 2 TAKING FIRST MOMENT OF AREA ABOUT THE EXTREME EDGE

PARALLEL TO YY AXIS

column number		first moment of area
○		3
5,10,15,20	25x99x4x2347.5	23.240E6 cm
4,19	42x99x2x1767	14.694E6
9,14	38x122x2x1767	16.384E6
3,18	42x99x2x1180	9.813E6
8,13	38x122x2x1180	10.941E6
2,17	42x99x2x593	4.931E6
7,12	38x122x2x593	5.498E6
1,6,11,16	25x99x4x12.5	0.124E6
□		
1	458x15x(483-299)	1.745E6
2	281x15x(483-140.5)	1.444E6
3	458x15x(483-299)	1.745E6
4	236x15x(483-7.5)	1.683E6
5	140x15x(483-281-91-7.5)	0.271E6
6	28x15x(483-7.5)	0.200E6
7	20x15x(483-281-91-7.5)	0.031E6
8	458x15x(2347.5-12.5-229)	14.468E6
9	458x15x(2347.5-12.5-229)	14.468E6
10	62x15x(2360-165-31)	2.013E6
11	62x15x(2360-165-62-194-31)	1.774E6
12	236x15x(2360-165-62-194-62+7.5)	6.671E6
13	20x15x(2360-165-7.5)	0.656E6
14	125x15x(2360-165-7.5)	4.102E6
15	28x15x(2360-165-62-194-62+7.5)	0.792E6
16	290x15x(1180-19-70-145)	4.165E6
17	290x15x(1180-19-70-145)	4.165E6
18	203x15x(1180-19-70-290+7.5)	2.462E6
19,20	(92+20)x15x(1180-19-70-7.5)	1.820E6
21,22	2x234x15x(1180+19+70+117)	9.730E6
23	203x15x(1180+19+70+234-7.5)	4.554E6
24	203x15x(1180+19+70+7.5)	3.887E6
	145119X	168.317E6

$\overline{X}$ = 1160 cm

APPENDIX 6.1

PREDICTION THEORY

A6.1 INTRODUCTION

The theory outlined in this chapter is based on some work by Kanda[4] which is related to an approach by Etkin[50] dealing with the along-wind response of a line-like structure.

Kanda's method was formulated for three dimensional bluff structures and emphasised the reduced frequency dependence of the along-wind force coefficient.

A treatment similar to that for the along-wind response was investigated, to describe the cross-wind response taking three factors into account for cases which the mean velocity was less than the critical one. The factors were as follows.

1/ Fluctuating force associated with the lateral components of turbulence.

2/ Vortex shedding which is dominant in a resonance condition.

3/ Aerodynamic negative damping which leads to galloping or self exciting oscillations when the mean velcity exceeds the critical velocity.

In order to predict the wind response of a tall structure in the along-wind direction a computer program was developed, (WREAN01)[4] This programe was later modified as RESPONSE. The predictions were developed from a mathematical model of the turbulence characteristics in a natural wind.

Approximations and simlifications were necessary to reduce the expression for the power spectral density of generalised force to a form suitable for computation.

A6.2 PREDICTIONS OF ALONG-WIND RESPONSE

The predictions were initially founded on the assumption of a strip theory relationship between the local drag and the total relative velocity for a two dimensional body. This theory was applied to a three dimensional body, by replacing the local drag with the net pressure, which was considered to act through the structure on the idealised surface normal to the mean wind direction,i.e.

$$P(y, z, t) = \tfrac{1}{2}\rho C_D(y, z, \xi)U'^2(y, z, t) + \rho B(z)C_M(y, z, \xi)\dot{U}'(y, z, t)$$

where

x,y,z = along-wind, cross-wind and vertical distance co-ordinates

t = time

P(y,z) = mean along-wind pressure

p(y,z,t) = turbulent component of along-wind pressure

P(y,z,t) = along-wind pressure = P(y,z) + p(y,z,t)

ρ = air mass density

B(z) = width of a structure

f = frequency

$\bar{U}(z)$ = mean along-wind velocity

u(y,z,t) = turbulent along-wind velocity component

$U(y,z,t) = \bar{U}(z) + u(y,z,t)$

$\overline{\Delta}(z)$ = mean along-wind structural displacement

$\delta(z,t)$ = dynamic along-wind structural displacement

$\Delta(z,t) = \overline{\Delta}(z) + \delta(z,t)$

$U'(y,z,t) = U(y,z,t) - \dot{\delta}(y,z,t)$

$\xi = f.B(z)/\overline{U}(z)$

$C_D(y,z,\xi)$ = drag coefficient

$C_M(y,z,\xi)$ = mass coefficient

By taking the time average and neglecting the second order terms in u and . then,

$$\overline{P}(y, z) = \tfrac{1}{2}\rho C_{D_o}(y, z)\,\overline{U}^2 \qquad \text{(A6.2)}$$

and

$$p(y, z, t) = \rho C_D(y, z, \xi)\,\overline{U}\,.\,u + \rho B(z)\,C_M(y, z, \xi)\,\dot{u} - \rho C_D(y, z, \xi)\,\overline{U}\cdot\dot{\delta} - \rho B(z)\,C_M(y, z, \xi)\,\ddot{\delta} \qquad \text{(A6.3)}$$

where C_{D_o} is the static or mean drag coefficient.

The last two terms of equation (A6.3) are not dependent on the turbulence but on the structural response. Consequently they were considered as the additional damping and mass in the equation of motion of a structure. Then the dynamic part of the along-wind net pressure, $p'(y,z,t)$, for the force contribution was written as,

$$p'(y,z,t) = \rho C_D(y,z,\xi)u \cdot \overline{U} + \rho B(z)\,C_M(y,z,\xi)\dot{u} \qquad \text{(A6.4)}$$

The associated dynamic displacement response .(z,t) was treated as a random function made up of components from the various independent modes of vibration. Then the equation of motion for

the n-th mode was written as

$$\ddot{q}_n(t) + 2\zeta_{T_n}(2\pi f_n)\dot{q}_n(t) + (2\pi f_n)^2 q_n(t) = \frac{F_n(t)}{M_{T_n}} \qquad \text{(A6.5)}$$

where q_n is the generalised displacement of the n-th mode;

$$\delta(z,t) = \sum_{n=1}^{N} \mu_n(z) \cdot q_n(t) \ ;$$

$\mu_n(z)$ is the n-th mode shape;

f_n is the n-th natural frequency;

$$M_{T_n} = \int_o^H \int_o^{B(z)} \{m(z) + \rho B(z)\ C_M(y,z,\xi)\}\mu_n^2(z)\ dy\ dz;$$

$m(z)$ is the mass of structure per unit surface area;

$\zeta_{T_n} = \zeta_n + \zeta_{A_n}$, total damping ratio;

ζ_n is the damping ratio of the structure of the n-th mode;

$$\zeta_{A_n} = \int_o^H \int_o^{B(z)} \frac{\rho C_D(y,z,\xi)\bar{U}(z)\ \mu_n^2(z)}{4\pi f_n\ M_{T_n}}\ dy\ dz; \quad \text{and}$$

F_n is the generalised force associated with the turbulence,

$$F_n(t) = \int_o^H \int_o^{B(z)} p'(y,z,t)\mu_n(z)\ dy\ dz \qquad \text{(A6.6)}$$

For the most lightly damped structures the cross-coupling between modes was assumed unlikely. Therefore the power spectral density of the response, $S_\delta(f)$ was written as a solution of equation (A6.5)

$$S_\delta(f) = \sum_{n=1}^{N} \mu_n^2(z) \; |\chi_n(f)|^2 \; S_{F_n}(f) \qquad \text{(A6.7)}$$

where

$$|\chi_n(f)|^2 = \frac{1}{(4\pi^2 M_{T_n})^2 \{ f^4 + f_n^4 + (4\zeta_{T_n}^2 - 2) f^2 f_n^2 \}}$$

Substitution of equation (A6.4) into (A6.6) yeilds the generalised force of the n-th mode, $F_n(t)$,as

$$F_n(t) = \int_0^H \int_0^{B(z)} \{\rho C_D(y,z,\xi)\bar{U}\cdot u + \rho C_M(y,z,\xi)B(z)\dot{u}\}\mu_n(z)\, dz\, dy \qquad \text{(A6.8)}$$

In equation (A6.8) $F_n(t)$was expressed as a function of t and ξ , but since for lightly damped structures only the components of response in the narrow band of frequency around resonance in a particular mode was considered to be of significance, therefore only the corresponding values of C_D and C_M were taken into account. This was considered to be adequate for small ζ_T (eg, ζ_T <2%).

Therefore $S_{F_n}(f)$ was defined as a Fourier transform of the auto-correlation function of $F_n(t)$ as follows,

$$S_{F_n}(f) = 2 \int_{-\infty}^{\infty} R_{F_n}(\tau) e^{-i2\pi f\tau} \, d\tau \qquad \text{(A6.9)}$$

where $$R_{F_n}(\tau) = E[F_n(t) \cdot F_n(t+\tau)] \qquad \text{(A6.10a)}$$

Further development of equation (A6.10a), by replacing the variables y,z with y_1 ,z_1, and y_2,z_2 corresponding to the integral

expression invloving $t+\tau$, leads to

$$R_{F_n}(\tau) = \int_0^H \int_0^H \int_0^B \int_0^B \{C^*_{D_n}(y_1,z_1)C^*_{D_n}(y_2,z_2)E[u_1(t)\cdot u_2(t+\tau)]$$

$$+ C^*_{D_n}(y_1,z_1)C^*_{M_n}(y_2,z_2)E[u_1(t)\cdot \dot{u}_2(t+\tau)]$$

$$+ C^*_{M_n}(y_1,z_1)C^*_{D_n}(y_2,z_2)E[\dot{u}_1(t)\cdot u_2(t+\tau)]$$

$$+ C^*_{M_n}(y_1,z_1)C^*_{M_n}(y_2,z_2)E[\dot{u}_1(t)\cdot \dot{u}_2(t+\tau)]\}$$

$$x \; dy_1\, dy_2\, dz_1\, dz_2 \qquad \text{(A6.10b)}$$

where $u_1(t), u_2(t)$ are turbulent velocity components at different positions (y_1,z_1) and (y_2,z_2) respectively, and

$$\left.\begin{aligned} C^*_{D_n}(y,z) &= \rho C_D(y,z,\xi_n)\bar{U}(z)\mu_n(z); \\ C^*_{M_n}(y,z) &= \rho C_M(y,z,\xi_n)B(z)\,\mu_n(z); \end{aligned}\right\} \qquad \text{(A6.11)}$$

Hence the power spectral density function of generalised force for the n-th mode was computed as

$$S_{F_n}(f) = 2\int_{-\infty}^{\infty}\int_0^H\int_0^H\int_0^B\int_0^B R_{u_1u_2}(\tau)\,\{C^*_{D_n}(y_1,z_1)\,C^*_{D_n}(y_2,z_2)$$

$$+ i2\pi f[C^*_{D_n}(y_1,z_1)\,C^*_{M_n}(y_2,z_2) - C^*_{M_n}(y_1,z_1)\,C^*_{D_n}(y_2,z_2)]$$

$$+ 4\pi^2 f^2\, C^*_{M_n}(y_1,z_1)\,C^*_{M_n}(y_2,z_2)\}\, dy_1\, dy_2\, dz_1\, dz_2$$

$$\times \; e^{-i2\pi f\tau} \; d\tau \qquad \text{(A6.12)}$$

Since the terms with brackets { } are independent of the integral variable τ, the Fourier integral was performed for the cross-correlation function as similar to equation (A6.9). It was assumed that C_D and C_M were constant with y, and had the same profile with z, and that in consequence,

$$C^*_{D_n}(z_1)\, C^*_{M_n}(z_2) - C^*_{M_n}(z_1)\, C^*_{D_n}(z_2) = 0 \qquad \text{(A6.13)}$$

Hence equation (A6.10) was rearranged and simplified as,

$$S_{F_n}(f) = \int_0^H \int_0^H \int_0^B \int_0^B S_{u_1 u_2}(f) \; \{C^*_{D_n}(z_1) C^*_{D_n}(z_2)$$

$$+ 4\pi^2 f^2 \, C^*_{M_n}(z_1) C^*_{M_n}(z_2)\} \; \times \; dy_1 \, dy_2 \, dz_1 \, dz_2 \qquad \text{(A6.14)}$$

Instead of using two coefficients $C_D(\xi)$ and $C_M(\xi)$ a dynamic along-wind force coefficient $\tilde{C}_D(\xi)$ was defined as

$$\tilde{C}_D(\xi) = C_D(\xi) \sqrt{1 + (2\pi f)^2 \, \frac{B^2 \cdot C_M^2(\xi)}{\bar{U}^2(z) \cdot C_D^2(\xi)}}$$

Then the definition equations (A6.11) was written accordingly as

$$\tilde{C}^*_{D_n}(z) = \rho \, \tilde{C}_D(\xi_n) \; \bar{U}(z) \mu_n(z)$$

$$= \sqrt{\{C^*_{D_n}(z)\}^2 + \{2\pi f \, C^*_{M_n}(z)\}^2}$$

Therefore equation (A6.14) became,

$$S_{F_n}(f) = \int_0^H \int_0^H \int_0^B \int_0^B S_{u_1 u_2}(f)\, \tilde{C}^*_{D_n}(z_1)\, \tilde{C}^*_{D_n}(z_2)\, dy_1\, dy_2\, dz_1\, dz_2 \quad (A6.15)$$

Generally the natural wind is not a homogeneous turbulent flow and so the cross-spectral density function consists of real and imaginary parts. However, since the power spectrum of the generalised force is a real function, the real part of the cross spectrum which for convenience was called the co-coherence, was taken into account and the imaginary part $Q_{u_1 u_2}$ was ignored. When the assumption equation (A6.13) was adopted and empolyed in the rearrangment of equation (A6.10), it yeilded

$$S_{F_n}(f) = \int_0^H \int_0^H \int_0^B \int_0^B C_{u_1 u_2}(f) \sqrt{S_{u_1}(f)\, S_{u_2}(f)}\; \tilde{C}^*_{D_n}(z_1)\, \tilde{C}^*_{D_n}(z_2) \times dy_1\, dy_2\, dz_1\, dz_2 \quad (A6.16)$$

where

$$S_{u_1 u_2}(f) = (C_{u_1 u_2}(f) - i\, Q_{u_1 u_2}(f)) \sqrt{S_{u_1}(f)\, S_{u_2}(f)}$$

A6.3 SIMPLIFICATION FOR COMPUTATION

In order to reduce the expression for the power spectral density of generalised force equation (A6.16) a form suitable for computation the assumptions and simplified equations listed below were considered.

1/

$$\bar{U}(z) = \left(\frac{z}{H}\right)^{\alpha} \bar{U}(H) \quad (A6.17)$$

2/

$$\sigma_u(z) = \left(\frac{z}{H}\right)^{-\alpha_T} \sigma_u(H) \tag{A6.18}$$

3/

$$\frac{f \cdot S_u(f,z)}{\sigma_u^2(z)} = k_1 \frac{\tilde{f}(z)}{(1 + \tilde{f}(z)^{\beta})^{5/3\beta}} \tag{A6.19}$$

where

$$\tilde{f}(z) = \frac{f \cdot L_h(z)}{\bar{U}(H)} \quad , \quad L_h(z) = L(H)\left(\frac{z}{H}\right)^{\alpha_L} = L_1(z)\left(\frac{H}{10}\right)^{\alpha}$$

$$L_1(z) = L(10)\left(\frac{z}{10}\right)^{\alpha_L} \quad \text{and} \quad k_1 = \frac{\beta\Gamma\left(\frac{5}{3\beta}\right)}{\Gamma\left(\frac{1}{\beta}\right)\Gamma\left(\frac{2}{3\beta}\right)}$$

4/

$$C_{u_1 u_2}(y_1, y_2, z_1, z_2, f) =$$

$$\exp\left(-\frac{f^*\sqrt{k_{hy}^2(z_m)(y_1-y_2)^2 + k_{hz}^2(z_m)(z_1-z_2)^2}}{\bar{U}(H)}\right) \tag{A6.20}$$

where $f^* = \sqrt{f^2 + \left(\frac{\bar{U}(10)}{k_2 L_h(z)}\right)^2}$, $z_m = \sqrt{z_1 z_2}$, $k_2 = \sqrt{10}$

$$k_{hy}(z_m) = k_y(H)\left(\frac{z_m}{H}\right)^{-\alpha_D} \quad \text{and} \quad k_{hz}(z_m) = k_2(H)\left(\frac{z_m}{H}\right)^{-\alpha_D}$$

5/

$$\mu(z) = \left(\frac{z}{H}\right)^{\alpha_\mu} \tag{A6.21}$$

6/ The projected area of the structure is rectangular in shape with constant width B (height H)

Substitution of equations (A6.19) and (A6.20) in equation (A6.16) gives,

$$S_{F_n}(f) = \int_0^H \int_0^H \int_0^B \int_0^B \exp\left\{ \frac{-f^* \sqrt{k_{hy}^2(z_m)(y_1-y_2)^2 + k_{hz}^2(z_m)(z_1-z_2)^2}}{\bar{U}(H)} \right\} \cdot \sigma_u(z_1)\sigma_u(z_2)$$

$$\times \; k_1 \sqrt{\frac{\frac{L_h(z_1)}{\bar{U}(H)}}{\left[1 + \left\{\frac{f \cdot L_h(z_1)}{\bar{U}(H)}\right\}\right]^{\beta\, 5/3\beta}} \cdot \frac{\frac{L_h(z_2)}{\bar{U}(H)}}{\left[1 + \left\{\frac{f \cdot L_h(z_2)}{\bar{U}(H)}\right\}\right]^{\beta\, 5/3\beta}}} \cdot \rho^2 \cdot \tilde{C}_{D_n}^2$$

$$\times \; \bar{U}(z_1)\, \bar{U}(z_2)\, \mu(z_1)\, \mu(z_2)\, dy_1\, dy_2\, dz_1\, dz_2 \qquad \text{(A6.22)}$$

When normalised co-ordnates; $y = By'$ and $z = Hz'$, were used and equations (A6.17), (A6.18) and (A6.21) were substituted in equation (A6.22),

$$S_{F_n}(f) = \left\{ \frac{\tilde{C}_{D_n} \cdot \rho \cdot \bar{U}^2(H) \cdot B \cdot H}{(1 + \alpha - \alpha_T + \alpha_\mu)} \right\}^2 \cdot \frac{\sigma_u^2(H)}{\bar{U}^2(H)} \cdot \frac{S_u(f \cdot H)}{\sigma_n^2(H)}$$

$$\times \; \psi^2(\alpha, \alpha_T, \alpha_\mu, \alpha_D, \alpha_L, \tilde{f}(H), f_B, f_H) \qquad \text{(A6.23)}$$

where

$$\psi^2(\alpha, \alpha_T, \alpha_\mu, \alpha_D, \alpha_L, \tilde{f}(H), f_B, f_H) =$$

$$(1 + \alpha - \alpha_T + \alpha_\mu)^2 \int_0^1 \int_0^1 \int_0^1 \int_0^1 z_1'^{\,\alpha-\alpha_T+\alpha_\mu} \cdot z_2'^{\,\alpha-\alpha_T+\alpha_\mu}$$

$$\times \exp\left[-\sqrt{\left\{ 1 + \frac{z_1'^{-\alpha_L} \cdot z_2'^{-\alpha_L}}{10\,\tilde{f}^2(H)} \right\} \left\{ f_B^2 (y_1' - y_2')^2 + f_H^2 (z_1' - z_2')^2 \right\}} \, z_1'^{-\alpha_D} z_2'^{-\alpha_D} \right]$$

$$\times \left\{ 1 + \tilde{f}^\beta(H) \right\}^{5/3\beta} \cdot \sqrt{\frac{z_1'^{\alpha_L}}{\left[1 + \left\{ \tilde{f}(H) z_1'^{\alpha_L} \right\}^\beta \right]^{5/3\beta}} \cdot \frac{z_2'^{\alpha_L}}{\left[1 + \left\{ \tilde{f}(H) z_2'^{\alpha_L} \right\}^\beta \right]^{5/3\beta}}}$$

$$\times \, dy_1' \, dy_2' \, dz_1' \, dz_2' \qquad \text{(A6.24)}$$

and $\alpha_T, \alpha_\mu, \alpha_D$, and α_L are power law exponents respectively of r.m.s. turbulent velcity, modal shape, decay constant k_{1y} and k_{1z} and the length scale L_1

By approximation the term height dependence of power spectral density in equation (A6.24) became,

$$\left[1 + \tilde{f}^\beta (H) \right]^{5/3\beta} \sqrt{\frac{z_1'^{\alpha_L}}{\left[1 + \left\{ \tilde{f}(H) z_1'^{\alpha_L} \right\}^\beta \right]^{5/3\beta}} \cdot \frac{z_2'^{\alpha_L}}{\left[1 + \left\{ \tilde{f}(H) z_2'^{\alpha_L} \right\}^\beta \right]^{5/3\beta}}}$$

$$\triangleq z_1'^{\alpha_L/2} \, z_2'^{\alpha_L/2} \left[\frac{1 + \tilde{f}^\beta (H)}{1 + \left\{ \tilde{f}(H) \, z_1'^{\alpha_L/2} \, z_2'^{\alpha_L/2} \right\}^\beta} \right]^{5/3\beta} \qquad \text{(A6.25)}$$

It was assumed that;

1/ the variation of α , α_T, α_μ, α_D, α_L, and $\tilde{f}(H)$ is negligible;

2/ $\alpha_T = \alpha_L = 0$

3/ $\alpha_D = \alpha$

4/ $\tilde{f}(H)$ is eliminated;and

5/ the function $\psi^2(\ .\ )$ is abreviated as $\psi^2(f_B, f_H)$

The mean deflection of the structure Δ (H) and the r.m.s. deflection $\sigma_\delta(H)$ at the top of structure was obtained by assumption of the same deflection mode, $\mu(z)$ for each as follows,

$$\overline{\Delta}(H) = \frac{1}{1 + 2\alpha + \alpha_\mu} \left\{ C_{D_o} \cdot \rho \frac{\overline{U}^2(H)}{2} \quad B \cdot H \right\} \cdot \frac{1}{k'}, \qquad \text{(A6.26)}$$

$$\sigma_\delta(H) = \frac{1}{1 + \alpha - \alpha_T + \alpha_\mu} \left\{ C_{D_o} \cdot \rho \frac{\overline{U}^2(H)}{2} \quad B \cdot H \right\} \cdot \frac{2\sigma_u(H)}{\overline{U}(H)}$$

$$x \left\{ \int_o^\infty \left(\frac{\tilde{C}_{D_n}}{C_{D_o}} \right) \frac{S_u(f,H)}{\sigma_u^2(H)} \quad \psi^2(f_B, f_H) \ |\chi(f)|^2 \ df \right\}^{\frac{1}{2}} \qquad \text{(A6.27)}$$

where

$k' = (2\pi f_1)^2 M_1$ (effective spring constant)

$M_1 = \frac{1}{1 + 2\alpha_\mu}$ H.B.D.γ (generalised mass for the fundamental mode)

$$\gamma = \frac{1 + 2\alpha_\mu}{H \cdot B \cdot D} \int_o^H \int_o^B m(z)\ \mu^2(z)\ dy\ dz$$

(average density of structure)

$$|\chi(f)|^2 = \frac{1}{k'^2 \left\{ \left(1 - \left(\frac{f}{f_1}\right)^2\right)^2 + 4\zeta_T^2 \left(\frac{f}{f_1}\right)^2 \right\}},$$

$\zeta_T = \zeta_S + \zeta_A$ (total damping ratio)

ζ_S is structural damping ratio for the fundamental mode and

$$\zeta_A = \frac{1 + 2\alpha_\mu}{1 + \alpha + 2\alpha_\mu} \quad \frac{\tilde{C}_{D_1}\ \bar{U}(H)\rho}{4\pi f_1\ D\ \gamma}$$

(aerodynamoic damping)

The ratio of r.m.s. to mean deflection was hence deduced by dividing equations (A6.27) into (A6.26),i.e.

$$\frac{\sigma_\delta(H)}{\bar{\Delta}(H)} = \frac{1 + 2\alpha + \alpha_\mu}{1 + \alpha - \alpha_T + \alpha_\mu} \cdot \frac{2\sigma_u(H)}{\bar{U}(H)}$$

$$x\left\{\int_o^\infty \left(\frac{\tilde{C}_{D_n}}{C_{D_o}}\right)^2 \frac{S_u(f,H)}{\sigma_u^2(H)} \quad \psi^2\ (f_B,\ f_H)\ |\chi(f)|^2 df\right\}^{\frac{1}{2}} \qquad \text{(A6.28)}$$

By approximation of the integral in equation (A6.28), and rearrangment

$$\frac{\sigma_\delta(H)}{\bar{\Delta}(H)} = r\left\{\left(\frac{\tilde{C}_{D_{qs}}}{C_{D_o}}\right)^2 \cdot B + \left(\frac{\tilde{C}_{D_1}}{C_{D_o}}\right)^2 R \cdot E \cdot S\right\}^{\frac{1}{2}} \qquad \text{(A6.29)}$$

where

$$r = \frac{1 + 2\alpha + \alpha_\mu}{1 + \alpha - \alpha_T + \alpha_\mu} \cdot \frac{2\sigma_u(H)}{\bar{U}(H)} \quad \text{(roughness factor)}$$

$$B = \int_o^{1.75f_1} \frac{S_u(f,H)}{\sigma_u^2(H)} \quad \psi^2\ (f_B,\ f_H)\ df \quad \text{(background excitation factor)}$$

$$= \text{function}\ (\alpha\ ,\ \alpha_T,\ \alpha_\mu,\ \alpha_D,\ \alpha_L,\ \tilde{f}_1(H),\ L_B,\ L_H)$$

$$\tilde{f}_1(H) = \frac{f_1 \cdot L(H)}{\bar{U}(H)}\ ,\ L_B = \frac{B \cdot k_y(H)}{L(H)}\ ,\ L_H = \frac{H \cdot k_z(H)}{L(H)}$$

$$R = \frac{\pi}{4\zeta_T} - 1.75$$ (resonance amplification factor)

$$E = \frac{f_1 \cdot S_u(f_1,H)}{\sigma_u^2(H)} = k_1 \frac{\frac{f_1 \cdot L(H)}{\bar{U}(H)}}{\left[1 + \left\{\frac{f_1 \cdot L(H)}{\bar{U}(H)}\right\}\right]^{\beta 5/3\beta}}$$ (gust power factor)

$$S = \psi^2(\alpha, \alpha_T, \alpha_\mu, \alpha_D, \alpha_L, \tilde{f}_1(H), F_B, F_H)$$ (size reduction factor)

$$F_B = \frac{f_1 \cdot B \cdot k_y(H)}{\bar{U}(H)}, \quad F_H = \frac{f_1 \cdot H \cdot k_z(H)}{\bar{U}(H)}$$

The expected value of maximum response displacement was obtained from the r.m.s. value multiplied by the peak factor,p,i.e.

$$\Delta_{max}(H) = \bar{\Delta}(H) + p \cdot \sigma_\delta(H)$$

The maximum r.m.s. acceleration was estimated and obtained from the power spectrum of r.m.s. displacement response,i.e.,

$$\ddot{\delta}_{max}(H) = p_a \sigma_{\ddot{\delta}}(H)$$

where

$$p_a = \sqrt{2 \ln f_1 T} + \frac{0.577}{\sqrt{2 \ln f_1 T}}$$

and T is the averaging period.

The WREAN 01 was hence developed on this theory to predict the wind response of a tall structure in the along-wind direction. Necessary input data and availabe output information for RESPONSE is summarised below.

INPUT DATA

H, B, D, f_1, γ α_μ and ζ for a structure;

$\bar{U}(z_r)$, α, $\sigma_u(z_r)/\bar{U}(z_r)$, α_T, $L(z_r)$, α_L, β, $k_y(z_r)$, $k_z(z_r)$, α_D, z_r for wind characteristics; and

C_{D_o}, $\tilde{C}_{D_{qs}}/C_{D_o}$, $\tilde{C}_{D_1}/C_{D_o}$

OUTPUT DATA AVAILABLE

$\bar{U}(H)$, $\sigma_u(H)/\bar{U}(H)$, $L(H)$, $k_y(H)$, $k_z(H)$

for confirmation of input data;

$\bar{\Delta}(H)$, $\sigma_\delta(H)$, $\sigma_{\ddot{\delta}}(H)$, $\Delta_{max}(H)$, $\ddot{\delta}_{max}(H)$

as a computation result; and r,B,E,S,G as intermediate factors where G = (gust factor)

$$G = \frac{\bar{\Delta}_{max}(H)}{\bar{\Delta}(H)} = 1 + p\,\frac{\sigma_\delta(H)}{\bar{\Delta}(H)}$$

APPENDIX 6.2

GRAPHS AFTER KANDA[4]

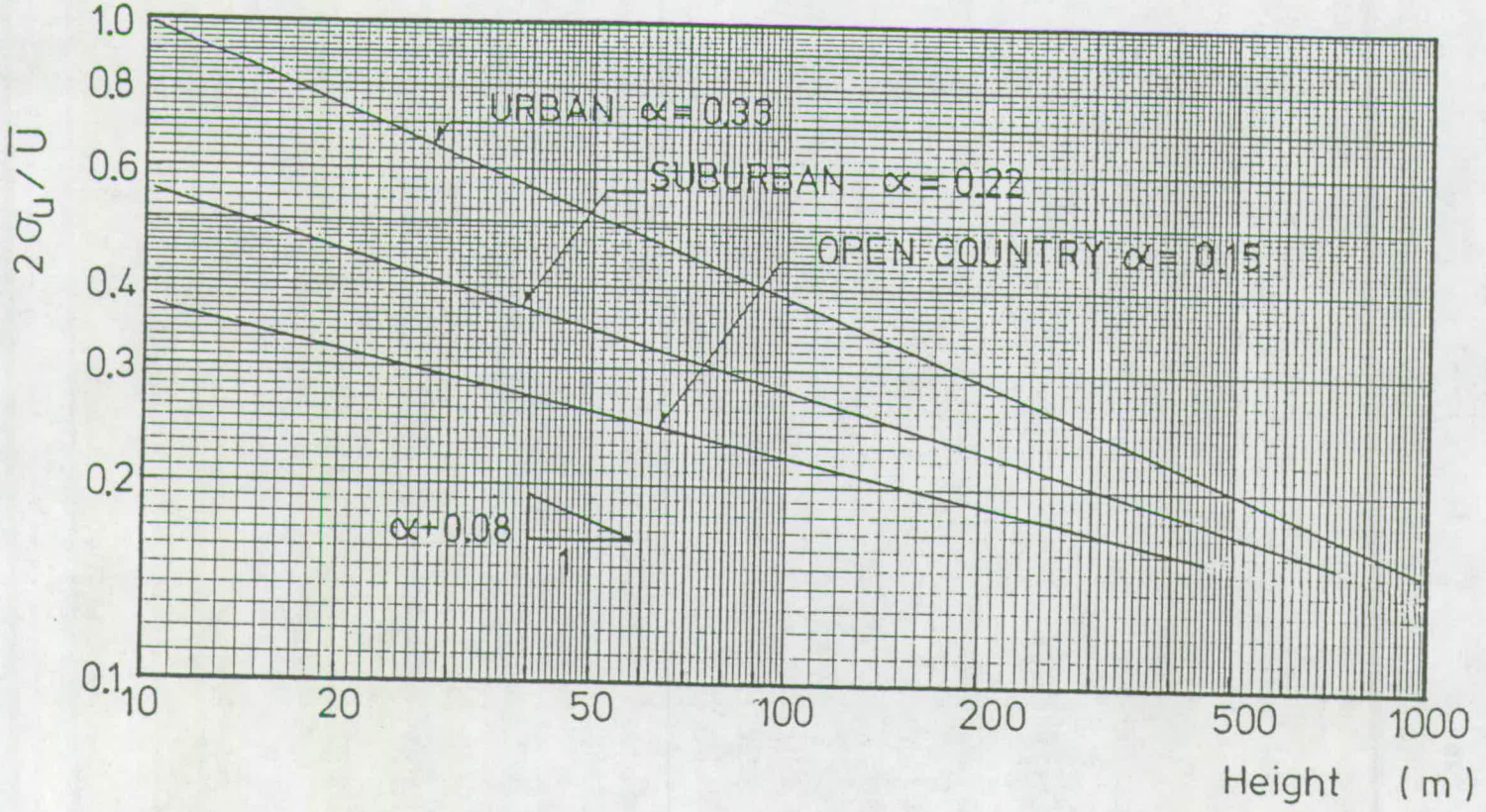

Figure A Turbulence intensity factor $\frac{2\sigma_u(H)}{\bar{U}(H)}$ (after Kanda[4])

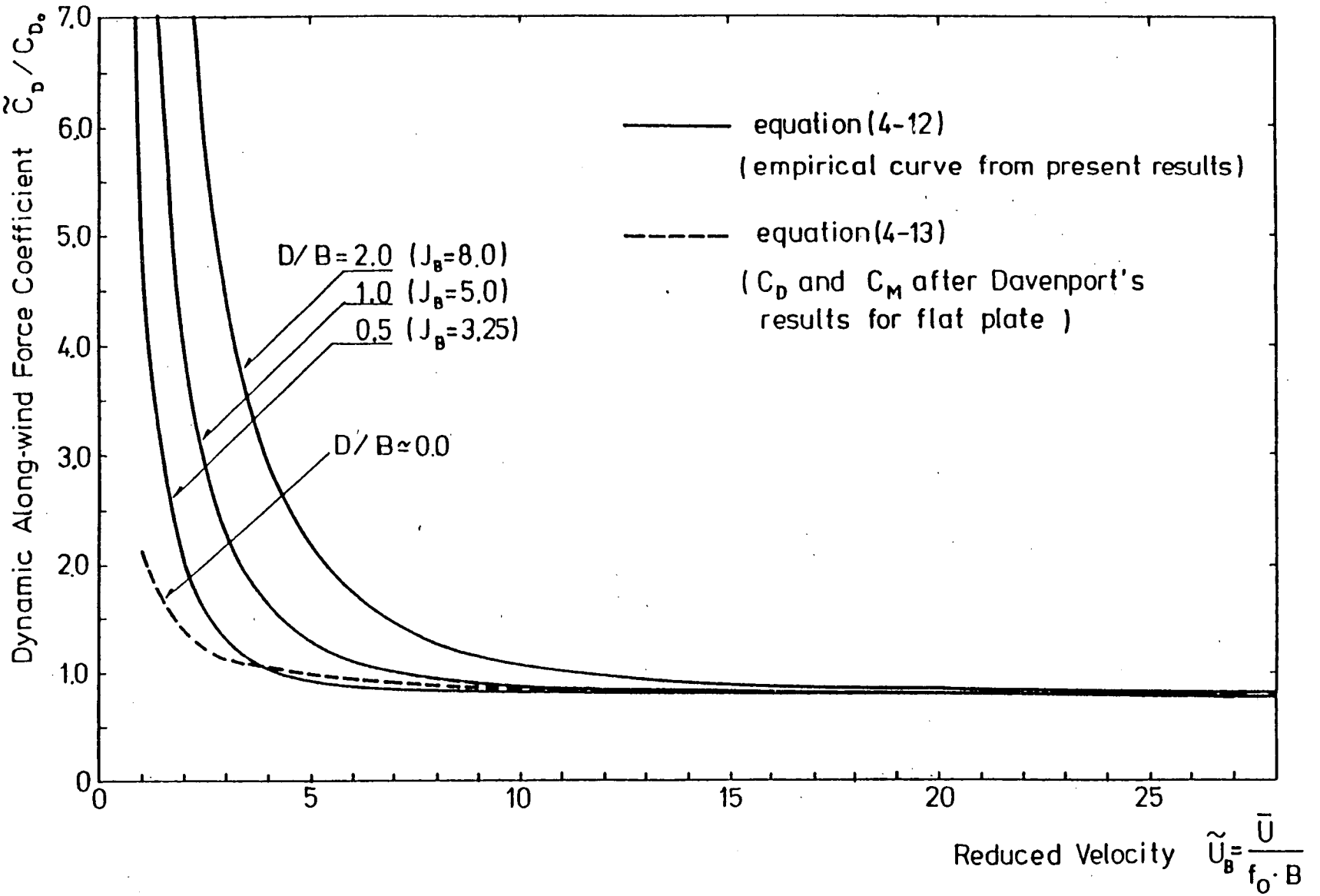

Figure B Proposed expression for $\tilde{C}_D$ against $\tilde{U}_B$ and $\frac{D}{B}$ presented in normalised form (*Kanda*[4])

APPENDIX 6.3

RESULTS OBTAINED BY THE RESPONSE PROGRAM

**** DYNAMIC WIND RESPONSE ANALYSIS RESULTS ****

NAME : RESPONSE Of JRC TO 6.1 M/S WIND (E-W)
SIZE OF STRUCTURE : H = 54.M B = 24.M D = 18.M F0=0.99HZ ZETA=0.71%
WIND CHARACTERISTICS AT Z=H (( ) SHOWS POWER EXPONENT OF PROFILE):

U(H) = 10.M/S (0.30) T.I. = 23.% (-0.08) L(H) = 1095.M (0.20) BETA = 2.0

DECAY FACTOR KY = 13.7 KZ = 11.7 (-0.41)

COEFFICIENTS :	C DST = 2.40	C DQS = 0.80	C DDR = 1.00

RESULTS: DEFLECTION X & ACCELERATION A AT Z=H
(MODAL SHAPE POWER EXPONENT = 1.0)

XMEAN = 0.0007M AERO.D.R. =0.032%

DAMPING RATIO 0.71%

AERODYNAMIC DAMPING EFFECT		N	Y
X RMS (M)		0.00022	0.00022
X MAX (M)		0.00148	0.00148
A RMS (G)		0.00013	0.00013
A MAX (G)		0.00056	0.00055
GUST FACTOR		2.25	2.25
PEAK FACTOR	X	3.72	3.71
	A	4.19	4.19

ROUGHNESS FACTOR	0.550	BACKGROUND EX.F.	0.574
GUST EX. FACTOR	0.021	SIZE RED. FACTOR	0.004

**** DYNAMIC WIND RESPONSE ANALYSIS RESULTS ****

NAME : RESPONSE OF JRC TO 32.5 M/S WIND (E-W)
SIZE OF STRUCTURE : H = 54.M B = 24.M D = 18.M FØ=Ø.99HZ ZETA=1.ØØ%
WIND CHARACTERISTICS AT Z=H (( ) SHOWS POWER EXPONENT OF PROFILE):

U(H) = 54.M/S (Ø.3Ø) T.I. = 12.% (-Ø.Ø8) L(H) = 1Ø6Ø.M (Ø.2Ø) BETA = 2.Ø

DECAY FACTOR KY = 13.7 KZ = 11.7 (-Ø.41)
COEFFICIENTS : C DST = 2.4Ø C DQS = Ø.8Ø C DDR = 2.4Ø

RESULTS: DEFLECTION X & ACCELERATION A AT Z=H
(MODAL SHAPE POWER EXPONENT = 1.Ø)

XMEAN = Ø.Ø186M AERO.D.R. =Ø.4Ø6%

DAMPING RATIO 1.ØØ%

AERODYNAMIC DAMPING EFFECT	N	Y
X RMS (M)	Ø.ØØ827	Ø.ØØ716
X MAX (M)	Ø.Ø53Ø9	Ø.Ø4841
A RMS (G)	Ø.Ø3Ø11	Ø.Ø2528
A MAX (G)	Ø.126Ø6	Ø.1Ø585
GUST FACTOR	2.85	2.6Ø
PEAK FACTOR X	4.17	4.16
A	4.19	4.19
ROUGHNESS FACTOR	Ø.284	BACKGROUND EX.F. Ø.579
GUST EX. FACTOR	Ø.Ø66	SIZE RED. FACTOR Ø.Ø72

**** DYNAMIC WIND RESPONSE ANALYSIS RESULTS ****

NAME : RESPONSE OF JRC TO 32.5 m/s WIND (E-W)
SIZE OF STRUCTURE : H = 54.M B = 24.M D = 18.M FØ=Ø.99HZ ZETA=1.ØØ%
WIND CHARACTERISTICS AT Z=H (( ) SHOWS POWER EXPONENT OF PROFILE):

U(H) = 54.M/S (Ø.3Ø) T.I. = 12.% (-Ø.Ø8) L(H) = 1Ø6Ø.M (Ø.2Ø) BETA = 2.Ø

DECAY FACTOR KY = 13.7 KZ = 11.7 (-Ø.41)
COEFFICIENTS : C DST = 2.4Ø C DQS = Ø.8Ø C DDR = 1.ØØ

RESULTS: DEFLECTION X & ACCELERATION A AT Z=H
(MODAL SHAPE POWER EXPONENT = 1.Ø)

XMEAN = Ø.Ø186M AERO.D.R. =Ø.169%

DAMPING RATIO 1.ØØ%

AERODYNAMIC DAMPING EFFECT	N	Y
X RMS (M)	Ø.ØØ452	Ø.ØØ435
X MAX (M)	Ø.Ø3718	Ø.Ø3645
A RMS (G)	Ø.Ø1261	Ø.Ø1165
A MAX (G)	Ø.Ø5278	Ø.Ø4877
GUST FACTOR	2.ØØ	1.96
PEAK FACTOR X	4.1Ø	4.Ø9
A	4.19	4.19

ROUGHNESS FACTOR Ø.284 BACKGROUND EX.F. Ø.579

GUST EX. FACTOR Ø.Ø66 SIZE RED. FACTOR Ø.Ø72

APPENDIX 6.4

RESULTS OBTAINED ACCORDING TO THE METHOD OUTLINED BY

ESDU 76001

Method of response prediction as outlined by ESDU 76001

$\overline{U}_{10} = 6,05$ hourly mean wind speed at a ref. height of 10m

$\alpha = 0,3$ power law exponent of mean wind speed

$Z_o = 1,0\ m$ surface roughness parameter

$h_o = 10\ m$ general obstical height

$d = h_o - 2,5\, Z_o$

$\tilde{Z} = 1/2\,(H - d) = 0.5(54 - 10 + 25) = 23,25\ m$

$\overline{U}_H = 6,05\left(\frac{54}{10}\right)^{0,3} = 10.03\ m/s$

$H = 54\ m$ $\quad w = 23,6\ m$ $\quad n_1 = 0,99\ Hz$ $\quad \zeta = 0,71\ \%$ $\quad m_1 = 3,23 \times 10^6\ kg$

$X_{Lu} = 25\,\tilde{Z}^{0,35} = 75,1$ $\qquad \tilde{n}_x = \frac{n_1 X_{Lu}}{\overline{U}_H} = \frac{0,99 \times 75,1}{10,03} = 7,41$

$Y_{Lu} = 10\,\tilde{Z}^{0,38} = 33,0$ $\qquad \tilde{n}_y = \frac{n_1 Y_{Lu}}{\overline{U}_H} = 3,26$ $\qquad \phi_{uu} = \frac{4\,\tilde{n}_x}{(1 + 70,8\,\tilde{n}_x)^{5/6}} = 0,0287$

$Z_{Lu} = 6,3\,\tilde{Z}^{0,45} = 25,9$ $\qquad \tilde{n}_z = \frac{n_1 Z_{Lu}}{\overline{U}_H} = 2,56$

$\frac{n\,w}{Y_{Lu}} = 0,71$ $\qquad \frac{n\,H}{Z_{Lu}} = 2,06$ $\qquad \frac{\sqrt{A}}{Z_{Lu}} = \frac{\sqrt{23,6 \times 54}}{25,9} = 1,38$

$I_u = \frac{\lambda}{\lg(\tilde{Z}/Z_o)}\,(0,867 + 0,556 \lg \tilde{Z} - 0,246 (\lg \tilde{Z})^2 = 0,282$ $\qquad \lambda = 0,76$ for $Z_o > 0,02m$

$B^2(\tilde{n}) = 2,25$ (Fig. 4) $\qquad J_H^2 = \frac{0,1}{1,0 \times 0,52 \times 0,89} = 0,216$ (Fig. 7)

$J_W^2 = \frac{0,23}{0,47 \times 1,0} = 0,489$ (Fig. 9)

$\bar{F}_1 = \left[0,5 \rho \times C_D \times (\overline{U}_H)^2 \times w \times H\right] / (2\alpha + 2) = \frac{0,5 \times 1,23 \times 1,0 \times 10,03^2 \times 23,6 \times 54}{(2 \times 0,3 + 2)} = 30,326 \times 10^3$

$n_1 S(n) = 4 \cdot J_H^2 \cdot J_W^2 \cdot (\bar{F}_1)^2 \cdot \phi_{uu} \cdot (I_u)^2 \cdot B^2(n)$

$= 1,995 \times 10^6\ N^2$

$g_D = \sqrt{2 \ln(n_1 T_o)} + \frac{0,577}{\sqrt{2 \ln(n_1 T_o)}}$ $\qquad T_o = 3600\ s$

$= 4,18$

$\ddot{X}_{max} = g_D \left[\sqrt{\frac{\pi n_1 S(n)}{4\zeta}} \times \frac{\mu}{m_1}\right]$ $\qquad \mu = 1,0$ mode shape function

$= 1,922 \times 10^{-2}\ m\,s^{-2}$

$= 19,6 \times 10^{-4}\ g$

Method of response prediction as outlined by ESDU 76001

$\overline{U}_{10} = 32,5$ hourly mean wind speed at a ref. height of 10m

$\alpha = 0,3$ power law exponent of mean wind speed

$Z_o = 1,0\,m$ surface roughness parameter

$h_o = 10\,m$ general obstacle height

$d = h_o - 2,5\,Z_o$

$\tilde{Z} = 1/2\,(H - d) = 0,5(54 - 10 + 25) = 23,25\,m$

$\overline{U}_H = 32,5\,(\frac{54}{10})^{0,3} = 54,0$ m/s

$H = 54\,m$ $\quad w = 23,6\,m$ $\quad n_1 = 0,99\,Hz$ $\quad \zeta = 1\,\%$ $\quad m_1 = 3,23 \times 10^6\,kg$

$X_{Lu} = 25\,\tilde{Z}^{0,35} = 75,1$ $\quad \tilde{n}_x = \frac{n_1 X_{Lu}}{\overline{U}_H} = \frac{0,99 \times 75,1}{54} = 1,38$

$Y_{Lu} = 10\,\tilde{Z}^{0,38} = 33,0$ $\quad \tilde{n}_y = \frac{n_1 Y_{Lu}}{\overline{U}_H} = 0,61$ $\quad \phi_{uu} = \frac{4\,\tilde{n}_x}{(1 + 70,8\,\tilde{n}_x)^{5/6}} = 0,092$

$Z_{Lu} = 6,3\,\tilde{Z}^{0,45} = 25,9$ $\quad \tilde{n}_z = \frac{n_1 Z_{Lu}}{\overline{U}_H} = 0,48$

$\frac{n\,w}{Y_{Lu}} = 0,708$ $\quad \frac{n\,H}{Z_{Lu}} = 2,06$ $\quad \frac{\sqrt{A}}{Z_{Lu}} = \frac{\sqrt{23,6 \times 54}}{25,9} = 1,38$

$I_u = \frac{\lambda}{\lg(\tilde{Z}/Z_o)}\,(0,867 + 0,556 \lg \tilde{Z} - 0,246 (\lg \tilde{Z})^2 = 0,282$ $\quad \lambda = 0,76$ for $Z_o > 0,02\,m$

$B^2(\tilde{n}) = 2,25$ (Fig. 4) $\quad J_H^2 = \frac{0,1}{1,0 \times 1,04 \times 0,89} = 0,108$ (Fig. 7)

$J_W^2 = \frac{0,23}{1,03 \times 1,0} = 0,233$ (Fig. 9)

$\bar{F}_1 = [0,5 \rho \times C_D \times (\overline{U}_H)^2 \times w \times H] / (2\alpha + 2) = \frac{0,5 \times 1,23 \times 1,0 \times 54^2 \times 23,6 \times 54}{(2 \times 0,3 + 2)} = 876 \times 10^3$

$n_1 S(n) = 4 \cdot J_H^2 \cdot J_W^2 \cdot (\bar{F}_1)^2 \cdot \phi_{uu} \cdot (I_u)^2 \cdot B^2(n)$

$= 1,029 \times 10^9\ N^2$

$g_D = \sqrt{2 \ln(n_1 T_o)} + \frac{0,577}{\sqrt{2 \ln(n_1 T_o)}}$ $\quad T_o = 3600\,s$

$= 4,18$

$\ddot{X}_{max} = g_D \left[\sqrt{\frac{\pi n_1 S(n)}{4 \zeta}} \times \frac{\mu}{m_1} \right]$ $\quad \mu = 1,0$ mode shape function

$= 0,368\ m s^{-2}$

$= 0,037\ g$

$X_{r.m.s} = \ddot{X}_{max} / (2\pi n_1)^2 \sqrt{2}$

$= 6,6\ mm$

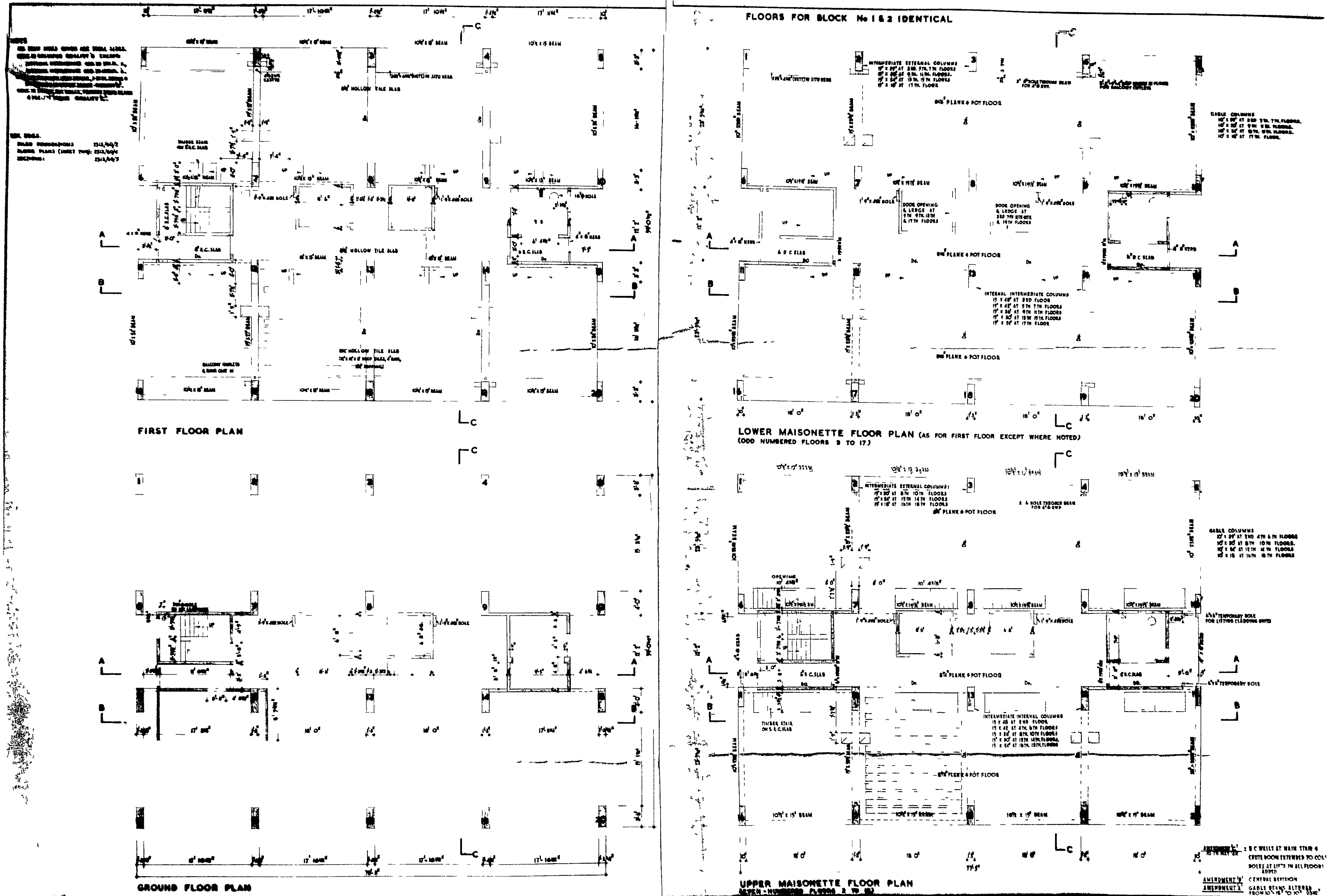

BLYTH & BLYTH M.I.C.E.
CHARTERED CIVIL ENGINEERS
CONSULTING STRUCTURAL ENGINEERS
135 GEORGE STREET EDINBURGH, 2

DRAWN BY R.B.C.S.
CHECKED BY
PASSED BY

CITY & ROYAL BURGH OF EDINBURGH

ARCHITECTS: ALISON & HUTCHISON & PARTNERS

CENTRAL LEITH REDEVELOPMENT
COUPER STREET SCHEME

FLOOR PLANS (SHEET ONE)

SCALE: ONE INCH TO EIGHT FEET.

DRAWING No 2513/60/3[C]

DATE DECEMBER 1960

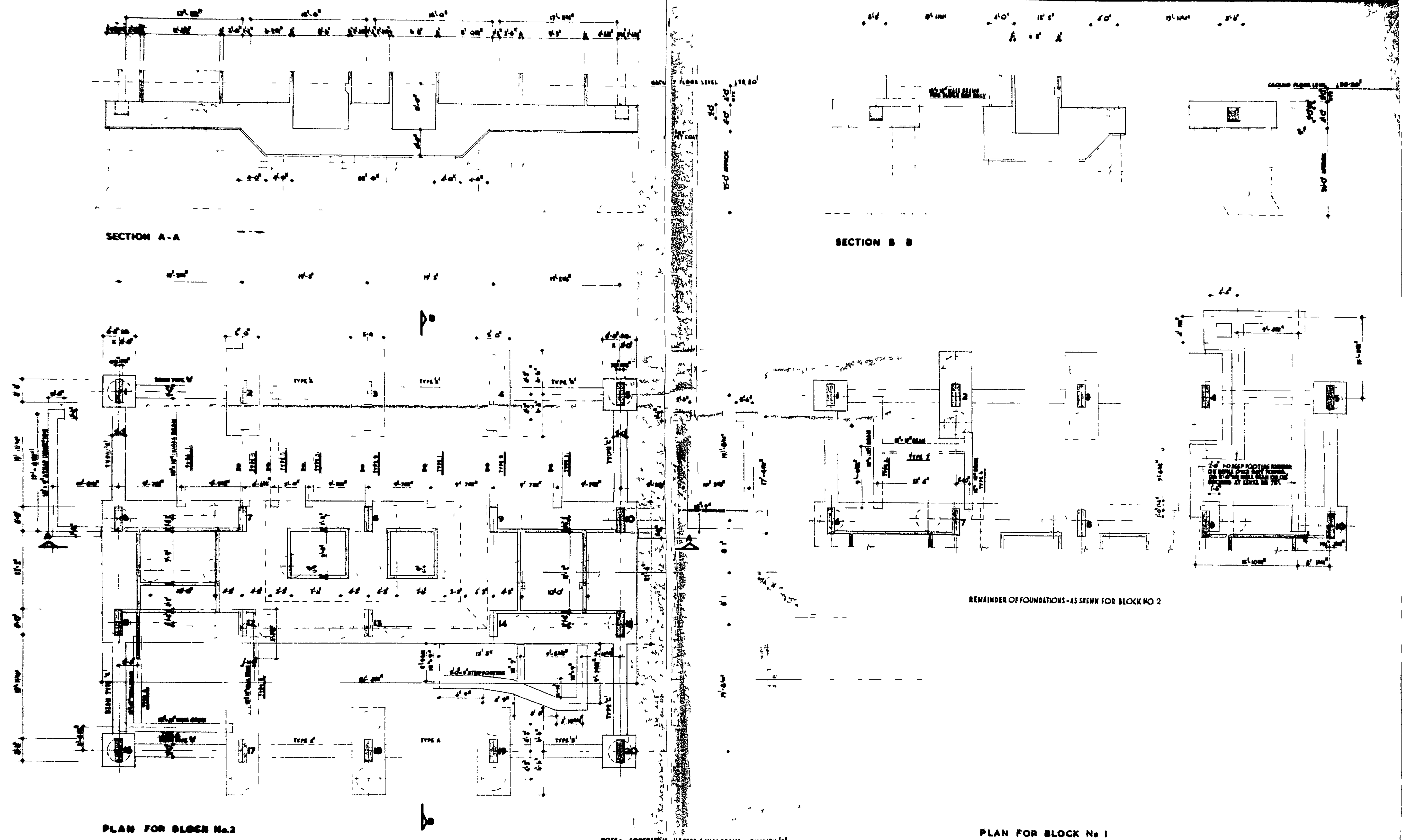

NOTE: CONCRETE IN PILECAPS & WALL BEAMS QUALITY 'B'
IN STRIP FOOTINGS 'C'
IN 2" CARPET COAT 'D'
ALL STRIP FOOTINGS TO BE REINFORCED WITH FABRIC
B.S. REF. NO 1221 A - 124, WEIGHING 5.17 LB/SQ YD

AMENDMENT 'C' ALTERATIONS AT WALL FOOTINGS ... FOR BLOCK NO. 1
AMENDMENT 'B' : DIMENSIONS TO POSITION OF WALL
R.C. WALLS AT MAIN STAIR & CHUTE ROOM
EXTENDED TO COLUMNS
AMENDMENT 'A' GENERAL REVISION

BLYTH & BLYTH M.M.I.C.E.
CHARTERED CIVIL ENGINEERS
CONSULTING STRUCTURAL ENGINEERS
135, GEORGE STREET, EDINBURGH, 2

DRAWN BY R.R.C.S.
CHECKED BY
PASSED BY

CITY & ROYAL BURGH OF EDINBURGH
ARCHITECTS ALISON & HUTCHISON & PARTNERS

CENTRAL LEITH REDEVELOPMENT
COWPER STREET SCHEME

PILED FOUNDATIONS
FOR BLOCKS No. 1 & 2
SCALE ONE INCH TO EIGHT FEET

DRAWING No 2513/60/2[C]
DATE DECEMBER 1960

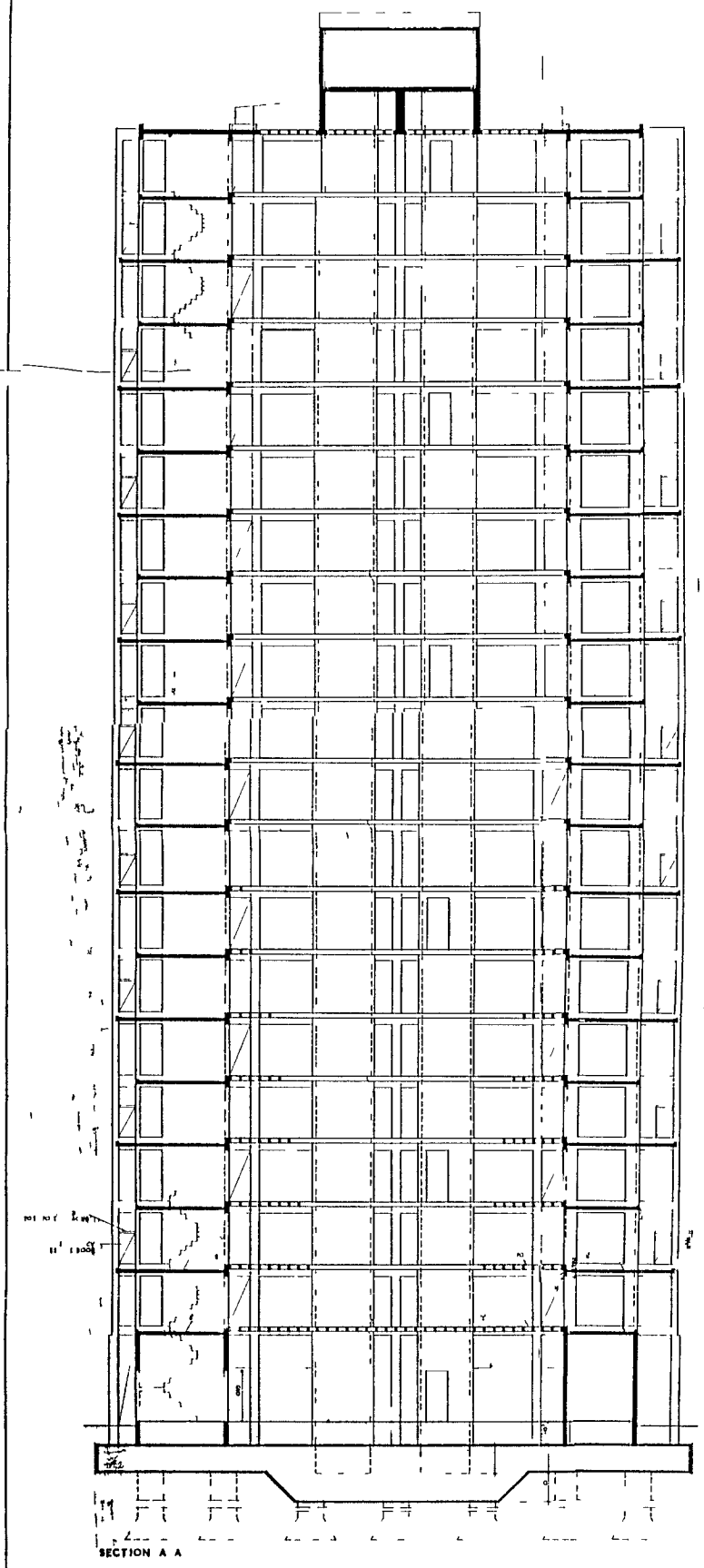

SECTION A A

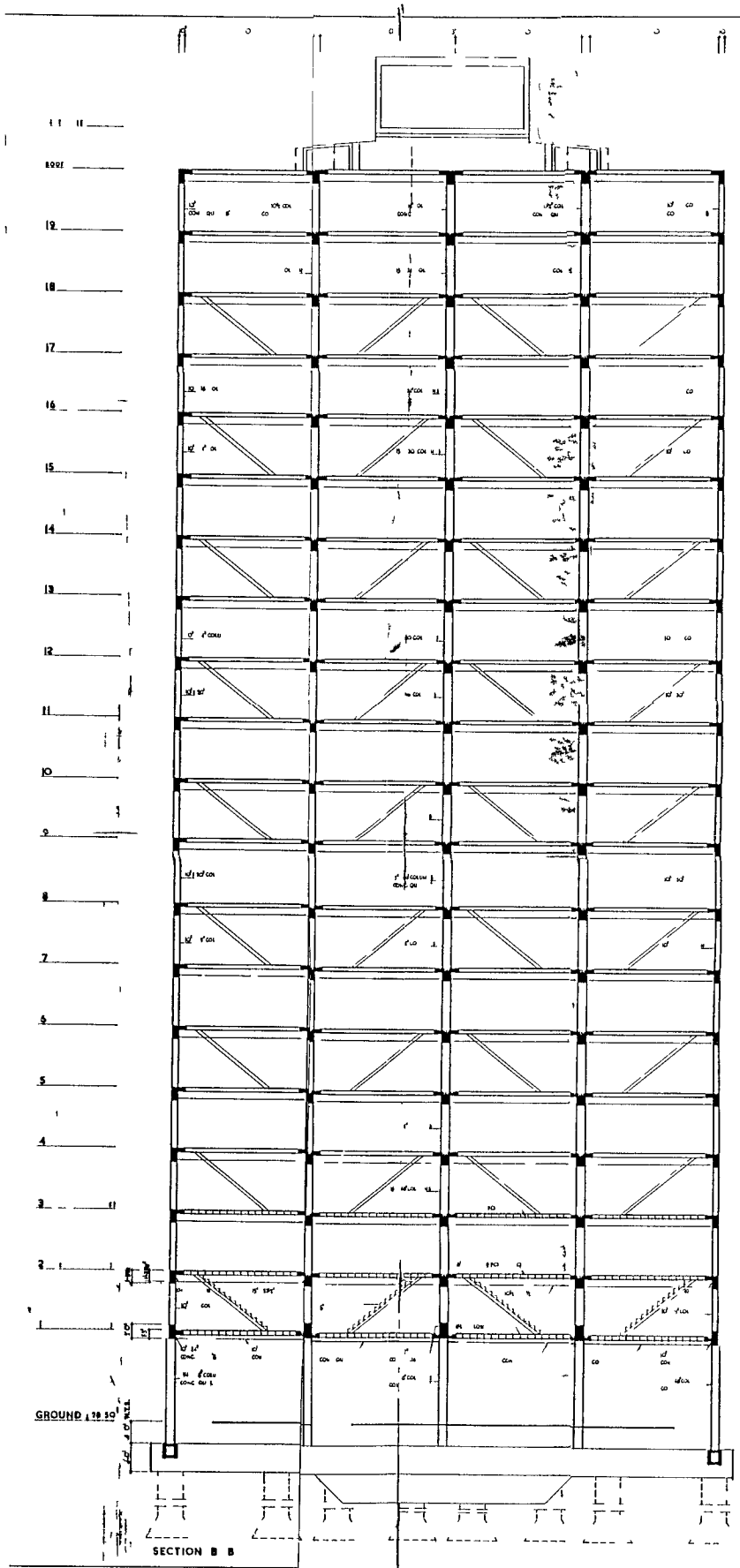

SECTION B B

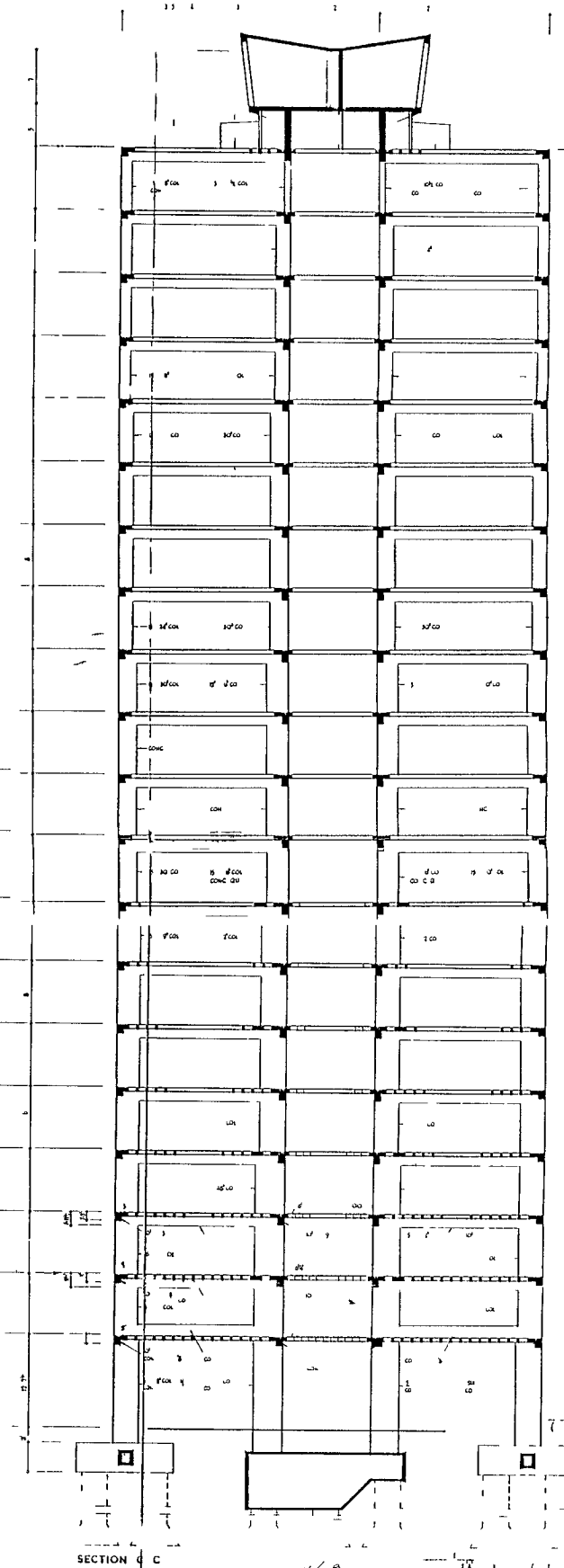

SECTION C C

BLYTH & BLYTH MESSRS
CIVIL ENGINEERS
CONSULTING STRUCTURAL ENGINEERS
RUSSELL STREET EDINBURGH 2

DRAWN BY
CHECKED BY
PASSED BY

CITY & ROYAL BURGH OF EDINBURGH

ARCHITECTS ALISON & HUTCHISON & PARTNERS

CENTRAL LEITH REDEVELOPMENT
COUPER STREET SCHEME

SECTIONS

SCALE ONE INCH TO EIGHT FEET

DRWG N 2513/60/S[illegible]

DATE JANUARY 1961